UNIVERSITY OF
BIRMINGHAM

Light Metal Amides and Imides For Hydrogen Storage

by

Alexandra L. Kersting

Supervisor: Dr Paul A. Anderson

A thesis submitted to the University of Birmingham for

the Degree of Doctor of Philosophy

The School of Chemistry

College of Engineering and Physical Sciences

The University of Birmingham

September 2011

ABSTRACT

The thermal decomposition of mixed cation amides, $Li_3Na(NH_2)_4$ and $LiNa_2(NH_2)_3$, with light metal hydrides, lithium hydride, sodium hydride and magnesium hydride, was investigated and hydrogen gas was identified as the major desorption product in all cases. Minimal ammonia was detected and therefore the mixed cation amides could be considered as hydrogen storage materials. The reactions were found to be similar to previously studied light metal amide-hydride systems like lithium amide/lithium hydride and lithium amide/magnesium hydride. Magnesium hydride caused the hydrogen desorption from the mixed cation amides to occur at a lower temperature than when they were heated with lithium hydride. The hydrogen desorption was also at a lower temperature than $LiNH_2$ + LiH and $2LiNH_2$ + MgH_2. Although hydrogen was desorbed when the mixed cation amides were heated with NaH, the amount was much smaller than for LiH and MgH_2, therefore making it less suitable as a hydrogen storage material.

Reactions in various ratios between $NaNH_2$ and MgH_2 were investigated to intermediate temperatures up to 350 °C. Thermal decomposition, Raman spectroscopy and thermogravimetric analysis were all employed to explore the decomposition and reaction pathways of these reactions. It was found that the products were analogous to those formed by lithium amide heated with magnesium hydride in similar ratios. The more hydride included in the reaction, the greater the hydrogen loss for the products. Three new phases were identified and each was attempted to be made pure in order to characterise them. Evidence for the formation of a mixed Na-Mg amide, Na-Mg imide and Na-Mg nitride, under different temperatures and reaction conditions, was obtained. Attempts to rehydrogenate the Na-Mg imide were successful, reforming magnesium amide and sodium hydride.

Sodium amide ($NaNH_2$) has been relatively neglected in the literature and so an examination of its decomposition products and reaction with sodium hydride, as a comparison to $LiNH_2$-LiH, were carried out. Using Raman and thermal decomposition techniques, it was proposed that a sodium imide may be formed, possibly with the same variable stoichiometry as observed for $LiNH_2$-Li_2NH. Rehydrogenation was attempted on this phase, but was unsuccessful.

ACKNOWLEDGEMENTS

I have many people to thank for their help in getting this thesis finished. First and foremost many thanks to my supervisor Paul Anderson for allowing me to do a PhD in the first place. Also, thanks to Phil Chater for all his help, advice, suggestions and cider on a Friday night.

Thanks to rest of Paul's group: Jim Prendergast, Matt Turnbull, Alvaro Mayoral Garcia, Ian Evans, David Hewett, Chao Zhao and Tom Carey for the opinions, ideas and comedy times. Thanks to all members of floor 5, past and present, for all the chats and procrastination.

For all the equipment time I've hogged in materials, thanks to David Book, Allan Walton, Vicky Mann and especially Dan Reed for also explaining all the intricacies of the TGA, DSC and Raman.

Thank you to my parents for allowing me the freedom to be a student all this time and for letting me return home to write up.

Thanks to Rachel and Simon for giving me a place to get away from everything when it got a bit overwhelming and to Ben for baby cuddles.

And of course, thanks to Rich...anyone that can put up with me whilst I write a thesis is worth their weight in gold.

CONTENTS

LIST OF ABREVIATIONS AND SYMBOLS

Abbreviation	*Description*
DFT	Density Functional Theory
DOE	Department of Energy
DSC	Differential Scanning Calorimetry
DTA	Differential Thermal Analysis
ESRF	European Synchrotron Radiation Facility
FCC	Face Centred Cubic
FTIR	Fourier Transform Infra Red Spectroscopy
IGA	Intelligent Gravimetric Analysis
MIM	Multiple Ion Monitoring
MS	Mass Spectrometry
PEM	Proton Exchange Membrane
PSD	Position Sensitive Detector
PTC	Positive Temperature Coefficient
QPA	Quantitative Phase Analysis
RGA	Residual Gas Analysis
RMM	Relative Molecular Mass
SAED	Selected Area Electron Diffraction
TGA	Thermogravimetric Analysis
TG-DTA	Thermogravimetric-Differential Thermal Analysis
TPA	Temperature Programmed Absorption
TPD	Temperature Programmed Desorption
XRD	X-ray Diffraction

1. INTRODUCTION

1. Hydrogen Economy

Hydrogen is the most abundant element in the universe; however, it does not exist in its elemental form. It is in this form that it is needed to be used as an energy vector. Therefore, hydrogen in its elemental form must be produced. At present, hydrogen is mostly produced from fossil fuels *via* steam reformation and the water gas shift reactions:

Equation 1-1 $$-(CH_2)-_n + H_2O \rightarrow CO + (n + 1)H_2$$

Equation 1-2 $$CO + H_2O \rightarrow CO_2 + H_2$$

Unfortunately, in gathering hydrogen from these reactions fossil fuels are used and CO_2 is released from these reactions and therefore the disadvantages outweigh the benefits. The ideal production of hydrogen would be independent from fossil fuels, from a limitless energy source and without the release of CO_2.

Electrolysis is one way of producing hydrogen cleanly, but this depends on the source of electricity. Electricity produced from renewable energy sources, such as photovoltaics, wind turbines and hydroelectricity provide the limitless 'green' energy required.

Nuclear power can also provide electricity without the CO_2 release, however there are harmful by-products from the radioactive waste and is therefore not ideal as a long term replacement for fossil fuels. In the short to medium term though, it can help meet our growing energy needs.

Hydrogen is important as fossil fuels are depleting and by burning them they are releasing CO_2, that was locked away underground, into the atmosphere. CO_2 is a greenhouse gas and has been linked to global climate change.[1]

The use of hydrogen is dependent on the challenges associated with production, storage and use. Storage is arguably the biggest challenge faced when considering the hydrogen economy.

Hydrogen can be combusted cleanly to give just water as the only product when burnt in oxygen. Hydrogen can also be used electrochemically in a fuel cell to produce electrical power. There are different types of fuel cell depending on their electrolyte: alkaline, phosphoric acid, molten carbonate, solid oxide and proton exchange membrane (PEM). PEM fuel cells have fast start up times, high efficiency from 65 °C and are good for mobile applications.

PEM fuel cells are, however, bad with contaminants in the hydrogen supply. With only 30 ppm NH_3 in the hydrogen supply there is a rapid drop in fuel cell performance that is not recoverable when the NH_3 is removed.

Hydrogen gas in its natural state fills a volume of 11 $m^3\ kg^{-1}$. This is massive and requires reduction to a more usable volumetric density. The usual ways of fulfilling this is through compression or liquefaction. This comes at the expense of the gravimetric density, that is the storage vessels in order to hold hydrogen at greater pressure than ambient reduce the gravimetric capacity of the system as a whole. Ideally, a compromise between the gravimetric and volumetric density would be reached. Here, we look at the storage of hydrogen within light metal amides and hydrides. The targets for the ideal hydrogen storage system have been outlined by the US Department of Energy (DOE).[2]

The original targets suggested by the US DOE have been replaced by more realistic goals. The current target for gravimetric capacity of a hydrogen storage system is 5.5 wt% in the year 2015 and ultimately 7.5 wt%. The delivery temperature target has been set at –40 to 85 °C with a delivery pressure of 5 bar for fuel cell applications. Recharging would ideally take no more than 2.5 minutes, it would need to be rapidly reversible to same standard throughout, withstand 1500 de/rehydrogenation cycles and be of low enough cost for widespread acceptance.

So far, there has been no single system which meets all the demanding criteria.

2. Using Hydrogen

Research into using hydrogen as an energy vector has expanded exponentially during the past few years. One of the most promising hydrogen storage media for use for a vehicular application is that of storing hydrogen in the solid state with light metals and non-metals. These metals and non-metals include lithium, sodium, magnesium, aluminium, boron and nitrogen in various combinations. Complex hydrides in particular demonstrate excellent hydrogen storage potential by their ability to contain within them high hydrogen mass (Table 1-1). Unfortunately, the reversibility (the ability to recombine the products after dehydrogenation with hydrogen) of these is poor.

Table 1-1 Selected complex hydrides and their hydrogen weight%.[3]

Hydride	*Wt%*	*Availability or Synthetic Reference*
$LiBH_4$	18.2	Commercially Available
$LiAlH_4$	10.5	Commercially Available
$Al(BH_4)_3$	20.0	[4]
$LiAlH_2(BH_4)_2$	15.2	[5]
$Mg(AlH_4)_2$	9.3	[6]
$Mg(BH_4)_2$	14.8	[7]
$Ca(AlH_4)_2$	7.7	[8]
$Ca(BH_4)_2$	11.4	Synthetic procedure to be developed
$NaAlH_4$	7.5	Commercially Available
$NaBH_4$	10.5	Commercially Available
$Ti(BH_4)_3$	12.9	[9]
$Ti(AlH_4)_4$	9.3	Synthetic procedure to be developed
$Zr(BH_4)_3$	8.8	[9]
$Fe(BH_4)_3$	11.9	Synthetic procedure to be developed

Light metal amides have recently shown better prospect of reversibility whilst maintaining a modest hydrogen weight%. Light metal amides have an additional problem of the possibility of ammonia release along with hydrogen. The challenge is now to utilise the maximum amount of hydrogen release with the minimal amount of ammonia release along with reasonable reversing conditions.

The reaction of lithium nitride (Li_3N) with hydrogen was originally investigated for hydrogen storage in 2002[10] and this system was found to reversibly absorb 11.5 wt% hydrogen (Equation 1-3). This made lithium amide ($LiNH_2$) reacted with LiH a realistic hydrogen storage system, as when heated alone $LiNH_2$ decomposes to lithium imide (Li_2NH) with the release of ammonia (Equation 1-4).

Equation 1-3 $Li_3N + 2H_2 \leftrightarrow Li_2NH + LiH + H_2 \leftrightarrow LiNH_2 + 2LiH$

Equation 1-4 $2LiNH_2 \leftrightarrow Li_2NH + NH_3$

Unfortunately, the reversing conditions are too harsh for the first part of Equation 1-3 to be practical, however the lithium amide-lithium imide conversion stores 6.5 wt% H_2 (1.85 hydrogen atoms) under 300 °C with favourable thermodynamics (ΔH = –45 kJ mol^{-1}).[10] The hydrogen desorption is thought to occur by one of two possible mechanisms. In the first, when $LiNH_2$ is heated with lithium hydride (LiH) it decomposes to lithium imide (Li_2NH) and ammonia (NH_3) (Equation 1-4) (ΔH = +84 kJ mol^{-1} NH_3)[11]. The NH_3 then reacts with LiH to form $LiNH_2$ with the release of hydrogen (H_2) (Equation 1-5). The enthalpy change was found to be –42 kJ mol^{-1} H_2.[11]

Equation 1-5 $LiH + NH_3 \rightarrow LiNH_2 + H_2$

These reactions continue until all the starting materials are used up.[12,13]

The second mechanism involves the direct reaction between $LiNH_2$ and LiH by the H^+ of $LiNH_2$ and H^- of LiH. This reaction forms hydrogen and the release of hydrogen is the driving force behind the reaction (Equation 1-6).[14,15]

Equation 1-6 $H^+ + H^- \rightarrow H_2$

The unit cell of $LiNH_2$ is shown in Figure 1-1. $LiNH_2$ has a tetragonal unit cell with lattice parameters a = 5.03 Å and c = 10.25 Å. It has been drawn with Li atoms on the unit cell edges and nitrogen forming N_4 tetragonal clusters.

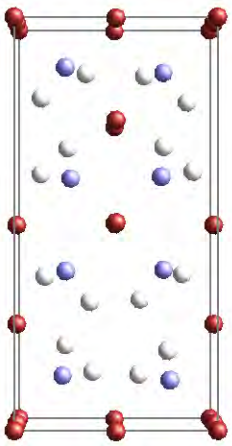

Figure 1-1 Crystal structure of $LiNH_2$. Nitrogen is shown in blue, lithium in red and hydrogen in grey. The unit cell is shown in black.[16]

The structure of Li_2NH is shown in Figure 1-2. It has cubic unit cell with lattice parameters of a = 5.057 Å. It is drawn as an anti-fluorite structure with nitrogen atoms on a face-centered cubic lattice.

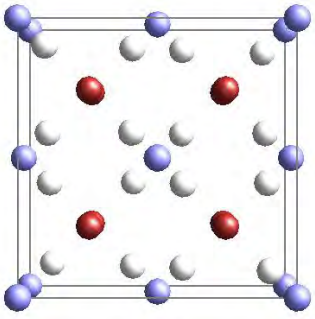

Figure 1-2 Crystal structure of Li_2NH. Nitrogen is shown in blue, lithium in red and hydrogen in grey. The unit cell is shown in black.[17]

Although $LiNH_2$ + LiH releases hydrogen without the desorption of ammonia, the temperature of 300 °C is still too high to be practical for a PEM fuel cell. Further improvements can be made to the $LiNH_2$-Li_2NH system have been found by substituting some lithium ions in the system for magnesium.

3. Li-Mg-N-H System

The decomposition temperature of LiH is 550 °C, whereas that of MgH_2 is much lower at around 280 °C. This shows LiH alone cannot be considered in this instance as a good hydrogen storage medium. MgH_2 alone (7.6 wt% H_2) has been investigated as a hydrogen storage material, but is still somewhat inadequate due to slow kinetics[18] as well as being fundamentally flawed by bad thermodynamics. ΔH_f (MgH_2) is −75 kJ mol^{-1} which means it will always be difficult (if not impossible) to remove the hydrogen below 280 °C.[19]

The lower stability of MgH_2 is due to magnesium hydride being partially ionic and partially covalent in its bonding, whereas lithium hydride is fully ionic, therefore much research has been conducted reacting $LiNH_2$ with MgH_2 in place of LiH.

The reaction between $LiNH_2$ and MgH_2 for hydrogen storage was first carried out in 2004 concurrently by 4 groups.[20,21,22,23] They all investigated slightly different factors in the reaction including different ratios between amide and hydride and variations using $Mg(NH_2)_2$ with LiH.

1. $2LiNH_2 + MgH_2$

Xiong *et al.*[20] heated lithium amide and magnesium hydride in a 2:1 ratio up to 350 °C in order that there was one amide unit for each hydrogen on the hydride. As with $LiNH_2$ and LiH only hydrogen, without any ammonia, was desorbed when lithium amide and magnesium hydride were reacted. It was found that the desorption temperatures, both onset and peak, of the hydrogen release were lower than for $LiNH_2$ + LiH. Powder X-ray Diffraction (XRD) was carried out on the sample after heating and comprised of peaks that did not match any previously identified Li-N-(H) compound. The sample was identified as $Li_2MgN_2H_2$ (Equation 1-7), with a cubic lattice with a = 10.03 Å.

Equation 1-7 $2LiNH_2 + MgH_2 \rightarrow Li_2MgN_2H_2 + 2H_2$

The sample was rehydrogenated under H_2 pressure at 90 bar and 180 °C. When the sample was hydrogenated completely it was found the temperature of this was dramatically reduced in comparison to the lithium system. The sample was cycled in order to assess the stability of the system. Little change in the temperature and intensity of hydrogen desorption/absorption showed a stable and reversible system. The XRD pattern showed the products of rehydrogenation to be $Mg(NH_2)_2$ and LiH rather than the original starting materials $LiNH_2$ and MgH_2 (Equation 1-8).

Equation 1-8 $2LiNH_2 + MgH_2 \rightarrow Li_2MgN_2H_2 + 2H_2 \leftrightarrow Mg(NH_2)_2 + 2LiH$

Xiong *et al.*[20] mention that amides of alkali and alkali earth metals consist of positively charged hydrogen ions bonded to N ions and conversely, the hydrogen in ionic hydrides is negatively charged. They suggested the high enthalpy of the reaction between these two opposing charged hydrogen ions could possibly drive the reaction between amides and hydrides (Equation 1-6).

At the same time, Luo[21] also published work on $2LiNH_2 + MgH_2$, directly comparing the absorption and desorption of $2LiNH_2 + MgH_2$ with $LiNH_2 + LiH$. Samples were ball-milled for 2 hours and heated to 300 °C for $LiNH_2 + LiH$ and 240 °C for $2LiNH_2 + MgH_2$. Hydrogen desorption started at 160 °C for the lithium only sample, whereas the Li-Mg sample started releasing at 100 °C. The samples were then subjected to pressure-composition isotherm measurements. The lithium only sample was compared to that of Chen *et al.*[10] and found to be similar, with any differences attributed to sample composition and preparation. The hydrogen pressure was found to be 1 bar at 280 °C. The Li-Mg sample was found to desorb a much higher H_2 wt% and therefore a greater pressure of 1.6 bar H_2 at 220 °C. The XRD pattern after dehydrogenation found there to be no Li_2NH or MgNH present and so Luo *et al.* concluded $Li_2MgN_2H_2$ was present, via Equation 1-7.

The Li-Mg-N-H sample was cycled 9 times and no degradation in desorption capacity was observed, which is important for hydrogen storage applications.

Yong Chen *et al.*[24] investigated the reaction of $2LiNH_2 + MgH_2$ ball-milled. They initially looked at the dehydriding profiles of the first 4 cycles of $2LiNH_2 + MgH_2$. It was seen that the first dehydrogenation profile was significantly slower than the subsequent 3. This was thought to be due to the first cycle being the interaction between $LiNH_2$ and MgH_2, whereas later cycles, as investigated by Luo and Sickafoose[25], were found to be reactions between

$Mg(NH_2)_2$ and LiH. Chen *et al.*[24] looked into the optimum dehydriding temperature for the starting reaction. It was found that 200 °C had substantially faster kinetics compared to 160 °C or 180 °C. Chen *et al.* suggested that in order to improve the kinetics of the lower temperature reactions, a suitable dopant to catalyze the reaction was necessary.

Luo *et al.*[26] looked into quantification of NH_3 release from the reaction of $2LiNH_2 + MgH_2$. The cycling of the Li-Mg-N-H system at 180 °C was found to have less capacity deterioration than the same reaction at 240 °C. This was due to less $Mg(NH_2)_2$ self-decomposition to MgNH at 180 °C.

Markmaitree *et al.*[27] found the reaction kinetics of $2LiNH_2 + MgH_2$ were more sluggish than $LiNH_2$ + LiH as it took longer for the former to reach equilibrium pressure. The two reactions were carried out with and without ball-milling. The $2LiNH_2 + MgH_2$ reaction always had more NH_3 desorbed from it, showing an overall poorer performance in terms of clean H_2 desorption. They confirmed the slow reaction between MgH_2 and NH_3, as suggested by Nakamori.[23] The more the samples were ball-milled, the less NH_3 was detected. This was thought to be due to smaller particle size and larger surface area of the MgH_2 and so greater opportunity for the NH_3 and MgH_2 to react, although not sufficient to alleviate the problem entirely. $2LiNH_2 + MgH_2$ heated to 210 °C for 5 hours formed MgNH and $Li_2Mg(NH)_2$ along with $LiNH_2$ and MgH_2 starting materials. There was no $Mg(NH_2)_2$ identified either by XRD or FTIR which is in conflict with Luo and Sickafoose who suggested a metathesis reaction occurred before the main reaction.[25] After heating for 10 hours, $LiNH_2$ had mostly disappeared as had MgNH; there was still a small amount of MgH_2 present as well as an increased amount of $Li_2Mg(NH)_2$. $Li_2Mg(NH)_2$ was characterised as being identical to the product formed by Luo and Sickafoose.[25] The suggested reaction scheme for this reaction

was the decomposition of lithium amide to imide and NH_3 (Equation 1-4), followed by the reaction of MgH_2 with NH_3 (Equation 1-9).

Equation 1-9 $MgH_2 + 2NH_3 \rightarrow Mg(NH_2)_2 + 2H_2$

The reaction between MgH_2 and NH_3 was found to be very slow.[28] The magnesium amide formed then goes on to decompose to MgNH with the release of NH_3 (first part of Equation 1-10). This occurs at a reasonable rate from 250 °C.[29] The ammonia recently formed then further reacts with MgH_2 and the reaction cycle continued.[27] The products from this cycle were MgNH and Li_2NH. These would then react to form $Li_2MgN_2H_2$ (Equation 1-11).[27]

Equation 1-10 $3Mg(NH_2)_2 \rightarrow 3MgNH + 3NH_3 \rightarrow Mg_3N_2 + 4NH_3$

Equation 1-11 $MgNH + Li_2NH \rightarrow Li_2MgN_2H_2$

This paper was the first to suggest the reaction between the two imides led to the mixed imide.[27] FTIR gave no indication of $Mg(NH_2)_2$ being present at any time. This was ascribed to the reaction in Equation 1-9 being slow.

Rijssenbeek[37] investigated the phase composition of $Li_2Mg(NH)_2$. $2LiNH_2 + MgH_2$ were ball-milled between 8 and 24 hours. There was no evidence of $Mg(NH_2)_2$ after milling, but a small amount of LiH was detected. The LiH was most likely present from metathesis between $LiNH_2$ and MgH_2, but $Mg(NH_2)_2$ did not appear as it is known to be non-crystalline after ball-milling.[30] $Li_2Mg(NH)_2$ first appeared after heating the starting materials to 280 °C. The desorption of H_2 and NH_3 was evidenced at this temperature. No further changes were

observed up to 330 °C. This was then labelled as α-$Li_2Mg(NH)_2$ (Figure 1-3). Complete hydrogen absorption was observed for α-$Li_2Mg(NH)_2$ and this reverted to $Mg(NH_2)_2$ and LiH. The α-$Li_2Mg(NH)_2$ was cycled. During the dehydrogenation phases of the cycling process, NH_3 was still evidenced, although in lesser amounts than the first desorption.

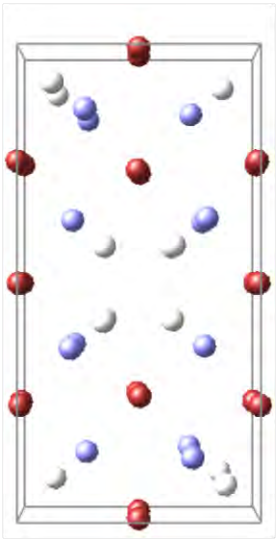

Figure 1-3 Crystal structure of α-$Li_2Mg(NH)_2$ Nitrogen is shown in blue, mixed lithium and magnesium sites in red and hydrogen in grey. The unit cell is shown in black.[37]

The XRD pattern observed at 330 °C was indexed to an orthorhombic unit cell, with space group *Iba*2 or *Ibam* with lattice parameters of $a \approx 10$ Å, $b \approx 5$ Å and $c \approx 5$ Å.[37] This structure is similar to that reported by Xiong *et al.*[33] using $Mg(NH_2)_2$-LiH (1:1) at 330 °C, whereas the 1:2 $Mg(NH_2)_2$ + LiH ratio at 250 °C gave only a cubic structure. Heating $2LiNH_2 + MgH_2$ to 350 °C caused a phase change to a primitive cubic phase, β-$Li_2Mg(NH)_2$.[37] Another transition occurred at 500 °C to a face centred cubic structure, γ-$Li_2Mg(NH)_2$. On cooling γ-$Li_2Mg(NH)_2$ reverted back to β-$Li_2Mg(NH)_2$, but α-$Li_2Mg(NH)_2$ was only formed from rehydrogenation followed by dehydrogenation at 280 °C. It was noted that using $Mg(NH_2)_2$ and LiH as starting

materials also formed the 3 phases of $Li_2Mg(NH)_2$, but the α-$Li_2Mg(NH)_2$ was sometimes difficult to detect and β-$Li_2Mg(NH)_2$ appeared at a lower temperature. A small amount of Mg_3N_2 was detected during some reactions at higher temperatures.

A fourth polymorph of $Li_2Mg(NH)_2$ was seen under different conditions.[37] Under high-pressure hydrogen (137 bar) and high temperatures (290 °C) δ-$Li_2Mg(NH)_2$ was formed with a tetragonal unit cell $a \approx 5.16$ Å, $c \approx 9.60$ Å (very close to α-$Li_2Mg(NH)_2$). However, when the temperature was cooled to below 280 °C, δ-$Li_2Mg(NH)_2$ reverted back to $Mg(NH_2)_2$ and LiH.

Full structural refinement was carried out for α-$Li_2Mg(NH)_2$.[37] Space group *Iba*2 was used and lattice parameters of $a = 9.78$ Å, $b = 4.99$ Å, $c = 5.20$ Å were refined. β-$Li_2Mg(NH)_2$ was refined to a primitive cubic unit cell with space group $P\text{-}4_3m$ and a lattice parameter of $a = 5.03$ Å. Xiong *et al.*[33] also reported a cubic structure, but with a unit cell with twice the lattice parameter. Rijssenbeek[37] attempted to index γ-$Li_2Mg(NH)_2$, but the XRD pattern was very similar to high temperature Li_2NH. It was indexed to a FCC cell with space group *Fm*–3*m* and $a \approx 5$ Å.

2. $Mg(NH_2)_2 + 2LiH$

Work was carried out by Xiong *et al.* in 2005.[31] This consisted of combining $Mg(NH_2)_2$ with 2LiH (the crystal structure of $Mg(NH_2)_2$ is shown in Figure 1-4). The reactants were ball-milled together for 2 days and then dehydrogenated by heating to 250 °C. The same $Li_2Mg(NH)_2$ phase as found the year before was formed.[20] The sample was then rehydrogenated under 90 bar H_2 up to 250 °C. This was found to reform $Mg(NH_2)_2$ and LiH. The hydrogen uptake started at 90 °C and became more rapid above 110 °C. Approximately 5.0 wt% H_2 was up taken below 200 °C in less than 50 minutes. The last of the hydrogen took

over 1 hour to be absorbed. The desorption occurred above 100 °C and more than 4.5 wt% was desorbed as the temperature reached 200 °C. The rest of the hydrogen desorbed much more slowly. For both the hydrogenation and dehydrogenation, the kinetics became slower towards completion of the reaction. As the hydrogen remained in the reaction vessel with the sample, the overpressure of hydrogen may suppress the last of the hydrogen release, therefore higher temperatures or gas removal system like a flowing line are required to complete the dehydrogenation more quickly.

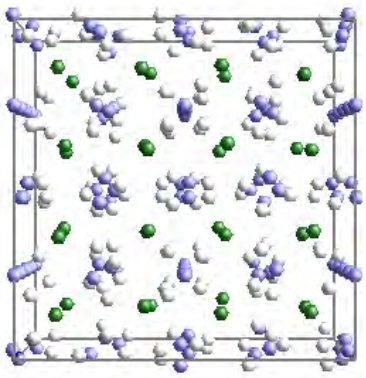

Figure 1-4 Crystal structure of $Mg(NH_2)_2$ Nitrogen is shown in blue, magnesium in green and hydrogen in grey. The unit cell is shown in black.[32]

Xiong *et al.*[31] also investigated this reaction by DSC. They found the hydrogen desorption started at around 100 °C and peaked at 200 °C. The $\Delta H_{desorption}$ was 44.1 kJ mol^{-1} H_2.

Figure 1-5 shows the reaction mechanism published by Xiong *et al.*[31] The mechanism shows the attraction between a $H^{\delta+}$ on the $Mg(NH_2)_2$ and $H^{\delta-}$ on LiH. This forms bonds concertedly between the $H^{\delta+}$ and $H^{\delta-}$ and the $Li^{\delta+}$ and $N^{\delta-}$. The bonds within lithium hydride and the nitrogen and hydrogen of $Mg(NH_2)_2$ break leaving an intermediate of '$LiMgN_2H_3$' and H_2. As this mechanism involves $H^{\delta+}$ and $H^{\delta-}$ (Equation 1-6) it was similar to that suggested by Chen

et al.[14] and Aguey-Zinsou *et al.*[15] for hydrogen release from $LiNH_2$ + LiH. For $Mg(NH_2)_2$ and LiH, Xiong *et al.* concluded that to decrease the activation energy of the reaction there needs to be a way of forming a greater attraction between H^+ and H^- of the amide and hydride respectively (Equation 1-6), or else weakening the Li-N and N-H bonds for rehydrogenation. This mechanism is not ammonia mediated, unlike the mechanisms proposed for much of the research previously discussed.

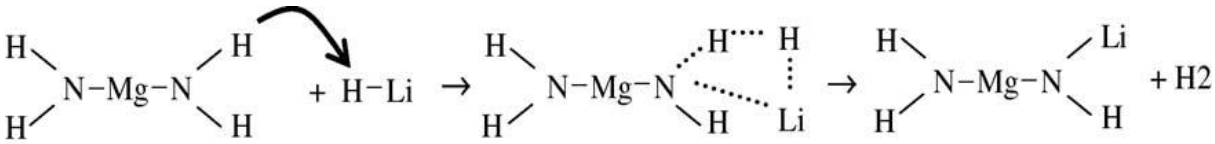

Figure 1-5 Possible reaction mechanism for the hydrogen desorption from $Mg(NH_2)_2$ + 2LiH.[31]

Xiong *et al.*[33] investigated $Mg(NH_2)_2$ + 2LiH, alongside 1:1 and 1:3 ratios. The reactants were ball-milled together for 20 h. The 1:2 mixture had better desorption characteristics than the 1:1 or 1:3 ratios. The hydrogen release was much greater than the 1:1 ratio and almost all the NH_3 desorption was suppressed. After cycling this mixture, all ammonia release was eliminated.

The 1:2 mixture was found to form $Li_2Mg(NH)_2$ at 250 °C, with a similar structure as previously reported by the same authors.[20,33] Mg_3N_2 was formed at 500 °C, but less than for the 1:1 ratio. The 1:3 mixture produced a Li-Mg-N-H complex at 240 °C similar to that in the 1:2 reaction mixture. Mg_3N_2 was again observed towards 500 °C.

The gas release from the 1:2 and 1:3 reactions were analysed quantitatively[33] using a gas reaction controller and applying soak and release modes. They both started to desorb

hydrogen at ~120 °C. Between 160–170 °C the rate of desorption increased, matching with temperature programmed desorption (TPD) data. Overall, the higher hydride content did not appear to increase the hydrogen desorption temperature. The 1:2 mixture gave 5 wt% H_2 by 230 °C, whereas the 1:3 reaction released 5.1 wt% H_2 by 330 °C. The hydrogen desorbed remained in the sample chamber and therefore provided a hydrogen over pressure which explained the lack of complete hydrogen desorption from the 1:3 mixture. Higher temperatures were required to remove more H_2.

The 1:2 mixture was more rapid than 1:3 for rehydrogenation at 70 bar.[33] At 100 °C the kinetics of adsorption were much quicker than 1:3. The slow kinetics of the 1:3 reaction mixture were blamed on possible sintering due to high temperature desorption or else the additional Li present in the sample.

Chen *et al.*[29] compared the reaction of $Mg(NH_2)_2$ + 2LiH with that of $Mg(NH_2)_2$ alone. They found the activation energies of the two reactions to be 88.1 kJ mol^{-1} and 130 kJ mol^{-1} respectively. This showed $Mg(NH_2)_2$ had a much larger kinetic barrier to overcome in order to liberate NH_3.

Chen *et al.*[29] commented that as the reaction rate is determined by the rate-determining step, the reaction between $Mg(NH_2)_2$ and LiH is unlikely to be started by the thermal decomposition of $Mg(NH_2)_2$. Isotopic exchange, of D for H, was also investigated and found to occur with relative ease which was supportive of a coordinated mechanism.

Liu *et al.*[34] investigated the effect of sodium compounds upon the Li-Mg-N-H system with partial substitution of $Mg(NH_2)_2$ for $NaNH_2$ and LiH for NaH. It was found that the hydrogen desorption kinetics of the Na containing reactions were markedly improved. NH_3 desorption was also reduced. The activation energies of the three samples, $Mg(NH_2)_2$ + 2LiH, $Mg(NH_2)_2$ +

1.6LiH + 0.4NaH and $0.8Mg(NH_2)_2$ + $0.4NaNH_2$ + 2LiH, were 105.5, 97.7, and 92.5 kJ mol^{-1} respectively. The Na-containing reactions desorbed their hydrogen quicker due to their lower activation energies. Unfortunately, less hydrogen was desorbed/adsorbed. The dehydrogenation products were different depending on the molar ratios between Li, Mg and Na.

NaH was added into the $Mg(NH_2)_2$-LiH mix [$Mg(NH_2)_2$-1.6LiH-0.4NaH].[34] There was no reaction when the starting materials were ball-milled together; therefore the starting materials were already in their lowest energy configuration or the activation energy for any reaction was not overcome. On heating it was observed that H_2 desorption started at 80 °C and peaked at 220 °C. The initial hydrogen loss was due to the formation of the mixed Li-Mg imide. The peak at 220 °C was thought to be from the reaction between $Mg(NH_2)_2$ and NaH. The products after hydrogen desorption were a $Li_2MgN_2H_2$-like phase, NaH and $NaNH_2$. On rehydrogenation $Mg(NH_2)_2$, LiH and NaH were all present.

When $NaNH_2$ was added to the $Mg(NH_2)_2$-LiH mix [$0.8Mg(NH_2)_2$-$0.4NaNH_2$-2LiH] the products after ball milling were found to be $Mg(NH_2)_2$, LiH, NaH and $LiNH_2$.[34] This revealed a salt metathesis reaction had occurred (Equation 1-12). The desorption started at 80 °C as before, but peaked at 230 °C. Again, the initial desorption was thought to be due to the reaction of $Mg(NH_2)_2$ and LiH. The peak was thought to be from $LiNH_2$ + NaH. The products after dehydrogenation were a cubic imide, NaH and $NaNH_2$. After rehydrogenation $Mg(NH_2)_2$, LiH, NaH, $NaNH_2$ and $LiNH_2$ were all present.

Equation 1-12 $NaNH_2 + LiH \rightarrow LiNH_2 + NaH$

Sudik *et al.*[35] investigated $Mg(NH_2)_2$ + 2LiH both unseeded and seeded with pre-decomposed $Li_2Mg(NH)_2$ added in excess to the reaction (5 wt%, 10 wt% and 15 wt%). All samples were ball-milled whether unseeded or with the seeded excess. It was found the 10 wt% $Li_2Mg(NH)_2$ lowered the desorption temperature by 40 °C, from 220 °C (for 0 wt% seeding) to 180 °C. The desorption curves indicated a two-step hydrogen release, the second stage being closer to the unseeded desorption curve. This suggested that not all the sample was exposed to the kinetically enhanced product seed. The activation energy of the seeded sample was lowered by 13% from 88.0 kJ mol^{-1} to 76.2 kJ mol^{-1} relative to the unseeded sample. The lowering of the desorption temperature aided the suppression of NH_3, although the temperature of NH_3 desorption was also lowered. Cycling the seeded sample continued to give lower temperatures of desorption although at 10 °C higher than on the first cycle. The relative desorption kinetics were found to be much quicker for the seeded sample than for the unseeded. At 220 °C the unseeded sample took an order of magnitude longer to fully desorb.

Liu *et al.*[36] looked at sintering their starting materials, $Mg(NH_2)_2$ + 2$LiNH_2$, in order to reduce particle size and increase mixing between the starting materials. The starting materials were first ball-milled for 36 hours, followed by heating to 315 °C under pure nitrogen gas. $Li_2Mg(NH)_2$ was formed along with the release of ammonia (Equation 1-13).

Equation 1-13 $Mg(NH_2)_2 + 2LiNH_2 \rightarrow Li_2Mg(NH)_2 + 2NH_3$

3 samples were then prepared from the sintered starting materials.[36] The first was $Li_2Mg(NH)_2$ hand-milled for 2 minutes. Samples 2 and 3 were ball-milled for 3 and 36 hours respectively.

The hydrogen uptake of all 3 samples was measured by heating them to 210 °C under 100 bar H_2. All samples absorbed about 5 wt% H_2. The onset of absorption was reduced by the ball-milling (particularly 36 h). The onset temperature for the hand-milled sample was 180 °C. By 180 °C the 36 hours ball-milled sample had already absorbed 3 wt% H_2.

The samples after their milling treatments were investigated *via* powder XRD and FTIR.[36] The hand-milled sample showed the presence of both orthorhombic α-$Li_2Mg(NH)_2$ and cubic β-$Li_2Mg(NH)_2$.[37] All the diffraction peaks were sharp indicating a well-ordered crystalline phase. By contrast, the ball-milled samples showed only the main peaks of β-$Li_2Mg(NH)_2$ and those were broad and less intense indicating a much less well-ordered state. The 2 ball-milled samples looked very similar, only that the sample milled for 36 hours had broader XRD peaks. The crystallite sizes for all 3 samples were calculated using the Scherrer equation and found to be about 41, 29 and 25 nm, respectively. The dramatic reduction in particle sizes between samples 1 and 2 explained the difference in the XRD patterns.

The FTIR spectra for the hand-milled sample showed the presence of 2 peaks in the imide region as well as very weak intensity absorbances from unreacted $LiNH_2$ (Figure 1-6).[36] The 2 peaks in the imide region were most likely from the two forms of $Li_2Mg(NH)_2$ present. The two ball-milled samples both had one peak in the imide region: this concurred with the XRD results for these samples. After rehydrogenation at 210 °C, the samples were dehydrided again. The kinetics of all the samples were very similar to their first dehydrogenation.

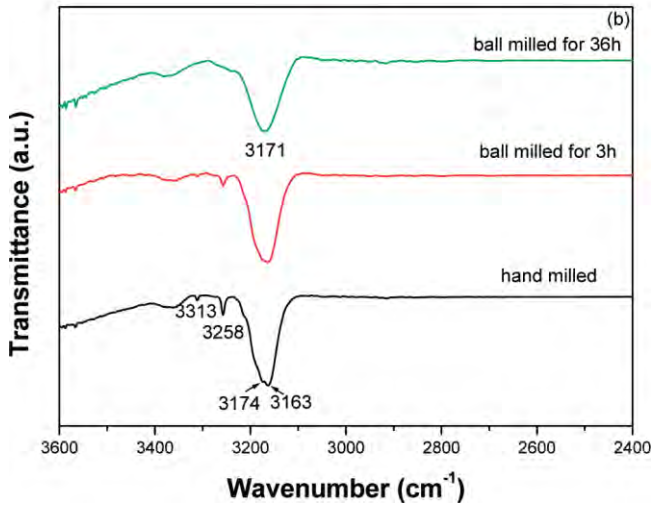

Figure 1-6 FTIR of $Li_2MgN_2H_2$ samples with different treatments.[36]

At the same time as Xiong *et al.*[31] above, Luo and Sickafoose[25] were examining the structural characteristics of the Li-Mg-N-H system. As it was already known that the reaction between $LiNH_2$ and MgH_2 was reversible back to $Mg(NH_2)_2$ and LiH (Equation 1-8), initially comparisons between desorption isotherms of $2LiNH_2 + MgH_2$ and $Mg(NH_2)_2 + 2LiH$ were carried out.

The desorption isotherms for $2LiNH_2 + MgH_2$ and $Mg(NH_2)_2 + 2LiH$ were virtually identical with any variations attributed to experimental error (Figure 1-7). Luo *et al.* were troubled as to why they should be so close in isothermal characteristics. XRD patterns of the milled $LiNH_2$ and MgH_2 mixture showed no reaction during ball-milling. The $2LiNH_2 + MgH_2$ mixture was heated to 220 °C under 100 bar H_2 for 2 h in order to establish which mechanism may be present. No desorption activity was expected under those conditions. The XRD after this experiment showed the presence of $Mg(NH_2)_2$ and LiH, as well as the starting materials $LiNH_2$ and MgH_2. This gave evidence of an incomplete salt metathesis reaction.

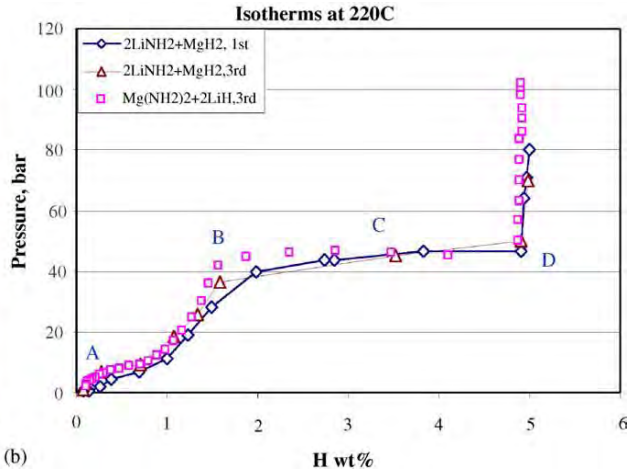

Figure 1-7 Desorption pressure-composition isotherms at 220 °C for the first and third desorption of the ($2LiNH_2$ + MgH_2) sample. Desorption isotherm for ($Mg(NH_2)_2$ + 2LiH) is included.[25]

Fourier transform infrared (FTIR) spectroscopy was used in this paper[25] to provide evidence on the makeup of the system throughout the hydriding/dehydriding cycle. The sample started in its dehydrided state. FTIR evidence showed the first dehydrided sample contained no $–NH_2$ bands and so was identified as an imide. The imide bands did not match MgNH or Li_2NH (as confirmed by XRD) and so were most likely from $Li_2Mg(NH)_2$. From XRD it was seen that the peak positions were slightly different at the start of hydriding to a short time after. The FTIR showed $–NH_2$ bands attached to Li, not Mg, without evidence for a new phase. Therefore, the following reaction was suggested:

Equation 1-14 $$Li_2MgN_2H_2 + 0.6H_2 \rightarrow Li_2MgN_2H_{3.2}$$

The authors chose this stoichiometry due to their observations above.

After rehydrogenation, there was evidence of $Mg(NH_2)_2$ and LiH in the XRD results. FTIR confirmed the presence of $Mg(NH_2)_2$. The following reaction was suggested for this region:

Equation 1-15 $$Li_2MgN_2H_{3.2} + 1.4H_2 \leftrightarrow Mg(NH_2)_2 + 2LiH$$

As the new phases of $Mg(NH_2)_2$ and LiH were formed gradually during absorption, the plateau observed during sorption isotherms was explained. The authors propose a pathway for the rehydriding reactions (Figure 1-8).

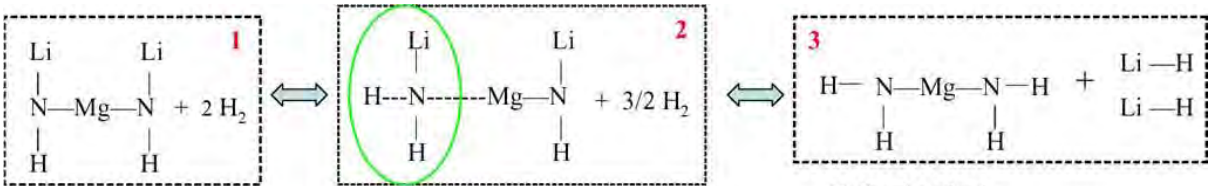

Figure 1-8 Proposed pathway for the sorption reaction of $Li_2Mg(NH)_2 + 2H_2$.[25]

Each box above (Figure 1-8) represents the sample at various times during the rehydrogenation.[25] Box 1 shows the starting materials for rehydrogenation- $Li_2MgN_2H_2$ and H_2. Box 2 shows the addition of one hydrogen to the imide forming the previously suggested $Li_2MgN_2H_{3.2}$ (Equation 1-14). The authors suggest the similarity in crystal structure between $Li_2MgN_2H_2$ and $Li_2MgN_2H_{3.2}$ in boxes 1 and 2 above could account for the similarity in the XRD patterns observed for both phases. The ringed section also highlights the presence of Li^+-NH_2^-, although still part of the mixed imide. The FTIR shows us that NH_2^- ions were coordinated to Li^+, which the authors have called $LiNH_2$, but these were still present as part of the mixed Li-Mg-imide-amide phase/phases, not as crystalline $LiNH_2$. Once the reaction is

complete (box 1 to 2), more hydrogen is added to form the bonds between Li and H and N and H of $Mg(NH_2)_2$. The transition from box 2 to 3 is not really a mechanistic progression, more a jump from the proposed intermediate to the fully hydrided phase.

This pathway (Figure 1-8)[25] is in contrast to Xiong *et al.*[31] who presented a possible mechanism for the dehydrogenation (Figure 1-5). Xiong *et al.* acknowledge the possible instability of the intermediate, but it is along the same mechanistic lines as Luo and Sickafoose.[25]

Janot *et al.*[38] compared the reactions $Mg(NH_2)_2 + 2LiH$ and $2LiNH_2 + MgH_2$. They attempted to gather preliminary data on the crystallographic unit cell of $Li_2Mg(NH)_2$ and found a cubic antifluorite structure, a = 10.06(1) Å. This was roughly twice the value of that suggested by Xiong *et al.*[20,33]

3. $3Mg(NH_2)_2 + 8LiH$

Concurrent with Xiong *et al.*[20] and Luo,[21] Leng *et al.*[22] also investigated the Li-Mg-N-H system. Leng *et al.*,[22] however, looked directly at the reaction between magnesium amide and lithium hydride in a 3:8 ratio. This indicated a product of Mg_3N_2 may be possible due to the addition of extra $Mg(NH_2)_2$ compared to the reactions seen previously. They suspected that the reaction between the $Mg(NH_2)_2$ and LiH would go *via* an NH_3-mediated solid-gas reaction like $LiNH_2$ + LiH (Equation 1-4 and Equation 1-5).

The mixture of $Mg(NH_2)_2$ (made by ball-milling MgH_2 under a pure NH_3 gas atmosphere of 4 bar) and LiH was ball milled under hydrogen gas for 2 h and then heated up to 400 °C.[22] A large amount of hydrogen desorption was observed. The temperature of desorption and the amount of hydrogen desorbed were both higher than the $LiNH_2$ + LiH reaction (as seen

above). Leng *et al.* attributed this to $Mg(NH_2)_2$ being less stable and more easily decomposed to imide and nitride than $LiNH_2$ (smaller enthalpy, larger entropy). The products after heating to 400 °C were characterised by XRD and found to be Mg_3N_2 and Li_2NH (Equation 1-16).

Equation 1-16 $3Mg(NH_2)_2 + 8LiH \rightarrow Mg_3N_2 + 4Li_2NH + 8H_2$

This reaction had a theoretical hydrogen capacity of about 7 wt% (in comparison to $2LiNH_2 + MgH_2$, 5.35 wt% H_2) and this was mirrored experimentally. In order to investigate the reversibility, the dehydrogenated sample was heated at 200 °C under 30 bar H_2. The starting materials were reproduced after rehydrogenation/dehydrogenation cycling, which indicated complete reversibility.

Leng *et al.*[22] suggested the reaction went by three elementary reactions:

(1) The decomposition of $Mg(NH_2)_2$ to MgNH and NH_3. This continues to Mg_3N_2 at higher temperatures (Equation 1-10).

(2) The NH_3 desorbed reacts with LiH present to form $LiNH_2 + H_2$ (Equation 1-5).

(3) The newly formed $LiNH_2$ decomposes to Li_2NH and further NH_3 (Equation 1-4). The NH_3 then reacts with more LiH, forming further $LiNH_2$ and undergoing further decomposition (Equation 1-5).

The products from the reaction carried out by Leng *et al.*[22] do not suggest $Li_2Mg(NH)_2$ was ever formed. The additional $Mg(NH_2)_2$ present pushed the reaction through to the most hydrogen deficient magnesium species, Mg_3N_2.

The rehydrogenation process could not simply follow the reverse of the suggested dehydrogenation reaction, as Li_2NH when rehydrogenated forms $LiNH_2$ and LiH. However, Mg_3N_2 does not rehydrogenate to $Mg(NH_2)_2$ and MgH_2[39] (or any other products). Rehydrogenation of Mg_3N_2 to $Mg(NH_2)_2$ and MgH_2 was however shown to occur by Nakamori et al. when mixed with Li_3N.[40]

4. $Mg(NH_2)_2 + 4LiH$

Nakamori *et al.*[23] investigated $Mg(NH_2)_2 + 4LiH$ to compare with the desorption characteristics of $Mg(NH_2)_2$ alone and when reacted with MgH_2. They found the decomposition of the two magnesium based reactions to be very similar in that they both desorbed NH_3 as a majority gas, possibly with a small amount of hydrogen. This indicated to them that the addition of MgH_2 to $Mg(NH_2)_2$ did not suppress the desorption of ammonia from $Mg(NH_2)_2$ as the addition of LiH does compared to $LiNH_2$ heated alone. It was concluded this was due to the reaction between LiH and NH_3 being "ultrafast",[41] whereas the analogous reaction between MgH_2 and NH_3 took in the region of a day to go to completion.

$Mg(NH_2)_2 + 4LiH$ were heated up to 600 °C. Mass loss began at approximately 150 °C; by 600 °C 6.5 wt% loss had been observed. This was less than the theoretical mass loss (9.1 wt% H_2) using Equation 1-17. It was seen from thermogravimetric-differential thermal analysis (TG-DTA) that more than 2 steps occurred during desorption (Figure 1-9). Only Mg_3N_2 and Li_3N were observed after dehydrogenation in a vacuum at 477 °C. The gas desorbed from the reaction was confirmed to be only hydrogen with no ammonia release observed. In comparison to the gas desorption temperature of $LiNH_2$ with LiH, Equation

1-18, Equation 1-17 occurred at over 100 °C lower. Nakamori *et al.*[23] put this down to the lower decomposition temperature of $Mg(NH_2)_2$ compared to $LiNH_2$.

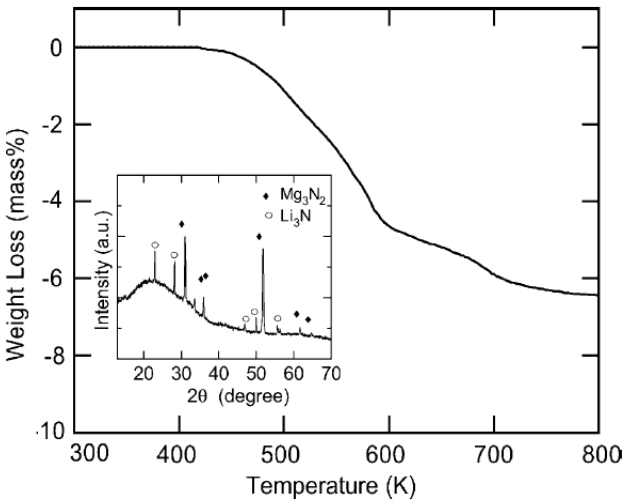

Figure 1-9 TG-DTA of the mixture of $Mg(NH_2)_2$ + 4LiH in argon flow at 0.1 MPa with a heating rate of 10 °C min^{-1}. The inset shows the powder XRD profile after dehydriding reaction of the mixture of $Mg(NH_2)_2$ + 4LiH. The closed diamonds and open circles show the peak positions of Mg_3N_2 and Li_3N.[23]

Equation 1-17 $3Mg(NH_2)_2 + 12LiH \leftrightarrow Mg_3N_2 + 4Li_3N + 12H_2$

Equation 1-18 $LiNH_2 + LiH \leftrightarrow Li_2NH + H_2$

Aoki *et al.*[42] focused on $3Mg(NH_2)_2$ + 12LiH due to the high hydrogen storage capacity of 9 wt%. The full reaction is seen in Equation 1-17. Up to 250 °C, only half the hydrogen was desorbed. The similarities noticed between the isotherms of $3Mg(NH_2)_2$ + 12LiH and $Mg(NH_2)_2$ + 2LiH imply the dehydrogenation reactions are similar. After dehydrogenation of the 3:12 mixture, two new phases were identified. One indexed with a tetragonal lattice, the other orthorhombic. The orthorhombic unit cell increased throughout hydrogen loss. (This is

different from interstitial hydrides.) Lattice parameters of the tetragonal and orthorhombic phases observed are shown in

Table 1-2 1–2.

Table 1-2 Lattice parameters of the tetragonal and orthorhombic phases observed (from Aoki *et al.*[42]).

Lattice Parameters H_2 *wt% loss*	*Tetragonal* *3.1*	*Orthorhombic* *3.5*	*Orthorhombic* *4.0*	*Orthorhombic* *4.9*
a/ Å	9.575	9.765	9.805	9.799
b/ Å	5.141	5.011	5.000	5.004
c/ Å	5.141	5.187	5.191	5.201

The tetragonal and orthorhombic phases corresponded to $Li_4Mg_3(NH_2)_2(NH)_4$ and $Li_{4+x}Mg_3(NH_2)_{2-x}(NH)_{4+x}$ (x = 0.4, 1, 2) respectively.[42] $Li_4Mg_3(NH_2)_2(NH)_4$, $Mg(NH_2)_2$ and LiH were all thought to coexist and the molar ratio of $Li_4Mg_3(NH_2)_2(NH)_4$ increased whilst the others decreased, throughout the plateau of the isotherm. The orthorhombic phase, $Li_{4+x}Mg_3(NH_2)_{2-x}(NH)_{4+x}$, formed at the sloping part of the isotherm. The final products were $Li_2MgN_2H_2$ and LiH. The authors suggest the temperature at 250 °C was the reason for the lack of continued reaction of the products.

5. $Mg(NH_2)_2$ + LiH

Xiong *et al.*[33] investigated $Mg(NH_2)_2$ and LiH in a 1:1 ratio. The reactants were ball-milled together for 20 h. The mixture started to desorb hydrogen at approximately 200 °C. There was less hydrogen comparatively than when compared to 1:2 and 1:3 mixtures also investigated by Xiong *et al*. A considerable amount of ammonia was also detected, starting at 150 °C and peaking at 270 °C. It was noted how the reaction between $Mg(NH_2)_2$ and xLiH

gave a lower decomposition temperature than the decomposition temperature of $Mg(NH_2)_2$ alone (~360 °C). It was suggested, therefore, that the NH_3 was not from the unreacted $Mg(NH_2)_2$ but from another –NH containing intermediate. Above 370 °C another large desorption of NH_3 was present. This may have been due to $Mg(NH_2)_2$ decomposition.

Powder XRD was then used in order to characterise the structural changes occurring.[33] The 1:1 mixture was examined by XRD after heating to 220 °C. The result was an XRD pattern that indicated a cubic structure with a = 5.033 Å (Figure 1-10). This is analogous to the structures noted by Xiong *et al.*[20] No $Mg(NH_2)_2$ or LiH was present. The ammonia released at higher temperature was suggested to have been the result of the Li-Mg-N-H structure decomposing. The decomposed structure (after heating to 370 °C) was tetragonal; a = 5.131 Å, c = 9.626 Å. By 500 °C, Mg_3N_2 had appeared as well as a post 220 °C compound, but with lower symmetry than the tetragonal phase.

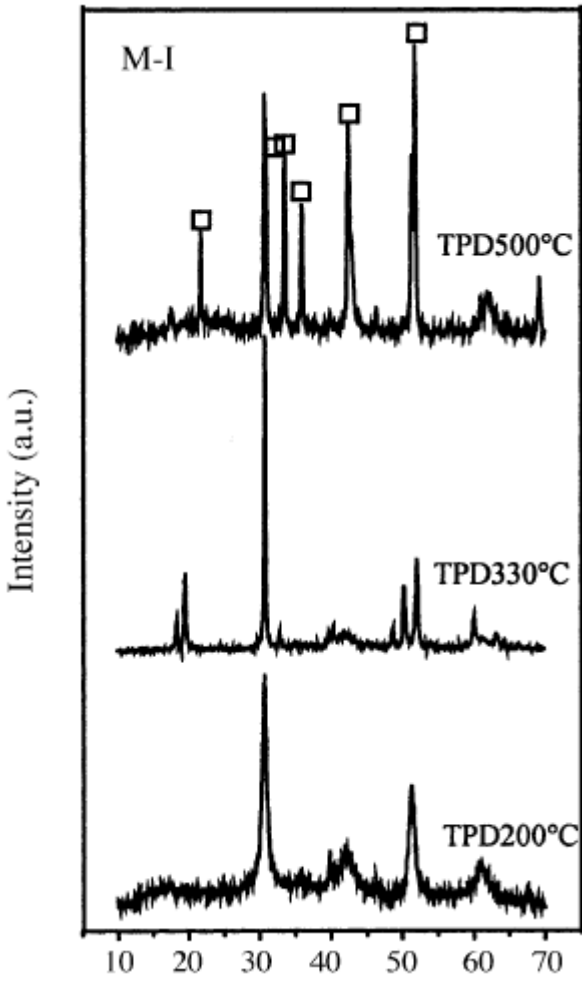

Figure 1-10 X-ray diffraction patterns of sample M-I after TPD test stopping at 220, 330 and 500 °C. Broad peaks at around 43.0 and 62.5° belong to MgO. Li_2O has diffraction peaks positioned at 33.6 and 56.4°; LiOH at 20.5, 32.6 and 35.8°.

By gravimetric methods the gas desorbed from the 1:1 ratio was found to be ½ NH_3 and ½ H_2 at 310 °C however, this did not match the equation Xiong *et al.* suggested (Equation 1-19).

Equation 1-19 $2Mg(NH_2)_2 + 2LiH \rightarrow Li_2Mg_2N_3H_3 + NH_3 + 2H_2$

The $Li_2Mg_2N_3H_3$ phase here (Equation 1-19) was previously characterised by Juza and Eberius, in 1962.[43] It was formed by reacting LiMgN with ammonia at 320–400 °C. Juza *et al.* indexed the phase to a tetragonal structure with a = 5.15 Å and c = 9.67 Å. Xiong *et al.*[33] formed this phase below 350 °C. The rehydrogenation of $Li_2Mg_2N_3H_3$ by Xiong *et al.* achieved an uptake of only 0.5 wt% between 70 and 210 °C. The structure has since been fully characterised and indexed in space group *I*-42*m* with lattice parameters a = 5.130 Å and c = 9.619 Å.[44]

6. $LiNH_2 + MgH_2$

Osborn *et al.*[45] combined $LiNH_2$ and MgH_2 in a 1:1 ratio. The DFT work of Alapati *et al.*[46] inspired this investigation due to a favourable thermodynamic driving force for the theoretical equation:

Equation 1-20 $LiNH_2 + MgH_2 \rightarrow LiMgN + 2H_2$

This reaction has a theoretical 8.2 wt% H_2 compared to 5.4 wt% for a 2:1 ratio. Their reaction relies on the decomposition of $LiNH_2$ to imide and ammonia (Equation 1-4) and then the reaction of ammonia with MgH_2 to $Mg(NH_2)_2$ and H_2 (Equation 1-9).

Unfortunately, a high concentration of ammonia was detected. A maximum of 3.4 wt% H_2 was desorbed. XRD after heating to 210 °C showed the presence of remaining MgH_2, newly formed LiH and $Li_2Mg_2(NH)_3$ as previously formed by Xiong *et al.* above.[33] None of the expected LiMgN was formed. The actual reaction scheme occurring was proposed to be:

Equation 1-21 $LiNH_2 + MgH_2 \rightarrow \frac{1}{3}Li_2Mg_2(NH)_3 + \frac{1}{3}MgH_2 + \frac{1}{3}LiH + H_2$

Equation 1-21 gives a theoretical 4.1 wt% H_2 release, much closer to the 3.4 wt% H_2 measured. The reaction overall was less promising for hydrogen storage purposes due to less H_2 being stored in the 1:1 system, ammonia desorption alongside hydrogen and unreacted starting material present. The proposed reaction of MgH_2 with NH_3 led to the unrealistic expectations of the authors.

Liu *et al.*[47] investigated the reaction of $LiNH_2$ + MgH_2 (1:1) using ball-milling and no external heat. The reactants were ball-milled together and hydrogen was released. As the starting materials did not desorb hydrogen when ball-milled alone this showed the reaction was occurring between the starting materials when ball-milled together. After 24 hours of ball-milling, $Mg(NH_2)_2$ was identified using FTIR. The powder XRD patterns taken at that time showed evidence of LiH. This showed further evidence of a metathesis reaction occurring to form $Mg(NH_2)_2$ and LiH.[25] Upon prolonged ball-milling (36 h), the $Mg(NH_2)_2$ XRD peaks started to diminish and new imide peak in its place began to be formed. XRD identified the new peaks as MgNH. No $Li_2Mg_2(NH)_3$ was detected at any time. This was put down to the different ball-milling time (36 h) used in comparison to Osborne *et al.* (3 h).[45] At 270 °C Mg_3N_2 was seen in XRD. This was quite a low temperature for the appearance of Mg_3N_2. After heating to 390 °C, Mg_3N_2, $Li_2Mg(NH)_2$ and LiH were all identified. Upon heating under hydrogen pressure (81 bar), the products were Mg_3N_2, LiH and $Mg(NH_2)_2$. The continued presence of Mg_3N_2 after attempted rehydriding gives further weight to the experiments of Kojima *et al.*,[39] whilst disagreeing with Nakamori *et al.*[40] and Leng *et al.*[22] As Nakamori *et al.*

had Li_3N present and Leng *et al.* had Li_2NH present in the rehydrogenation reactants the lithium products may be necessary for Mg_3N_2 to rehydride.

7. $3Mg(NH_2)_2 + 2Li_3N$

Ma *et al.*[48] investigated the reaction between $3Mg(NH_2)_2$ and $2Li_3N$ in hope of enhancing capacity and mitigating NH_3 desorption. The reaction was heated to 240 °C under dynamic vacuum. α-$Li_2Mg(NH)_2$ was formed. Only NH_3 was desorbed (Equation 1-22).

Equation 1-22 $$3Mg(NH_2)_2 + 2Li_3N \rightarrow 3Li_2Mg(NH)_2 + 2NH_3$$

It was suggested this reaction had occurred via a 3-step mechanism. Firstly the $Mg(NH_2)_2$ decomposed to MgNH and NH_3 (Equation 1-10). The NH_3 then reacted with Li_3N to form Li_2NH (Equation 1-23).

Equation 1-23 $$2Li_3N + NH_3 \rightarrow 3Li_2NH$$

The two imides then combined to form $Li_2Mg(NH)_2$ (Equation 1-11). Upon hydrogenation, the mixed imide hydrided back to $Mg(NH_2)_2$ and LiH (Equation 1-8).

Varying of the ratio between the two starting materials ($xLi_3N + 3Mg(NH_2)_2$, x = 2, 2.1, 2.3, 2.5, 3) was also investigated. It was found that when heated to 200 °C for 120 minutes the 2.3:3 mixture desorbed 4.9 wt% H_2. Further increase in the amount of Li_3N reduced the amount of H_2 desorbed down to 4.25 wt%. The cycling stability was found to be very good and less ammonia was detected with this sample. Upon rehydrogenation the products were

$Mg(NH_2)_2$, $LiNH_2$ and LiH. During rehydrogenation Li_2NH may have been formed, but due to its structural similarity to $Li_2Mg(NH)_2$ this was difficult to ascertain. When the products from rehydrogenation were dehydrided again, $Li_2Mg(NH)_2$ was formed from the reaction of $Mg(NH_2)_2$ and LiH, however $LiNH_2$ and the remaining LiH were stable at the temperatures tested. No difference in the desorption mechanism was encountered with the use of more Li_3N. This was different to the various ratios of $Mg(NH_2)_2$/LiH investigated by others.[20,21,22,23] $LiNH_2$ is thought to be an important intermediate in the formation of $Li_2Mg(NH)_2$. The $LiNH_2$ may provide favourable nucleation/growth sites. This is thought to be similar to the effect of product seeding.

8. Conclusions

Table 1-3 Summary of the Li-(Mg-)N-H systems discussed above.

Reactants	*Properties*
$LiNH_2$ + LiH	Possible 11.5 wt% hydrogen release, 6.5 wt% hydrogen release below 300 °C
$2LiNH_2 + MgH_2$	Lower H_2 desorption temperature than $LiNH_2$-LiH system, $Li_2Mg(NH)_2$ formed, rehydrogenated at 180 °C under 90 bar H_2, temperature, stability on cycling with products: $Mg(NH_2)_2$ + 2LiH, more ball milling = less NH_3
$Mg(NH_2)_2$ + 2LiH	*α*-, *β*-, *γ*-, *δ*-$Li_2Mg(NH)_2$ formed, rehydrogenated under 90 bar H_2 and 250 °C, reformed $Mg(NH_2)_2$ and LiH, rapid hydrogen uptake above 110 °C, 5 wt% uptake below 200 °C, remaining H_2 desorbed slower, seeding with $Li_2Mg(NH)_2$ decreased desorption temperature
$3Mg(NH_2)_2 + 8LiH$	Desorption temperature higher than $LiNH_2$-LiH, Mg_3N_2 and Li_2NH formed, 7 wt% H_2 desorbed, rehydrogenated under 30 bar H_2 and 200 °C
$Mg(NH_2)_2 + 4LiH$	Up to 250 °C 4.5 wt% loss, up to 600 °C 6.5 wt% H_2 loss (theoretical 9.1 wt%), Mg_3N_2 and Li_3N as products, $Li_4Mg_3(NH_2)_2(NH)_4$ and $Li_{4+x}Mg_3(NH_2)_{2-x}(NH)_{4+x}$ (x = 0.4, 1, 2) intermediates identified
$Mg(NH_2)_2$ + LiH	Started to desorb H_2 at 200 °C, less H_2 desorbed than 1:2 or 1:3, ammonia detected from 150 °C, $Li_2Mg_2N_3H_3$ formed, only 0.5 wt% H_2 uptake up to 210 °C on rehydriding
$LiNH_2 + MgH_2$	3.4 wt% H_2 desorbed on heating, ammonia detected, $Li_2Mg_2(NH)_3$ formed, when ball-milled with no heating H_2 desorbed, no ammonia, $Mg(NH_2)_2$ and LiH formed after 24 h rehydriding, MgNH formed after 36 h
$3Mg(NH_2)_2 + 2Li_3N$	Heated to 240 °C under dynamic vacuum, $Li_2Mg(NH)_2$ formed, NH_3 desorbed, no hydrogen, 2.3:3 ratio of starting materials gave 4.9 wt% H_2 after 120 mins at 200 °C

In conclusion, it can be seen that the Li-Mg-N-H system overall seems to have kinetics and thermodynamics more promising for hydrogen storage than the $LiNH_2$-LiH system, in particular $Mg(NH_2)_2$/LiH starting materials after undergoing ball-milling to reduce particle

size. $Mg(NH_2)_2$/LiH would also be better starting materials than $LiNH_2$/MgH_2 as $Mg(NH_2)_2$ is less reactive with the atmosphere than $LiNH_2$. Using $Mg(NH_2)_2$ and LiH is also of benefit as LiH has a greater reactivity with NH_3 than MgH_2. The best ratio of $Mg(NH_2)_2$:LiH was 3:8. This desorbed 7 wt% H_2 on heating at 400 °C after 2 hours ball-milling under hydrogen.[22] It appeared the best rehydriding conditions used were 30 bar H_2 and 200 °C for this reaction. Although the desorption temperature was higher than other literature published, the higher hydrogen content and lower hydrogen pressure required to reverse back to starting materials was most promising in comparison to other systems reviewed here.

The partial substitution of lithium for magnesium in the lithium amide lattice appears to destabilise the system and encourages hydrogen desorption at a lower temperature than for $LiNH_2$/LiH.

4. Aims

The aims of the research carried out within this thesis concerns the reactions of light metal hydrides with various light metal amides reactions not previously studied. The mixed cation amides $Li_3Na(NH_2)_4$ and $LiNa_2(NH_2)_3$ were heated with LiH, NaH and MgH_2 in order to establish whether hydrogen was desorbed and if so whether the mixed cations within the amides destabilised the temperature at which the reactions desorbed hydrogen in comparison to $LiNH_2$ and $NaNH_2$ respectively.

The reactions of $NaNH_2$ and MgH_2 in various ratios were investigated using thermal decomposition, Raman spectroscopy and thermogravimetric analysis in order to establish whether there was a similar reaction mechanism to that of $LiNH_2$ and MgH_2. The products

from heating $NaNH_2$ + MgH_2 were then put under a hydrogen atmosphere in order to attempt rehydrogenation.

Finally, it was realised that the decomposition characteristics of $NaNH_2$ had been relatively neglected in the literature and so an examination of its decomposition products and reaction with sodium hydride, as a comparison to $LiNH_2$/LiH, were carried out, using Raman and thermal decomposition techniques.

---

[1] T. M. Letcher, Climate Change - Observed Impacts on Planet Earth, Elsevier, 2009

[2] US Department of Energy Targets for Onboard Hydrogen Storage Systems for Light-Duty Vehicles Technical report, Office of Energy Efficiency and Renewable Energy and The FreedomCAR and Fuel Partnership, 2009

[3] D. K. Slattery, M. D. Hampton, Proceedings of the 2002 U.S. DOE Hydrogen Program Review

[4] H. I. Schlesinger, H. C. Brown, E. K. Hyde, *J. Am. Chem Soc.,* 75 (1953) 209–213

[5] British Patents 840,572 and 863,491

[6] E. C. Ashby, R. D. Schwartz, B. D. James, *Inorg. Chem.,* 9 (1970) 325–332

[7] E. C. Ashby, R. D. Schwartz, *Inorg. Chem.,* 11 (1972) 925–929

[8] A. E. Finholt, G. D. Barbaras, G. K. Barbaras, G. Urry, T. Wartik, H. I. Schlesinger*, J. Inorg. Nucl. Chem.,* 1 (1955) 317–325

[9] H. R. Hoekstra, J. J. Katz, *J. Am. Chem. Soc.,* 71 (1949) 2488–2492

[10] P. Chen, Z. Xiong, J. Luo, J. Lin, K. L. Tan, *Nature,* 420 (2002) 302–304

[11] T. Ichikawa, N. Hanada, S. Isobe, H. Leng, H. Fujii, *J. Alloys Compds*., 404–406 (2005) 435–438

[12] O. Ruff, H. Goeres, *Chem. Ber.,* 44 (1910) 502–506

[13] T. Ichikawa, N. Hanada, S. Isobe, H. Leng, H. Fujii, *J. Phys. Chem. B,* 108 (2004) 7887–7892

[14] P. Chen, Z. T. Xiong, J. Z. Luo, J. Y. Lin, K. L. Tan, *J. Phys. Chem. B,* 107 (2003) 10967–10970

[15] K-F. Aguey-Zinsou, J. Yao, Z. X. Guo, *J. Phys. Chem. B,* 111 (2007) 12531–1253

[16] J. Yang, Q. Cai, Y. Z. Wang, W. B. Yelon, W. J. James, *Materials Research Soc. Symposia Proceedings,* 971 (2007) 1-6

[17] K. Ohoyama, Y. Nakamori, S-I. Orimo, K. Yamada, J. Phys. Soc. Jpn. 74 (2005) 483-487

[18] J. K. Nörskov, A. Houmüller, P. Johasson, A.S. Pedersen. *J. Less-Common Met.,* 46 (1981) 257–260

[19] A. Zaluska, L. Zaluski, J.O. Strőm-Olsen, *J. Alloys Compds.,* 288 (1999) 217–225

[20] Z. Xiong, G. Wu, J. Hu, P. Chen, *Adv. Mater.,* 16 (2004) 17, 1522–1525

[21] W. Luo, *J. Alloys Compds.,* 381 (2004) 284–287

[22] H.Y. Leng, T. Ichikawa, S. Hino, N. Hanada, S. Isobe, H. Fujii, *J. Phys. Chem. B,* 108 (2004) 8763–8765

[23] Y. Nakamori, G. Kitahara, S. Orimo, *J. Pow. Sources,* 138 (2004) 309–312

[24] Y. Chen, C-Z. Wu, P. Wang, H-M. Cheng, *Int. J. Hydrogen Energy*, 31 (2006) 1236–1240

[25] W. Luo, S. Sickafoose, *J. Alloys Compds*., 407 (2006) 274–281

[26] W. Luo, K. Stewart, *J. Alloys Compds.,* 440 (2007) 357–361
[27] T. Markmaitree, W. Osborn, L. L. Shaw, *Int. J. Hydrogen Energy,* 33 (2008) 3915–3924
[28] H.Y. Leng, T. Ichikawa, S. Hino, N. Hanada, S. Isobe, H. Fujii *J. Pow. Sources*, 156 (2006) 166–170
[29] P. Chen, Z. T. Xiong, L. F. Yang, G. T. Wu, W. F. Luo, *J. Phys. Chem. B,* 110 (2006) 14221–14225
[30] F. Dolci, E. Napolitano, E. Weidner, S. Enzo, P. Moretto, M. Brunelli, T. Hansen, M. Fichtner, W. Lohstroh, *Inorg. Chem*., 50 (2011) 1116–1122
[31] Z. Xiong, J. Hu, G. Wu, P. Chen, W. Luo, K. Gross, J. Wang *J. Alloys Compds.*, 398 (2005) 235–239
[32] H. Jacobs, *Zeitschrift für Anorganische und Allgemeine Chemie*, 382, (1971) 97-109
[33] Z. Xiong, G. Wu, J. Hu, P. Chen, W. Luo, J. Wang, *J. Alloys Compds.,* 417 (2006) 190–194
[34] Y. Liu, J. Hu, Z. Xiong, G. Wu, *J. Mater. Res.*, 22, 5 (2007) 1339–1345
[35] A. Sudik, J. Yang, D. Halliday, C. Wolverton, *J. Phys. Chem. B,* 111 (2007) 6568–6573
[36] Y. Liu, K. Zhong, K. Luo, M. Gao, H. Pan, Q. Wang, *J. Am. Chem. Soc.*, 131 (2009) 1862–1870
[37] J. Rijssenbeek, *J. Alloys Compds.,* 454 (2008) 233–244
[38] R. Janot, J-B, Eymery, J-M. Tarascon, *J. Pow. Sources,* 164 (2007) 496–502
[39] Y. Kojima, Y. Kawai, N. Ohba, *J. Pow. Sources,* 159 (2006) 81–87
[40] Y. Nakamori, G. Kitahara, K. Miwa, S. Towata, S. Orimo, *Appl. Phys. A,* 80 (2005) 1–3
[41] Y. H. Hu, E. Ruckenstein, *J. Phys. Chem. A*, 107 (2003) 9737–9739
[42] M. Aoki , T. Noritake, G. Kitahara, Y. Nakamori, S. Towata, S. Orimo, *J. Alloys Compds.,* 2007, 428, 307–311
[43] R. Juza, E. Eberius, *Naturwissenschaften,* 49 (1962) 104
[44] E. Weidner, F. Dolci, J. J. Hu, W. Lohstroh, T. Hansen, D. J. Bull, M. Fichtner, *J. Phys. Chem. C,* 113 (2009) 15772–15777
[45] W. Osborn, T. Markmaitree, L. L. Shaw, *J. Pow. Sources, 127* (2007) 376–378
[46] S. V. Alapati, J. K. Johnson, D. S. Sholl, *J. Phys. Chem. B,* 110 (2006) 8769–8776
[47] Y. Liu, K. Zhong, M. Gao, J. Wang, H. Pan, Q. Wang, *Chem. Mater.,* 20 (2008) 3521–3527
[48] P. Ma, H-B. Dai, Z-Z. Fang, X-D. Kang, Y. Liang, P-J. Wang, P. Wang, H-M. Cheng*, J. Phys. Chem. B,* 113 (2009) 9944–9949

2. EXPERIMENTAL

1. Crystallography

Crystallography describes the arrangement of atoms in the solid state (although not all solids are crystalline). Atoms in the solid state form a regular arrangement in 3 dimensions. A 'unit cell' is the smallest regular, repeating unit of atoms which completely describes the atomic arrangement and symmetry of the crystal structure. This is present in all ideal crystals and demonstrates the full symmetry of the crystal structure. By translating the unit cell it is possible to form the full crystal lattice. The lattice is defined by locating equivalent positions, which are known as lattice points. The unit cell can be described by the three lengths of the edges (*a*, *b* and *c*), as well as the angles between them (*α*, *β* and *γ*). These are known as lattice parameters (Figure 2-1).

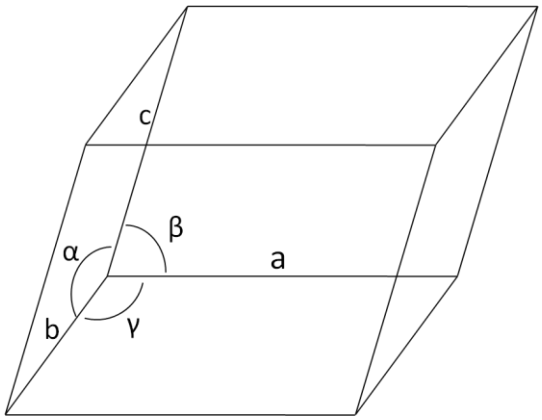

Figure 2-1 General three-dimensional unit cell definition.

The lattice parameters may take any values and therefore Figure 2-1 shows a cell with no symmetry. As the symmetry increases, the unit cell develops relationships between various

cell parameters and seven primitive (P) crystal systems can be formed. Primitive cells have only one lattice point. 14 lattice types can be formed if body centring (I) and face centring (F and C) are introduced. The body centred lattice has an additional lattice point at the centre of the unit cell and face centred lattices have lattice points at the centre of every unit cell face (F-centring only). These additional F and C, as well as P lattices are known as the 14 Bravais lattices (Table 2-1).

Table 2-1 Dimensions and essential symmetry features of the seven crystal systems.

7 Lattice Systems	*Unit Cell Dimensions*	*Essential Symmetry*	*Allowed Lattices*
Cubic	a=b=c; α=β=γ=90 °	Four threefold axes	P, I, F
Tetragonal	a=b≠c; α=β=γ=90 °	One fourfold axis	P, I
Orthorhombic	a≠b≠c; α=β=γ=90 °	Three twofold axes	P, I, F, C
Hexagonal	a=b≠c; α=β=90 °, γ=120 °	One sixfold axes	P
Trigonal	a=b=c; α=β=γ≠90 °	One threefold axis	R
Monoclinic	a≠b≠c; α=γ=90 °, β≠90 °	One twofold axis	P, C
Triclinic	a≠b≠c; α≠β≠γ≠90 °	None	P

1. Crystal Structures

The lattice parameters, atomic positions within the unit cell and the internal symmetry of the unit cell can completely describe the crystal structure of a material. Atomic positions are described as fractional coordinates in each direction along the unit cell from one corner of the cell. With the inclusion of atoms to the unit cell, further translational symmetry elements to those required for the description of Bravais lattices must be considered. The arrangement of the atoms can give rise to screw axes and glide planes. 230 ‘spaces groups’ can be derived when all of the possible 3-D symmetry arrangements are combined. Space groups completely describe the symmetry of the crystal structure.

2. Lattice Vectors, Planes and Miller Indices

An unambiguous description of the directions and planes of crystals is very important in diffraction and crystallography. The directional vectors in a lattice must pass through the origin. Any point on a vector can be described as fractions of unit cell lengths *a*, *b* and *c*. These fractions, in turn, are multiplied up to whole numbers to give the conventional form $[uvw]$. Any directional coordinate going in the opposite direction is identified by a negative, e.g. $[\bar{u}vw]$ (Figure 2-2).

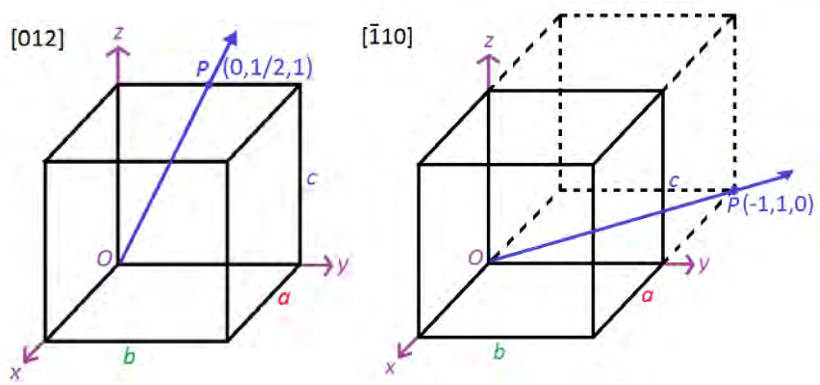

Figure 2-2 Examples of lattice vectors.

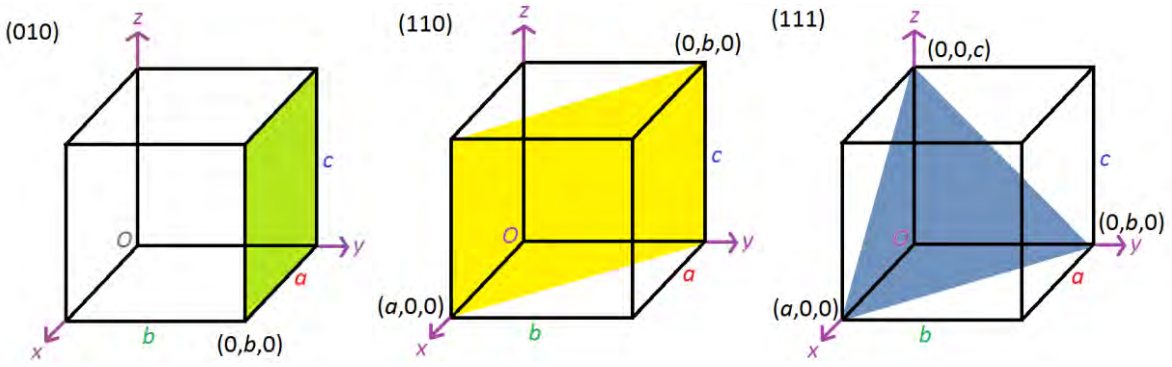

Figure 2-3 Lattice planes with different Miller indices.

A lattice plane (Figure 2-3) is formed by the connection of several lattice points in 3-D. Each lattice point must sit on a lattice plane. A lattice plane is defined by how it intersects the unit cell vectors, *a*, *b* and *c*. This is described by Miller indices. For each of *a*, *b* and *c*, there is an equivalent Miller index *h*, *k* and *l* respectively. The reciprocals of the fractions along *a*, *b* or *c* are written as (*hkl*). Therefore, any equivalent lattice plane will have the same (*hkl*) value. The perpendicular distance that separates equivalent lattice planes is known by *d*-spacing (d_{hkl}). *d* can be derived for a cubic system by Equation 2-1.

Equation 2-1 $$d = \frac{a}{\sqrt{h^2+k^2+l^2}}$$

3. Bragg's Law

Bragg's treatment of the diffraction of X-rays was based on considering crystals as layers of atoms which behave as reflecting planes, where the angle of incidence equals the angle of reflection. (These layers of atoms may be regarded as lying in planes, which are described by the Miller indices, as described above.) Some X-rays are considered to be reflected by the first planes of atoms, those that are not continue travelling through the crystal until reflected by another plane (Equation 2-2). The reflections are observed only when *n* is an integer, that is, when completely constructive interference occurs between the waves of X-rays (Figure 2-4 and Equation 2-3). All other values of *n* destroy the scattering, therefore do not result in any peaks.

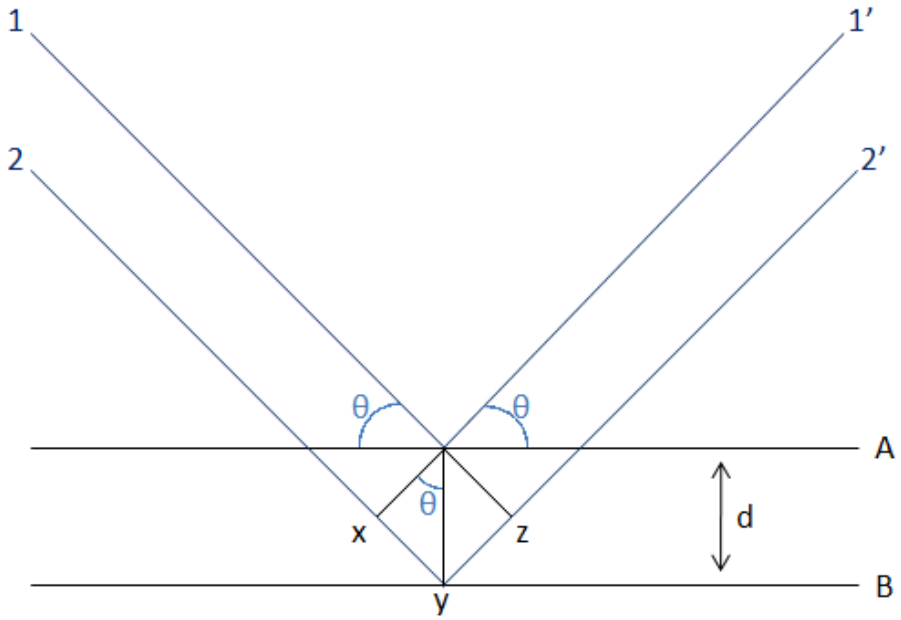

Figure 2-4 Diagram of the derivation of Bragg's Law.

Equation 2-2 $$(xy + yz) = (d_{hkl}sin\theta + d_{hkl}sin\theta) = 2d_{hkl}sin\theta$$

For completely constructive interference, the change in phase of the reflected (or diffracted) wave must be equal to an integer multiple of the wavelength:

Equation 2-3 $$n\lambda = 2d_{hkl}sin\theta_n$$

where *n* is an integer. While in theory *n* can take any integer value, in practice the diffracted intensity falls off rapidly with increasing *n* (higher order reflections), so the Bragg equation is frequently simplified further to:

Equation 2-4 $$\lambda = 2d_{hkl}sin\theta_n$$

Only scattering events where *n* is an integer will give rise to *n* observed diffracted intensity, with all other values giving rise to completely destructive interference when summed over all scattering events. The angle of the observed diffracted beam gives the separation of the planes of atoms giving rise to that diffracted beam (known as the *d*-spacing), whereas the intensity of the beam gives information on the properties of the scatterers.

2. X-ray Diffraction

An X-ray diffraction (XRD) experiment comprises shining a monochromatic source of radiation onto a sample, with a movable detector placed in a defined geometry relative to the source and sample. It is generally a non-destructive technique which reveals information regarding the crystallographic structure and chemical composition of materials.

In a laboratory setting, X-rays are produced when a beam of electrons are accelerated and collide with a metal anode target inside a vacuum tube. These electrons induce electronic transitions within the atoms of the target. When these atoms relax, well defined electronic transitions within the atoms lead to the emission of radiation of characteristic wavelengths. In this study, a Cu target was exclusively used, but others including Mo, Cr, Fe and Co can be used.

The X-rays emitted from the metal anode source form a divergent beam containing a spectrum of X-rays. The spectrum comprises characteristic discrete wavelengths, which correspond to the energy of atomic transitions of the metal target and a background spectrum known as *Bremsstrahlung*. *Bremsstrahlung* (brake radiation) is produced from the deceleration of a charged particle (electron) when deflected by another charged particle, for

an electron usually an atomic nucleus (target). As the moving particle loses kinetic energy, a photon (X-ray) is produced (due to conservation of energy). The total X-ray spectrum is continuous with additional peaks at certain energies which are characteristic of the target material. For the experiments here a copper radiation source was used, as shown in Figure 2-5.

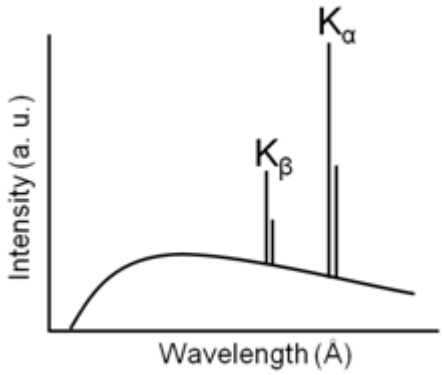

Figure 2-5 Cu X-ray emission spectrum.

A single, intense beam of radiation is required for X-ray diffraction. Monochromation is necessary to select the single most intense part of the spectrum. There are two types of monochromation often used in laboratory X-ray sources. The first is a crystal monochromator. This is a single crystal set at a specific orientation, θ_m, so that the Bragg equation is satisfied:

Equation 2-5 $$\lambda = 2d_{hkl}sin\theta_m$$

where $d_{(hkl)}$ is the d-spacing of an intense Bragg reflection.

Crystal monochromators are typically made from Si, Ge, quartz or graphite. A single wavelength can be selected using this method of monochromation. The second type of monochromator is a Göbel mirror. This is formed from curved multi-layer crystals made up of alternating strongly and weakly scattering materials. The multi-layer spacing determines the wavelength of the radiation that is reflected. This produces a parallel X-ray beam. Göbel mirrors are unable to monochromate the radiation adequately to differentiate between the two strongest types of Cu radiation: Kα_1 and Kα_2 (shown in Figure 2-5).

Scintillation counters are the most common form of X-ray detectors. A phosphorescent crystal fluoresces when struck by the photons emitted by the X-rays. A photomultiplier tube then detects and amplifies the fluorescence from the crystal. The signal is directly proportional to the number of photons hitting the crystal. This is a point detector as only data from a single 2θ angle can be measured at any time. Position sensitive detectors (PSD) are becoming more popular as they can collect data over a 2θ range to reduce data collection time. The detector records the 2θ angle at which each X-ray is detected.

Accurate relative positioning between the X-ray beam, sample and detector is essential in diffraction. A goniometer is used to measure the relative angles between the components. There are two common geometries of diffractometers: reflection (Bragg-Brentano) and transmission (Debye-Scherrer).

1. Synchrotron X-ray Diffraction

A synchrotron is a particle accelerator in which a magnetic field and electric field are synchronised to produce a high energy, focussed beam of charged particles. Synchrotron radiation is emitted when charged particles change their velocity (or direction). Many

wavelengths are emitted and can be selected using monochromation. Synchrotron X-ray sources have the advantage of being very intense, perfectly polarised sources of X-ray radiation.

Powder synchrotron X-ray diffraction data were collected on beam line ID31 at the European Synchrotron Radiation Facility (ESRF), in Grenoble, France, at a wavelength and step-size of 0.79986916 Å and 0.003 ° respectively. Borosilicate capillaries of 0.9 mm were filled in a glove bag under flowing nitrogen. Once the samples were tightly packed, the capillary was sealed with 0.7 mm diameter glass rod, removed from the glove bag and sealed with a gas torch. No signs of oxidation of samples from the loading and sealing processes were observed.

The sealed capillaries were spun at 100 r.p.m. perpendicular to the X-ray beam to improve randomisation of the individual crystal orientations. Reflections from a silicon standard were used to determine the exact wavelength and zero point. The samples were scanned for 15 minutes and in this time no noticeable radiation damage, in the form of anisotropic peak shift or broadening, was observed.

Powder synchrotron X-ray data were also collected on beam line I11 at the Diamond Light Source, in Didcot, UK at a wavelength and step-size of 0.825594 Å and 0.002 °, respectively.

2. Laboratory X-ray Diffraction

Laboratory powder X-ray data were collected on a Siemens D5000 diffractometer in transmission mode. A copper X-ray source was monochromated using a germanium monochromator. This gave Cu $K_{\alpha 1}$ radiation with a wavelength of 1.54056 Å. Samples were

prepared by grinding in an argon filled glove box and sealed on a metal disc between two layers of Scotch® Magic™ tape. Samples were rotated perpendicular to the X-ray beam.

Samples were also collected on a Bruker AXS D8 diffractometer in transmission mode. A copper X-ray source was monochromated using a germanium monochromator. This gave Cu Kα_1 radiation with a wavelength of 1.54056 Å. Samples were prepared as above.

3. Rietveld Analysis

It is not always possible to grow large single crystals in order to gain structural information. Rietveld analysis can be used on powder diffraction samples. The conventional problem with powder diffraction is the inability to differentiate between overlapping peaks. The Rietveld method creates virtual separation of the overlapping peaks, thereby allowing accurate determination of the structure. Rietveld analysis requires the unit cell size and shape, atomic positions, occupancies and thermal motion parameters in order to build a structural model. Experimental parameters such as peak profile and background shape are then combined with the structural model to calculate a diffraction pattern. A least-squares method is used to vary these parameters until the difference between the measured and calculated diffraction profiles is at a minimum. The S_y function is minimised during the least squares refinement:

Equation 2-6 $$S_y = \sum_i w_i (y_i - y_{ci})^2$$

where

$w_i = {}^1/_{y_i}$,
$y_i = observed\ intensity\ at\ the\ \mathrm{i}th\ step$,
$y_{ci} = calculated\ intensity\ at\ the\ \mathrm{i}th\ step, and\ the\ sum\ is\ over\ all\ data\ points$.[1,2]

The Rietveld method is used to refine the structural model as opposed to structure solution, therefore the best starting model as possible is necessary. However, the Rietveld method can be used in structure solution, as well as being vital in the last step of structure determination, when the final refinement of the structural determination is performed. Crystal structure determination is carried out in a number of steps. Firstly, the diffraction pattern is indexed and the crystal system and lattice parameters are determined. The space group, followed by approximate structure are then identified. Finally the Rietveld method is used to refine the structure.

In carrying out a Rietveld refinement the observed pattern along with a calculated pattern and the difference line are produced. Ideally the difference line would be straight for a perfect fit. However, in order to assess how different variations affect the calculated pattern, a series of statistics are produced. These give a numerical indication as to how good the fit is. The statistical value based on the fitting of the complete calculated pattern to that of the observed pattern is known as the '*R*-weighted pattern', R_{wp} (Equation 2-7).

Equation 2-7 $$R_{wp} = \left[\frac{\sum w_i[y_i(obs) - y_i(calc)]^2}{\sum w_i[y_i(obs)]^2}\right]^{1/2}$$

This equation includes the S_y value being minimised and therefore is a good indication as to how the refinement is progressing. The R_{wp} value can appear artificially high if not all peaks in the pattern are accounted for. This, however, can be easily identified by viewing the difference line. The value may appear too low if the background is high as it is easier to fit

well to slow changing background, than to peaks. It is therefore possible to find a background corrected version of this and other *R*-values can be calculated (Equation 2-8).

Equation 2-8 $$R'_{wp} = \left[\frac{\sum w_i[y_i(obs)-y_i(calc)]^2}{\sum w_i[y_i(obs)-Bkg_i]^2}\right]^{1/2}$$

The R_{wp} finally reached should agree with the statistically expected *R*-value, R_{exp} (Equation 2-9), which gives the best possible *R*-value based upon the quality of the data.

Equation 2-9 $$R_{exp} = \left[\frac{N-P-C}{\sum w_i[y_i(obs)]^2}\right]^{1/2}$$

where
$N = number\ of\ observables,$
$P = number\ of\ parameters,$
$C = number\ of\ constraints\ used.$

The calculation to work out the statistical significance of the difference between R_{wp} and R_{exp} is given by Equation 2-10. χ^2 is the square of the ratio between R_{wp} and R_{exp}; the lower the value of χ^2, the better the fit. χ^2 includes the number of refined parameters and is therefore a useful statistic as the fit to the observed data tends to increase as the number of refined parameters increases. If the χ^2 value is very small it can indicate that poor quality data outweighs the errors associated with the structural model and a high background, (which is easily modelled and significantly reduce the χ^2 value).

Equation 2-10 $$\chi^2 = \left[\frac{R_{wp}}{R_{exp}}\right]^2$$

It is also very important to consider the quality of the structural model in terms of chemical sense. The atomic distances between bonding and non-bonding atoms must be sensible as well as the bonding angles. Fractional occupancies should also be reasonable for the suggested chemical composition of the sample.

4. Quantitative Phase Analysis

Rietveld analysis has been shown to provide very accurate estimates of the relative and/or absolute amounts of constituent phases in the mixture. X-ray and neutron diffraction have shown the effectiveness of this technique, known as quantitative phase analysis (QPA[1]). QPA is reliant on the following equation:

Equation 2-11 $$W_p = \frac{S_p(ZMV)_p}{\sum_{i=1}^{n} S_i(ZMV)_i}$$

where *W* is the relative weight fraction of phase *p* in a mixture of *n* phases, and *S*, *Z*, *M* and *V* are the Rietveld scale factor, the number of formula units per unit cell, the mass of the formula unit (in atomic mass units) and the unit cell volume (in Å^3), respectively.[2] If an internal standard phase, *s*, is added to the phase mixture in the weight fraction W_s, then the absolute weight fractions of the other identified components, *p*, are given by:

Equation 2-12 $$W_p = \frac{W_s S_p (ZMV)_p}{S_s (ZMV)_s}$$

A reduction from unity of the sum of the determined weight fractions of the *n* identified constituents can provide an estimate as to the amount of non-crystalline or amorphous material present in the sample.

The intensity of Bragg peaks can be affected by preferred orientation, extinction, micro-absorption and sample representability. Preferred orientation can cause the most deviation. It arises when there is a stronger tendency for the crystallites in a powder to be oriented more one way then all others. Rapidly spinning the sample during data collection essentially removes the possible effects of preferred orientation. This can cause a deviation of the determined weight fractions from their true values. Extinction effects are most pronounced when mixture components have radically different crystallite and grain sizes. Micro-absorption is most prominent when phases present have very different absorption coefficients. One advantage of QPA is that the effects of preferred orientation and extinction effects can be taken into account.

5. TOPAS

The powder diffraction data was analysed using the computer program Topas.[3] Initially the diffraction patterns of pure samples of the constituent phases were used. The lattice parameters, atomic positions, thermal parameters and pseudo-Voigt peak shape parameters were refined for each phase, as well as using a suitable emission profile and Lorentz-

polarisation factor with sample height error included. The background was described with a Chebyshev polynomial. Once the observed diffraction data of the pure phases gave a good Rietveld refinement, the atomic positions and thermal parameters were fixed.

In Figure 2-6 a typical powder XRD pattern as produced by Topas is shown. The 2θ value is on the *x*-axis, the counts are on the *y*-axis. The identified products are in the key in the top right hand corner. They are listed as Rietveld refined phases first, with the weight% value included. This is only established from the Rietveld phases. The phases with 0 wt% are Pawley refined and therefore have no wt% value given. The observed powder XRD pattern is shown by the black line, with the fitting for both Rietveld and Pawley phases with the red line to the observed phases, in this example, of $NaNH_2$ (blue tick marks), NaH (black tick marks) and $Mg_{(1-0.5x)}Na_x(NH)$ (green tick marks). The difference line between the experimental and calculated X-ray patterns is shown in grey. There are unidentified peaks present which have not been fitted by the red line. At ~51 ° the red line is not fitted to the observed powder XRD at all. This is due to the region being excluded to stop the fitting to an inappropriate peak.

The weight% given here for $NaNH_2$ and NaH can be converted to mole% by dividing the weight% by the RMM of the phase.

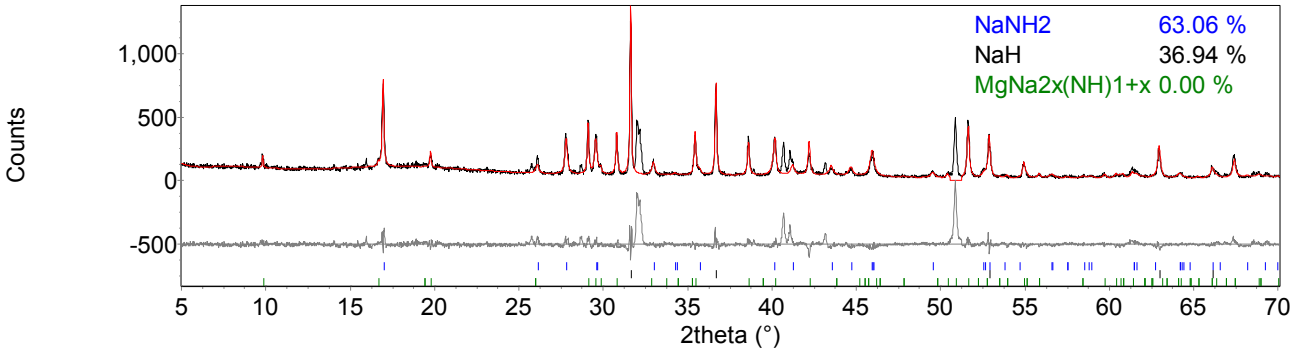

Figure 2-6 Typical powder XRD pattern as produced by Topas.

3. Solid State Synthesis

The starting materials used react with atmospheric water and oxygen. This required all manipulations of the starting materials to be carried out under inert conditions. All samples were prepared in an argon filled glove box (MBraun, Unilab, <1 ppm O_2, 0.1 ppm H_2O), using an analytical balance (up to ±0.1 mg accuracy) to weigh out the samples in the desired molar ratios.

The starting materials were intimately ground together using a mortar and pestle. Once ground, they were transferred into a quartz reaction tube (½" O/D) and sealed with a Young's tap *via* an Ultra-Torr® fitting, before being removed from the glove box. The T-piece was specially designed in order that gas may be passed through the top of the T-piece, allowing purging of the line, before opening the Young's tap so the sample was kept at atmospheric pressure whilst maintaining an inert atmosphere (Figure 2-7(a)).

The preparation of the reactions occurred under an inert atmosphere, specifically flowing argon gas. The Young's taps were attached to plastic tubing which was connected to sulphuric acid bubblers. The argon passed over the samples went *via* these bubblers on the

inlet and outlet in order that any moisture present in the gas stream would dissolve in the acid, therefore not contaminating the samples.

The reaction tube was then clamped into place inside a vertical furnace (Lenton Furnaces, LTF 12/25/250 fitted with a Eurotherm 3216P1 controller and an insulating plug at the base of the work tube to improve thermal uniformity), ensuring the reaction mixture was within the centre of the hot zone of the furnace (Figure 2-7(b)). The reactions were heated at a ramp rate of 2 °C min^{-1} in order to ensure heating of the sample did not overshoot the desired temperature. Reaction mixtures were typically heated for 12 hours before the power was turned off and the reaction products allowed to cool naturally at approximately 3 °C min^{-1}.

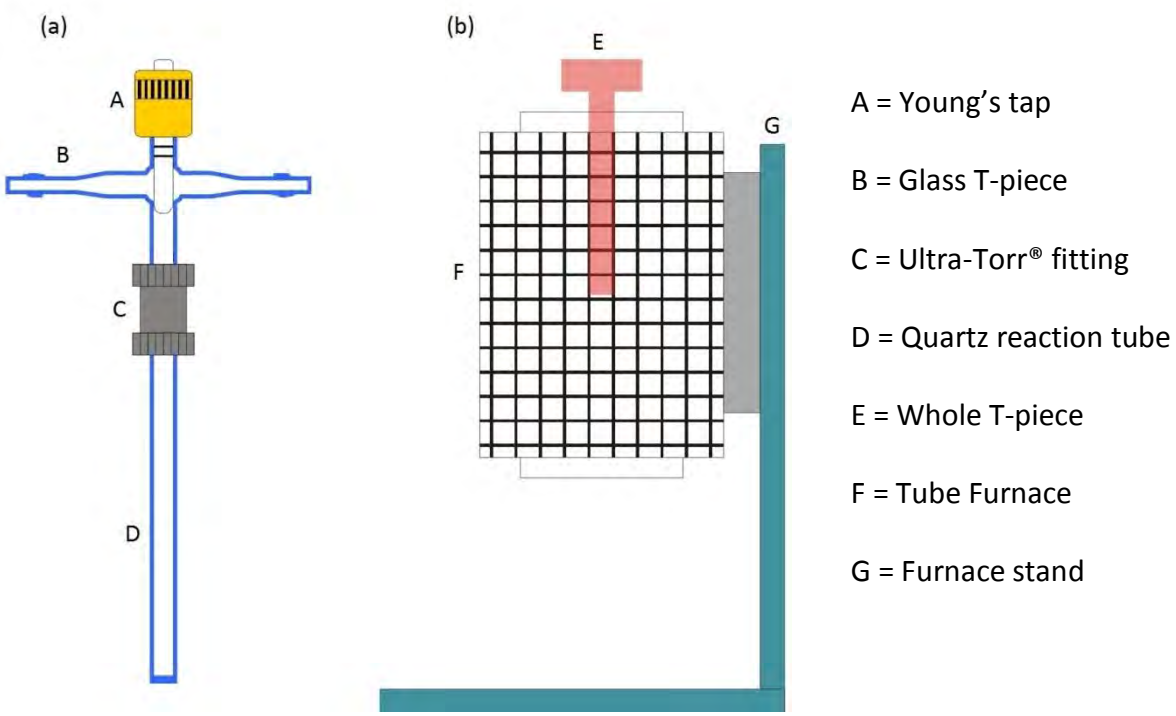

Figure 2-7 Solid state synthesis set-up of (a) breakdown of components of T-piece and (b) whole T-piece in tube furnace.

4. Differential Scanning Calorimetry

Differential scanning calorimetry (DSC, Figure 2-8) measures the heat flow into or out of a sample in relation to a reference whilst heating the sample with a linear temperature ramp. Information regarding exothermic and endothermic events such as melting, crystallisation and reactions can be gleaned from using DSC. Quantitative and qualitative information can also be garnered. DSC is an experimental technique that involves measuring the energy required in order to keep a near-zero temperature difference between a test substance (S) and an inert reference material (R) while the samples are subjected to an identical temperature programme. The reference material is usually an empty sample pan and lid. There is a direct relationship between the difference in energy supplied to the sample (S) and reference (R) and the enthalpy of the reaction or phase change giving rise to the energy difference.

DSC is a more advanced version of differential thermal analysis (DTA). DTA involves looking at the temperature difference, ΔT, when a sample and inert reference material are subjected to the same heating programme. The temperature is monitored by thermocouples. ΔT is then plotted against time or furnace temperature. If the sample were to undergo an endothermic event, the temperature of the sample would lag behind that of the reference material, until the melting is completed and normal heating can resume. DSC looks at the difference in energy required in order to keep both the sample and the reference material at the same temperature when heated or cooled. This enables DSC to be fully quantitative, whereas DTA is at best semi-quantitative.

For DSC experiments presented in this thesis, heat-flux DSC was used. The test sample and reference material are enclosed within the same heating block with high thermal

conductivity in order to establish good heat flow between S and R. The enthalpy changes that occur to S cause a temperature difference between S and R. This results in heat flow between S and R (due to good thermal contact). The temperature difference between S and R is recorded and by using calibration experiments can be further related to the enthalpy change of the specimen.

In heat-flux DSC, the energy required to maintain a constant temperature of both S and R is a measure of the energy changes in S relative to R. DSC can detect very small energy changes between S and R as long as both S and R are subject to the same temperature programme (Figure 2-8). The data from DSC can be quantifiable so long as the sample mass is carefully measured and careful calibration is undertaken.

DSC measurements were performed on a calibrated Netzsch DSC 204 HP Phoenix, which was housed inside a flowing argon glove box. Samples of approximately 8 mg were loaded into a shallow aluminium pan and fitted with an aluminium lid, edges turned up. A hole was pierced in the top of the lid prior to it being transferred into the glove box. This was to allow any gas desorbed to escape. The sample was spread evenly over the base of the pan in order to allow uniform heating of the sample. The sample mass was measured to 0.001 mg accuracy. The reference was another Al pan and lid. An argon atmosphere of 3 bar was maintained inside the DSC at 100 ml min^{-1} flow rate. Typical experiments involved a ramp at 2 min^{-1} to 250 or 350 °C, a dwell time of 20 minutes followed by cooling at 2 °C min^{-1} to room temperature. The wobble at the start of traces is caused by an initial start-up deflection.

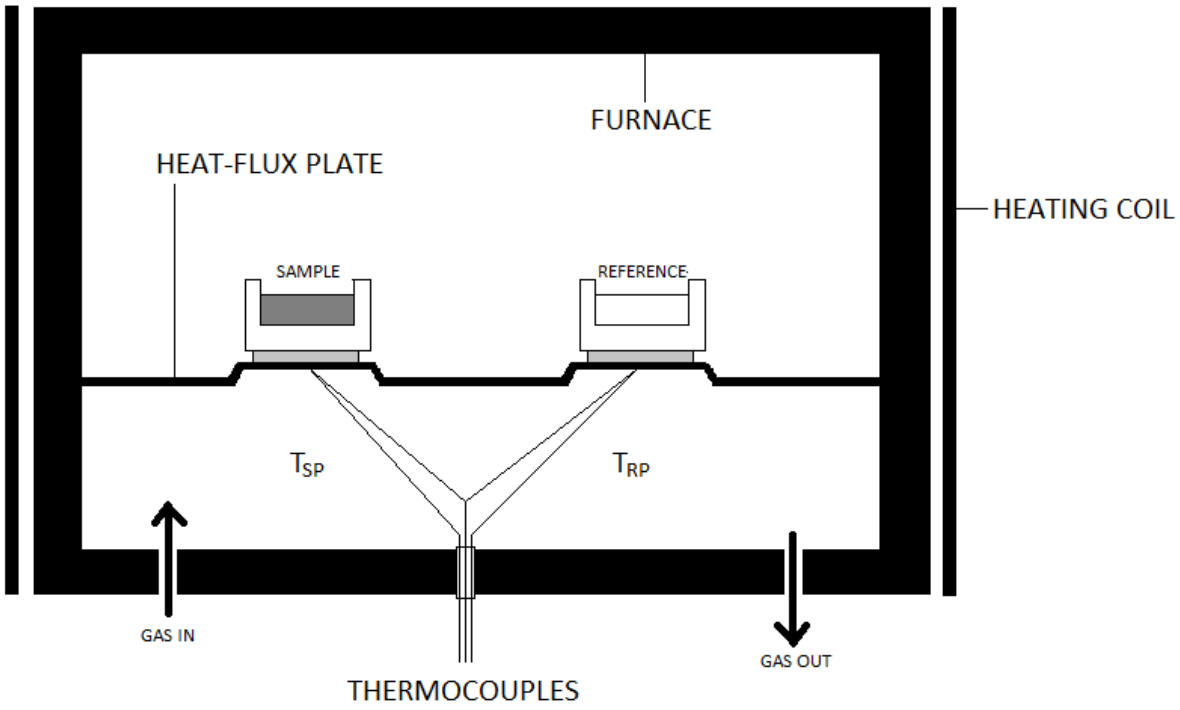

Figure 2-8 Diagram of differential scanning calorimeter.

5. Thermogravimetric Analysis

Thermogravimetric analysis (TGA) is a thermal analysis technique used to analyse the mass loss of a sample with respect to a change in temperature under a controlled atmosphere. It can be used with mass spectrometry (MS) in order to monitor the gases desorbed from the sample during heating and therefore assign specific mass losses to specific gaseous products (Figure 2-9).

TGA is reliant on precise measurements of weight, temperature and rate of temperature change. A baseline measurement must be carried out before experiments are conducted. Temperature gradients, air buoyancy, convection currents within the furnace tube and other factors contribute to a buoyancy effect, that is: when a sample is heated under argon, the apparent weight changes with the increase in temperature. This is due to the change in

weight of the displaced gas. The sample therefore appears to gain weight on heating. This affect can be removed by heating the empty crucible under the same conditions as the samples would be. This baseline is then subtracted from the experimental run.

The TGA (Netzsch TG209) was contained within an argon filled flowing glovebox. Two calibration runs were conducted by heating the empty crucible pan at 2 °C min^{-1} to 350 °C with one heated with an isothermal heating run at 350 °C for 1 hour, the other with immediate cooling. All experiments were cooled at 2 °C min^{-1} to room temperature. The experiments in this study were carried out under argon gas at 1 bar pressure. Samples of approximately 20 mg were loaded into an alumina crucible pan and the lid (with a small hole in the top) was placed on top (as used for the baseline measurement).

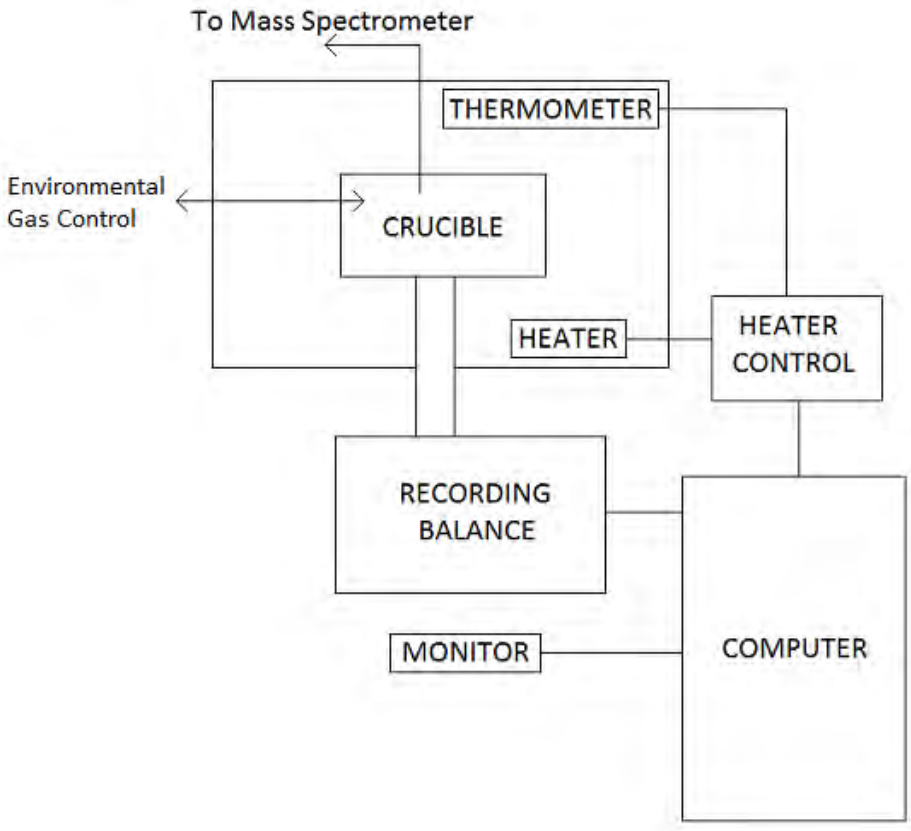

Figure 2-9 Block diagram of thermogravimetric analyser.

6. Raman Spectroscopy

Raman spectroscopy is a technique used to study vibrational, rotational and other low-frequency modes in a system. It involves the scattering of monochromatic light from infrared to ultraviolet which is used to irradiate the sample. The incident light interacts with the molecule polarising the electron cloud surrounding the constituent nuclei to form a short-lived “virtual state”. The virtual state is unstable and on relaxing back to the ground state emits a photon. Usually the difference in energy between the emitted and absorbed photons is very small and so the process can be treated as elastic scattering, also known as Rayleigh scattering (Figure 2-10). Occasionally nuclear motion can be induced in the molecule. In this event, a significant amount of energy is transferred between the photon and the molecule. This is inelastic Raman scattering of which there are two types, Stokes and anti-Stokes scattering. Stokes scattering involves the emitted photon having less energy than the absorbed photon. This is caused by the molecule being excited from its ground vibrational state to a higher energy vibrational state. Anti-Stokes scattering involves the emitted photon having more energy than the absorbed photon. This is caused by the molecule starting in a higher vibrational state. If this energy is transferred to the absorbed photon, the photon is emitted with more energy than the photon absorbed. At room temperature most molecules are in their ground state and therefore a Stokes shift is observed most often. As the temperature of the sample is increased, so does the ratio of anti-Stokes to Stokes scattering.

In order for the molecule to exhibit Raman scattering a change in the molecular polarisation potential with respect to the vibrational coordinate is required. The amount of polarisability change will determine the intensity of the Raman scattering. The most intense bands

observed in Raman spectra are usually symmetric vibrations. The symmetry of the molecule determines the vibrations which will be active.

Raman spectra in this study were collected on a Renishaw InVia Raman microscope using an Ar ion laser at a wavelength of 488 nm. Samples were loaded in an Instec sample cell in an argon filled glove box. The sample cell was then transferred to the microscope and argon gas was flowed over the sample at 1 bar pressure during data collection.

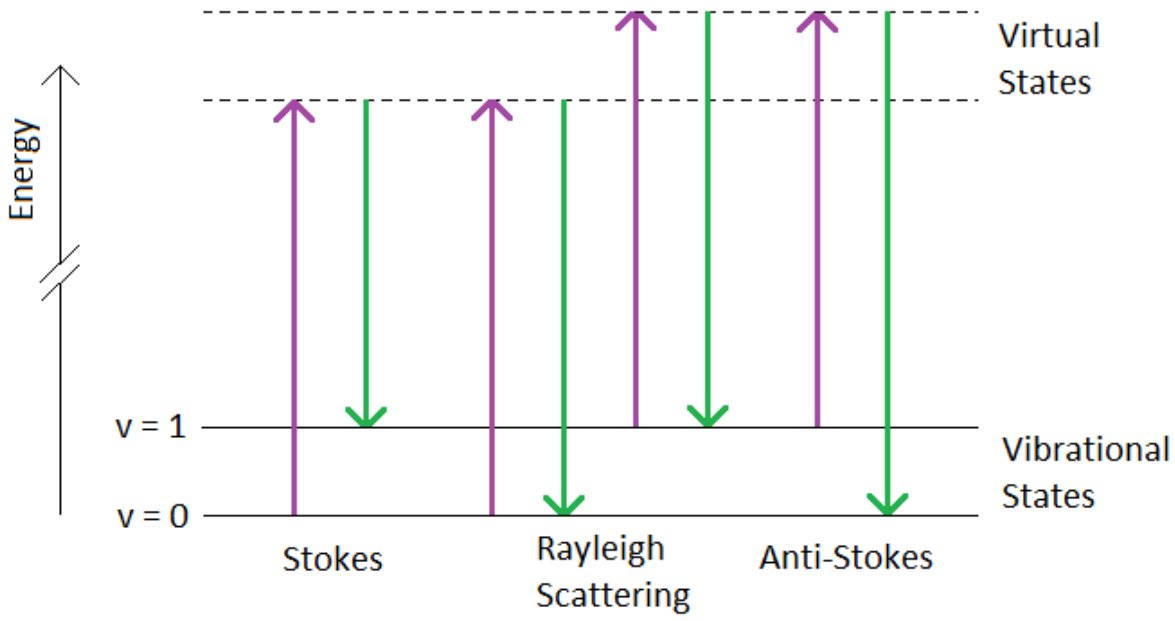

Figure 2-10 Diagram of Raman scattering processes. The incident energy and scattered energy are represented in purple and green respectively.

7. Temperature Programmed Desorption

Temperature programmed desorption (TPD) is a generic term used to describe an apparatus set-up that can control the heating rate and atmospheric conditions of a solid sample. The gaseous products are monitored in relation to the temperature of the sample (Figure 2-11).

In this study, TPD was carried out under flowing argon and products were monitored using mass spectrometry (TPD-MS). A mass flow controller (Hastings 200 Series, Teledyne) was used to control a constant rate of argon at 100 ml min^{-1} flowing over the sample. The sample (~0.1 g) was weighed into a quartz reaction tube (7 mm O/D, 4 mm I/D) inside an argon filled glove box and sealed upright in the reaction chamber. The sealed reaction chamber was then transferred onto the TPD apparatus without exposing the sample to the atmosphere. A barrel heater was placed around the reaction chamber. The barrel heater was controlled by an internal thermocouple that was placed within the sample. As the thermocouple was in contact with the sample it was sometimes possible to see endothermic and exothermic events within the temperature trace of the TPD. The gaseous desorption products were monitored using a quadrupole mass spectrometer (HPR-20, Hiden Analytical) using a Faraday cup detector.

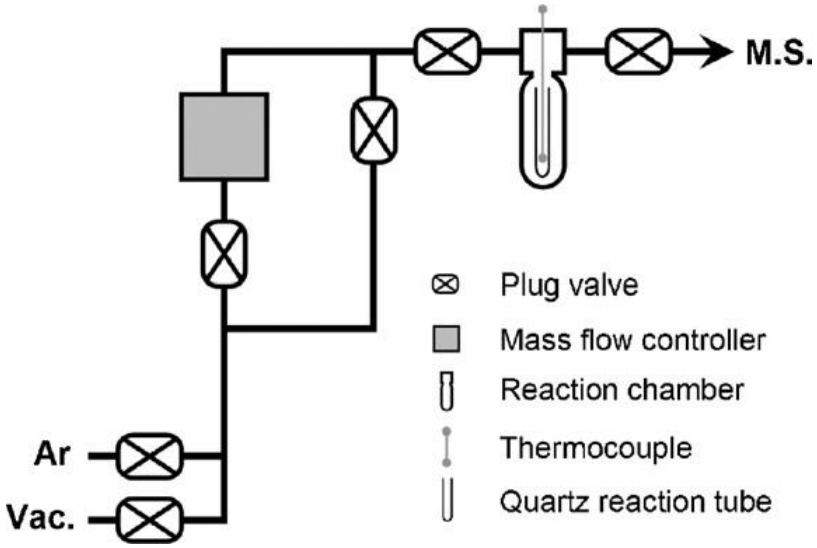

Figure 2-11 Schematic diagram of the TPD-MS apparatus.[4]

1. Calibration

In order to determine the true total sensitivity of the mass spectrometer towards hydrogen and ammonia, a calibration gas was used (BOC Speciality Gases, 4736 ppm H_2, 4898 ppm NH_3, balance Ar). Determining NH_3 in a mass spectrometer is problematic as the $NH_3^{\bullet+}$ mass fragment has the same *m/z* value as $OH^{\bullet+}$ fragment of water, which is frequently present in high vacuum systems such as mass spectrometers. Therefore, the $NH_2^{\bullet+}$ fragment of NH_3 was used to determine the true amount of NH_3. $NH_2^{\bullet+}$ is approximately 80% of the intensity of the $NH_3^{\bullet+}$ fragment.

The calibration gas was connected to the TPD apparatus under the control of the mass flow controller in the same way as for the argon carrier gas described above. The mass flow for the calibration gas was 20 ml min^{-1}. The observed partial pressures (P_n) for mass channels (*m/z*) 2 ($H_2^{\bullet+}$), 16 ($NH_2^{\bullet+}$), 17 ($NH_3^{\bullet+}/OH^{\bullet+}$), 18 ($H_2O^{\bullet+}$), 28 ($N_2^{\bullet+}$), 32 ($O_2^{\bullet+}$) and 40 ($Ar^{\bullet+}$) were recorded until a constant signal was reached. In order to determine the background levels of

mass channels 2 ($H_2^{\bullet+}$) and 16 ($NH_2^{\bullet+}$), the equivalent mass spectrum data were also collected for the pure argon carrier gas.

The observed partial pressure signals of H_2 and NH_2 (P_2 and P_{16}) were converted to fractions (χ_2 and χ_{16}) of the observed argon signal (P_{40}):

Equation 2-13 $$\chi_2 = \frac{P_2}{P_{40}} \qquad \chi_{16} = \frac{P_{16}}{P_{40}}$$

The observed fractional signals determined for H_2 and NH_2 for the pure argon carrier gas (χ_2^0 and χ_{16}^0) were deducted from the respective fractional signals from the calibration gas. This gave background subtracted fractional signals. These fractional signals were then divided by the true molar fraction as provided by the calibration gas certificate, to give the relative sensitivity, RS, values for H_2 and NH_3 (Equation 2-14).

Equation 2-14 $$R_{H_2} = \frac{\chi_2 - \chi_2^0}{4.736 \times 10^{-3}} \qquad R_{NH_3} = \frac{\chi_{16} - \chi_{16}^0}{4.898 \times 10^{-3}}$$

The observed values for H_{2^+} and NH_{2^+} from the TPD-MS experiments could then be corrected to true values by using these determined relative sensitivity values.

When collecting TPD-MS data the same mass channels were recorded as for the calibration using the same data collection routine. The background signals for mass channels 2 (H_{2^+}) and 16 (NH_{2^+}) were determined by allowing the MS to collect data for an appropriate period of time before the TPD-MS experiment was started. The data collected were then converted to a fraction of the argon signal (χ_2 and χ_{16}, Equation 2-13). For the *m/z* 2 and 16 mass

channels, the background signal determined before starting the experiment was then subtracted from the following signals. The corrected fractional signal was then divided by the determined RS value to give the corrected molar fractions of H_2 and NH_3 in the gas stream, given by $\chi^*_{H_2}$ and $\chi^*_{NH_3}$ (Equation 2-15).

Equation 2-15 $$\chi^*_{H_2} = \frac{\chi_2 - \chi^0_2}{R_{H_2}} \qquad \chi^*_{NH_3} = \frac{\chi_{16} - \chi^0_{16}}{R_{NH_3}}$$

Accurate values for the relative amounts of H_2 and NH_3 released could then be established from this corrected TPD-MS data.

Pseudo-gravimetric data could be produced by using a mass flow controller in the TPD-MS experiment to control the flowing gas stream. The molar fractions of H_2 and NH_3 at t, ($\chi^*_{H_2}$ (t) and $\chi^*_{NH_3}$(t)) were by the corrected MS data at regular time intervals (δt) determined by the rate of the MS data collection (approximately one spectrum every 20 seconds). The volume of each gas (V_{H_2} and V_{NH_3}) released during the timescale for one MS spectrum could be determined by knowing the flow rate of the argon carrier gas (100 ml min^{-1}). The total volume (ml) of each gas desorbed during a certain time interval, *V*(t) could therefore also be deduced (Equation 2-16).

Equation 2-16 $V_{H_2}(t) = \sum_{t=0}^{t} 100 \times \delta t \times \chi^*_{H_2}(t) \qquad V_{NH_3}(t) = \sum_{t=0}^{t} 100 \times \delta t \times \chi^*_{NH_3}(t)$

The molar volumes of H_2 and NH_3 at room temperature and pressure are 24.804 l mol^{-1} and 24.532 l mol^{-1} respectively.[5]

Once the volume of gas released had been calculated it could be multiplied by 4.032×10^{-5} mol ml^{-1} and 4.076×10^{-5} mol ml^{-1}, respectively, in order to estimate the number of moles of H_2 and NH_3 released. If the starting mass of the sample and molecular mass were known, the number of moles of each gas released could be expressed in terms of the number of moles of the starting sample.

A simulated mass of each gas released could be calculated by multiplying the molecular mass of the gas by the calculated number of moles of the gas released (Equation 2-17 and Equation 2-18). The calculated mass of gas released could then be subtracted from the initial sample mass (m_s, grams) and expressed as a percentage of the starting mass. Therefore, a simulated gravimetric plot could be plotted.

Equation 2-17
$$\mathrm{wt\%(t)} = 100 \times \frac{m_s - \sum_{t=0}^{t} V_{\mathrm{H_2}}(\mathrm{t}) \times 4.032 \times 10^{-5} \times 2.02}{m_s}$$

Equation 2-18
$$\mathrm{wt\%(t)} = 100 \times \frac{m_s - \sum_{t=0}^{t} V_{\mathrm{NH_3}}(\mathrm{t}) \times 4.076 \times 10^{-5} \times 16.02}{m_s}$$

This form of data analysis allows for a more complete examination of the desorbed gases in relation to the starting sample despite it being a complex method. Much more information can be deduced from the TPD-MS set-up than merely identification of desorbed gases.

8. Mass Spectrometry

TPD apparatus described above was coupled to a quadrupole mass spectrometer (MS) (HPR-20, Hiden Analytical). The detection limit of the MS was approximately 5 ppm in the argon carrier gas stream.

MS is an analytical technique used to measure the mass to charge (*m/z*) ratio of charged particles. Mass spectrometers can scan across a range of *m/z* values and establish the relative amount of each observed. Specific *m/z* ratios can be monitored in order to determine the amount of any given analyte. Species are ionised and then electromagnetic fields manipulate the ions differently depending on their *m/z* ratio. MS must be carried out at low pressure in order to stop the ions colliding with other species and losing their charge. MS consists of three main processes: ionisation, separation and detection.[6]

1. Ionisation

Ionisation of species can occur in many different ways. In this study, electron ionisation (EI, formerly known as electron impact) is the only ionisation method used. Ionisation converts atoms/molecules into gas-phase ionic species by the removal or addition of an electron or proton (Equation 2-19).

Equation 2-19 $$M + e^- \rightarrow M^{+\bullet} + 2e^-$$

where
$M = analyte\ molecule\ being\ ionised,$
$e^- = electron,$
$M^{+\bullet} = resulting\ ion.$

The electrons are produced from thermionic emission by heating a wire filament that has an electric current running through it. The neutral analyte molecules are introduced to the ion source in a direction perpendicular to the electron beam. The electron beam knocks an electron from atoms to create a singly charged cation. Some double ionisation does occur but these ions are discarded by the analyser. As the species are monitored by their *m/z* ratio,

singly charged species are preferable. The energy of the electron beam is usually tuned to avoid multiple ionisations. The radical cation products are then accelerated towards the mass analyser by a repeller electrode. The ionisation process can give rise to fragmentation of larger molecules, as excess ionisation energy can cause the ionised species to break up into smaller fragments. These smaller species will also be detected by their *m/z* ratio. For larger, organic samples, this fragmentation pattern can be useful for phase identification and can give important structural information about the analyte.

2. Separation

The ionic species are separated according to their *m/z* ratio by an analyser. A quadrupole mass analyser is the most common type of mass analyser now used in MS (Figure 2-12). Originally species were separated by bending their flight radius depending on their *m/z* ratio. The frequency of the oscillation is chosen in order to selectively stabilise one *m/z* ratio, and therefore this ratio reaches the detector at the expense of the other *m/z* ratios. The other ionic species get scattered or neutralised in collisions and are therefore not detected.

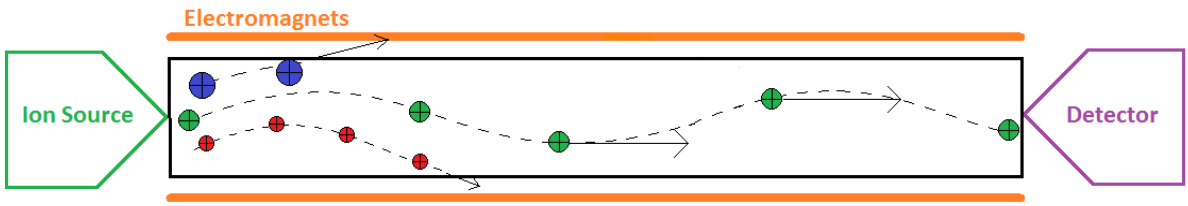

Figure 2-12 Schematic diagram of a quadrupole mass spectrum analyser.

3. Detection

The detector records the ion current produced when an ion hits a surface. The signal is then amplified and the data output as a mass spectrum. A Faraday cup detector was used in this study to collect and measure the separated ions. A Faraday cup is a conductive cup designed to catch charged particles in vacuum. The current resulting from the impact can be measured. The current is directly proportional to the number of ions hitting the surface.

4. Overview

The analyte is contained in an argon carrier gas which is sampled through a heated capillary. The gas then passes into the vacuum system of the mass spectrometer *via* the capillary. The capillary has a small diameter in order to restrict the amount of gas entering the system so the low pressure required can be maintained. The vacuum system is heated in order to reduce the water concentration present in the system as water is ever-present (in low concentrations) in high vacuum appliances (Figure 2-13).

Here, the mass spectrum was first collected over the *m/z* range of 1 to 50 to identify which species were present. Multiple ion monitoring mode (MIM) was then used to detect only the ions of interest. This enabled an increase in the rate of data collection.

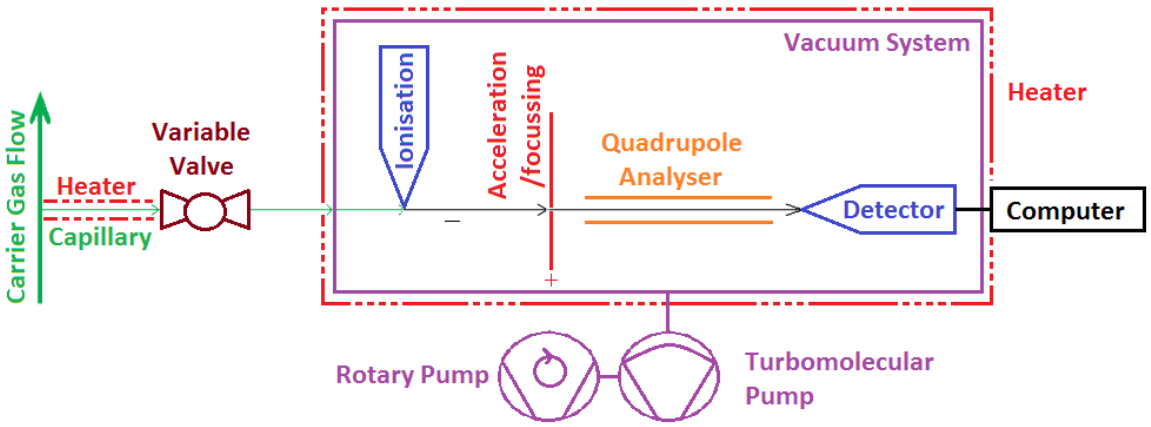

Figure 2-13 Schematic diagram of a mass spectrometer with the principal components labelled.

9. Intelligent Gravimetric Analysis

An Intelligent Gravimetric Analyser (IGA, Hiden Analytical) is a pressure controlled thermo-gravimetric balance with complete control of the environment. The sample is loaded into a crucible (quartz crucibles were made in-house for this study) and placed on a hang-down attached to a microbalance head. The weight of the sample is then monitored under different environmental conditions so that weight changes can be observed with changing temperature and pressure. The temperature of the sample is controlled by using an external furnace which surrounds the reaction tube accommodating the sample hang-down. The sample temperature is monitored using a positive temperature coefficient (PTC) sensor placed next to the sample (Figure 2-14).

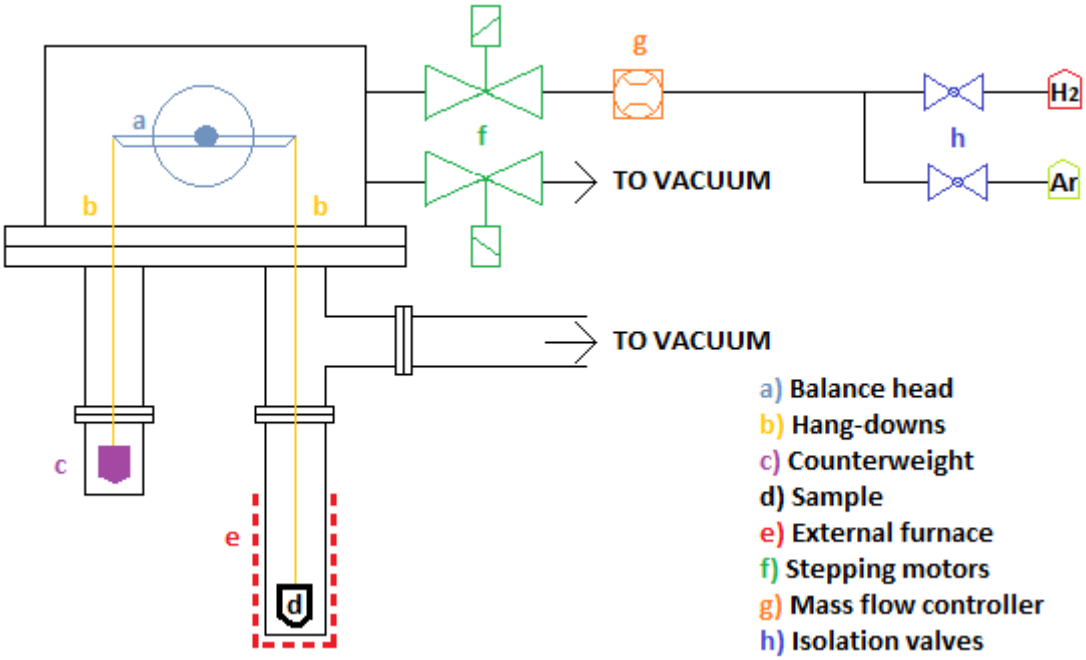

Figure 2-14 Schematic diagram of IGA apparatus.

1. Pressure Control Mode

The IGA used in this study had stepping motors on the gas inlet and outlet so the pressure inside the reactor could be controlled precisely from 50 mbar to 20 bar. An assortment of gases can be connected to the inlet, but here only Ar and H_2 were used. In pressure control mode, pressure is set and a ramp rate selected. The IGA then admits gas up to the desired pressure by continually admitting small amounts of gas *via* the inlet stepping motor. The pressure is then maintained at the set-point value by continually allowing gas in whilst monitoring the sample mass. The outlet is connected to a vacuum system and the pressure is reduced by continually bleeding small amounts of gas out into the vacuum system. The pressure control mode was used to observe the hydrogenation of samples under a hydrogen atmosphere.

2. Inert Sample Loading

The sample was able to be loaded without contact with the atmosphere by using a portable glove box. The dry mass of the sample crucible was weighed and recorded, before being taken into a glove box where the sample was loaded into it. The sample and crucible were removed from the glove box, sealed in a sample cartridge. The sample cartridge was inserted into the portable glove box whilst it was attached to the IGA. The portable glove box was then purged of air by cycling with argon between 1050 mbar and 1250 mbar 100 times. After this, the sample cartridge was opened and the sample crucible was transferred to the hang-down using a mechanical arm.

10. High Pressure Rig

The high pressure rig allows samples to be exposed to high temperature and pressures of various gases. For these experiments argon and hydrogen gases were connected (Figure 2–15).

The high pressure rig is capable of hydrogenating samples at pressures of up to 100 bar and temperatures up to 640 °C. Samples of ~0.1 g were loaded into a quartz reaction tube (7 mm O/D, 4 mm I/D) in an argon filled glove box. Up to four of these were then loaded into the high pressure cell. The bolts on this were tightened to 60 Nm in the glove box before removing and tightening further to 90 Nm. The cell was supported inside a vertical furnace and connected to the control manifold. The manifold was purged of air by cycling with argon and then the whole system, including the high pressure cell, was purged of argon with 100% hydrogen. The system was cycled with hydrogen at ~3 bar and down to rough vacuum

(~1 x 10^{-3} mbar). The argon was used as an intermediate gas in order to eliminate the risk of explosion between air and hydrogen gas, if air was purged directly with hydrogen. The system was then pressurised to the desired pressure with hydrogen. The pressure in the cell increases with the increase in temperature and the initial pressure was set to ensure the final pressure was as desired (under heating). The sample was heated to the desired set point inside a vertical slit furnace. The temperature was monitored using an internal thermocouple.

Once the reactor was cool, it was vented to ~3 bar before evacuating and cycling between ~3 bar argon and rough vacuum. The high pressure cell was then returned to the argon glove box to remove and weigh the samples. The pressure was measured to ~± 5 bar on an analogue pressure gauge.

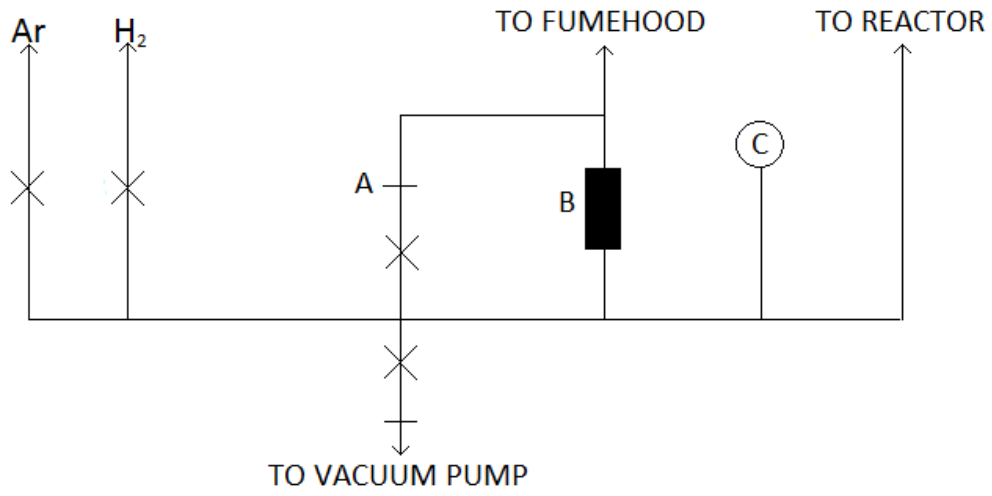

A = Vent to fumehood
B = Pressure Release Valve
C = Analogue Pressure Gauge

Figure 2-15 Schematic diagram of high pressure rig.

[1] A. G. De la Torre, M. A. G. Aranda, *J. Appl. Cryst.*, 36 (2003) 1169–1176

[2] R.E. Dinnebarbier, S. J. L. Billinge, *Powder Diffraction. Theory and Practice*, RSC Publishing (2008)

[3] Topas, general profile and structure analysis software for powder diffraction data. A. A. Coelho; Bruker AXS, Karlsruhe, Germany, 3.0 ed., 2004.

[4] P. A. Chater, P. A. Anderson, J. W. Prendergast, A. Walton, V. S. J. Mann, D. Book, W. I. F. David, S. R. Johnson, P. P. Edwards, *J. Alloys Compds.,* 446–447 (2007) 350–354

[5] National Institute of Standards and Technology NIST Standard Reference Database 69: NIST Chemistry WebBook (2008)

[6] P. Price, *J. Am. Soc. Mass Spectrom.,* 2 (1991) 336–348

3. $Li_3Na(NH_2)_4$ and $LiNa_2(NH_2)_3$

1. Introduction

The mixed amides $Li_3Na(NH_2)_4$, $Li_5Na(NH_2)_6$ and $LiNa_2(NH_2)_3$ were first synthesised by Harbrecht and Jacobs, in 1982,[1] using supercritical ammonia and the lithium and sodium metals in molar ratios from 1:3 to 3:1 (Equation 3-1 and Equation 3-2). The ammonia was between 1.7 and 4.3 kbar in an autoclave at 157–197 °C for between 4 and 20 days.

Equation 3-1 $$8Li + 2Na + 10NH_3 \rightarrow Li_3Na(NH_2)_4 + Li_5Na(NH_2)_6 + 5H_2$$

Equation 3-2 $$2Li + 4Na + 6NH_3 \rightarrow 2LiNa_2(NH_2)_3 + 3H_2$$

The lattice parameters for the three mixed amides are given in Table 3-1. The $LiNa_2(NH_2)_3$ and $Li_3Na(NH_2)_4$ lattice parameters were backed up by single crystal X-ray structure determination, however $Li_5Na(NH_2)_6$ lattice parameters were determined by Weissenberg and precession photographs.

Table 3-1 Lattice parameters of $LiNa_2(NH_2)_3$, $Li_3Na(NH_2)_4$ and $Li_5Na(NH_2)_6$ (from Jacobs *et al.*[1])

Lattice Parameters	*$LiNa_2(NH_2)_3$*	*$Li_3Na(NH_2)_4$*	*$Li_5Na(NH_2)_6$*
a/ Å	6.278(2)	5.072(4)	5.072(3)
c/ Å	11.142(4)	11.478(5)	34.36(1)
Space group	$P4_2/m$	*I*-4	*I*-4

These mixed amides are important because of their high hydrogen content ($LiNa_2(NH_2)_3$ 6.0 wt%; $Li_3Na(NH_2)_4$ 7.5 wt%; $Li_5Na(NH_2)_6$ 7.9 wt%) although the addition of sodium

decreases gravimetric content compared to $LiNH_2$. It is however possible that the mixing of the cations might cause destabilisation of the amide, which with the addition of a light metal hydride could cause the material to release hydrogen, at a lower temperature than lithium amide under the same conditions. This can be compared to $LiNH_2$ which is known to be destabilised by the addition of Mg (from MgH_2) into the lattice and therefore reduce the temperature at which hydrogen is desorbed.[2]

Equation 3-3 and Equation 3-4 were carried out in the solid state by Lowton *et al.*[3] in 2008. Lattice parameters have been confirmed for both $Li_3Na(NH_2)_4$ and $LiNa_2(NH_2)_3$ (Table 3–2).

Equation 3-3 $3LiNH_2 + NaNH_2 \rightarrow Li_3Na(NH_2)_4$

Equation 3-4 $LiNH_2 + 2NaNH_2 \rightarrow LiNa_2(NH_2)_3$

Table 3-2 Lattice parameters of $LiNa_2(NH_2)_3$ and $Li_3Na(NH_2)_4$ (from Lowton *et al.*[3])

Lattice parameters	*$LiNa_2(NH_2)_3$*	*$Li_3Na(NH_2)_4$*
a/ Å	6.2838(1)	5.081(1)
c/ Å	11.1485(2)	11.511(5)
Space Group	*$P4_2/m$*	*I*-4

We decided to prepare the mixed amides and study their reactions with common light metal hydrides. The light metal hydrides chosen were: LiH, NaH and MgH_2. Alone, these hydrides are not practical because, as previously mentioned, LiH decomposes above 550 °C, which is too high. Similarly, NaH decomposes at 425 °C and MgH_2, although a light and cheap material, suffers from slow desorption kinetics.

2. Results

1. Preparation of $Li_3Na(NH_2)_4$

$Li_3Na(NH_2)_4$ was prepared in house from heating $3LiNH_2$ (Sigma-Aldrich, hydrogen storage grade) + $NaNH_2$ (Sigma-Aldrich, hydrogen storage grade) to 200 °C for 12 hours. The powder XRD pattern produced is shown below (Figure 3-1). The lattice parameters were tetragonal a = 5.08124 Å, c = 11.506 Å. These parameters compare well with the literature values published by Lowton *et al.*[3] of a = 5.081 Å, c = 11.511 Å.

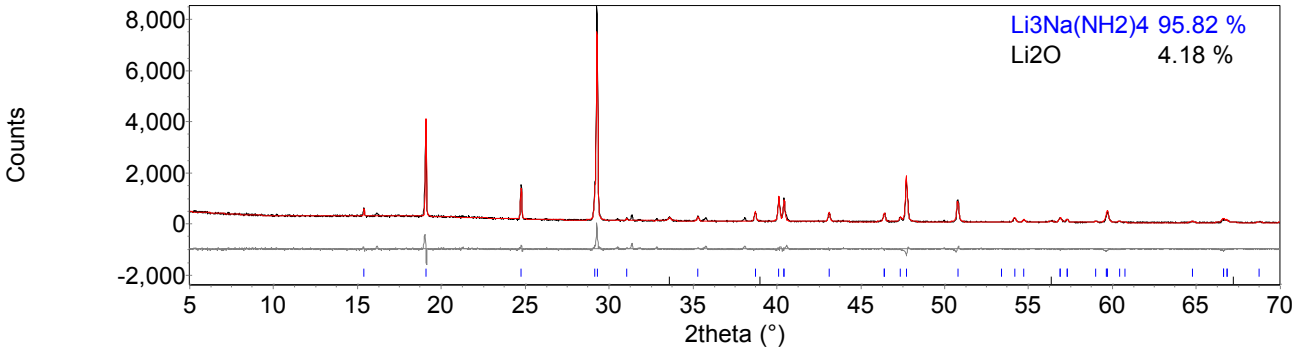

Figure 3-1 $Li_3Na(NH_2)_4$, formed in house from $3LiNH_2$ + $NaNH_2$ heated to 200 °C for 12 hours. R_{wp} = 11.425, R_{exp} = 6.833, X^2 = 2.8.

It was found on heating $Li_3Na(NH_2)_4$ alone to 350 °C for 1 hour that $LiNa_2(NH_2)_3$ and $LiNH_2$ were the products, along with remaining $Li_3Na(NH_2)_4$ (Equation 3-5 and Figure 3-2).

Equation 3-5 $$2Li_3Na(NH_2)_4 \rightarrow LiNa_2(NH_2)_3 + 5LiNH_2$$

After 4 hours, heating the $LiNH_2$ previously present in the products had disappeared (Figure 3-3).

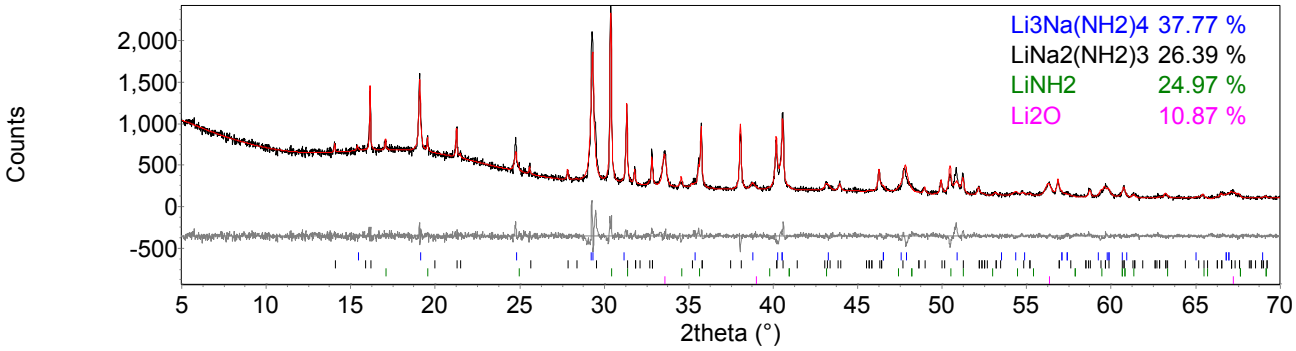

Figure 3-2 Powder XRD pattern of $Li_3Na(NH_2)_4$, heated to 350 °C for 1 hour on a flowing line. The observed powder XRD pattern (black line) was fitted using a Rietveld fit (red line) to the observed phases $Li_3Na(NH_2)_4$ (blue tick marks), $LiNa_2(NH_2)_3$ (black tick marks), $LiNH_2$ (green tick marks) and Li_2O (pink tick marks). R_{wp} = 7.000, R_{exp} = 5.020, X^2 = 1.9.

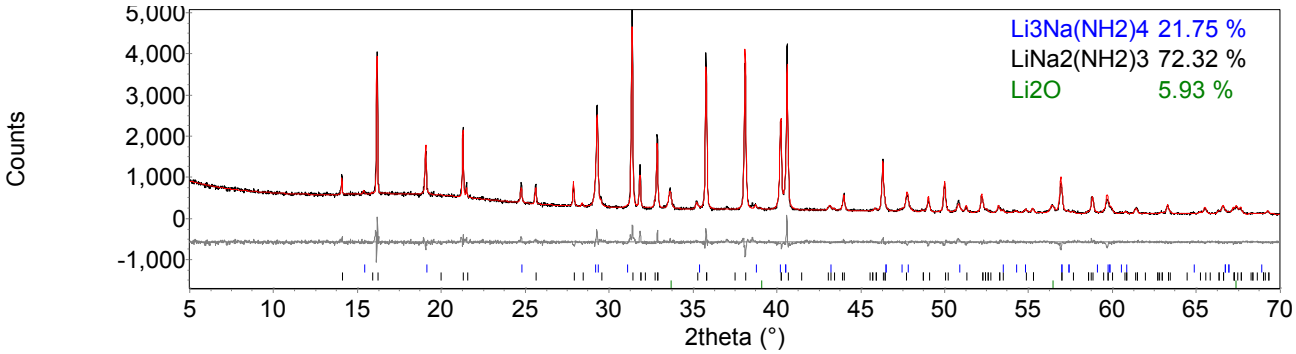

Figure 3-3 Powder XRD pattern of $Li_3Na(NH_2)_4$, heated to 350 °C for 4 hours on a flowing line. The observed powder XRD pattern (black line) was fitted using a Rietveld fit (red line) to the observed phases $Li_3Na(NH_2)_4$ (blue tick marks), $LiNa_2(NH_2)_3$ (black tick marks) and Li_2O (green tick marks). R_{wp} = 7.348, R_{exp} = 4.914, X^2 = 2.2.

2. Preparation of $LiNa_2(NH_2)_3$

$LiNa_2(NH_2)_3$ was formed in house from heating $LiNH_2$ + $2NaNH_2$ to 200 °C for 12 hours (Figure 3-4). The $LiNa_2(NH_2)_3$ was characterised by using the lattice parameters published by Lowton *et al*.[3] The lattice parameters of our tetragonal $LiNa_2(NH_2)_3$ starting material were found to be a = 6.30 Å and c = 11.19 Å. This was in comparison to Lowton *et al*. lattice parameters of a = 6.28 Å and c = 11.15 Å.

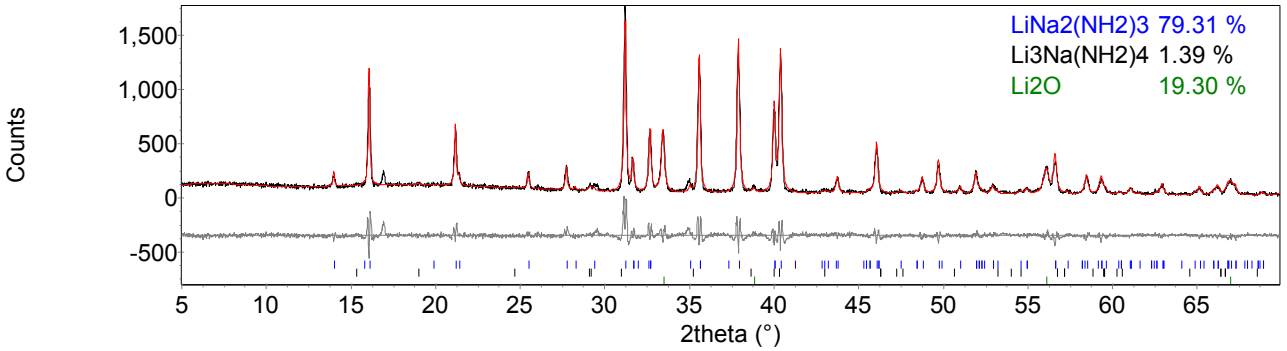

Figure 3-4 $LiNa_2(NH_2)_3$, formed in house from $LiNH_2$ + $2NaNH_2$ heated to 200 °C for 12 hours. R_{wp} = 15.575, R_{exp} = 8.985, X^2 = 3.0.

On heating $LiNa_2(NH_2)_3$ for 1 hour at 350 °C, the products were a mix of $LiNa_2(NH_2)_3$ starting material and $Li_3Na(NH_2)_4$ (Figure 3-5). The lattice parameters of $Li_3Na(NH_2)_4$ were larger than in the literature.[3] This suggested there was less Li and more Na present in the unit cell. This may account for the lack of $NaNH_2$ present as it could be expected that:

Equation 3-6 $3LiNa_2(NH_2)_3 \rightarrow Li_3Na(NH_2)_4 + 5NaNH_2$

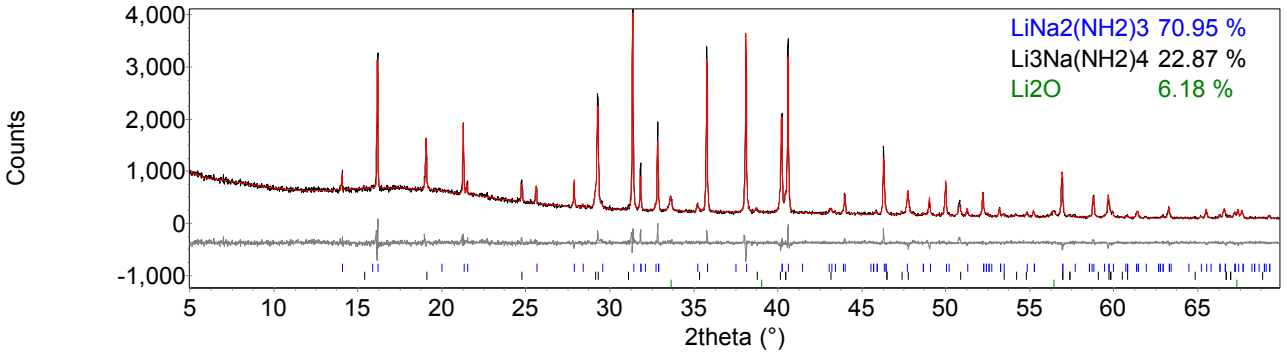

Figure 3-5 Powder XRD pattern of $LiNa_2(NH_2)_3$, heated to 350 °C for 1 hour on a flowing line. The observed powder XRD pattern (black line) was fitted using a Rietveld fit (red line) to the observed phases $Li_3Na(NH_2)_4$ (blue tick marks), $LiNa_2(NH_2)_3$ (black tick marks) and Li_2O (green tick marks). R_{wp} = 6.737, R_{exp} = 5.005, X^2 = 1.8.

No gas was desorbed from either mixed cation amide when heated alone. It seemed the two mixed cation amides formed an equilibrium between them.

3. $Li_3Na(NH_2)_4$ + 4LiH

$Li_3Na(NH_2)_4$ was heated with LiH (Sigma-Aldrich, 95%) in a 1:4 ratio. This ratio was chosen in order to react one mole of amide with one mole of hydride, as with the $LiNH_2$ – LiH system.

1. Temperature Programmed Desorption-Mass Spectrometry

The reaction was carried out on a TPD-MS apparatus at a heating rate of 2 °C min^{-1} to 350 °C. As can be seen from Figure 3-6, the reaction predominantly gave off hydrogen with a very small amount of ammonia desorbed at the peak of hydrogen desorption. The hydrogen desorption proceeded slowly as soon as heating started. At 235 °C the rate of hydrogen desorption increased and peaked at 315 °C, before rapidly decreasing back to the background level of hydrogen release. This drop off in hydrogen release occurred concurrently with the isothermal heating of the sample. The shape of the hydrogen desorption appears to be that of two separate hydrogen desorption reactions. The first being the slow desorption up to 235 °C, the second above 235 °C. The products after heating were analysed by powder XRD and identified as Li_2NH and NaH.

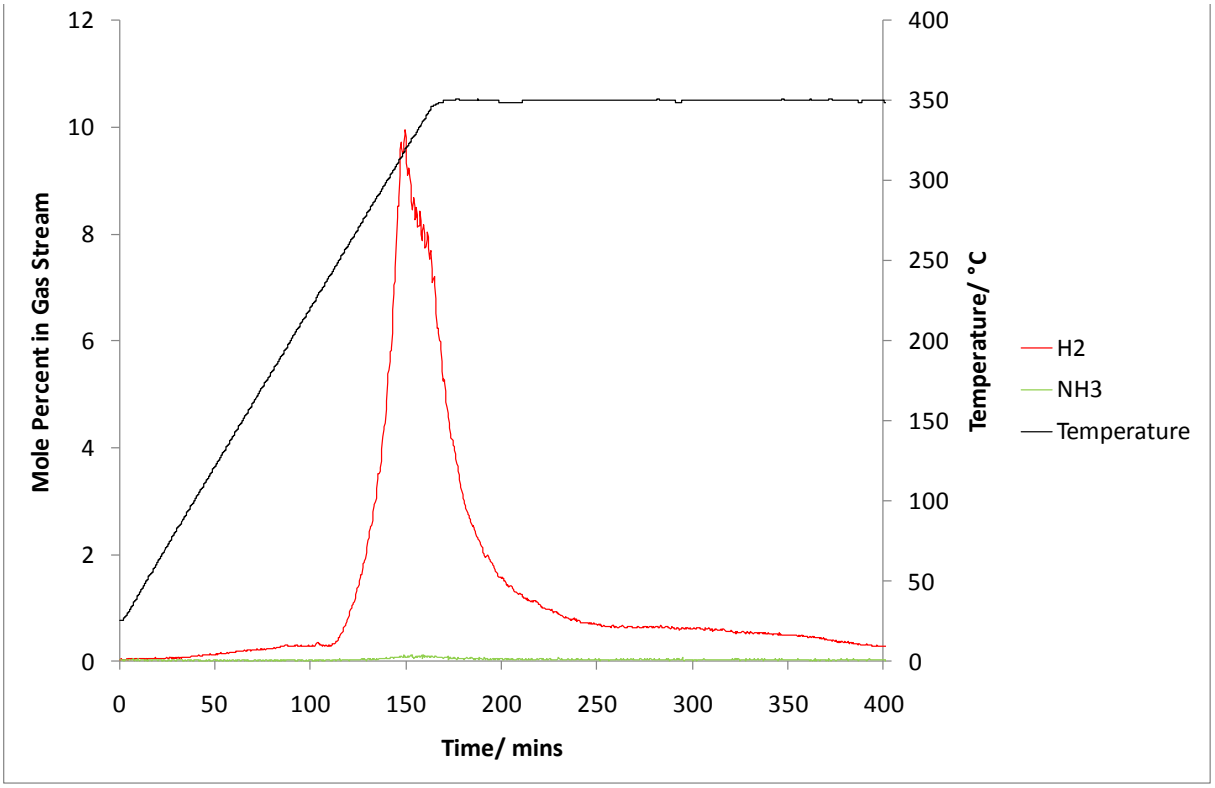

Figure 3-6 Thermal decomposition analysis of $Li_3Na(NH_2)_4$ + 4LiH in a TPD-MS apparatus. The temperature trace is shown in black and the mole percent of H_2 and NH_3 released are shown in red and green respectively.

When the $Li_3Na(NH_2)_4$ + 4LiH mixture was heated on the flowing line at 350 °C for 12 hours the products were Li_2NH, $LiNa_2(NH_2)_3$ and Na, together with a significant amount of lithium oxide (Figure 3-7). The oxide present in XRD patterns was most likely from the reaction of the sample with the Scotch® Magic™ tape used to make up the sample for XRD.

The XRD pattern includes the weight percent (wt%) of the known phases that have been refined by the Rietveld method, using computer program Topas.[4]

The weight percents calculated by Topas can be converted to mole percents by dividing the weight percent by the relative molecular mass (RMM). The mole fraction can in turn be

calculated by summing the mole percents and dividing the individual mole percents by the sum total for Rietveld phases in each XRD.

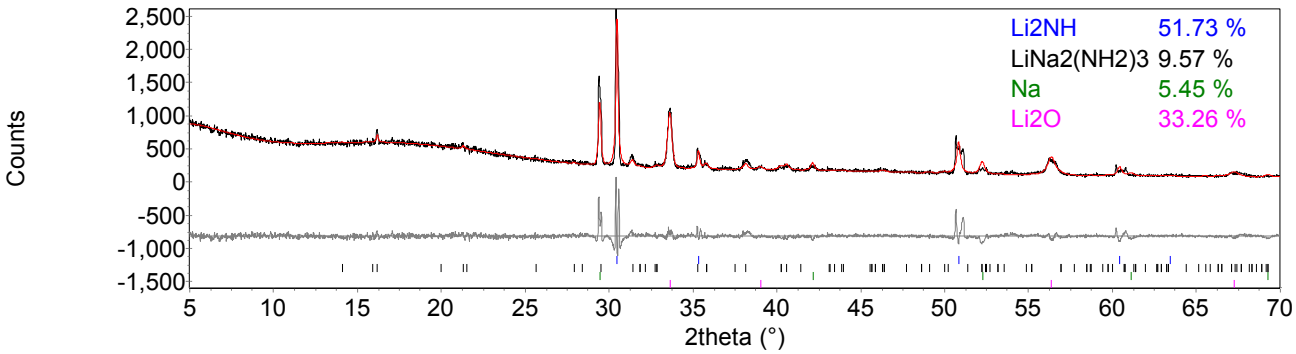

Figure 3-7 Powder XRD pattern of $Li_3Na(NH_2)_4$ + 4LiH, heated to 350 °C for 12 hours under flowing argon. The observed powder XRD pattern (black line) was fitted using a Rietveld fit (red line) to the observed phases Li_2NH (blue tick marks), $LiNa_2(NH_2)_3$ (black tick marks), Na (green tick marks and Li_2O (pink tick marks). R_{wp} = 11.034, R_{exp} = 5.503, X^2 = 4.0.

There was no NaH present under these reaction conditions in comparison to TPD-MS results. However, Na metal was present instead. Under these conditions it is known NaH decomposes to Na with the release of hydrogen (Equation 3-7). This should account for the tail of hydrogen present during the isothermal heating.

Equation 3-7 $2NaH \rightarrow 2Na + H_2$

The majority product under both these conditions was Li_2NH, however on heating under argon for 12 hours, $LiNa_2(NH_2)_3$ was also present.

2. Discussion

For the reaction to have gone to completion only imide, not amide as present here, should have been present in the products. As it was $LiNa_2(NH_2)_3$ that was present in the products, not the $Li_3Na(NH_2)_4$ starting material, it is suggested that $LiNa_2(NH_2)_3$ is more stable.

We concluded that the $Li_3Na(NH_2)_4$ + 4LiH stoichiometry was not correct to maximise the hydrogen from this system. In order for the reaction to go stoichiometrically, more LiH was needed. Therefore, we investigated:

Equation 3-8 $Li_3Na(NH_2)_4 + 5LiH \rightarrow 4Li_2NH + NaH + 4H_2$

4. $Li_3Na(NH_2)_4$ + 5LiH

1. *Temperature Programmed Desorption-Mass Spectrometry*

As before, the reaction was first carried out on TPD-MS apparatus. From Figure 3-8, it can be seen hydrogen was the only gas desorbed from this reaction. There was a slow rise in hydrogen desorption from heating onset and the peak of the hydrogen desorption was still at nearly 350 °C with a similar desorption profile as the 1:4 mixture. Figure 3-8 also shows a comparison between the hydrogen release from $Li_3Na(NH_2)_4$ + 5LiH to $Li_3Na(NH_2)_4$ heated with 4NaH and $2MgH_2$, sections 3.2.6 and 3.2.7 respectively.

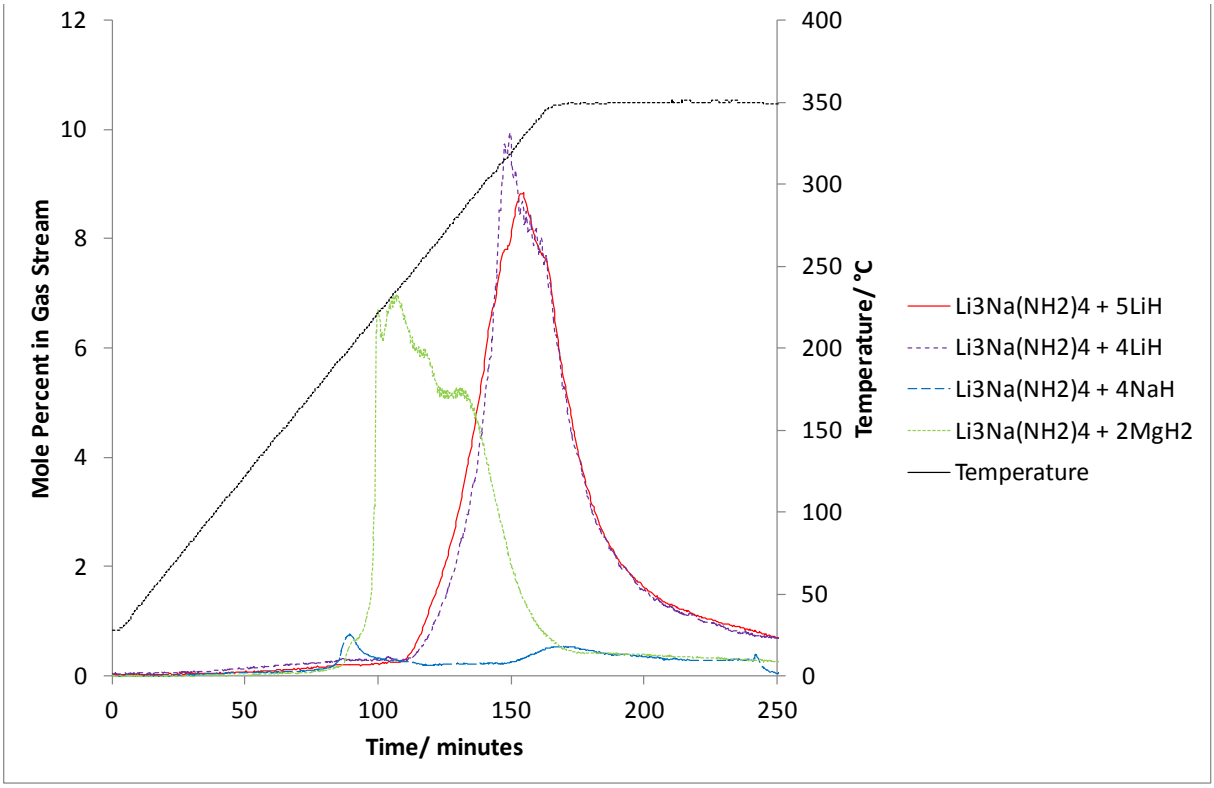

Figure 3-8 Thermal decomposition analysis of hydrogen release from $Li_3Na(NH_2)_4$ + 5LiH (red trace) in a TPD-MS apparatus in comparison to $Li_3Na(NH_2)_4$ + 4LiH (purple trace), $Li_3Na(NH_2)_4$ + 4NaH (blue trace) and $Li_3Na(NH_2)_4$ + $2MgH_2$ (green trace). The temperature trace is shown in black.

The solid products present after TPD-MS, identified by their powder XRD pattern were Li_2NH and NaH (Figure 3-9). As no mixed cation amides were present in the products this implied that the reaction had gone to completion with the additional mole of LiH. Also, any further dehydrogenation would come from the decomposition pathways of the individual products.

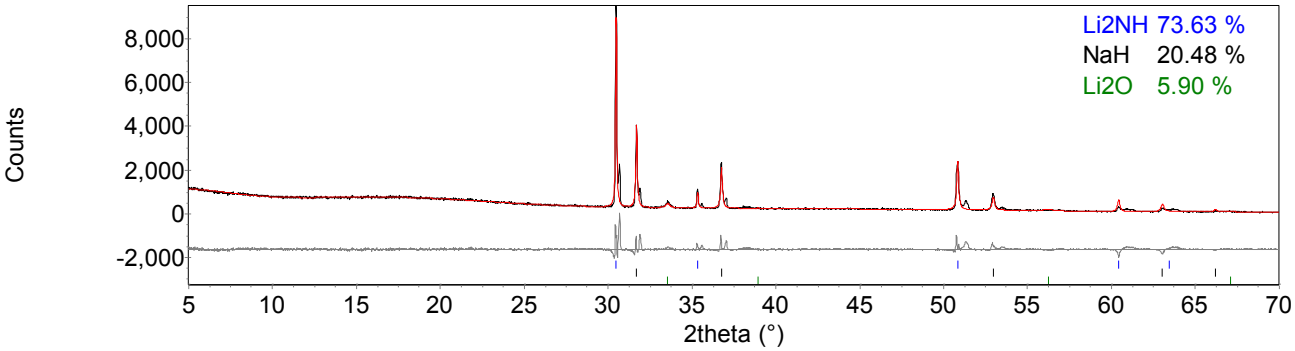

Figure 3-9 Powder XRD pattern of $Li_3Na(NH_2)_4$ + 5LiH, after TPD-MS to 350 °C. The observed powder XRD pattern (black line) was fitted using a Rietveld fit (red line) to the observed phases Li_2NH (blue tick marks), NaH (black tick marks) and Li_2O (green tick marks). R_{wp} = 13.806, R_{exp} = 4.784, X^2 = 8.3.

These results from heating $Li_3Na(NH_2)_4$ with 5LiH were consistent with the products of Equation 3-8.

2. *Thermogravimetric Analysis*

The starting materials, $Li_3Na(NH_2)_4$ + 5LiH, were heated to 350 °C on TGA-MS apparatus, at a rate of 2 °C min^{-1} to 350 °C where heating ceased (Figure 3-10). It was found that only hydrogen gas was desorbed. No ammonia was seen above the detection limit of the mass spectrometer. The hydrogen was desorbed in one main release with two peaks. The desorption started at ~190 °C and the peaks occurred at ~270 and ~330 °C. The desorption started at a slightly lower temperature than when the reaction was heated on TPD-MS apparatus. The first peak of the hydrogen desorption on TGA-MS apparatus was at a lower temperature than for TPD-MS apparatus.

The overall mass loss from this experiment was 4.3 wt%. This was in comparison to a theoretical mass loss of 5.5 wt% for the products NaH and Li_2NH, Equation 3-8.

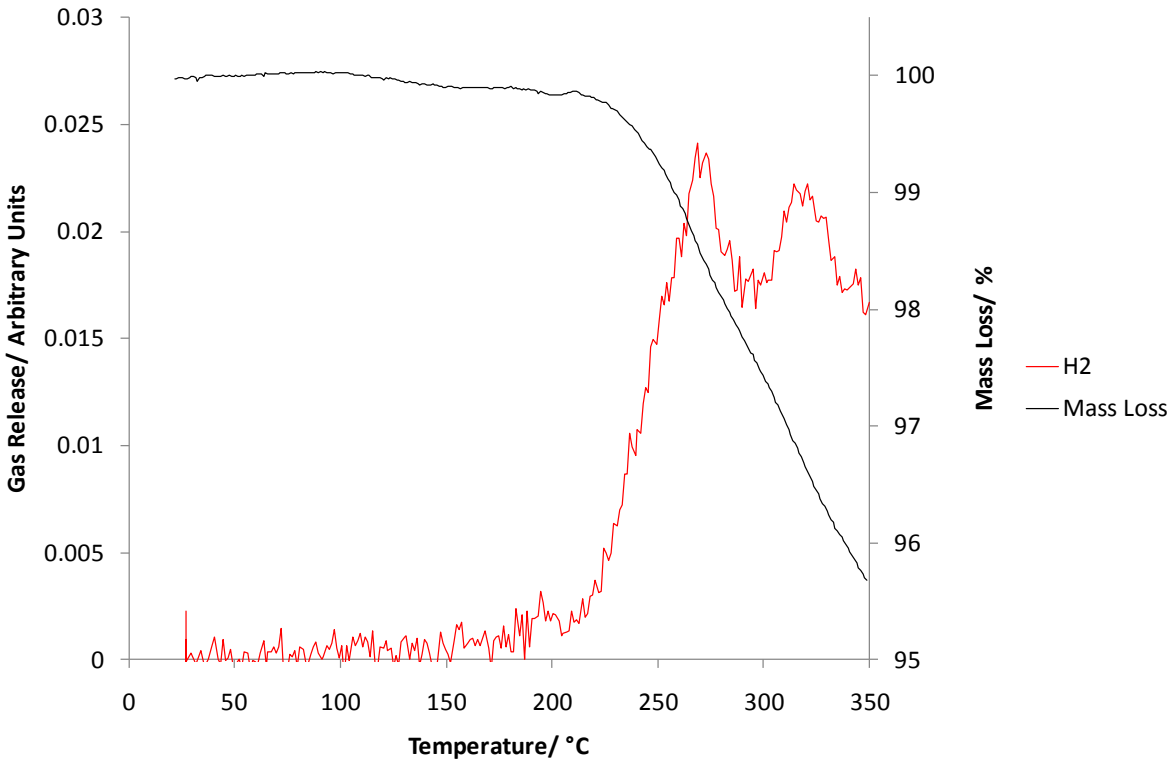

Figure 3-10 TGA-MS of the $Li_3Na(NH_2)_4$ + 5LiH reaction. The H_2 release is shown in red and the percentage mass loss is shown in black

3. Flowing Line Reactions

In order to establish the reaction pathway from reactants to products, the same reaction was carried out under different conditions. The $Li_3Na(NH_2)_4$ + 5LiH starting materials were heated to 150 °C for 12 and 24 hours, 200 °C for 12 and 24 hours and 250 °C, 300 °C and 350 °C for 12 hours on the flowing line.

After heating to 150 °C for 12 hours, the products were Li_2NH, $LiNa_2(NH_2)_3$ and NaH (Figure 3-11) with the $Li_3Na(NH_2)_4$ and LiH starting materials as the majority phases present. There was approximately twice as much $LiNa_2(NH_2)_3$ present after heating for 24 hours (Figure 3-12) compared to 12 hours heating.

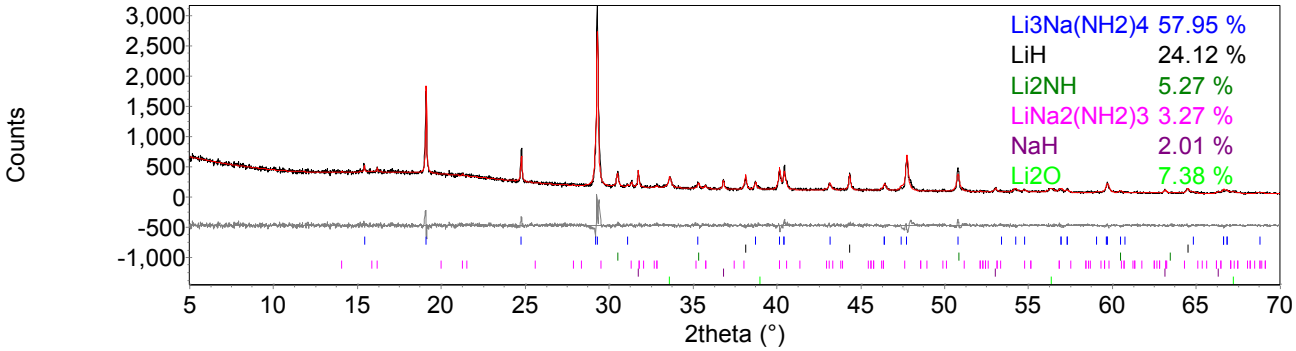

Figure 3-11 Powder XRD pattern of $Li_3Na(NH_2)_4$ + 5LiH, heated to 150 °C for 12 hours on flowing line. The observed powder XRD pattern (black line) was fitted using a Rietveld fit (red line) to the observed phases $Li_3Na(NH_2)_4$ (blue tick marks), LiH (black tick marks), Li_2NH (green tick marks), $LiNa_2(NH_2)_3$ (pink tick marks), NaH (purple tick marks) and Li_2O (light green tick marks). R_{wp} = 8.888, R_{exp} = 6.469, X^2 = 1.9.

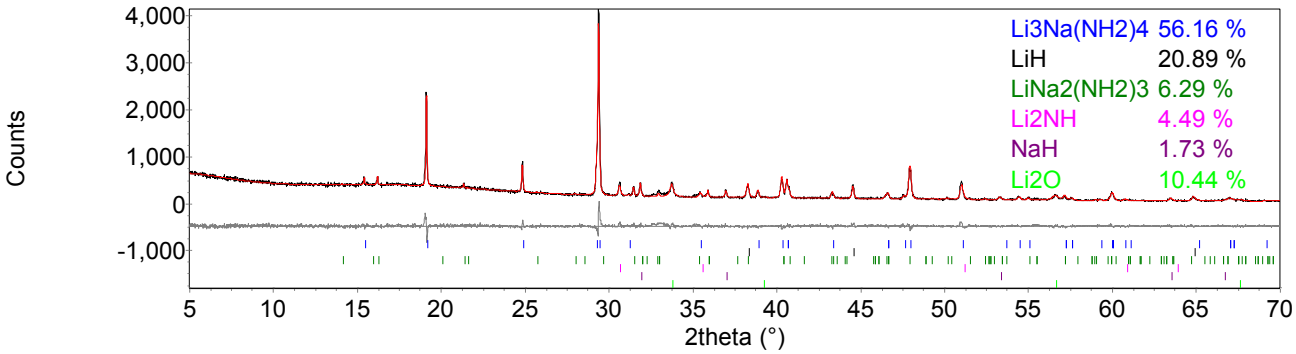

Figure 3-12 Powder XRD pattern of $Li_3Na(NH_2)_4$ + 5LiH, heated to 150 °C for 24 hours on flowing line. The observed powder XRD pattern (black line) was fitted using a Rietveld fit (red line) to the observed phases $Li_3Na(NH_2)_4$ (blue tick marks), LiH (black tick marks), $LiNa_2(NH_2)_3$ (green tick marks), Li_2NH (pink tick marks), NaH (purple tick marks) and Li_2O (light green tick marks). R_{wp} = 8.627, R_{exp} = 6.411, X^2 = 1.8.

$Li_3Na(NH_2)_4$ + 5LiH was heated to 200 °C for 12 (Figure 3-13) and 24 hours. The products for both were the same: $LiNH_2$, Li_2NH and NaH, along with remaining $Li_3Na(NH_2)_4$ and LiH.

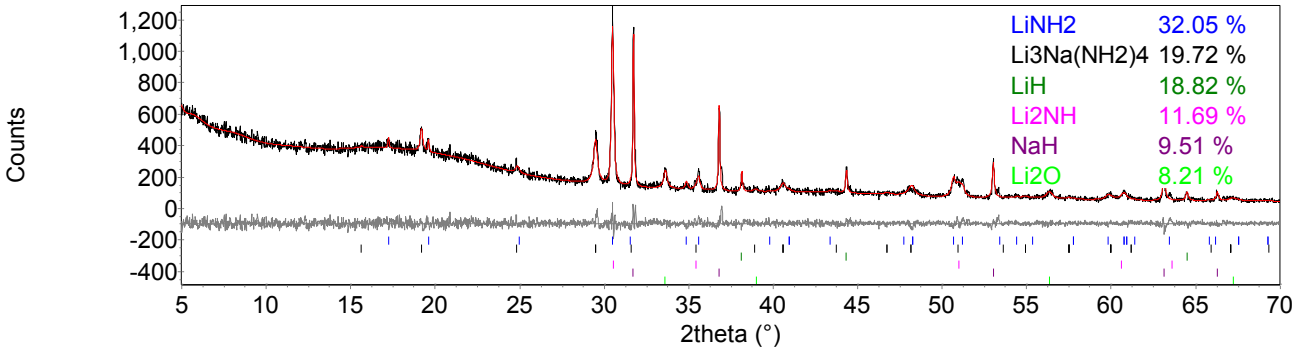

Figure 3-13 Powder XRD pattern of $Li_3Na(NH_2)_4$ + 5LiH, heated to 200 °C for 12 hours on flowing line. The observed powder XRD pattern (black line) was fitted using a Rietveld fit (red line) to the observed phases $Li_3Na(NH_2)_4$ (blue tick marks), LiH (black tick marks), Li_2NH (green tick marks), $LiNa_2(NH_2)_3$ (pink tick marks), NaH (purple tick marks) and Li_2O (light green tick marks). R_{wp} = 8.231, R_{exp} = 6.881, X^2 = 1.4.

After heating to 250 °C, there was still a mix of $LiNH_2$ and Li_2NH present (Figure 3-14) alongside NaH. There was also LiH present, but this was a smaller amount than observed after reaction at 200 °C. $Li_3Na(NH_2)_4$ was no longer present at 250 °C. Between 200 and 250 °C the most significant hydrogen desorption started (Figure 3-8).

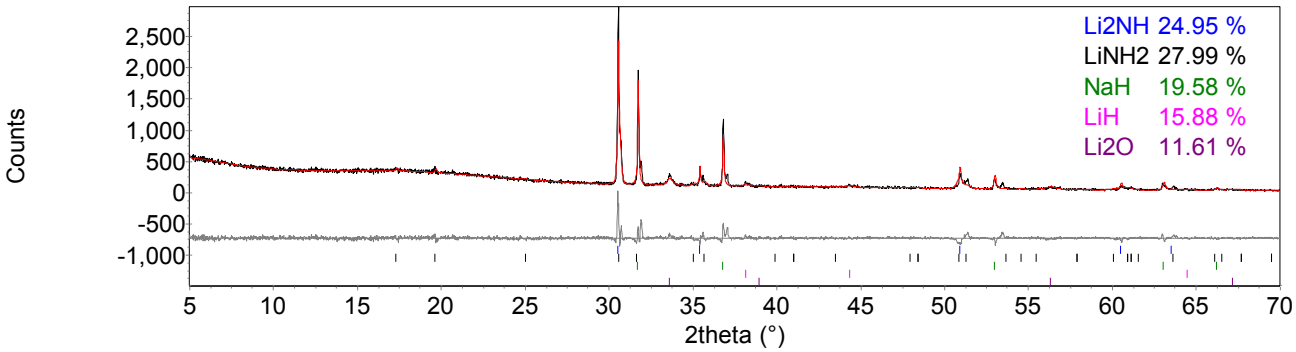

Figure 3-14 Powder XRD pattern of $Li_3Na(NH_2)_4$ + 5LiH, heated to 250 °C for 12 hours on flowing line. The observed powder XRD pattern (black line) was fitted using a Rietveld fit (red line) to the observed phases Li_2NH (blue tick marks), $LiNH_2$ (black tick marks), NaH (green tick marks), LiH (pink tick marks) and Li_2O (purple tick marks). R_{wp} = 11.734, R_{exp} = 7.161, X^2 = 2.7.

After heating to 300 °C for 12 hours the imide forming reaction had gone to completion and only Li_2NH, NaH and Li_2O were present in the products (Equation 3-8 and Figure 3-15).

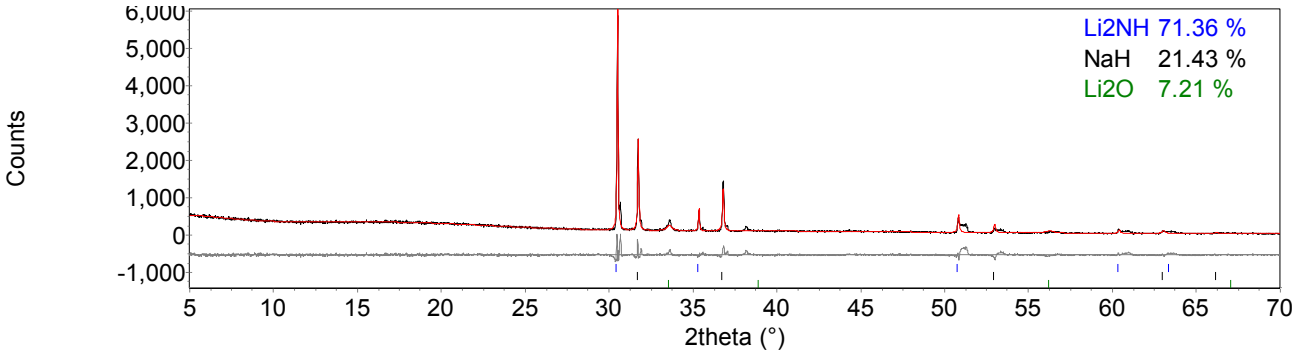

Figure 3-15 Powder XRD pattern of $Li_3Na(NH_2)_4$ + 5LiH, heated to 300 °C for 12 hours on flowing line. The observed powder XRD pattern (black line) was fitted using a Rietveld fit (red line) to the observed phases Li_2NH (blue tick marks), NaH (black tick marks) and Li_2O (green tick marks). R_{wp} = 13.758, R_{exp} = 7.051, X^2 = 3.8.

The starting materials were then heated to 350 °C for 12 hours. The majority products were Li_2NH and NaH as for 300 °C, but with the addition of Na from the decomposition NaH (Equation 3-7).

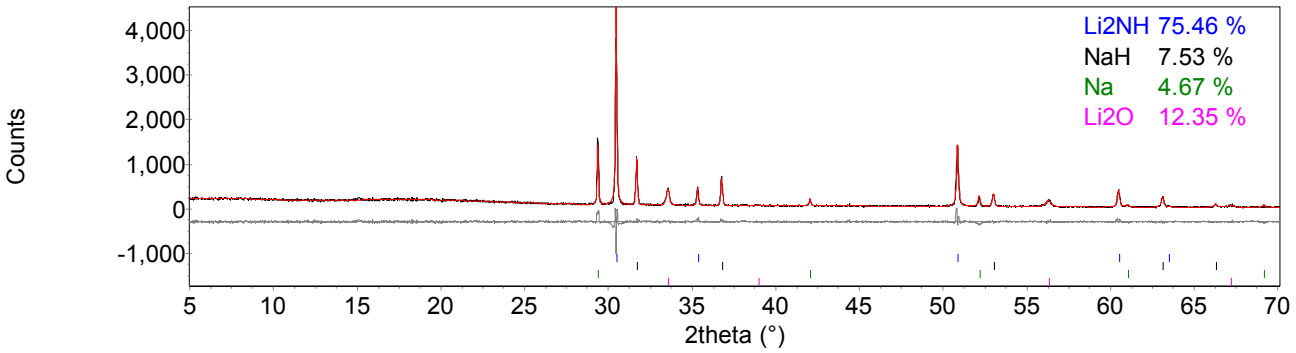

Figure 3-16 Powder XRD pattern of $Li_3Na(NH_2)_4$ + 5LiH, heated to 350 °C for 12 hours on flowing line. The observed powder XRD pattern (black line) was fitted using a Rietveld fit (red line) to the observed phases Li_2NH (blue tick marks), NaH (black tick marks), Na (green tick marks) and Li_2O (pink tick marks). R_{wp} = 11.404, R_{exp} = 8.461, X^2 = 1.8.

The full reaction can be described as:

Equation 3-9 $2Li_3Na(NH_2)_4 + 10LiH \rightarrow 8Li_2NH + (2-x)NaH + xNa + (8+½x)H_2$

4. *Rehydrogenation*

The products from $Li_3Na(NH_2)_4$ + 5LiH heated at 350 °C for 12 hours (Figure 3-16) were subjected to rehydrogenation in order to establish whether the reaction was reversible. After heating the previously formed products [Li_2NH and NaH] under hydrogen gas at 100 bar, 200 °C for 48 hours, the new, post-hydrogenation products were examined by XRD and found to be $LiNH_2$, LiH and NaH (present before hydriding) (Figure 3-17).

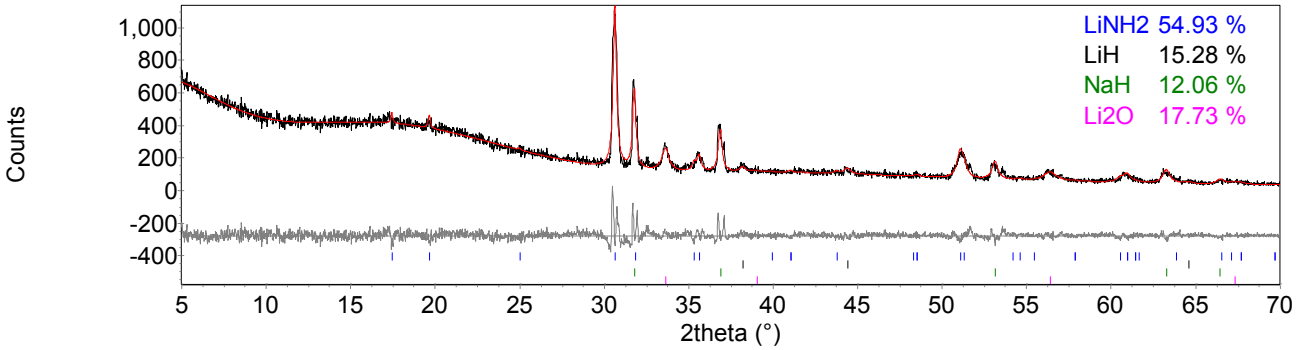

Figure 3-17 Powder XRD pattern of products from $Li_3Na(NH_2)_4$ + 5LiH (heated to 350 °C, 12 hours) rehydrogenated under 200 °C, 100 bar H_2, 48 hours. The observed powder XRD pattern (black line) was fitted using a Rietveld fit (red line) to the observed phases $LiNH_2$ (blue tick marks), LiH (black tick marks), NaH (green tick marks) and Li_2O (pink tick marks). R_{wp} = 9.430, R_{exp} = 6.724, X^2 = 2.0.

5. *Discussion*

From Figure 3-8, it was shown that up to 240 °C there was slow but significant hydrogen desorption. At these temperatures it would be unlikely Li_2NH would form due to a reaction

between $LiNH_2$ and LiH as this known not to occur below 275 °C under these conditions (Equation 3-10). An alternative reason for the hydrogen release could be the diffusion of Li^+ ions, from LiH, into $Li_3Na(NH_2)_4$ and H^+ diffusing out. The H^+ diffusing out could combine with the H^- remaining from LiH, forming H_2. This would result in '$Li_{3+x}Na(NH_2)_{4-x}NH_x$' forming along with H_2. When x = 2½, $Li_{5½}Na(NH_2)_{1½}(NH)_{2½}$ would be formed. This can be rewritten as $5Li_2NH + LiNa_2(NH_2)_3$. As this diffusion process was likely to be slow, this would account for the small amount of H_2 desorbed and also the small amount of $LiNa_2(NH_2)_3$ formed. The wt% calculated by Topas of the Li_2NH and $LiNa_2(NH_2)_3$ were found to be in a 5:1 mole ratio (Figure 3-12). Although the amount of hydrogen appeared small (0.2 wt%), it was very much below the temperature of hydrogen desorption traditionally attributed to amide-hydride hydrogen release of about 300 °C.

The presence of $LiNH_2$ as well as Li_2NH within the products after heating the starting materials to 200 °C suggested that a second pathway may be present. Significant hydrogen release from this reaction was observed under these conditions from 225 °C.

Equation 3-10 $LiNH_2 + LiH \rightarrow Li_2NH + H_2$

The presence of $LiNH_2$ may have resulted from a metathesis occurring between the $Li_3Na(NH_2)_4$ and LiH. If Li^+ were to diffuse into $Li_3Na(NH_2)_4$ (as before) and Na^+ were to diffuse out and combine with H^- (from LiH), the products would be $LiNH_2$ and NaH. Obviously Na^+ is much larger than H^+; therefore the rate of diffusion was likely to be much slower than the other suggested pathway at 150 °C whereas any increase in temperature would also assist the diffusion of Na^+ out of $Li_3Na(NH_2)_4$. The structural similarity between $Li_3Na(NH_2)_4$ and

$LiNH_2$ (both tetragonal with space group *I*-4) may cause a topotactic reaction to occur between them. The N atoms would remain in the same place and Li^+ and Na^+ ions would diffuse around them. This would aid the ease of which Li^+ and Na^+ can diffuse into and out of the structure respectively.

The main desorption would most likely to be due to the formation of Li_2NH from $LiNH_2$. In forming Li_2NH, NH_3 is also desorbed. The NH_3 then reacts with LiH forming more $LiNH_2$ (this reaction is known to be ultra-fast[5]). This would continue until all the LiH was exhausted (Equation 3-11). This reaction uses up the excess LiH present.

Equation 3-11 $LiNH_2 \rightarrow ½Li_2NH + ½NH_3 \rightarrow ½NH_3 + ½LiH \rightarrow ½LiNH_2$

An overall reaction scheme is shown in Table 3-3. This shows the temperatures at which each product was formed.

Table 3-3 Overall reaction scheme $Li_3Na(NH_2)_4$ + 5LiH of heated to various temperatures. The products from each temperature are shown.

Temp/ °C	*Reaction Scheme*	*Products*	
Onset of heating–235	$2Li_3Na(NH_2)_4 + 2½Li^+ – H^+ \rightarrow$	$2Li_{5½}Na(NH_2)_{1½}(NH)_{2½}, H_2 \rightarrow$	$5Li_2NH$, $LiNa_2(NH_2)_3$
150–235	$Li_3Na(NH_2)_4 + Li^+ – Na^+ \rightarrow$	$Li_4(NH_2)_4$, NaH →	$4LiNH_2$, NaH
225–315	$LiNH_2$ + LiH →	Li_2NH, H_2	
350	NaH →	Na, H_2	

The products present after rehydriding were $LiNH_2$ and LiH along with NaH that was present before. The method for the main hydrogen desorption from $Li_3Na(NH_2)_4$ + 5LiH was one of

Li^+ diffusion into $Li_3Na(NH_2)_4$ and Na^+ diffusion out. Due to the stability of $LiNH_2$ and NaH, it would be unlikely to be thermodynamically preferable to reform $Li_3Na(NH_2)_4$ by reverse diffusion and only the rehydrogenation of the individual products to their fully hydrogenated state was possible (Equation 3-12).

Equation 3-12 $4Li_2NH + Na + 4½H_2 \rightarrow 4LiNH_2 + 4LiH + NaH$

5. $Li_3Na(NH_2)_4 + 3LiH$

In order to clarify the pathways of the reactions occurring within the dehydrogenation of $Li_3Na(NH_2)_4 + 5LiH$, $Li_3Na(NH_2)_4 + 3LiH$ was investigated at 350 °C.

Heating to 350 °C for 12 hours under argon produced the powder XRD pattern shown in Figure 3-18. The products were Li_2NH, $LiNa_2(NH_2)_3$, Na and NaH. These products back up the results from $Li_3Na(NH_2)_4 + 4LiH$ in that $LiNa_2(NH_2)_3$ was formed if not enough LiH was present. We can presume both mechanisms discussed above are at work here as $LiNa_2(NH_2)_3$ and NaH/Na were both present, although much more $LiNa_2(NH_2)_3$ was present than NaH/Na. This indicated the Li^+/H^+ diffusion may predominate, due to the lack of LiH available to diffuse at higher temperatures.

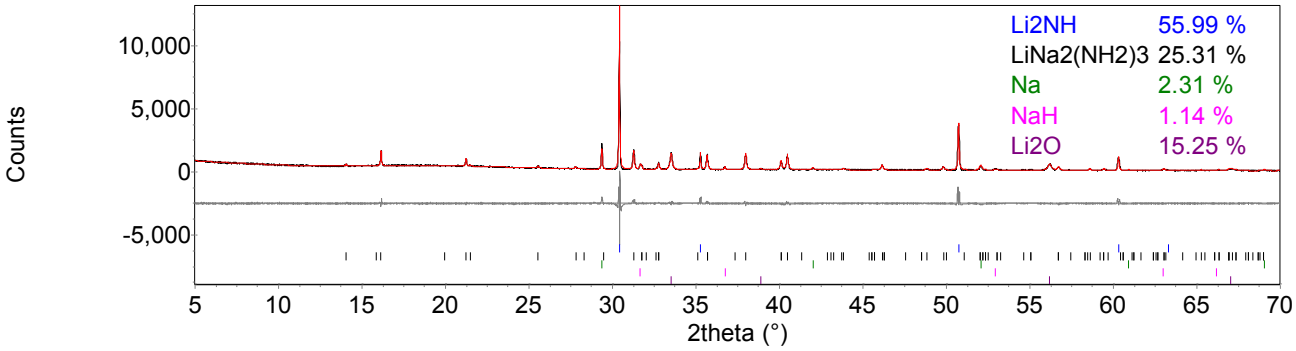

Figure 3-18 Powder XRD pattern of $Li_3Na(NH_2)_4$ + 3LiH, heated to 350 °C for 12 hours on flowing line. The observed powder XRD pattern (black line) was fitted using a Rietveld fit (red line) to the observed phases Li_2NH (blue tick marks), $LiNa_2(NH_2)_3$ (black tick marks), Na (green tick marks), NaH (pink tick marks) and Li_2O (purple tick marks). R_{wp} = 12.337, R_{exp} = 5.436, X^2 = 5.2.

6. $Li_3Na(NH_2)_4$ + 4NaH

$Li_3Na(NH_2)_4$ was heated with NaH (Sigma-Aldrich, 95%) in a 1:4 ratio. This ratio was chosen in order to react one mole of amide with one mole of hydride, as with the $LiNH_2$-LiH system.

1. Temperature Programmed Desorption-Mass Spectrometry

The reaction was carried out on a TPD-MS apparatus at a heating rate of 2 °C min^{-1} up to 350 °C (Figure 3-19). The TPD-MS trace showed a small amount of H_2 was desorbed from this reaction. No other gases were desorbed during heating. The release of hydrogen started soon after heating was started, 60 °C. At 160 °C the rate at which hydrogen was desorbed increased rapidly. This desorption peaked at 195 °C and then rapidly fell away to background hydrogen desorption levels. At 300 °C the rate of desorption increased again. This peaked at 350 °C before decreasing as isothermal heating took place. In the furnace power at 190 °C there was a very small endotherm; this coincided with the peak of the first hydrogen

desorption. The comparison between this hydrogen desorption and that of $Li_3Na(NH_2)_4$ + 4LiH, $Li_3Na(NH_2)_4$ + 5LiH and $Li_3Na(NH_2)_4$ + $2MgH_2$ is shown in Figure 3-8.

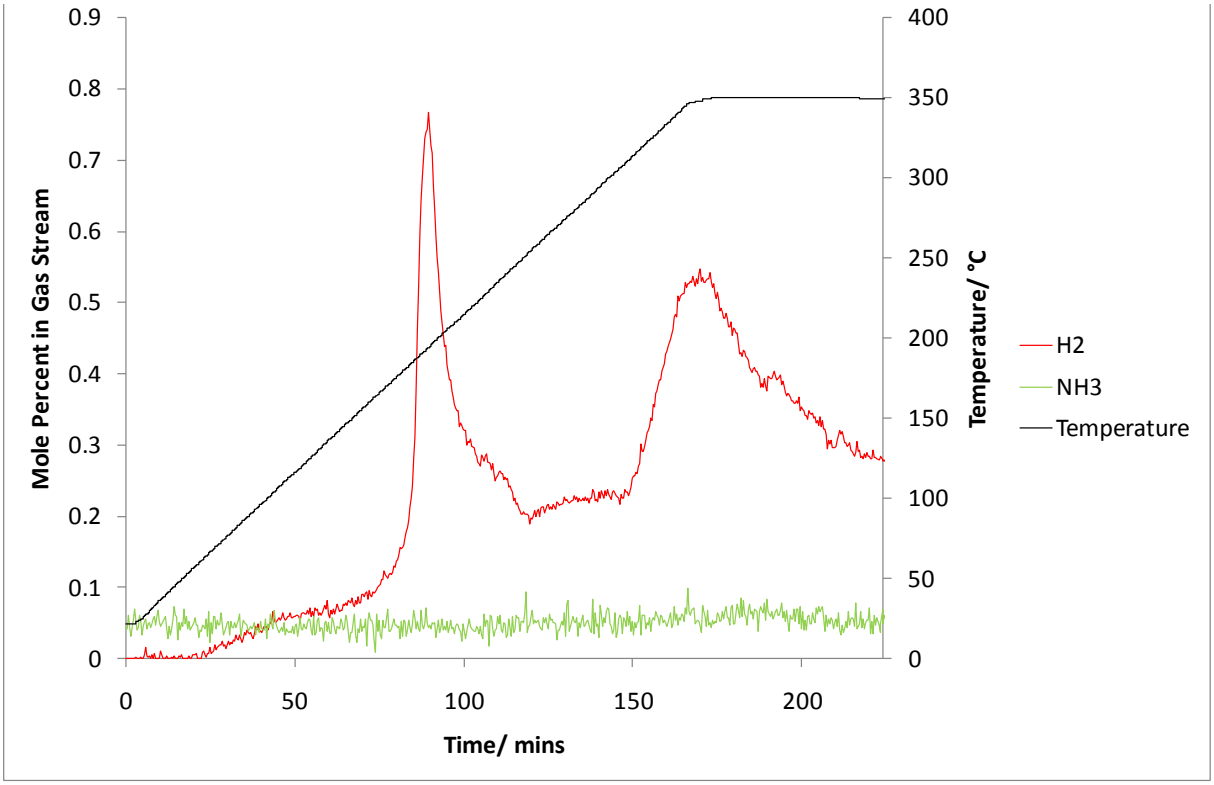

Figure 3-19 TPD-MS analysis of the $Li_3Na(NH_2)_4$ + 4NaH reaction. The temperature trace is shown in black and the mole percents of H_2 and NH_3 released are shown in red and green respectively.

2. *Flowing Line Reactions*

The reaction was then heated up to intermediate temperatures in an attempt to establish the pathway for desorption. $Li_3Na(NH_2)_4$ + 4NaH was first heated up to 150 °C for 12 hours and the products analysed using powder XRD (Figure 3-20). The products from this reaction were newly formed $NaNH_2$ and $LiNa_2(NH_2)_3$ and a large amount of Li_2O, as well as $Li_3Na(NH_2)_4$ and NaH starting materials.

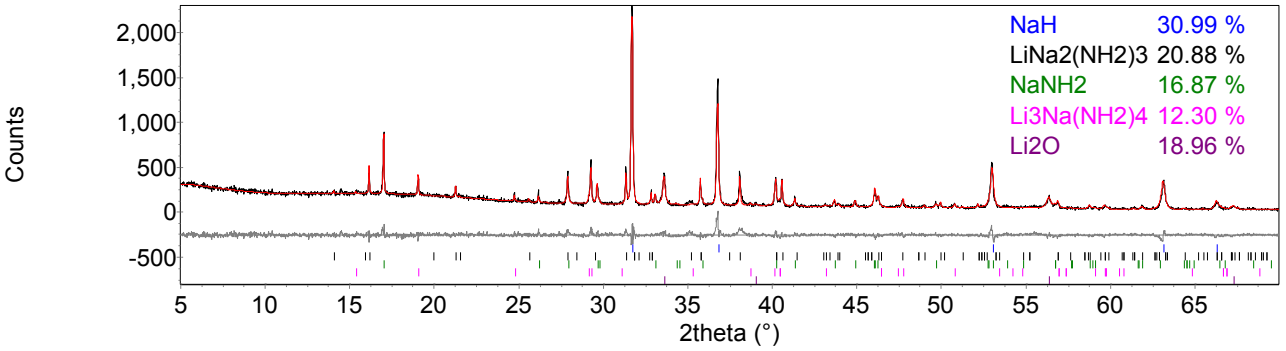

Figure 3-20 Powder XRD pattern of $Li_3Na(NH_2)_4$ + 4NaH, after heating 150 °C for 12 hours. The observed powder XRD pattern (black line) was fitted using a Rietveld fit (red line) to the observed phases NaH (blue tick marks), $LiNa_2(NH_2)_3$ (black tick marks), $NaNH_2$ (green tick marks), $Li_3Na(NH_2)_4$ (pink tick marks) and Li_2O (purple tick marks). R_{wp} = 11.379, R_{exp} = 8.587, X^2 = 1.8.

The products after heating the starting materials to 250 °C were $LiNa_2(NH_2)_3$ and $NaNH_2$ as for heating to 150 °C, along with the continued presence of NaH and Li_2O (Figure 3-21). There was a hydrogen desorption at 200 °C, but no hydrogen deficient species were present upon heating to 250 °C. (Although in the context of other desorptions, this one was very small, 0.5 wt%)

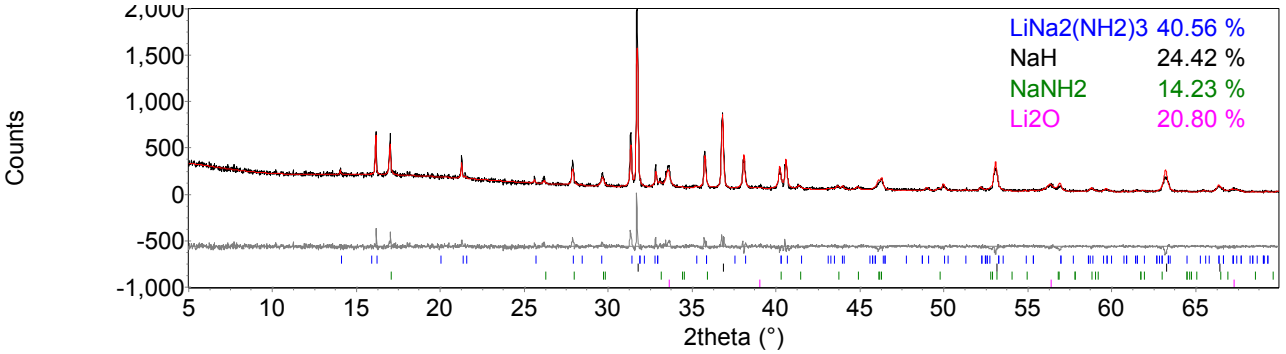

Figure 3-21 Powder XRD pattern of $Li_3Na(NH_2)_4$ + 4NaH, after heating 250 °C for 12 hours. The observed powder XRD pattern (black line) was fitted using a Rietveld fit (red line) to the observed phases $LiNa_2(NH_2)_3$ (blue tick marks), NaH (black tick marks), $NaNH_2$ (green tick marks) and Li_2O (pink tick marks). R_{wp} = 12.116, R_{exp} = 8.799, X^2 = 1.9.

The starting materials were heated together to 350 °C for 20 minutes. The products after analysing using powder XRD were $LiNa_2(NH_2)_3$ and a very small amount of sodium metal (Figure 3-22) and remaining starting materials. It was clear that starting materials were still present, particularly NaH.

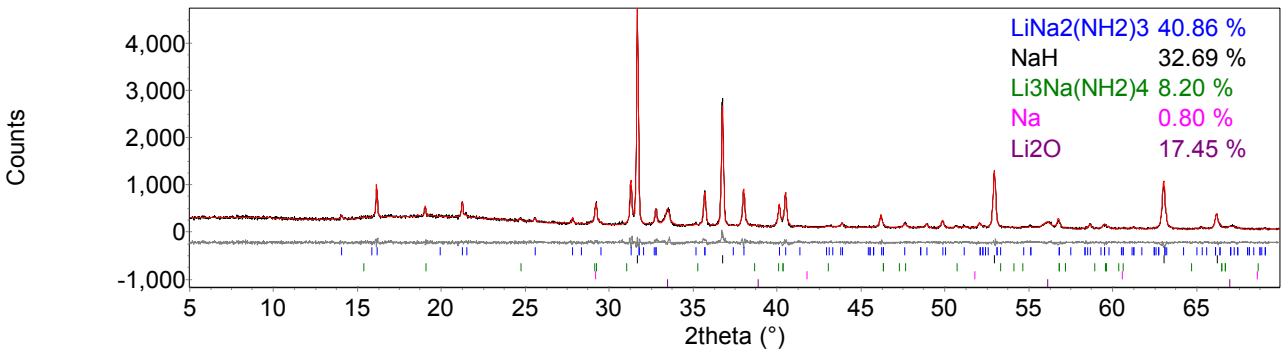

Figure 3-22 Powder XRD pattern of $Li_3Na(NH_2)_4$ + 4NaH, after heating 350 °C for 20 minutes. The observed powder XRD pattern (black line) was fitted using a Rietveld fit (red line) to the observed phases $LiNa_2(NH_2)_3$ (blue tick marks), NaH (black tick marks), $Li_3Na(NH_2)_4$ (green tick marks), Na (pink tick marks) and Li_2O (purple tick marks). R_{wp} = 8.217, R_{exp} = 6.613, X^2 = 1.5.

After heating to 350 °C for 12 hours the products were $NaNH_2$, $LiNa_2(NH_2)_3$ Na and a small amount of NaH (starting material) (Figure 3-23). The Na present was most likely from the decomposition of NaH (Equation 3-7).

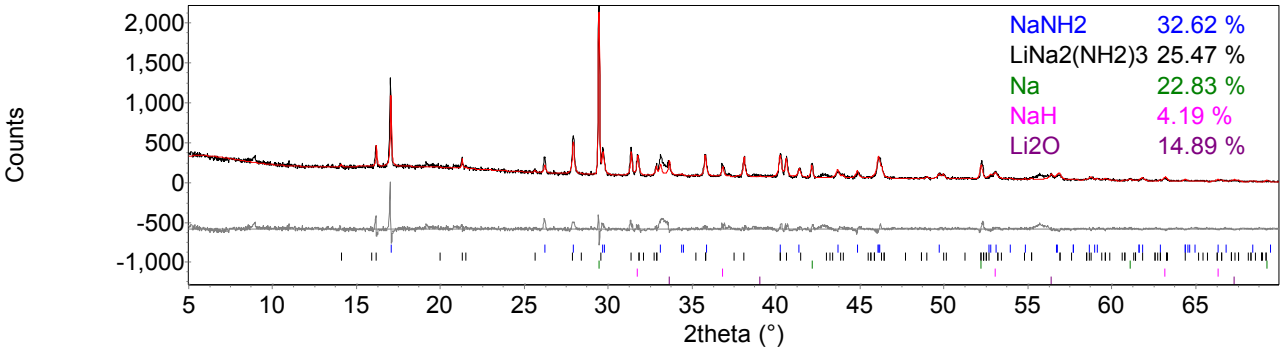

Figure 3-23 Powder XRD pattern of $Li_3Na(NH_2)_4$ + 4NaH, after heating 350 °C for 12 hours. The observed powder XRD pattern (black line) was fitted using a Rietveld fit (red line) to the observed phases $NaNH_2$ (blue tick marks), $LiNa_2(NH_2)_3$ (black tick marks), Na (green tick marks), NaH (pink tick marks) and Li_2O (purple tick marks). R_{wp} = 15.245, R_{exp} = 8.631, X^2 = 3.1.

3. Discussion

The amount of $Li_3Na(NH_2)_4$ starting material had decreased after heating to 150 °C and exhausted by 250 °C. Its presence at 350 °C, upon heating for 20 minutes, was most probably due to the reaction time shortened. $NaNH_2$ was present upon heating for 12 hours at 150, 250 and 350 °C, but not heated for 20 minutes at 350 °C. This indicated the $NaNH_2$ required hours in which to form. The $NaNH_2$ may have been formed from the $Li_3Na(NH_2)_4$, therefore explaining the inverse relationship between their presence in the products.

NaH was present up to 350 °C when it was found to decompose to Na metal and hydrogen gas (Equation 3-7). It appeared that all the NaH did not partake in the reaction and merely decomposed to Na when the reaction temperature was high enough. This would coincide with the second hydrogen desorption in Figure 3-19.

It could be tentatively suggested that the oxidation of $Li_3Na(NH_2)_4$ could form Li_2O and $LiNa_2(NH_2)_3$. If the Li^+ from $Li_3Na(NH_2)_4$ were to diffuse out in order to form Li_2O and Na^+ from NaH were to diffuse into $Li_{3-x}Na_{1+x}(NH_2)_4$, when x = 2, $LiNa_3(NH_2)_4$ would form. This can

be rewritten as $LiNa_2(NH_2)_3 + NaNH_2$. The remaining NaH would then go on to decompose to its constituent elements (Equation 3-7). An overall equation for the products is suggested in Equation 3-13.

Equation 3-13 when $x = 2$;

$$Li_{3-x}Na_{1+x}(NH_2)_4 + (4-x)NaH + x/4O_2 \rightarrow LiNa_3(NH_2)_4 + 2NaH + x/2Li_2O + H_2$$

$$\rightarrow LiNa_2(NH_2)_3 + NaNH_2 + (2-y)NaH + yNa + x/2Li_2O + (1+½y)H_2$$

The reaction gave a hydrogen loss of 0.5 wt%. If only NaH was responsible for the hydrogen desorbed then there was a theoretical mass loss of 2.0 wt% H_2.

7. $Li_3Na(NH_2)_4 + 2MgH_2$

$Li_3Na(NH_2)_4$ was heated with MgH_2 (Alfa Aesar, 98%) in a 1:2 ratio. This ratio was used in order to keep the amide and hydride in a 1:1 ratio.

1. *Temperature Programmed Desorption-Mass Spectrometry*

$Li_3Na(NH_2)_4 + 2MgH_2$ was first examined on a TPD-MS apparatus at a heating rate of 2 °C min^{-1} up to 350 °C. In Figure 3-24, it can be seen that hydrogen was the predominant gas desorbed, but a very small amount of ammonia also appeared to be released. The hydrogen desorption started at a slow rate at 115 °C. The rate increased steeply at 180 °C. The desorption peaked quickly at 215 °C and slowly dropped whilst maintaining a broad desorption. The desorption dropped back to almost background levels by 350 °C, although a small tail of desorption continued to be observed. At 215 °C there was a fluctuation in the

temperature trace. When comparing the temperature trace to the furnace power it can be seen there was a drop in power followed by a rise at the same temperature (Figure 3-25). The mass loss on heating $Li_3Na(NH_2)_4 + 2MgH_2$ for 300 minutes was calculated to be 2.8 wt%. The products after heating $Li_3Na(NH_2)_4 + 2MgH_2$ to 350 °C on the TPD-MS apparatus were α-$Li_2Mg(NH)_2$, β-$Li_2Mg(NH)_2$ and Na as well as some unidentified peaks (Figure 3-26). The comparison between this hydrogen desorption and that of $Li_3Na(NH_2)_4 + 4LiH$, $Li_3Na(NH_2)_4 + 5LiH$ and $Li_3Na(NH_2)_4 + 4NaH$ is shown in Figure 3-8.

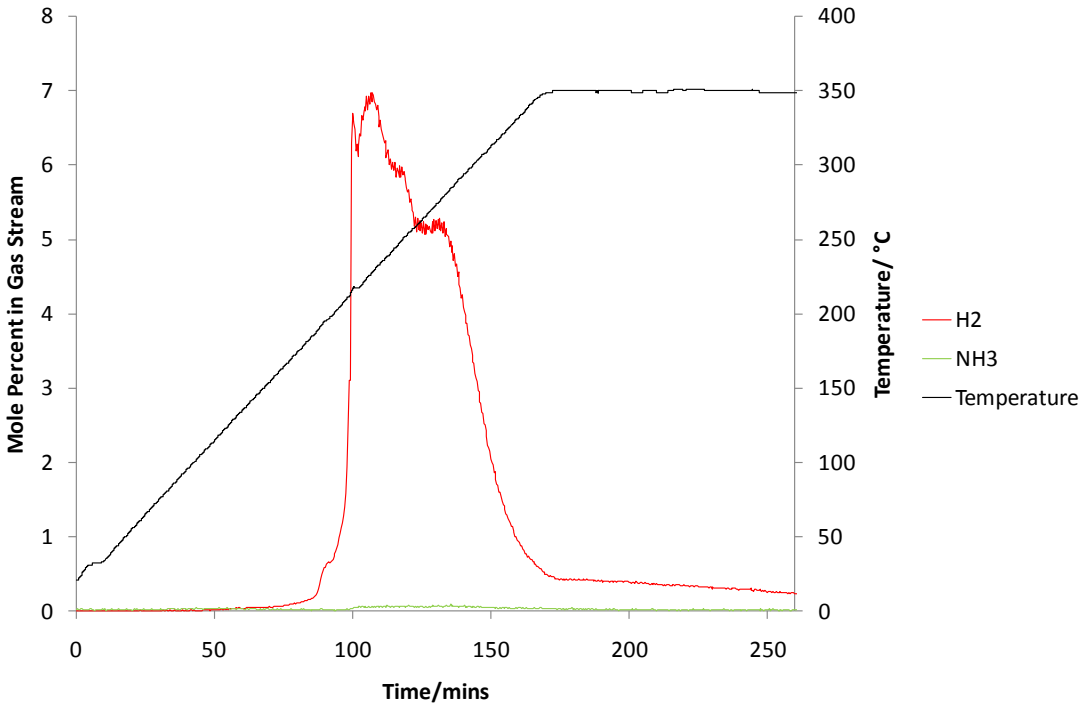

Figure 3-24 TPD-MS analysis of $Li_3Na(NH_2)_4 + 2MgH_2$. The temperature trace is shown in black and the mole percentages of H_2 and NH_3 released are shown in red and green respectively.

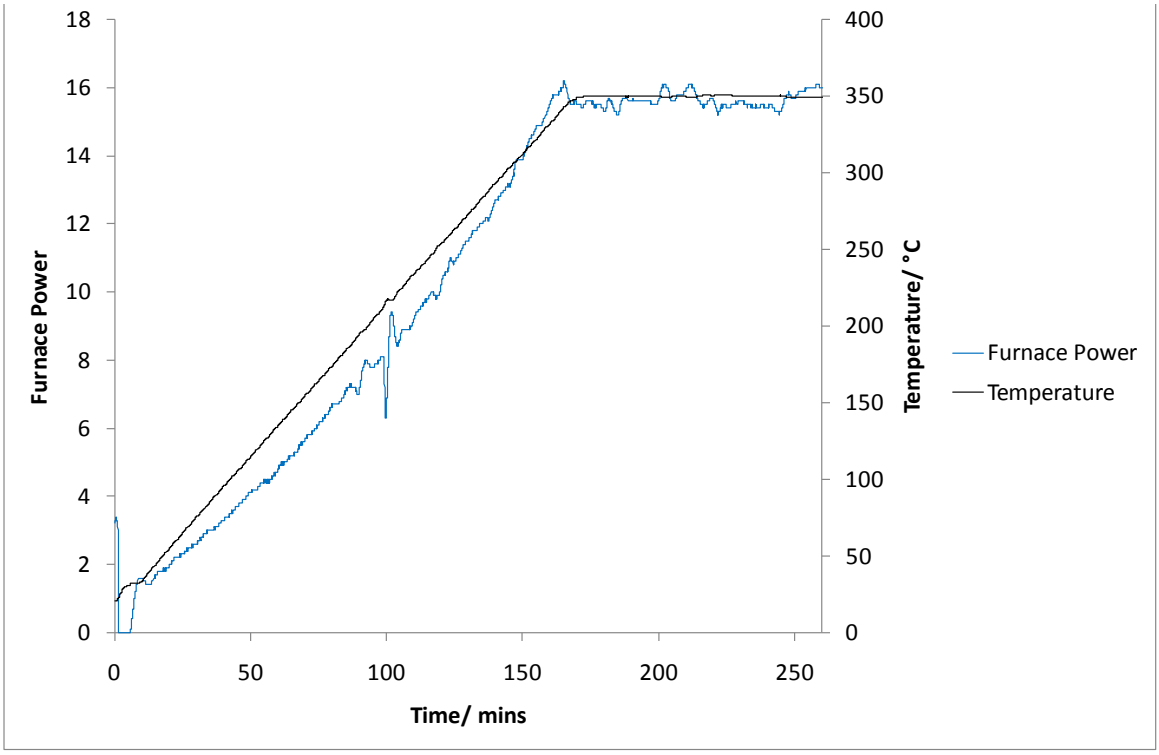

Figure 3-25 Furnace power during the TPD-MS analysis of $Li_3Na(NH_2)_4$ + $2MgH_2$. The furnace power and temperature are shown in blue and black respectively.

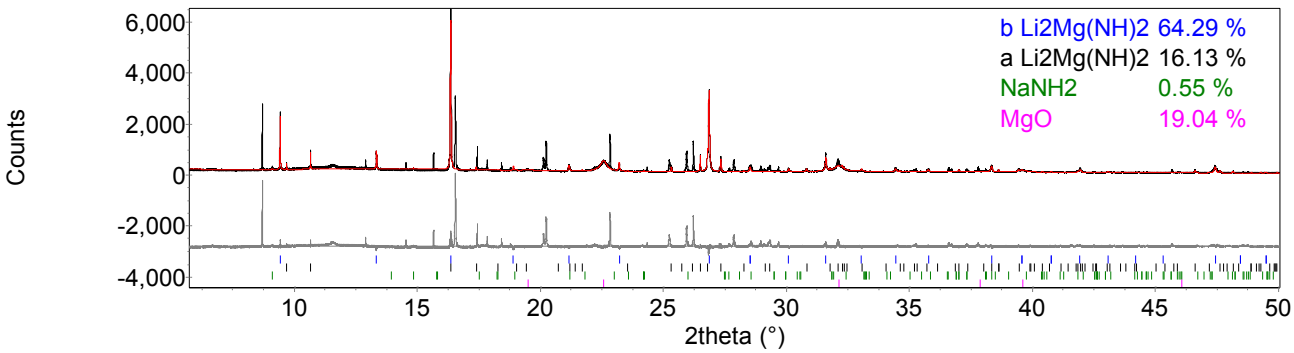

Figure 3-26 Powder XRD pattern of $Li_3Na(NH_2)_4$ + $2MgH_2$, heated to 350 °C on a TPD-MS apparatus. The observed powder XRD pattern (black line) was fitted using a Rietveld fit (red line) to the observed phases *β*-$Li_2Mg(NH)_2$ (blue tick marks), *α*-$Li_2Mg(NH)_2$ (black tick marks), $NaNH_2$ (green tick marks) and MgO (pink tick marks). R_{wp} = 28.531, R_{exp} = 7.457, X^2 = 14.6.

2. *Flowing Line Reactions*

The reaction was then carried out at 300 °C for 12 hours on a flowing line. The products from this reaction were *α*-$Li_2Mg(NH)_2$ and NaH as well as the same unidentified peaks as present

after TPD-MS, but in a smaller amount (Figure 3-27). The reaction was then carried out at 350 °C for 20 minutes (Figure 3-28) and repeated for 12 hours (Figure 3-29). The products at 350 °C after 20 minutes were the same as for 300 °C heated for 12 hours, with the addition of some Li_2NH and $NaNH_2$ (Figure 3-28). α-$Li_2Mg(NH)_2$ was the majority product in both reactions.

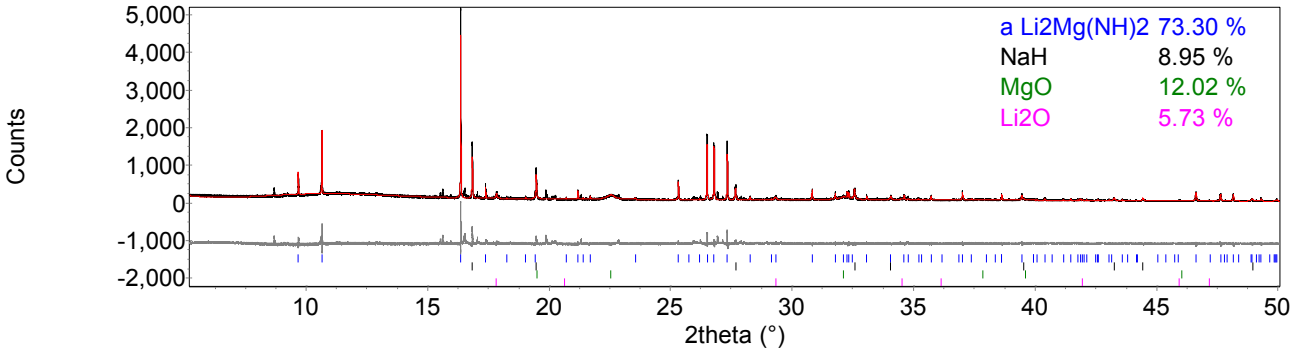

Figure 3-27 Powder XRD pattern of $Li_3Na(NH_2)_4$ + $2MgH_2$, heated to 300 °C for 12 hours on a flowing line under argon. The observed powder XRD pattern (black line) was fitted using a Rietveld fit (red line) to the observed phases α-$Li_2Mg(NH)_2$ (blue tick marks), NaH (black tick marks), MgO (green tick marks) and Li_2O (pink tick marks). R_{wp} = 18.841, R_{exp} = 9.101, X^2 = 4.3.

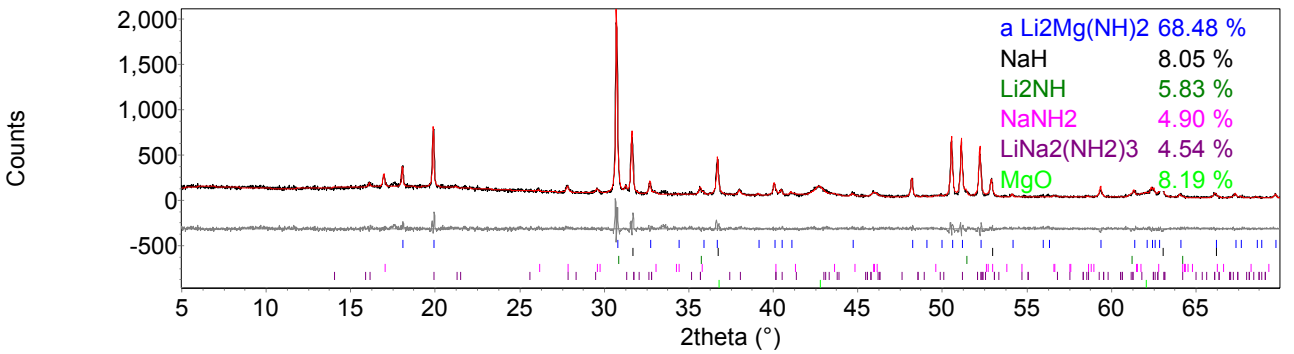

Figure 3-28 Powder XRD pattern of $Li_3Na(NH_2)_4$ + $2MgH_2$, heated to 350 °C for 20 minutes on a flowing line under argon. The observed powder XRD pattern (black line) was fitted using a Rietveld fit (red line) to the observed phases α-$Li_2Mg(NH)_2$ (blue tick marks), NaH (black tick marks), Li_2NH (green tick marks), $NaNH_2$ (pink tick marks), $LiNa_2(NH_2)_3$ (purple tick marks) and MgO (light green tick marks). R_{wp} = 13.052, R_{exp} = 9.791, X^2 = 1.8.

Upon heating $Li_3Na(NH_2)_4$ + $2MgH_2$ to 350 °C for 12 hours β-$Li_2Mg(NH)_2$ appeared as a product alongside a much smaller amount of α-$Li_2Mg(NH)_2$ (Figure 3-29). This was consistent with the post TPD XRD results.

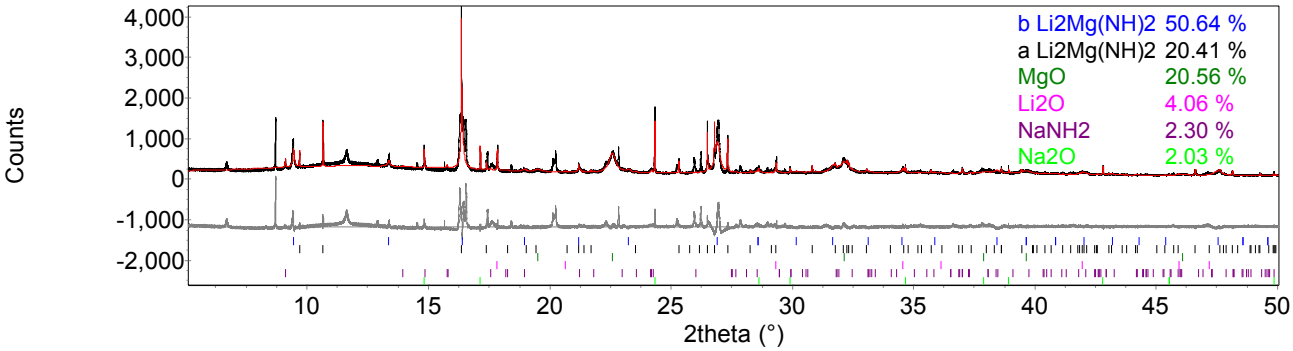

Figure 3-29 Powder XRD pattern of $Li_3Na(NH_2)_4$ + $2MgH_2$, heated to 350 °C for 12 hours on flowing line under argon. The observed powder XRD pattern (black line) was fitted using a Rietveld fit (red line) to the observed phases β-$Li_2Mg(NH)_2$ (blue tick marks), α-$Li_2Mg(NH)_2$ (black tick marks), $NaNH_2$ (green tick marks), Na_2O (pink tick marks), MgO (purple tick marks) and Li_2O (light green tick marks). R_{wp} = 17.386, R_{exp} = 7.315, X^2 = 3.7.

The starting materials were heated to 550 °C for 4 hours. The products were Li_2NH, Mg_3N_2 and β-$Li_2Mg(NH)_2$ (Figure 3-30).

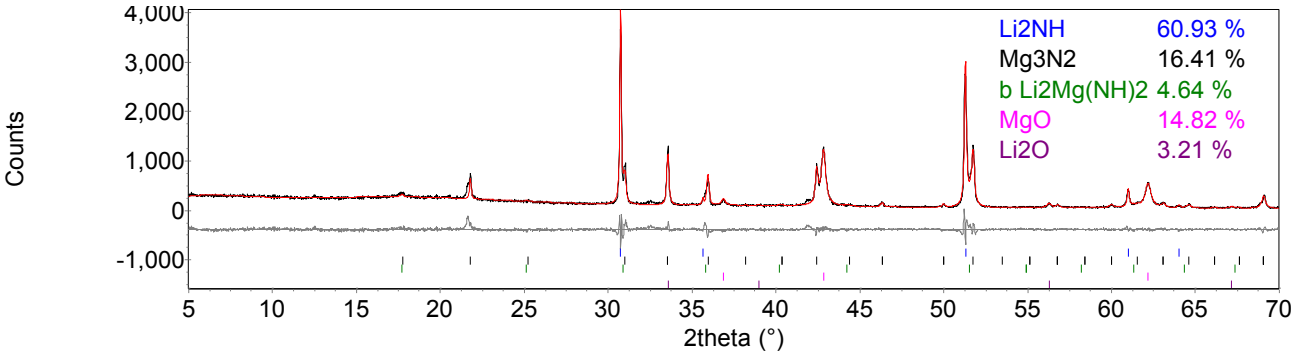

Figure 3-30 Powder XRD pattern of $Li_3Na(NH_2)_4$ + $2MgH_2$, heated to 550 °C for 4 hours on a flowing line under argon. The observed powder XRD pattern (black line) was fitted using a Rietveld fit (red line) to the observed phases Li_2NH (blue tick marks), Mg_3N_2 (black tick marks), *β*-$Li_2Mg(NH)_2$ (green tick marks), MgO (pink tick marks) and Li_2O (purple tick marks). R_{wp} = 11.416, R_{exp} = 7.001, X^2 = 2.7.

3. Discussion

The fluctuation in the temperature trace (Figure 3-24) accompanied by the drop in the furnace power followed quickly by a rise (Figure 3-25), was indicative of an exothermic event occurring in the sample. As this coincided with the hydrogen desorption peak the exotherm can be assigned to the sudden increase in loss of hydrogen. This is not ideal for a hydrogen storage medium as the hydrogen loss would need to be endothermic in order to be thermodynamically reversible.

The products from heating on a TPD-MS apparatus were *α*-$Li_2Mg(NH)_2$, *β*-$Li_2Mg(NH)_2$ and a very small amount of $NaNH_2$, as well as the unidentified peaks. The lack of sodium present in the known products implied sodium would be part of the compound(s) giving rise to the unidentified peaks. The lattice parameters of the mixed Li-Mg imides were as expected and so it appeared no partial substitution of sodium into the mixed Li-Mg imides had occurred.

The presence of *β*-$Li_2Mg(NH)_2$ at 350 °C Figure 3-29) was expected as *β*-$Li_2Mg(NH)_2$ transforms from *α*-$Li_2Mg(NH)_2$ at around 350 °C. The heating of the starting materials for

12 hours enabled β-$Li_2Mg(NH)_2$ to form, whereas heating at 350 °C for 20 minutes (Figure 3-28) was not prolonged enough for α-$Li_2Mg(NH)_2$ to transform.

The products after heating to 350 °C for 12 hours were consistent with those after heating on TPD-MS. The products after heating to 300 °C for 12 hours gave no $NaNH_2$, but there was NaH. After heating to 350 °C for 20 minutes there was the presence of both $NaNH_2$ and NaH and after prolonged heating for 12 hours, only NaH was present, with no $NaNH_2$. The longer heating time at 350 °C completed the conversion of $NaNH_2$ to NaH. This may not have been a direct conversion as no ammonia was seen to be desorbed (Figure 3-24).

The products after heating the sample to 550 °C for 4 hours were all identified and completely devoid of sodium. The other products: Li_2NH, Mg_3N_2 and β-$Li_2Mg(NH)_2$ were hydrogen deficient. A possible equation could be suggested (Equation 3-14). At heating to 550 °C it was possible that ammonia was desorbed (although we had no evidence for this as the TPD-MS was not carried out up to 550 °C). The lack of sodium present in the known products on heating to above 350 °C was most probably due to the NaH formed (Figure 3-28) decomposing to Na (Equation 3-7) and the Na metal then vaporising off.

Equation 3-14 $2Li_3Na(NH_2)_4 + 4MgH_2 \rightarrow 2Li_2NH + Li_2Mg(NH)_2 + 2Na + Mg_3N_2 + 7H_2 + 2NH_3$

Products from $Li_3Na(NH_2)_4 + 2MgH_2$ could be compared with those from $2LiNH_2 + MgH_2$. On heating $Li_3Na(NH_2)_4 + 2MgH_2$ up to 350 °C the known products were α-$Li_2Mg(NH)_2$, β-$Li_2Mg(NH)_2$, a small amount of $NaNH_2$ and hydrogen. In comparison, $2LiNH_2 + MgH_2$ heated to 350 °C gives the products of α-$Li_2Mg(NH)_2$ and β-$Li_2Mg(NH)_2$ and accompanied by hydrogen release.

The products are very similar to each other. The presence of sodium within the $Li_3Na(NH_2)_4$ + $2MgH_2$ reaction appeared to form $NaNH_2$ and be part of the compound(s) giving rise to the unidentified peaks. The lithium and magnesium form the mixed Li-Mg imide as if sodium was not present. The $NaNH_2$ had metathesised with both LiH and MgH_2 to form NaH (pages 82 and 152). This suggested that here the mixed Li-Mg imides were more stable than NaH.

8. $LiNa_2(NH_2)_3$ + 3LiH

$LiNa_2(NH_2)_3$ was originally heated with LiH in the ratio 1:3. This was in order to maintain a 1:1 ratio between amide and hydride- as with $LiNH_2$-LiH system.

1. *Temperature Programmed Desorption-Mass Spectrometry*

It can be seen from the TPD-MS data that only hydrogen was desorbed from the reaction (Figure 3-31). There was no evidence of ammonia desorption. There were two main hydrogen desorption regions. The lower temperature desorption started at about 50 °C with a slow release. An endothermic event occurred at 100 °C, although this was not reflected in the furnace power. Shortly after this, the rate of hydrogen desorption increased and formed an isolated desorption that decreased at 230 °C. There was a 'blip' in the desorption trace at 190 °C. This was present when the reaction was repeated. The fluctuation was accompanied by an exotherm in the temperature trace. Closer inspection of the furnace power (Figure 3-32) showed a drop in power followed by a rise. This confirmed the presence of an exothermic reaction in the sample. The main hydrogen desorption started at about 240 °C, peaking at 310 °C, before decreasing and then slowly tailing off. This was a much greater hydrogen desorption compared to the first desorption. At the peak of the hydrogen

desorption a small endotherm in the temperature trace was seen. This was confirmed by an increase in furnace power.

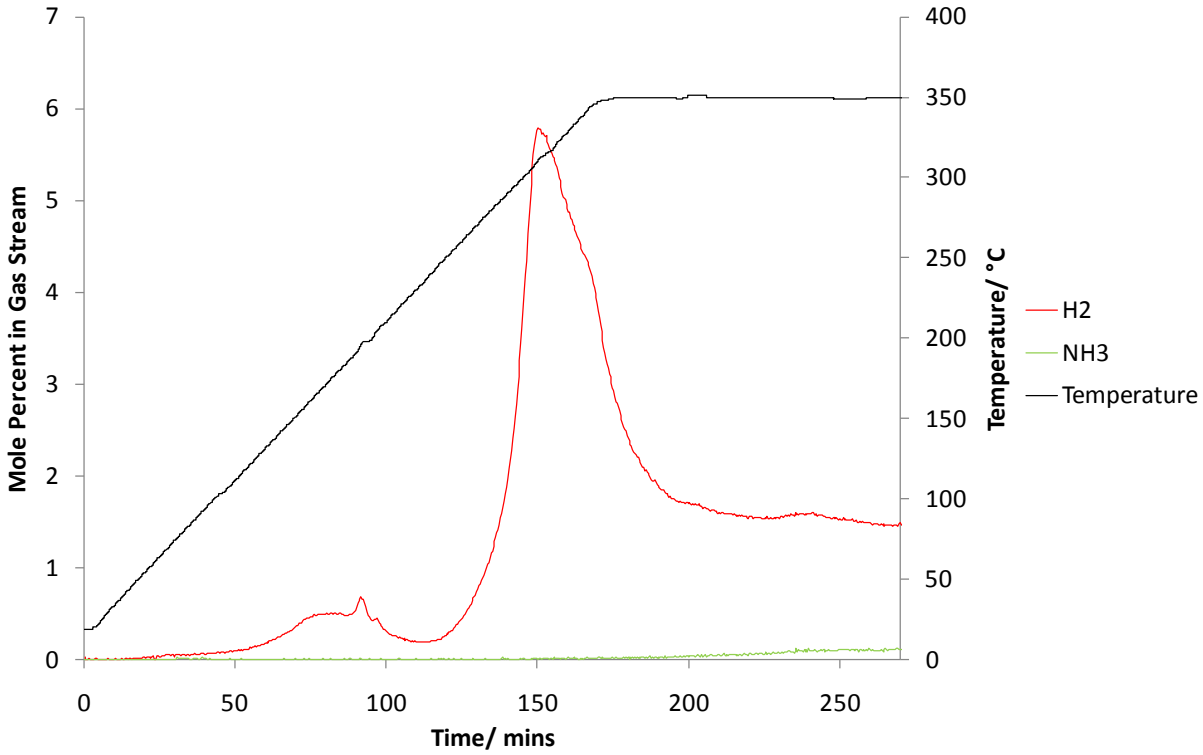

Figure 3-31 Thermal decomposition analysis of $LiNa_2(NH_2)_3$ + 3LiH in a TPD-MS apparatus. The temperature trace is shown in black and the mole percents of H_2 and NH_3 released are shown in red and green respectively.

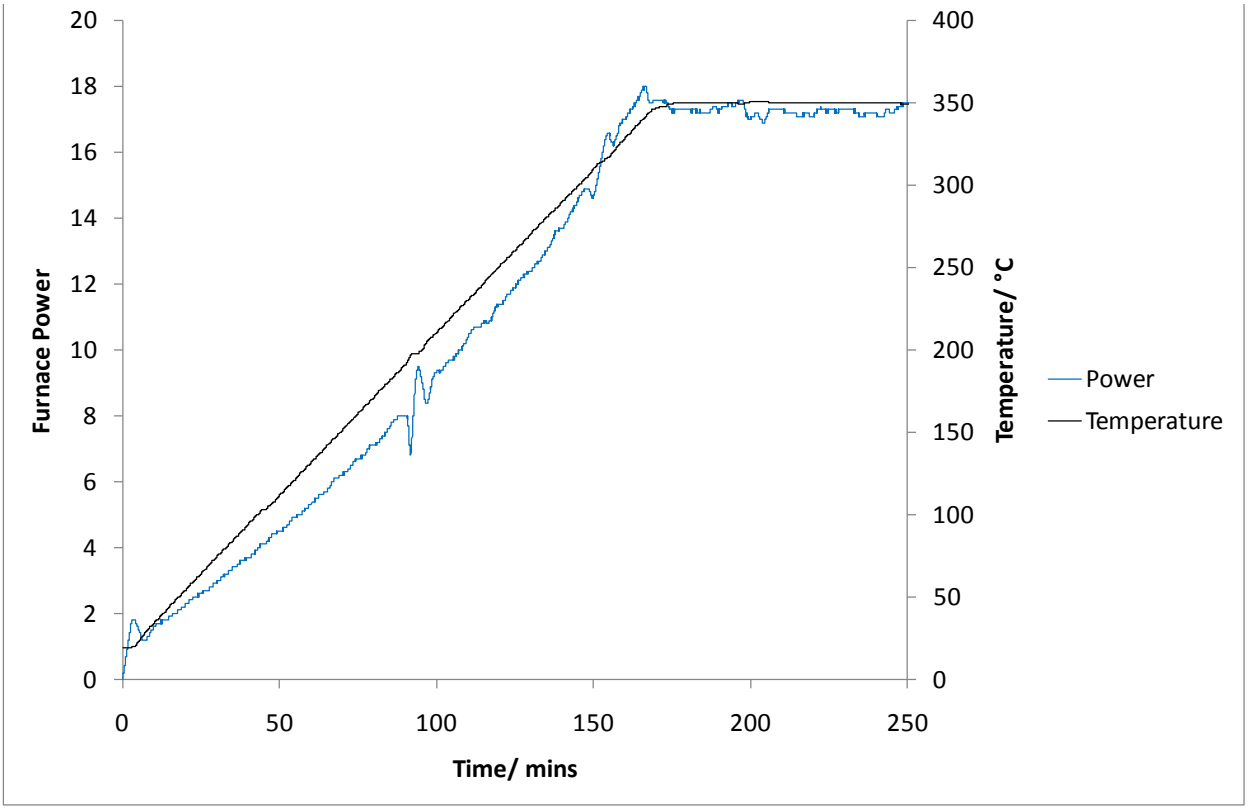

Figure 3-32 Furnace power during the TPD-MS analysis of $LiNa_2(NH_2)_3$ + 3LiH. The furnace power and temperature are shown in blue and black respectively.

The products after heating the reaction on TPD-MS were Li_2NH, $NaNH_2$, Na, a very small amount of NaH and remaining $LiNa_2(NH_2)_3$ starting material (Figure 3-33).

The equation for this reaction could be written as:

Equation 3-15 $LiNa_2(NH_2)_3 + 3LiH \rightarrow 2Li_2NH + NaNH_2 + (1\text{-}x)NaH + xNa + (2½+x)H_2$

A total of 3.3 wt% H_2 was desorbed in comparison to 4.0 wt% theoretically possible from this reaction when heated up to 350 °C for 300 minutes. This was the equivalent of 2 moles of H_2 released.

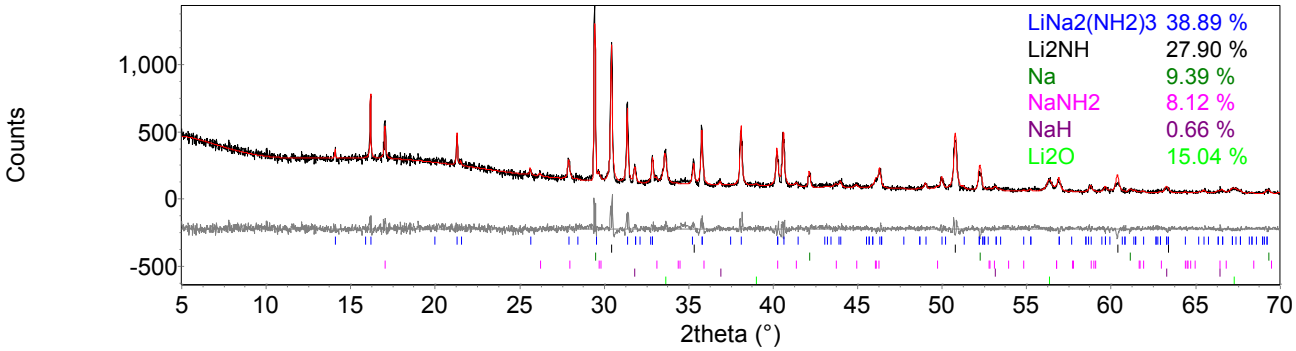

Figure 3-33 Powder XRD pattern of $LiNa_2(NH_2)_3$ + 3LiH heated to 350 °C on TPD-MS apparatus. The observed powder XRD pattern (black line) was fitted using a Rietveld fit (red line) to the observed phases $LiNa_2(NH_2)_3$ (blue tick marks), Li_2NH (black tick marks), Na (green tick marks), $NaNH_2$ (pink tick marks), NaH (purple tick marks) and Li_2O (light green tick marks). R_{wp} = 9.962, R_{exp} = 7.396, X^2 = 1.8.

There was still amide starting material present in the products suggesting the reaction had not gone to completion. Therefore, more LiH was required in order to complete the dehydrogenation of $LiNa_2(NH_2)_3$ to Li_2NH and other products. $LiNa_2(NH_2)_3$ + 5LiH was then investigated on the TPD-MS apparatus.

9. $LiNa_2(NH_2)_3$ + 5LiH

1. *Temperature Programmed Desorption-Mass Spectrometry*

The hydrogen desorption curve from TPD-MS was very similar to $LiNa_2(NH_2)_3$ + 3LiH, but there was slightly more hydrogen desorbed in the major peak (Figure 3-34). Figure 3-34 also shows the comparison of hydrogen desorption from $LiNa_2(NH_2)_3$ + 5LiH, $LiNa_2(NH_2)_3$ + 3LiH, $LiNa_2(NH_2)_3$ + 3NaH and $2LiNa_2(NH_2)_3$ + $3MgH_2$ Again, there was a fluctuation in the temperature trace at 190 °C.

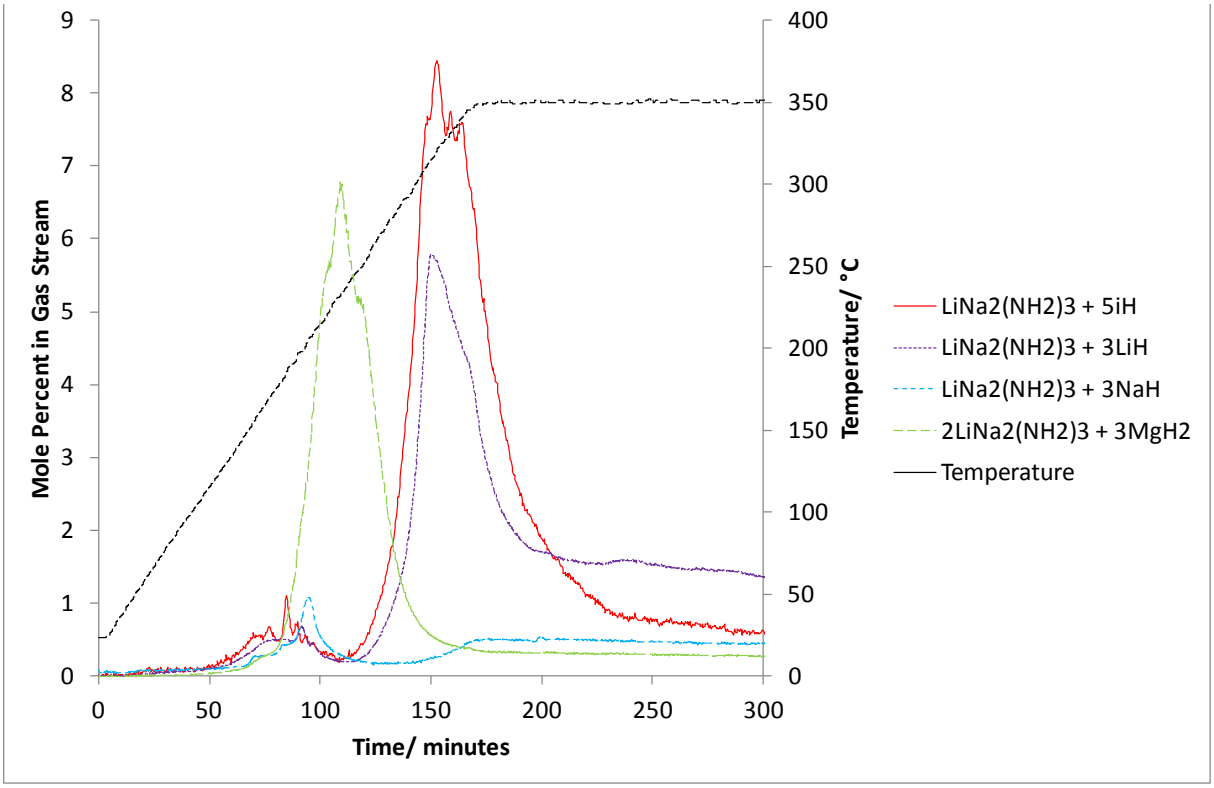

Figure 3-34 Thermal decomposition analysis of hydrogen release from $LiNa_2(NH_2)_3$ + 5LiH (red trace) in a TPD-MS apparatus in comparison to $LiNa_2(NH_2)_3$ + 3LiH (purple trace), $LiNa_2(NH_2)_3$ + 3NaH (blue trace) and $2LiNa_2(NH_2)_3$ + $3MgH_2$ (green trace). The temperature trace is shown in black.

The products from this reaction were Li_2NH, NaH and Na (Figure 3-35). As no $LiNa_2(NH_2)_3$ remained, it appeared the amide to imide reaction had gone to completion. It could be seen that the additional two moles of LiH was necessary to complete the reaction. The complete reaction can be written as:

Equation 3-16 $$LiNa_2(NH_2)_3 + 5LiH \rightarrow 3Li_2NH + (2\text{-}x)NaH + xNa + (3+½x)H_2$$

4.0 wt% H_2 total was desorbed from this reaction when heated for 300 minutes; 2.8 moles of H_2. The theoretical mass loss is 5.7 wt%.

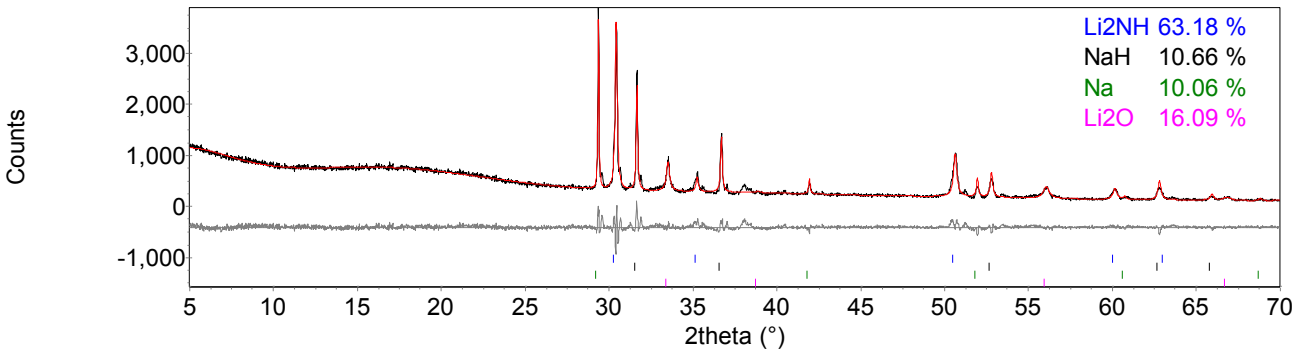

Figure 3-35 Powder XRD of $LiNa_2(NH_2)_3$ + 5LiH heated to 350 °C on a TPD-MS apparatus. The observed powder XRD pattern (black line) was fitted using a Rietveld fit (red line) to the observed phases Li_2NH (blue tick marks), NaH (black tick marks), Na (green tick marks) and Li_2O (pink tick marks). R_{wp} = 8.031, R_{exp} = 4.737, X^2 = 2.9.

2. Flowing Line Reactions

The starting materials were then heated to intermediate temperatures in order to establish the mechanism of desorption occurring. The starting materials were initially heated to 150 °C and held for 12 hours. 150 °C was part way through the first desorption (Figure 3-34). The products from the reaction after powder XRD were found to be $Li_3Na(NH_2)_4$, NaH, Li_2NH and a very small amount of $NaNH_2$, as well as $LiNa_2(NH_2)_3$ and LiH starting materials (Figure 3-36).

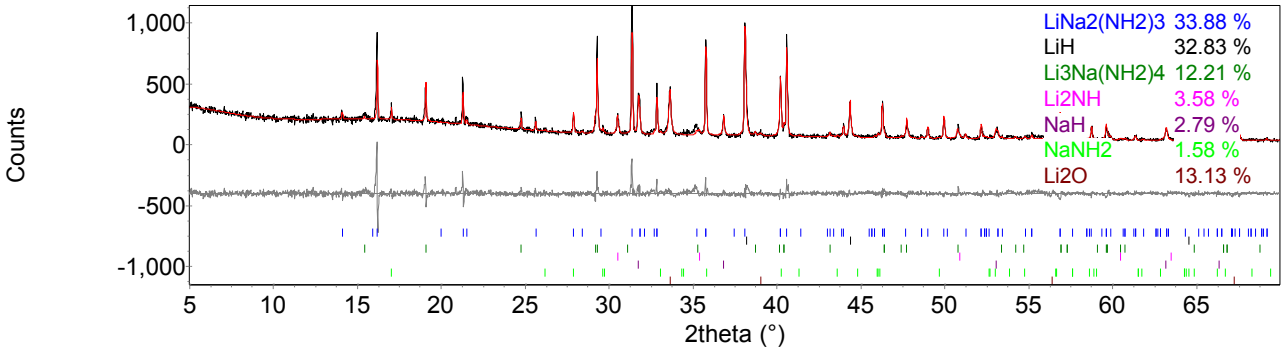

Figure 3-36 Powder XRD pattern of $LiNa_2(NH_2)_3$ + 5LiH, heated to 150 °C for 12 hours on flowing line. The observed powder XRD pattern (black line) was fitted using a Rietveld fit (red line) to the observed phases $LiNa_2(NH_2)_3$ (blue tick marks), LiH (black tick marks), $Li_3Na(NH_2)_4$ (green tick marks), Li_2NH (pink tick marks), NaH (purple tick marks), $NaNH_2$ (light green tick marks) and Li_2O (brown tick marks). R_{wp} = 13.080, R_{exp} = 8.612, X^2 = 2.3.

The reaction was then carried out at 200 °C. This was towards the end of the first desorption (Figure 3-34) and also shortly after the endothermic event occurring at 190 °C. The products were found to be LiH starting material along with $LiNH_2$, $Li_3Na(NH_2)_4$, NaH and Li_2NH. $LiNa_2(NH_2)_3$, starting material, had been consumed by this temperature (Figure 3-37). The hydrogen desorption may be in some way related to the consumption of the $LiNa_2(NH_2)_3$.

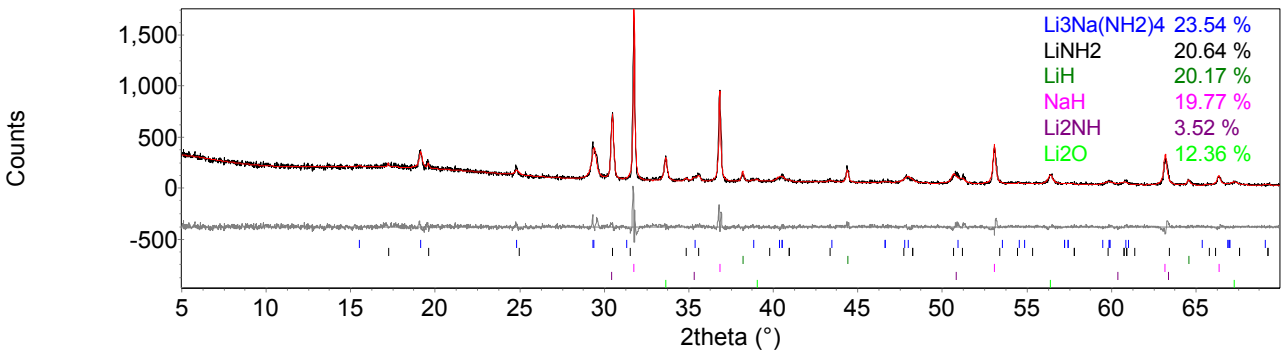

Figure 3-37 Powder XRD pattern of $LiNa_2(NH_2)_3$ + 5LiH, heated to 200 °C for 12 hours on flowing line. The observed powder XRD pattern (black line) was fitted using a Rietveld fit (red line) to the observed phases $Li_3Na(NH_2)_4$ (blue tick marks), $LiNH_2$ (black tick marks), LiH (green tick marks), NaH (pink tick marks), Li_2NH (purple tick marks) and Li_2O (light green tick marks). R_{wp} = 11.627, R_{exp} = 8.814, X^2 = 1.7.

The reaction carried out at 250 °C coincided with the very start of the second, major desorption (Figure 3-34). Neither mixed cation amide was present in the products. LiH starting material was present as well as $LiNH_2$, NaH and Li_2NH (Figure 3-38). It appeared that the second hydrogen peak was due to the reaction between $LiNH_2$ and LiH.

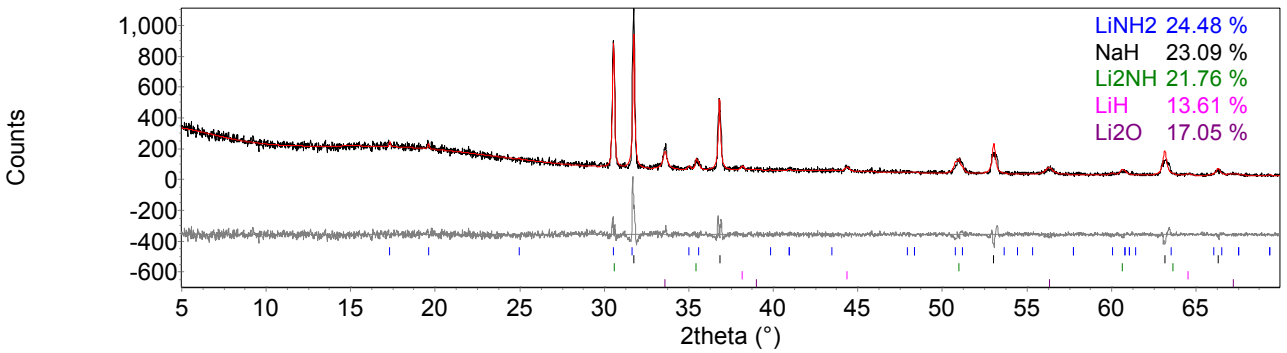

Figure 3-38 Powder XRD pattern of $LiNa_2(NH_2)_3$ + 5LiH, heated to 250 °C for 12 hours on flowing line. The observed powder XRD pattern (black line) was fitted using a Rietveld fit (red line) to the observed phases $LiNH_2$ (blue tick marks), NaH (black tick marks), Li_2NH (green tick marks), LiH (pink tick marks) and Li_2O (purple tick marks). R_{wp} = 12.071, R_{exp} = 9.153, X^2 = 1.7.

3. Discussion

$NaNH_2$ was only visible in the products from the reaction carried out to 150 °C, with the additional LiH. It had been expected that more $NaNH_2$ would be observed throughout the reaction at different temperatures, if the same mechanism of Li^+ and H^+ diffusion took part here. $NaNH_2$ should still be formed by the low temperature Li^+/H^+ diffusion. However, further work carried out below showed it was possible for $NaNH_2$ to react with LiH to form $LiNH_2$ and NaH in a metathesis reaction (Equation 3-17).

Hu *et al.*[6] investigated improvements to the Li-Mg-N-H hydrogen storage system. They used $NaNH_2$ as an additive in order to improve kinetics of hydrogen desorption. $Mg(NH_2)_2$, LiH and $NaNH_2$ were ball-milled together. For $0.8Mg(NH_2)_2$–$0.4NaNH_2$–2LiH, the powder XRD pattern

post milling showed the presence of $Mg(NH_2)_2$, LiH, NaH, and $LiNH_2$. It was noted that a metathesis reaction had occurred between the $NaNH_2$ and LiH in order to form the $LiNH_2$ and NaH present post milling (Equation 3-17).

The standard formation enthalpies of $NaNH_2$, LiH, $LiNH_2$, and NaH are −123.8, −90.5, −179.5, and −56.3 kJ mol^{-1}, respectively.[7] The enthalpy change of Equation 3-17 was calculated to be −21.5 kJ mol^{-1}.

The possible metathesis between $NaNH_2$ and LiH was investigated under the same conditions as here. The starting materials were heated together to 350 °C for 2 hours. The products were $LiNH_2$ (2 moles) and NaH (2 moles) (Figure 3-39), as hypothesised. There was no evidence of Li_2NH from a reaction between $LiNH_2$ and LiH (Equation 3-10).

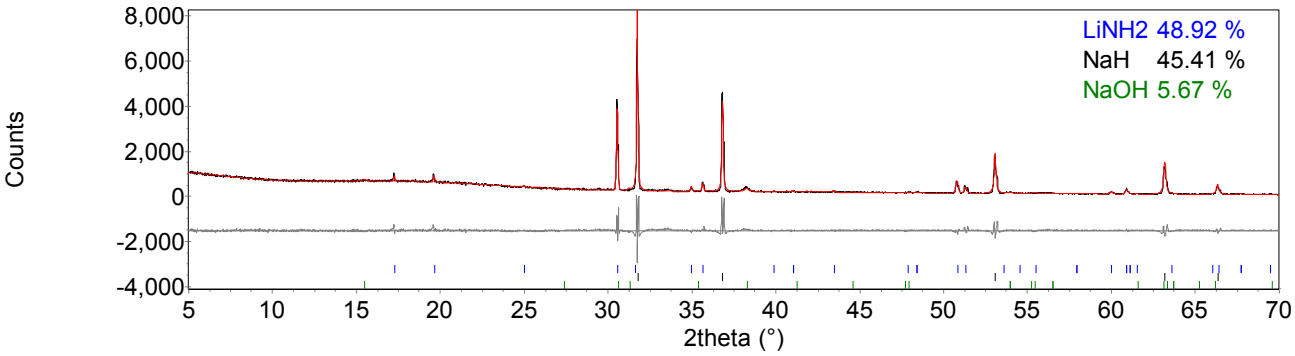

Figure 3-39 Powder XRD pattern of $NaNH_2$ + LiH, heated to 350 °C for 2 hours on flowing line. The observed powder XRD pattern (black line) was fitted using a Rietveld fit (red line) to the observed phases $LiNH_2$ (blue tick marks), NaH (black tick marks) and NaOH (green tick marks). R_{wp} = 11.904, R_{exp} = 5.026, X^2 = 5.6.

The metathesis would explain the lack of $NaNH_2$ observed in the products from the reaction of $LiNa_2(NH_2)_3$ + 5LiH.

Equation 3-17 $NaNH_2 + LiH \rightarrow LiNH_2 + NaH$

$NaNH_2$ was present in the products of $LiNa_2(NH_2)_3$ + 3LiH, Equation 3-15, as not enough LiH was added to the reaction to perform a metathesis reaction with the $NaNH_2$ (only 3 moles). The $LiNH_2$ formed from both the Li^+/Na^+ diffusion discussed previously (section 3.4.5) and as a result of Equation 3-17 could then go on to further react with LiH present to form Li_2NH (Equation 3-10). This would result in the large hydrogen desorption starting at 240 °C (Figure 3-34).

There was both NaH and $NaNH_2$ present in the products of both $LiNa_2(NH_2)_3$ + 3LiH and $LiNa_2(NH_2)_3$ + 5LiH. This suggested similar pathways to those discussed in section 3.2.4 were occurring in these reactions. This was due to NaH and $NaNH_2$ each being the product of one of the pathways. The first, thought to predominate at lower temperatures, involved the diffusion of Li^+ ions into and diffusion of H^+ ions out of $LiNa_2(NH_2)_3$. The H^+ combined with H^- remaining from LiH to form H_2 which was the cause of the low temperature H_2 desorption. This pathway may be more prominent here, in comparison to $Li_3Na(NH_2)_4$ + *x*LiH, as a much greater hydrogen peak was present in the lower temperature heating region (up to 240 °C).

$LiNa_2(NH_2)_3$ with H^+ diffusing out and Li^+ diffusing in would form $Li_{1+x}Na_2(NH_2)_{3-x}(NH)_x$ ($0 \leq x \leq 1$). When x = 1, '$Li_2Na_2(NH_2)_2NH$' would form. This can be rewritten as Li_2NH + '$Na_2(NH_2)_2$', which in turn can be rewritten as $Li_2NH + 2NaNH_2$.

At higher temperatures the LiH may again (as per section 3.2.4) be able to undergo a metathesis with $LiNa_2(NH_2)_3$ with Li^+ diffusing into the $LiNa_2(NH_2)_3$ which would be accompanied by Na^+ diffusing out of the sample. This would form $Li_{1+x}Na_{2-x}(NH_2)_3$. When x = 2, $Li_3(NH_2)_3$ + 2NaH would be formed. This can be rewritten as $3LiNH_2$ + 2NaH. The $LiNH_2$ present can then further react with LiH to form Li_2NH (Equation 3-10). Na was present in the products instead of NaH, due to NaH decomposing to Na and H_2 (Equation 3-7). The H_2 from

the decomposition of NaH would most likely be the cause of the tail of hydrogen visible during the isothermal heating. The greater size of Na^+ ions hinders their ionic mobility and therefore this pathway would be assisted by higher temperatures. The overall reaction scheme is shown in Table 3-4. The products from each temperature are shown.

Table 3-4 Overall reaction scheme $LiNa_2(NH_2)_3 + 5LiH$ of heated to various temperatures. The products from each temperature are shown.

Temp/ °C	*Reaction Scheme*	*Products*	
Onset of heating–240	$LiNa_2(NH_2)_3 + Li^+ - H^+ \rightarrow$	$Li_2Na_2(NH_2)_2(NH)$, $½H_2$ $\rightarrow$	$Li_2NH + Na_2(NH_2)_2$ $(2NaNH_2)$
Throughout heating	$NaNH_2 + LiH \rightarrow$	$LiNH_2 + NaH$	
200–350	$LiNa_2(NH_2)_3 + 2Li^+ - 2Na^+ \rightarrow$	$Li_3Na_0(NH_2)_3 \rightarrow$	$Li_3(NH_2)_3$ $(3LiNH_2)$ $+ 2NaH$
240–350	$LiNH_2 + LiH \rightarrow$	Li_2NH, H_2	
350	$NaH \rightarrow$	Na, $½H_2$	

It is interesting to note that at no time is an unidentified phase present. An unidentified phase could have suggested the presence of a mixed Li-Na imide i.e. '$Li_3Na(NH)_2$' or '$Li_2Na_4(NH)_3$' forming. As the structure of $Li_3Na(NH_2)_4$ is based on $LiNH_2$ units it is possible the structure of $Li_3Na(NH_2)_4$ would still be maintained if less H were present (*cf.* $LiNH_2 \rightarrow Li_2NH$). It would theoretically also result in the loss of ammonia (Equation 3-18).

Equation 3-18 $\quad Li_3Na(NH_2)_4 + 2LiH \rightarrow Li_5Na(NH)_3 + 2H_2 + NH_3$

Mixed cation imides are known in the form of $Li_2Mg(NH)_2$ and $Li_2Ca(NH)_2$. However, these involve lithium and a group 2 metal, and in comparison it does not appear that lithium and

another group 1 metal are able to form a mixed imide by this method. Theoretically, it seems it would not be possible to form the mixed group 1 cation imides without the desorption of NH_3 as there would be too much nitrogen present in the amide to charge balance the it within the imide.

10. $LiNa_2(NH_2)_3 + 3NaH$

$LiNa_2(NH_2)_3$ was heated with NaH in a 1:3 ratio. This ratio was used in order to ensure a 1:1 amide to hydride ratio as for the $LiNH_2$-LiH system.

1. *Temperature Programmed Desorption-Mass Spectrometry*

The reaction was originally heated at a rate of 2 °C min^{-1} to 350 °C on TPD-MS apparatus. The gas desorption profile is shown in Figure 3-40. It can be seen that only hydrogen was desorbed. There was no evidence of ammonia desorption. The hydrogen desorption occurred in two main stages, although a slow rate of hydrogen desorption appeared shortly after heating began. The rate of hydrogen desorption increased at 140 °C and rose to 200 °C during which time there were two 'steps' in the desorption (157 and 179 °C). At this peak there was an event in the temperature trace. This was confirmed by the furnace power graph (Figure 3-41), which showed an increase in furnace power followed by a drop, before resuming the prescribed heating run. The first desorption ceased at 250 °C. A second desorption started at about 300 °C and rose to a maximum at 350 °C where isothermal heating was reached. The hydrogen desorption dropped very slowly in the stable temperature region. A comparison of this hydrogen release in comparison to that of $LiNa_2(NH_2)_3 + 3LiH$, $LiNa_2(NH_2)_3 + 5LiH$ and $2LiNa_2(NH_2)_3 + 3MgH_2$ is shown in Figure 3-34.

The products after heating on TPD-MS were analysed by powder XRD (Figure 3-42). They were found to be $NaNH_2$, Na and Li_2O.

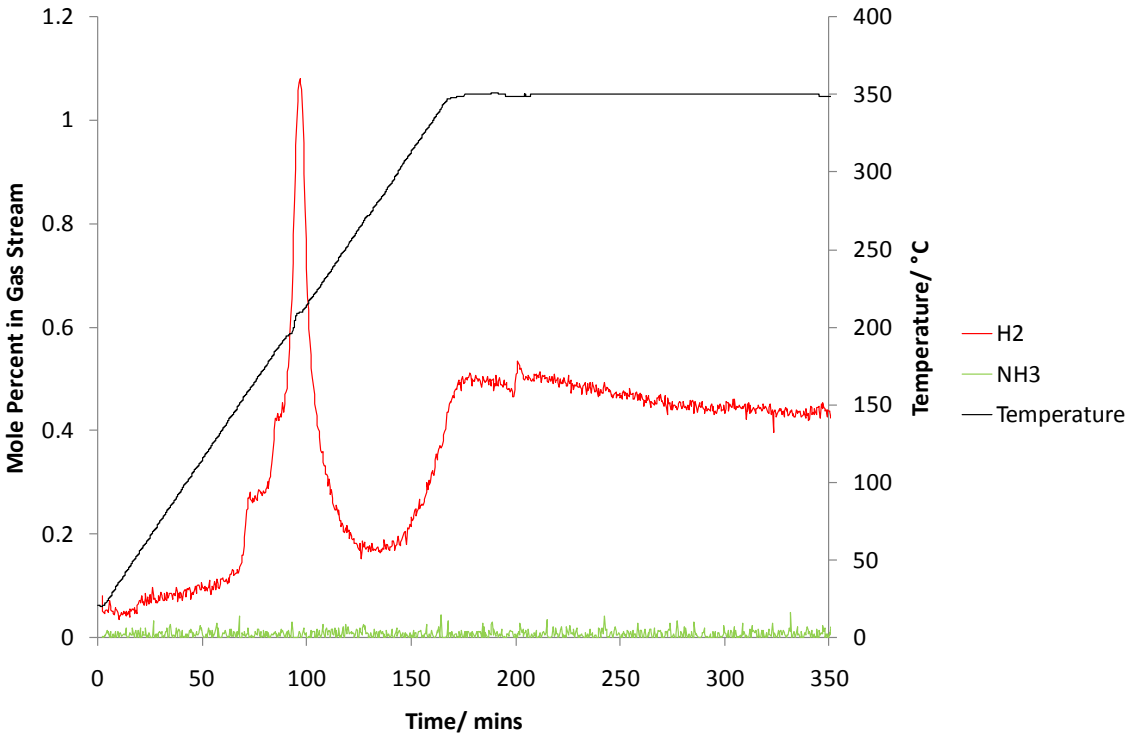

Figure 3-40 Thermal decomposition analysis of $LiNa_2(NH_2)_3$ + 3NaH in a TPD-MS apparatus. The temperature trace is shown in black and the mole percents of H_2 and NH_3 released are shown in red and green respectively.

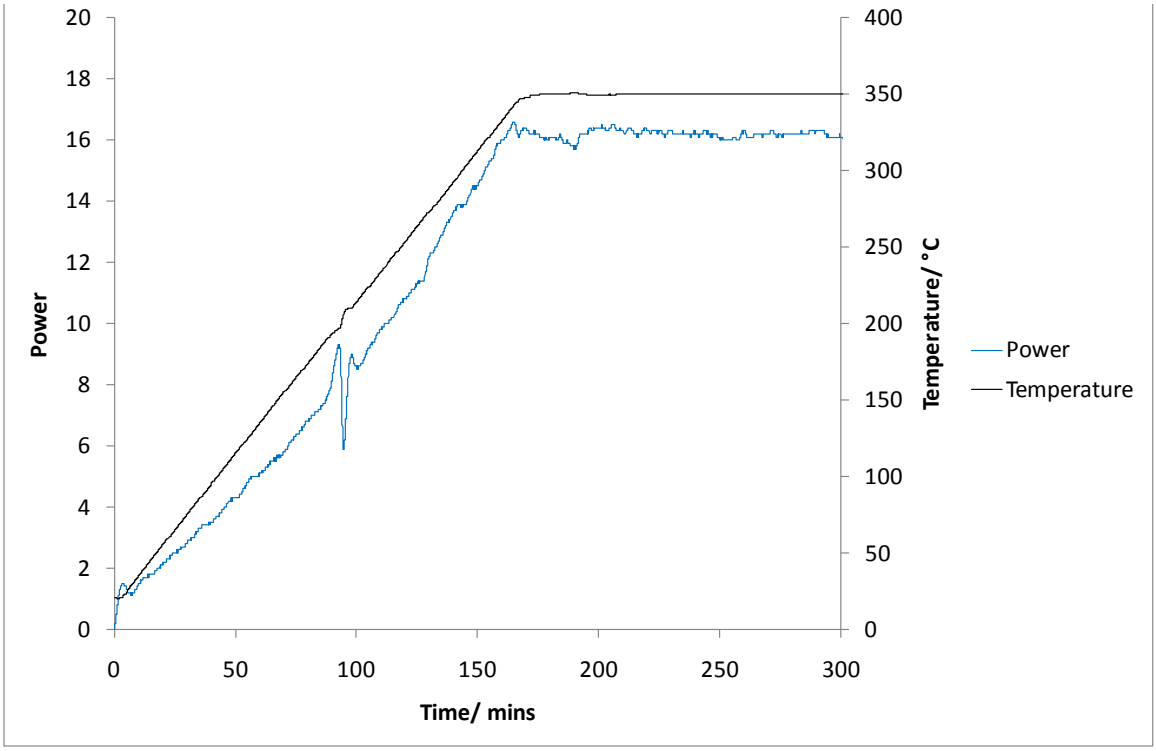

Figure 3-41 Furnace power during the TPD-MS analysis of $LiNa_2(NH_2)_3$ + 3NaH reaction. The furnace power and temperature are shown in blue and black respectively.

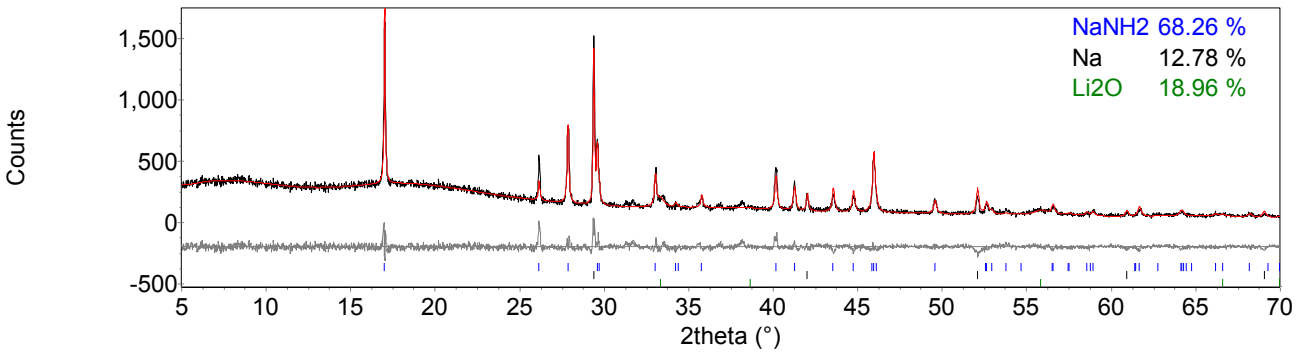

Figure 3-42 Powder XRD pattern of $LiNa_2(NH_2)_3$ + 3NaH heated to 350 °C on a TPD-MS apparatus. The observed powder XRD pattern (black line) was fitted using a Rietveld fit (red line) to the observed phases $NaNH_2$ (blue tick marks), Na (black tick marks) and Li_2O (green tick marks). R_{wp} = 10.167, R_{exp} = 7.432, X^2 = 1.9.

2. *Flowing Line Reactions*

The starting materials were heated together up to 140 °C for 12 hours in order to know what products were present when the rate of hydrogen desorption first increased. The phases

present after analysis using powder XRD were starting materials, $LiNa_2(NH_2)_3$ and NaH, as well as $NaNH_2$ and $Li_3Na(NH_2)_4$ (Figure 3-43). It was suggested previously, from thermal decomposition data (Figure 3-41), that $NaNH_2$ was present at 200 °C. It can be seen here that it was present from at least 140 °C. For $Li_3Na(NH_2)_4$ + 4NaH, $NaNH_2$ was also present from a low temperature: 150 °C.

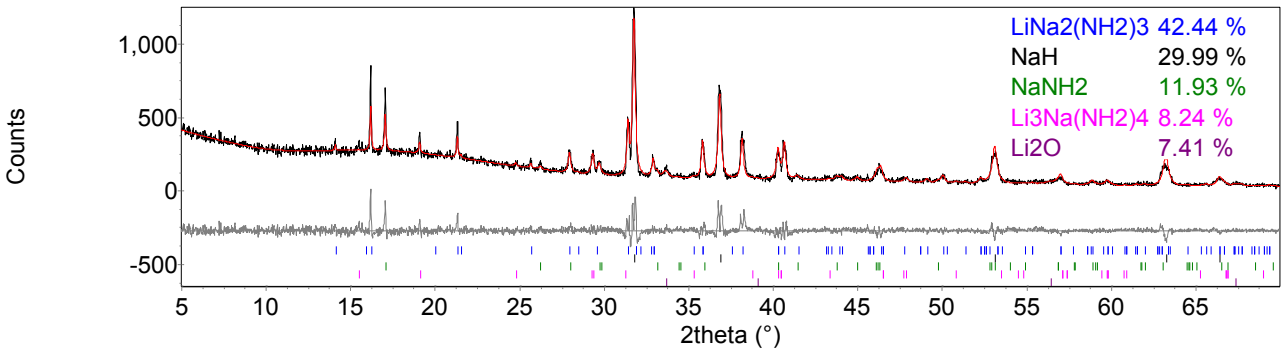

Figure 3-43 Powder XRD pattern of $LiNa_2(NH_2)_3$ + 3NaH heated to 140 °C for 12 hours on flowing line. The observed powder XRD pattern (black line) was fitted using a Rietveld fit (red line) to the observed phases $LiNa_2(NH_2)_3$ (blue tick marks), NaH (black tick marks), $NaNH_2$ (green tick marks), $Li_3Na(NH_2)_4$ (pink tick marks) and Li_2O (purple tick marks). R_{wp} = 11.645, R_{exp} = 7.814, X^2 = 2.2.

The products present after heating to 260 °C were investigated in an attempt to establish what phases were present between the two main hydrogen desorptions. These were starting materials again, as well as $NaNH_2$ and Li_2O, as before (Figure 3-44). No $Li_3Na(NH_2)_4$ was present as it had been at 140 °C.

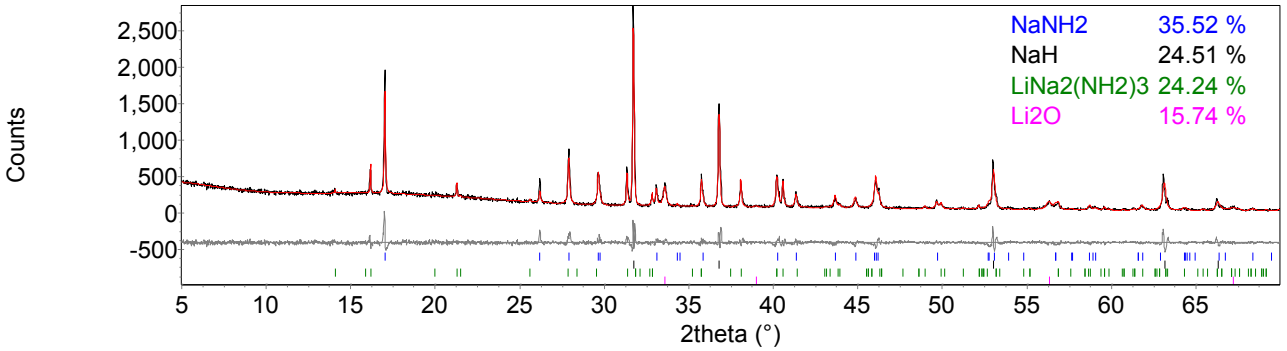

Figure 3-44 Powder XRD pattern of $LiNa_2(NH_2)_3$ + 3NaH heated to 260 °C for 12 hours on flowing line. The observed powder XRD pattern (black line) was fitted using a Rietveld fit (red line) to the observed phases $NaNH_2$ (blue tick marks), NaH (black tick marks), $LiNa_2(NH_2)_3$ (green tick marks), and Li_2O (pink tick marks). R_{wp} = 11.486, R_{exp} = 7.543, X^2 = 2.3.

When the reaction was carried out on the flowing line for 20 minutes to 350 °C the products were similar to heating on TPD-MS: $NaNH_2$, but this time $LiNa_2(NH_2)_3$ was also present along with NaH starting material (Figure 3-45).

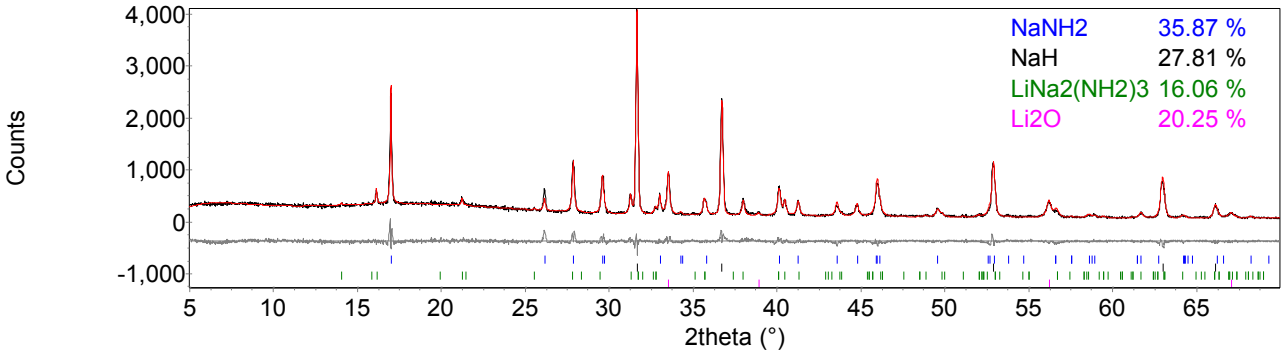

Figure 3-45 Powder XRD pattern of $LiNa_2(NH_2)_3$ + 3NaH heated to 350 °C for 20 minutes on a flowing line. The observed powder XRD pattern (black line) was fitted using a Rietveld fit (red line) to the observed phases $NaNH_2$ (blue tick marks), NaH (black tick marks), $LiNa_2(NH_2)_3$ (green tick marks) and Li_2O (pink tick marks). R_{wp} = 9.183, R_{exp} = 6.262, X^2 = 2.1.

The products after heating the starting materials to 350 °C for 12 hours were $NaNH_2$ and Na, as well as a large amount of Li_2O and NaH remaining (Figure 3-46). In comparison to heating for 20 minutes, the $LiNa_2(NH_2)_3$ had disappeared and more Li_2O was present. The difference

between products from heating on TPD-MS apparatus (Figure 3-42) and flowing line for 12 hours was the lack of NaH from TPD-MS heating, having formed Na, whereas after 12 hours on the flowing line both NaH and Na were present

Heating for 12 hours appeared to cause the $LiNa_2(NH_2)_3$ present (Figure 3-45) to react and not be present (Figure 3-46).

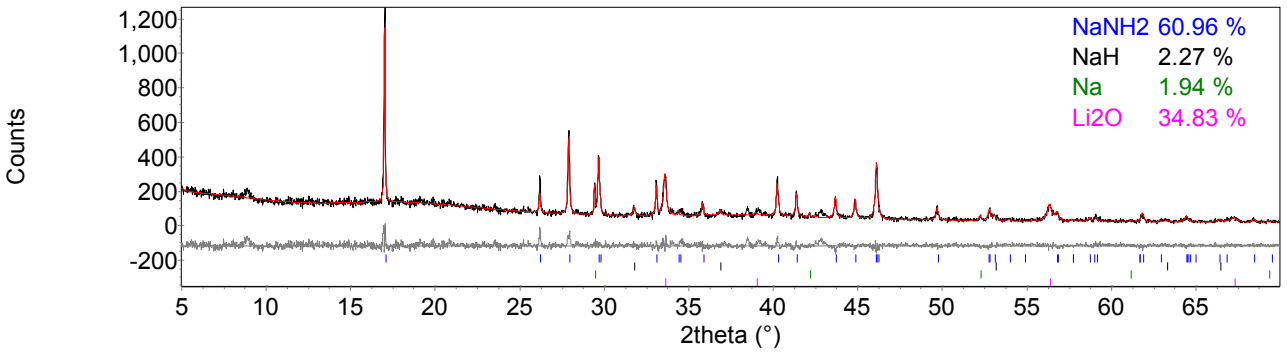

Figure 3-46 Powder XRD pattern of $LiNa_2(NH_2)_3$ + 3NaH heated to 350 °C for 12 hours on a flowing line. The observed powder XRD pattern (black line) was fitted using a Rietveld fit (red line) to the observed phases $NaNH_2$ (blue tick marks), NaH (black tick marks), Na (green tick marks) and Li_2O (pink tick marks). R_{wp} = 13.251, R_{exp} = 10.684, X^2 = 1.5.

$Li_3Na(NH_2)_4$ was only observed after heating to 140 °C for 12 hours. The first two steps in the hydrogen desorption appeared to occur in the same temperature region as the two endothermic events occurring at about 200 °C, as shown by differential scanning calorimetry (DSC) (Figure 3-47). A sample of $LiNa_2(NH_2)_3$ + 3NaH was heated at 2 °C min^{-1} up to 350 °C, held there for 20 minutes and then cooled at 2 °C min^{-1} to room temperature. This was carried out under a 3 bar argon atmosphere flowing at 100 ml min^{-1}.

The main hydrogen desorption seemed to be exothermic as the DSC power increased. The second main hydrogen desorption occurred alongside an endothermic event in the DSC

power. The same endotherm occurred at the end of heating $Li_3Na(NH_2)_4$ + 4NaH on DSC to 350 °C (Figure 3-48).

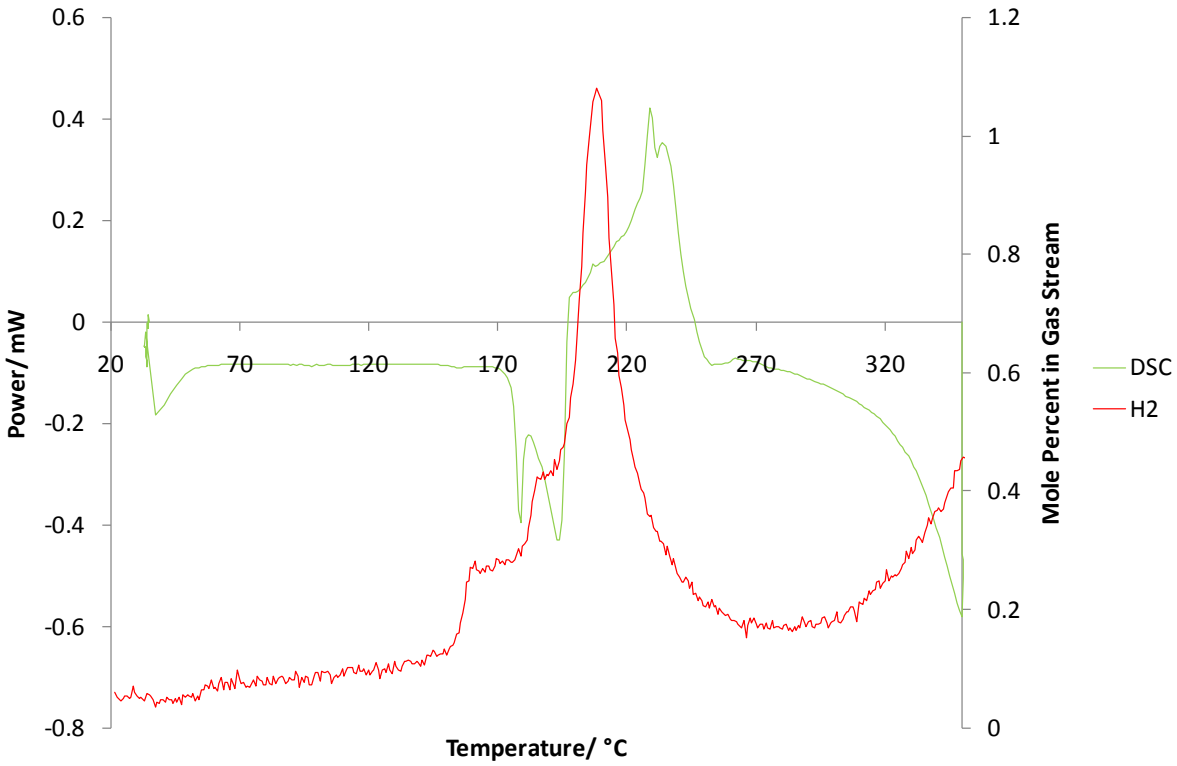

Figure 3-47 Comparison between DSC power and H_2 desorption from the $LiNa_2(NH_2)_3$ + 3NaH reaction heated to 350 °C.

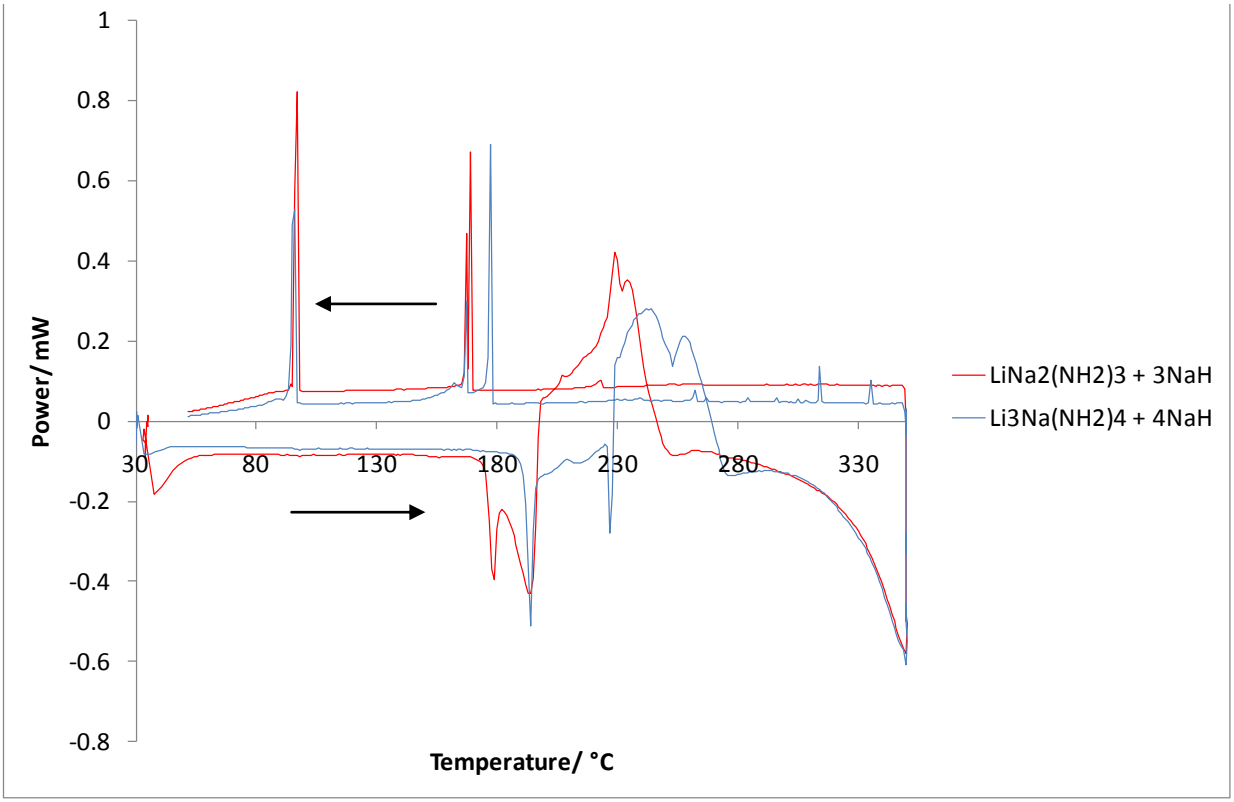

Figure 3-48 Comparison of DSC power for the $Li_3Na(NH_2)_4$ + 4NaH and $LiNa_2(NH_2)_3$ + 3NaH reactions.

The comparison of hydrogen desorption from $LiNa_2(NH_2)_3$ + 3NaH and $Li_3Na(NH_2)_4$ + 4NaH is shown in Figure 3-49. It can seen there was a greater H_2 desorption tail during isothermal heating for $LiNa_2(NH_2)_3$ + 3NaH.

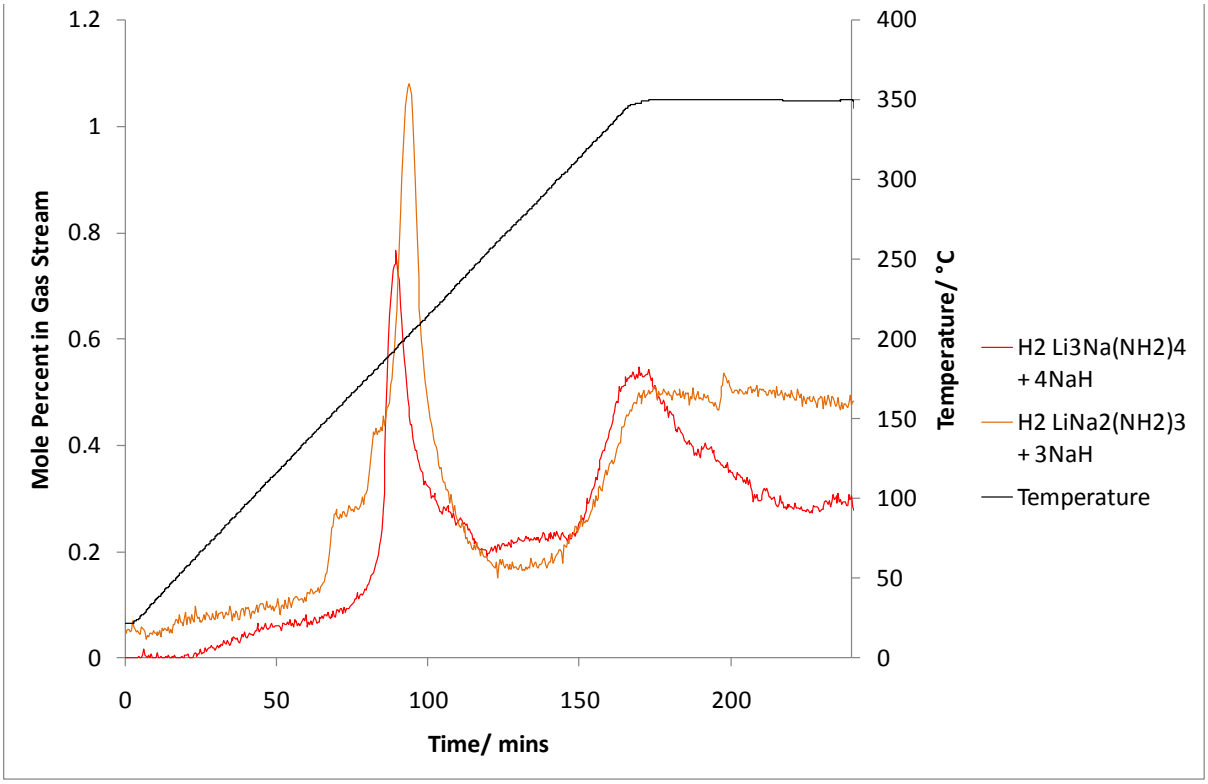

Figure 3-49 Comparison of TPD-MS of $LiNa_2(NH_2)_3$ + 3NaH and $Li_3Na(NH_2)_4$ + 4NaH. The temperature trace is shown in black and the mole percents of H_2 released for $LiNa_2(NH_2)_3$ + 3NaH and $Li_3Na(NH_2)_4$ + 4NaH are shown in orange and red respectively.

3. Discussion

The $NaNH_2$ and $Li_3Na(NH_2)_4$ were formed at very low temperatures, possibly from the transformation of $LiNa_2(NH_2)_3$ to $Li_3Na(NH_2)_4$ and $NaNH_2$ (Equation 3-6). It had been shown that the mixed cation amides formed an equilibrium (Sections 3.2.1 and 3.2.2).

The melting point temperature of $NaNH_2$ is 210 °C, very close to the endothermic event noticed at 200 °C (Figure 3-41). Melting is endothermic and this could explain the fluctuation in the temperature trace and furnace power at 200 °C. This would suggest $NaNH_2$ was present in the reaction mixture at 200 °C and remained further unreacted up to 350 °C, as it was present in the products then. The endotherm was also present in the DSC trace (Figure 3-47).

The products from $LiNa_2(NH_2)_3$ + 3NaH were $NaNH_2$, Na and Li_2O. These products were the same as those identified for $Li_3Na(NH_2)_4$ + 4NaH, but without $LiNa_2(NH_2)_3$.

From the molar amounts of Li and Na in the products (Figure 3-46) the sample was deficient in Na-containing products. It is possible that sodium was lost through sodium vapour when NaH decomposed to Na and H_2 (Equation 3-7).

These products could be formed by the same mechanism as tentatively suggested in section 3.2.4. That is, oxidation of $LiNa_2(NH_2)_3$ causes Li^+ to diffuse out of $LiNa_2(NH_2)_3$ and Na^+ from NaH to diffuse into $LiNa_2(NH_2)_3$, forming Li_2O. This would notionally form $Na_3(NH_2)_3$, which can be rewritten as $3NaNH_2$. The H^- remaining from NaH would form H_2. NaH remaining would decompose at 350 °C to form Na (Equation 3-7).

Equation 3-19

when x = 1, $2Li_{1-x}Na_{2+x}(NH_2)_3 + (6-2x)NaH + ½O_2 \rightarrow 2Na_3(NH_2)_3 + 4NaH + Li_2O + H_2 \rightarrow 6NaNH_2 + (4-y)NaH + yNa + Li_2O + (1+½y)H_2$

A hydrogen loss of 1.6 wt% was found from the TPD-MS apparatus. This compared favourably to the theoretical mass loss of 1.7 wt% if only the NaH were to desorb H_2. The long slow H_2 desorption during isothermal heating (Figure 3-40) was most likely from the decomposition of NaH to Na (Equation 3-7).

11. $2LiNa_2(NH_2)_3 + 3MgH_2$

$LiNa_2(NH_2)_3$ was heated with MgH_2 in a 2:3 ratio. This was in order to maintain a 1:1 ratio between amide and hydride as with the $LiNH_2$ + LiH system.

1. *Temperature Programmed Desorption-Mass Spectrometry*

$2LiNa_2(NH_2)_3 + 3MgH_2$ was initially examined on a TPD-MS apparatus at a heating rate of 2 °C min^{-1} up to 350 °C (Figure 3-50). The reaction released only hydrogen with no evidence for ammonia desorption. The hydrogen desorption started at 75 °C at a slow rate which started to increase at 140 °C and was fastest from 170 °C, up to a peak at 230 °C. After reaching 230 °C, the rate of hydrogen desorption decreased to almost background levels by 290 °C. The mass loss after heating $2LiNa_2(NH_2)_3 + 3MgH_2$ for 300 minutes was calculated to be 2.2 wt%.

The products after heating this reaction to 350 °C were found to be *α*-$Li_2Mg(NH)_2$, *β*-$Li_2Mg(NH)_2$, Li_2NH and Na along with a large amount of oxidation (Figure 3-51). In addition there were also unidentified peaks present. The *β*-$Li_2Mg(NH)_2$ appeared in the products after TPD-MS here and not in $Li_3Na(NH_2)_4 + 2MgH_2$ (section 3.2.7) due to the heating in the TPD-MS apparatus being for longer than for $Li_3Na(NH_2)_2 + 2MgH_2$. The hydrogen desorption here can be compared to that of $LiNa_2(NH_2)_3 + 3LiH$, $LiNa_2(NH_2)_3 + 5LiH$ and $LiNa_2(NH_2)_3 + 3NaH$ is shown in Figure 3-34.

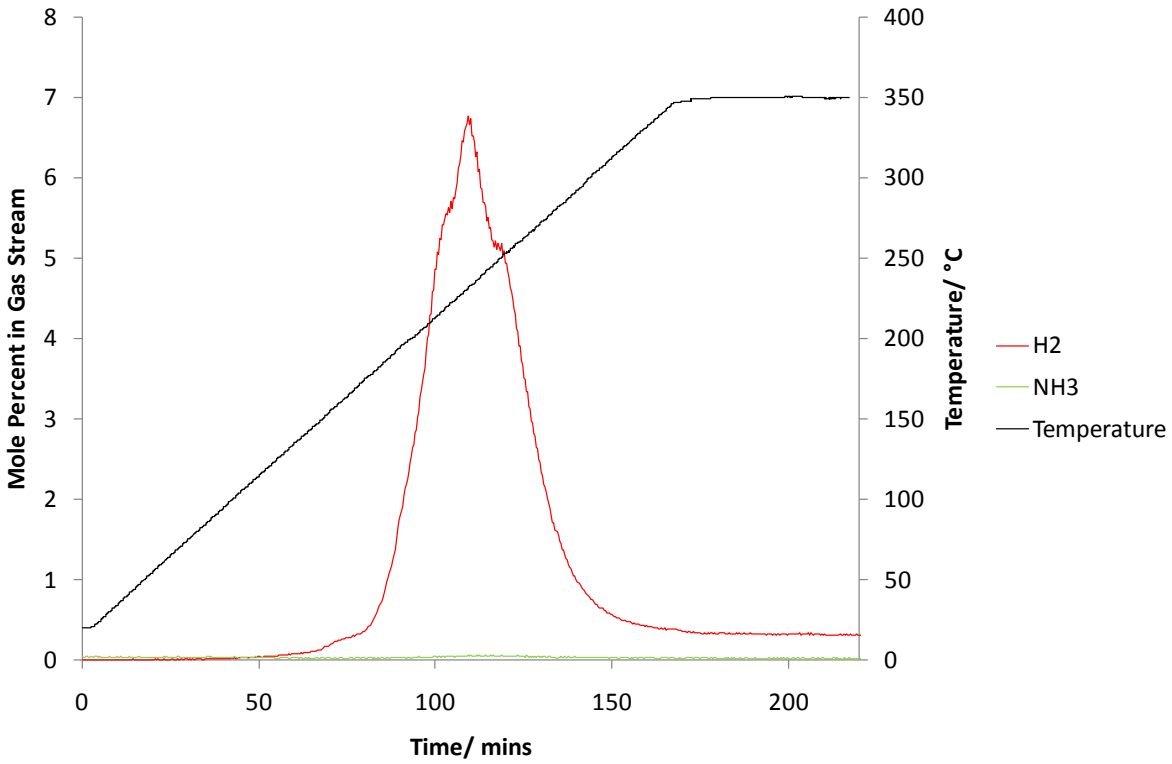

Figure 3-50 TPD-MS analysis of $2LiNa_2(NH_2)_3 + 3MgH_2$. The temperature trace is shown in black and the mole percentages of H_2 and NH_3 released are shown in red and green respectively.

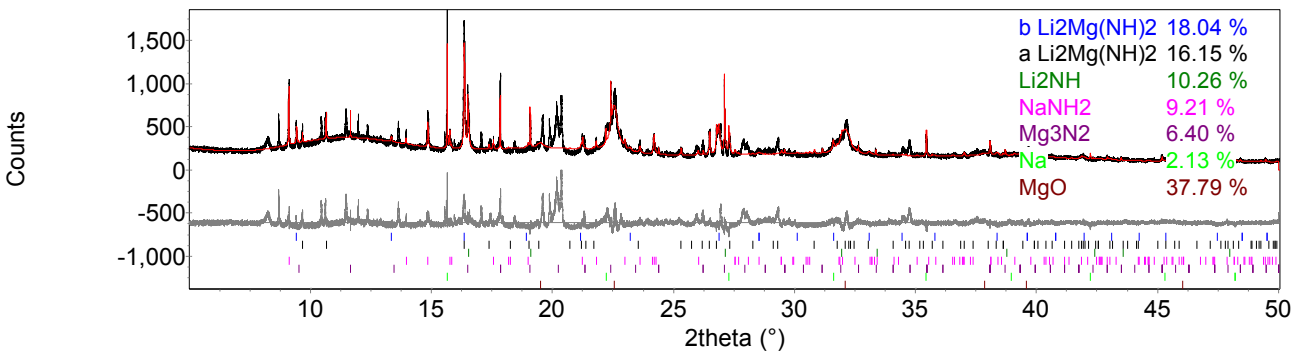

Figure 3-51 Powder XRD pattern of $2LiNa_2(NH_2)_3 + 3MgH_2$, heated to 350 °C on TPD-MS apparatus. The observed powder XRD pattern (black line) was fitted using a Rietveld fit (red line) to the observed phases β-$Li_2Mg(NH)_2$ (blue tick marks), α-$Li_2Mg(NH)_2$ (black tick marks), Li_2NH (green tick marks), $NaNH_2$ (pink tick marks), Mg_3N_2 (purple tick marks), Na (light green tick marks) and MgO (brown tick marks). R_{wp} = 15.394, R_{exp} = 4.758, X^2 = 10.5.

2. *Flowing Line Reactions*

After heating the reaction mixture to 300 °C for 12 hours the products were $NaNH_2$, $LiNa_2(NH_2)_3$, NaH and MgO, as well as lots of unidentified peaks (Figure 3-52).

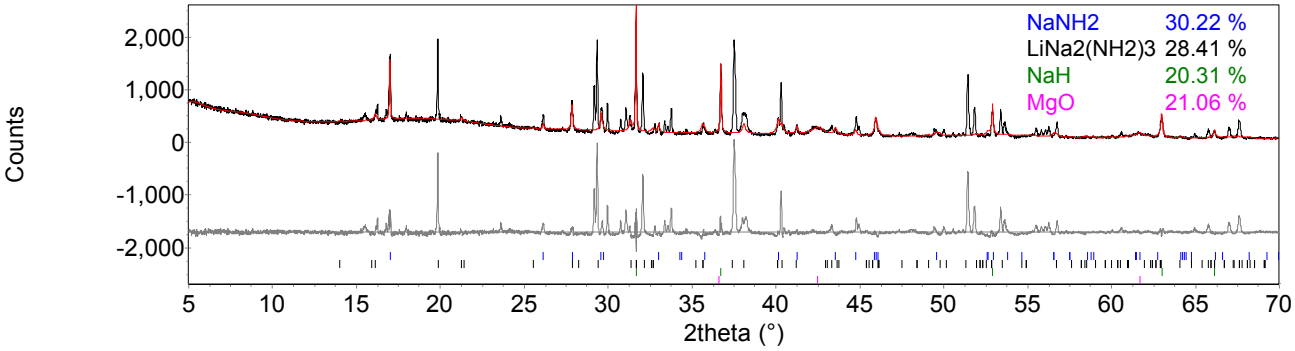

Figure 3-52 Powder XRD pattern of $2LiNa_2(NH_2)_3 + 3MgH_2$, heated to 300 °C for 12 hours on a flowing line under argon. The observed powder XRD pattern (black line) was fitted using a Rietveld fit (red line) to the observed phases $NaNH_2$ (blue tick marks), $LiNa_2(NH_2)_3$ (black tick marks), NaH (green tick marks) and MgO (pink tick marks). $R_{wp} = 26.097$, $R_{exp} = 5.825$, $X^2 = 20.1$.

The reaction mixture was also heated to 350 °C for 12 hours (Figure 3-53). The products from this were *β*-$Li_2Mg(NH)_2$, $NaNH_2$ and Na, as well as unidentified peaks. The unidentified peaks were different to those in Figure 3-52.

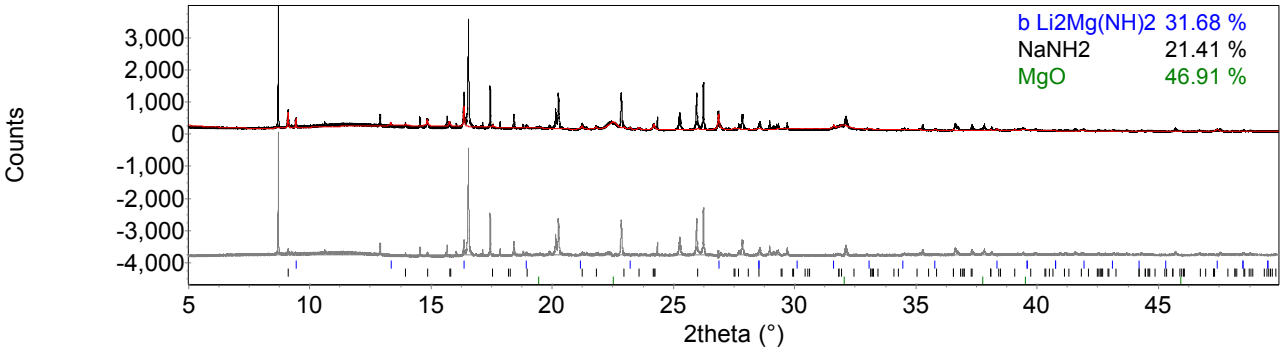

Figure 3-53 Powder XRD pattern of $2LiNa_2(NH_2)_3 + 3MgH_2$, heated to 350 °C for 12 hours on flowing line under argon. The observed powder XRD pattern (black line) was fitted using a Rietveld fit (red line) to the observed phases *β*-$Li_2Mg(NH)_2$ (blue tick marks), $NaNH_2$ (black tick marks) and MgO (green tick marks). R_{wp} = 30.545, R_{exp} = 7.718, X^2 = 15.7.

$2LiNa_2(NH_2)_3 + 3MgH_2$ was heated together to 350 °C for 36 hours. The products were the same as for the 12 hour heating (Figure 3-53). The unidentified peaks were in the same places. The amounts of the known products were similar.

3. Discussion

The furnace power and temperature trace (Figure 3-50) of $2LiNa_2(NH_2)_3 + 3MgH_2$ showed no fluctuations. This was unlike when $Li_3Na(NH_2)_4$ was heated with MgH_2 where an exothermic event was observed at 180 °C.

The products after heating $2LiNa_2(NH_2)_3 + 3MgH_2$ to 350 °C for 12 hours (Figure 3-53) were similar to those after heating the same reaction on a TPD-MS apparatus (Figure 3-51). The products were *β*-$Li_2Mg(NH)_2$, $NaNH_2$, MgO and a lot of unidentified peaks. These unidentified peaks were present in both XRD patterns. There were also additional unidentified peaks within the TPD XRD pattern.

$LiNa_2(NH_2)_3$ has a majority of sodium cations within it compared to $Li_3Na(NH_2)_4$ in which the majority of cations are lithium. The reaction between $LiNa_2(NH_2)_3$ and MgH_2 can therefore

be compared to that of the sodium-rich $NaNH_2$ and MgH_2 reactions (sections 4.2.2 and 4.2.3).

The products after heating $2LiNa_2(NH_2)_3 + 3MgH_2$ to 350 °C on a TPD-MS apparatus were α-$Li_2Mg(NH)_2$, β-$Li_2Mg(NH)_2$, Li_2NH, $NaNH_2$, Mg_3N_2 and Na along with the release of hydrogen. The $Li_2Mg(NH)_2$ appeared to form as if no sodium was present at all. In comparison, the products from the sodium-rich reactions with MgH_2 were the mixed Na-Mg imide, $NaNH_2$, Mg_3N_2 and NaH/Na also with the release of hydrogen (Figure 7-4 and Figure 7-13). It could be seen that the products from both reactions were similar with only the extra Li present forming Li_2NH. However, as the composition of the unidentified phases was unknown a full comparison could not be carried out.

$2LiNa_2(NH_2)_3 + 3MgH_2$, heated to 350 °C for 12 hours (Figure 3-53), $Li_3Na(NH_2)_4 + 2MgH_2$ heated on TPD-MS (Figure 3-26) and $2LiNa_2(NH_2)_3 + 3MgH_2$ heated to 350 °C on TPD-MS had the same unidentified peaks, but $2LiNa_2(NH_2)_3 + 3MgH_2$ heated on TPD-MS also had additional unidentified peaks present.

Some of the unidentified peaks from $2LiNa_2(NH_2)_3 + 3MgH_2$, heated to 350 °C on TPD-MS (Figure 3-51) were the same as the starting materials heated to 300 °C for 12 hours (Figure 3-52), however many were new. It is interesting to note there was no α-$Li_2Mg(NH)_2$ formed after heating to 300 °C for 12 hours, as shown in Figure 3-52, whereas in the $Li_3Na(NH_2)_4 + 2MgH_2$ mixture under the same conditions, it was present (Figure 3-27).

Attempts were made to characterise the unidentified products from the reactions $Li_3Na(NH_2)_4 + 2MgH_2$ and $2LiNa_2(NH_2)_3 + 3MgH_2$, however all proved unsuccessful. It was unclear in most cases whether the unidentified peaks belonged to one or more phases.

Although under some conditions $2LiNH_2 + MgH_2$ desorbs hydrogen at a lower temperature than $LiNH_2 + LiH$[8,9] it could be seen under the conditions here that the release of hydrogen occurred at the same temperature for both reactions. It was possible to compare the hydrogen desorptions for the reactions of mixed cation amides with LiH and MgH_2. It can be seen from Figure 3-54 that both the mixed cation amides, when heated with MgH_2, desorbed hydrogen at almost 100 °C lower than when heated with LiH. The reaction of the mixed cation amides with LiH occurred at the same temperature as $LiNH_2 + LiH$ and $2LiNH_2 + MgH_2$ under these conditions. The benefit of the addition of MgH_2 to the mixed cation amides was clear.

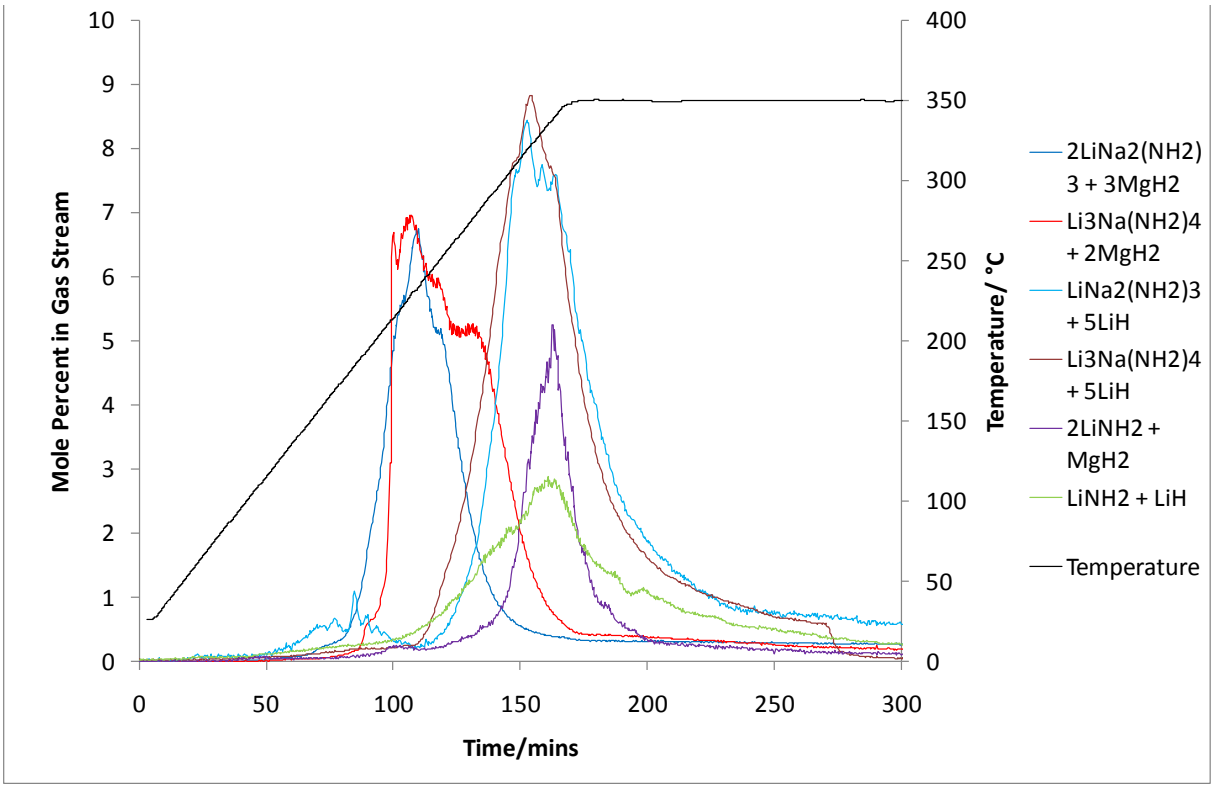

Figure 3-54 Comparison TPD-MS analysis of $Li_3Na(NH_2)_4 + 4LiH$, $LiNa_2(NH_2)_3 + 3LiH$, $Li_3Na(NH_2)_4 + 2MgH_2$ and $LiNa_2(NH_2)_3 + 3MgH_2$ with $2LiNH_2 + MgH_2$ and $LiNH_2 + LiH$.

[1] H. Jacobs, B. Harbrecht *Journal of the Less-Common Metals,* 85 (1982) 87–95
[2] Y. Nakamori, S. Orimo, *J. Alloys Compds*., 370 (2004) 271–275
[3] R. L. Lowton, M. O. Jones, W. I. F. David, S. R. Johnson, M. Sommariva, P. P. Edwards, *J. Mater. Chem*., 18 (2008) 2355–2360
[4] Topas, general profile and structure analysis software for powder diffraction data, A. A. Coelho; Bruker AXS, Karlsruhe, Germany, 3.0 ed., 2004
[5] Y. H. Hu, E. Ruckenstein, *J. Phys. Chem. A,* 107 (2003) 9737–9739
[6] Y. Liu, J. Hu, Z. Xiong, G. Wu*, J. Mater. Res*., 22 (2007) 5, 1339–1345
[7] D.R. Lide, *CRC Handbook of Chemistry and Physics,* 87th edition
[8] Z. Xiong, G. Wu, J. Hu, P. Chen, *Adv. Mater.,* 16 (2004) 17, 1522–1525
[9] W. Luo, *J. Alloys Compds.,* 381 (2004) 284–287

4. xNaNH$_2$ + yMgH$_2$

1. Introduction

The use of $LiNH_2$ in solid-state hydrogen storage materials has been well researched. $LiNH_2$ has been combined with LiH,[1,2,3] MgH_2,[4,5,6,7] CaH_2,[8,9,10,11] $LiAlH_4$[12] as well as forming mixed cation amides $Li_3Na(NH_2)_4$, $LiNa_2(NH_2)_3$[13,14] and $K_2Li(NH_2)_3$.[15] However, the use of sodium amide in place of $LiNH_2$ for hydrogen storage has not been investigated as extensively.

The use of sodium amide over lithium amide would be preferable because of the cost of lithium vs. sodium. Lithium costs 550 €/kg whereas sodium is cheaper by almost a factor of 4. This is largely due to the greater abundance of sodium than lithium. Also, the increase in lithium use in batteries is likely to have the effect of pushing the price up. Unfortunately, sodium weighs more than lithium and so will have a detrimental effect on the mass to hydrogen ratio. Sodium amide itself is less stable than lithium amide. This can be seen in the contrasting enthalpy of formation: $LiNH_2$ –179.5 kJ mol^{-1}; $NaNH_2$ –123.8 kJ mol^{-1}. This lower stability should assist in the release of hydrogen from an amide/hydride system containing sodium amide.

The reactions between $LiNH_2$ and MgH_2 and $Mg(NH_2)_2$ and LiH have previously been discussed in the introduction (section 1). The electronegativity difference between Li and Mg (Li, 0.98; Mg, 1.31, Pauling scale) in the Li-Mg-N-H system is said to be one driving force in the decreased temperature desorption between Li-Mg-N-H and Li-N-H systems.[16] The difference in electronegativity between the cations means there is weaker ionic interaction for sodium with

the $[NH_2]^-$ anion.[17] The electronegativity difference between Na and Mg (Na, 0.93) is greater than that between Li and Mg. Therefore, if an intermediate of Na-Mg-N-H can be formed (although not suggested before) it could release hydrogen at a lower temperature than $Li_2Mg(NH)_2$. The attraction between the H^- in the ionic NaH and $H^{\delta+}$ in the amide should aid hydrogen desorption, as it has with LiH.[1,2]

At the time we started research into the Na-Mg-N-H system, no other research had been carried out. In 2010, Dolotko *et al.*[18] reported investigations into the reaction $2NaNH_2 + 3MgH_2$. Dolotko *et al.*[18] ball-milled the starting materials for 15 minutes to ensure complete mixing of the reactants. The reactants were pressed into pellets and then placed in an autoclave and evacuated. The sample was heated to the selected temperature and held there until the pressure stabilised and then quenched using forced air (5–10 minutes cooling time). They argued that as the kinetics of the original reaction are slow, the kinetics of the reverse reaction should also be slow.

The reaction was initially carried out to 395 °C and about 5 wt% H_2 desorption was observed. The only gas found by the residual gas analyser (RGA) was hydrogen with no evidence of ammonia. The H_2 release observed by Dolotko *et al.*[18] began at 130 °C and appeared to be composed of two parts. The first step occurred between 130 and 270 °C, but was slow up to 210 °C. The second step occurred above 330 °C. Reactions at intermediate temperatures were then carried out in order to establish the desorption mechanism. The final products at 390 °C were Mg_3N_2 and NaH.

Dolotko *et al.* tried to rehydride their fully decomposed sample (Mg_3N_2 + NaH). They did this with a pressure of 190 bar hydrogen and 395 °C for 48 hours until the autoclave pressure stabilised. 2.1 wt% hydrogen was taken up; anything lower than this temperature was unsuccessful for hydrogen absorption. After hydrogenation at 395 °C, the products were MgNH along with remaining Mg_3N_2 and NaH.

Earlier, Xiong *et al.*[19] investigated the opposite reaction, that between $Mg(NH_2)_2$ and NaH in the molar ratios 1:1, 2:3 and 1:2. These sodium rich ratios are analogous to the Li rich reaction between $LiNH_2$ and MgH_2. The decomposition of $Mg(NH_2)_2$ alone was initially investigated and then used as a basis for comparison by adding NaH to the reaction. $Mg(NH_2)_2$ was synthesised in house by the reaction of NH_3 with milled Mg powder at 300 °C overnight. Both $Mg(NH_2)_2$ alone and the mixtures were all ball-milled (2 days and 1 day respectively). The addition of NaH to $Mg(NH_2)_2$ greatly changed the temperature programmed desorption (TPD) features of $Mg(NH_2)_2$ alone.

$Mg(NH_2)_2$ when decomposed alone desorbed NH_3 preferentially, whereas when mixed with NaH, the release of H_2 was observed, although NH_3 was still desorbed to a lesser amount. This was in contrast to Dolotko *et al.* who only observed H_2 desorption with their system.

The temperature at which H_2 was desorbed was lower with the $Mg(NH_2)_2$-NaH mixtures than those of milled $Mg(NH_2)_2$ or NaH individually.[20] Xiong *et al.* suggested this indicated a lower kinetic barrier in place for these reactions. It was also suggested that an intermediate of $Mg(NH_2)_2$-NaH may have formed which reduced the activation energy although the nature of this intermediate was not determined. The 1:1 ratio gave a TPD signal that showed a large

amount of NH_3 desorbed (similar to $Mg(NH_2)_2$ alone). The increased amount of NaH added to the subsequent reactions suppressed desorption of NH_3 considerably, but not completely. N_2, which was observed mainly in the 1:1 reaction, was not seen until 400 °C with additional NaH. Extra NaH significantly improved the suppression of gases other than H_2. Xiong *et al.* suggested the Na stabilised the –N or –NH of the units in the reacting mixture, although exactly what they mean by this is unclear. This stability seems to have been lost at temperatures above 400 °C.

The reversibility of the Mg-Na-N-H system was investigated.[19] The mixtures were pre-desorbed to 190 °C followed by temperature programmed absorption (TPA) under H_2 at 11 bar. The 1:1 mixture started to absorb H_2 at slightly above room temperature. The mixtures with increased NaH absorbed H_2 at higher temperatures. Absorption and desorption cycling was carried out for all mixtures was obtained at 160, 180 and 200 °C. For $Mg(NH_2)_2$-NaH (1:1), 1.75 wt% H_2 was reabsorbed. For 2:3 this increased to 2.17 wt% H_2. The 1:2 mixture gave 1.83 wt% H_2 absorption and showed that the extra 0.5 moles of NaH did not enhance the storage capacity of the mixture.

Powder X-ray diffraction (XRD) was used to analyse the 2:3 sample when dehydrogenated at 190 °C. The result was that the $Mg(NH_2)_2$ and NaH had completely disappeared and an unidentified phase was seen. No attempt was made to characterise this compound. When put under H_2 pressure at 140 °C, this phase rehydrided back to $Mg(NH_2)_2$ and NaH. The same phase was observed under repeated rehydriding/dehydriding cycles.

As this thesis was being written, a third paper was published. Sheppard *et al.*[21] ball milled a 1:1 mixture of $NaNH_2$ and MgH_2 for 3 hours. After ball-milling the starting materials for 3 hours, the

products were $NaNH_2$ and MgH_2, as well as a small amount of NaH. This showed a metathesis had already started to occur, although no $Mg(NH_2)_2$ was visible, which was put down to milling-induced amorphisation.

The ball-milled starting materials were then subjected to heating on a TPD-MS apparatus between room temperature and 370 °C.[21] 3 main hydrogen desorptions were found to occur up to 330 °C. Hydrogen was desorbed almost immediately on heating and a sizable peak occurred at 140 °C. This was concurrent with a small desorption of ammonia. There were hydrogen desorption peaks at 191 and 230 °C and then desorption of hydrogen increased at 280 °C up to 315 °C where ammonia was again desorbed. Above 335 °C, N_2, NH_3 and H_2 production increased. Sheppard *et al.* were unsure whether N_2 was desorbed directly from the sample or from the decomposition of NH_3.

Sheppard *et al.*[21] then examined the phases present at various temperatures after heating on TPD-MS. They repeated the experiment and halted it at 165, 267, 225 and 370 °C. After heating to 165 °C they found the products to be MgH_2, NaH and $NaMgH_3$. There were also other broad diffraction peaks they were unable to identify. To improve the crystallinity, the sample was placed under 200 bar hydrogen and heated to 300 °C. After heating the 165 °C sample under hydrogen pressure, some of the unidentified peaks were found to be $Mg(NH_2)_2$. Other unidentified peaks were found to have disappeared and MgNH peaks had emerged. The authors say the lack of discernible hydrogen evolution during this annealing process suggests that the phase associated with the unidentified peaks converted to MgNH without a detectable hydrogen release.

The sample heated to 267 °C was found to have increased amounts of NaH and $NaMgH_3$, whilst all MgH_2 and $Mg(NH_2)_2$ had disappeared.[21] The unidentified phase found at 165 °C was seen again, this time with a peak shift. Sheppard *et al.* identified this phase as the same as formed by Xiong *et al.*[19] above.

At 335 °C, the peaks of the unidentified phase were sharper and Mg_3N_2 was first observed as a product.[21] There was no $NaMgH_3$ present. Upon further investigation of the unidentified phase, they indexed it to a trigonal space group, possibly *P*3*c*1, with lattice constants a = 6.11 Å and c = 17.90 Å.

The XRD pattern of the sample heated to 370 °C was found to contain Na metal, Mg_3N_2 and another unidentified phase.[21] Sheppard *et al.* reasoned the Na present was due to the decomposition of NaH under residual gas analysis (RGA) conditions. In order to increase the crystallinity of the second unidentified phase, the ball-milled starting materials were first evacuated at 200 °C for 18 hours before being evacuated at 280 °C for 18 hours. The phase was thought to be monoclinic (space group *C*2) with lattice parameters of a = 13.92 Å, b = 3.58 Å, c = 12.39 Å and β = 115.8 °.

Sheppard *et al.*[21] then used Fourier transform infrared spectroscopy (FTIR) to examine the conversion between amide, imide and nitride. The sample after heating to 165 °C was found to have broad absorption features between 3150 and 3300 cm^{-1}. Although poorly resolved, the position of the peaks were consistent with those of alkali and alkaline-earth amides. After desorption up to 267 °C, the FTIR spectrum of the sample had lost all features present at 165 °C and a single broad absorption at 3171 cm^{-1} was present. This was indicative of an imide; either a

new unknown structure of MgNH as the peak did not match those of the known structure of MgNH, or alternatively they suggest the presence of a mixed Na-Mg imide. Further heating of the sample to 335 °C found the peak at 3171 cm^{-1} was sharpened as XRD peaks were found to have similarly sharpened. The FTIR spectrum for 370 °C was devoid of discernible features. This was consistent with the conversion of imide phases to their nitrides. As there was so much Mg_3N_2 present in the XRD pattern it was not possible to define the unknown phase as nitride, but the absence of N-H bonding in the FTIR spectrum ruled out the possibility of amide or imide being formed.

The mass of hydrogen desorbed from the sample at different temperatures was measured.[21] Up to 165 °C 0.5 wt% H_2 was desorbed, this was associated with the formation of a small amount of imide-like phase. Between 165–267 °C a yield of 2.0 wt% H_2 was attributed to complete decomposition of $Mg(NH_2)_2$ to the imide-like unknown phase. Between 267 and 335 °C 0.8 wt% H_2 was desorbed. This was assigned to the decomposition of $NaMgH_3$ and the formation of Mg_3N_2. A total of 3.3 wt% H_2 was desorbed; just over half the total hydrogen in the sample.

Sheppard *et al.*[21] attempted to quantify the Na content of their two unknown phases using XRD by mixing samples with a known amount of an internal standard. This process deteriorated the already poorly crystalline XRD peaks, making quantification impossible.

In the following chapter sodium amide will be used in place of lithium amide in the reaction with magnesium hydride. In order to establish the best possible ratio between reactants, 4 ratios were investigated. $2NaNH_2 + 3MgH_2$ was investigated (without ball-milling). In order to

compare with $2LiNH_2 + MgH_2$, $2NaNH_2 + MgH_2$ was investigated. In order to compare reaction schemes with Xiong *et al.*,[19] $3NaNH_2 + 2MgH_2$ and $NaNH_2 + MgH_2$ were investigated. These reactions had the same number of each metal ion present in order to compare $Mg(NH_2)_2$ +NaH based reactions with $NaNH_2 + MgH_2$ based reactions, but the amide:hydride ratios were different. The full range of ratios were:

$2NaNH_2 + 3MgH_2$; $2NaNH_2 + MgH_2$; $3NaNH_2 + 2MgH_2$ and $NaNH_2 + MgH_2$.

In addition to the reactions above, $NaH + MgH_2$ and $Mg(NH_2)_2 + NaNH_2$ were also investigated in response to findings from the initial $xNaNH_2 + yMgH_2$ reactions.

2. Results

1. $2NaNH_2 + 3MgH_2$

1. *Temperature Programmed Desorption-Mass Spectrometry*

$NaNH_2$ and MgH_2 were heated together in a 2:3 ratio. The reaction was initially carried out on a TPD-MS apparatus at a heating rate of 2 °C min^{-1} to 350 °C. The investigation into this system initially investigated the desorption characteristics in order to see whether there was any similarity with the Li-Mg-N-H system in desorption of hydrogen gas alone, without any accompanying ammonia.

It can be seen from Figure 4-1 that hydrogen was the only gas observed with no evidence of any ammonia desorbed above the detection limit of the mass spectrometer. The hydrogen trace showed the desorption starting from 120 °C with a number of distinct peaks. The first peak at 150 °C was accompanied by a fluctuation in the temperature trace. The rate of hydrogen

desorption decreased between 150 and 180 °C when the rate increased again quite quickly. This peaked at 255 °C before the rate of desorption diminished. The rate again increased for the third and fourth desorptions at 292 °C. The third desorption peaked at 320 °C. The rate decreased, but a shoulder of hydrogen appeared once the temperature had reached 350 °C. The hydrogen desorption then slowly tailed off during isothermal heating. A comparison between this hydrogen desorption and that of the other $x\mathrm{NaNH_2} + y\mathrm{MgH_2}$ reactions can be seen in Figure 4-30.

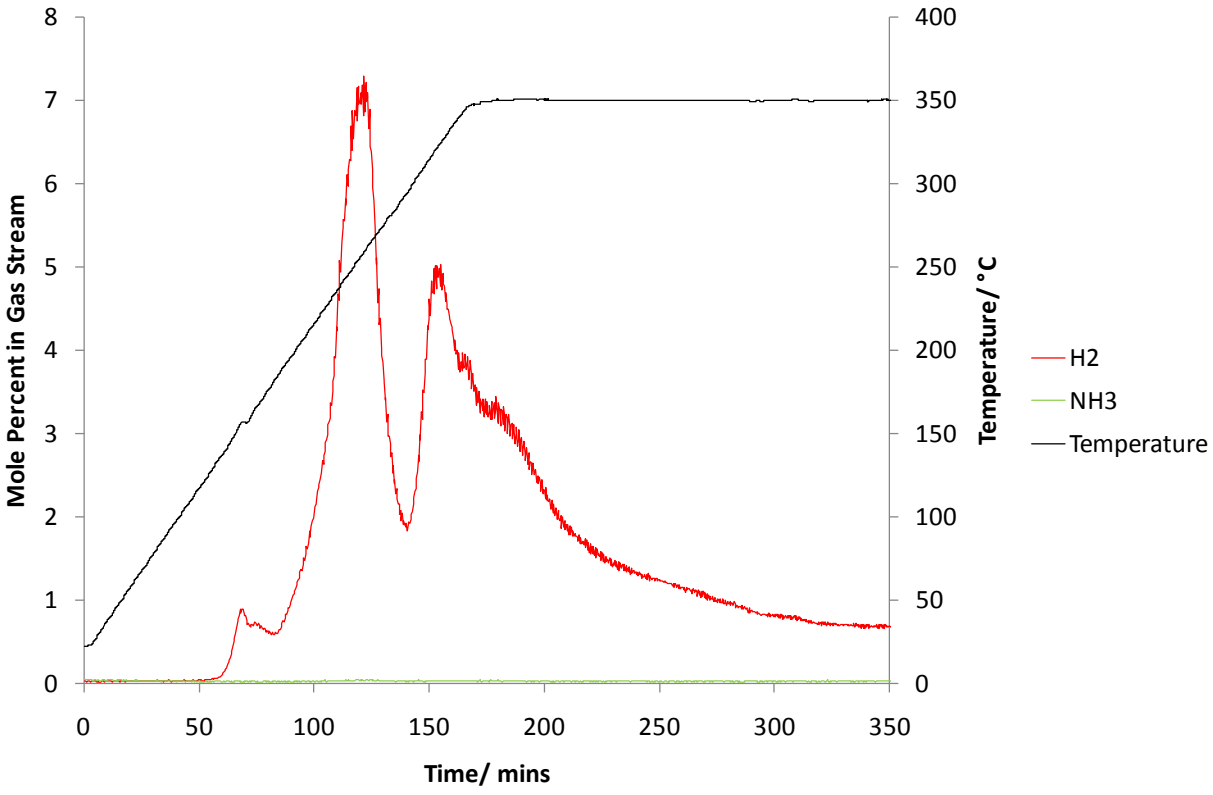

Figure 4-1 TPD-MS analysis of the $2\mathrm{NaNH_2} + 3\mathrm{MgH_2}$ reaction. The temperature trace is shown in black and the MS traces for H_2 and NH_3 are shown in red and green, respectively.

The temperature trace was then compared to that of the furnace power (Figure 4-2). It was seen that the fluctuation in the temperature trace at 150 °C was accompanied by a fluctuation in the furnace power. The temperature trace had a small increase followed by a small drop. The furnace power showed a decrease in power at 150 °C followed by an increase. This indicated this fluctuation was due to an exothermic event.

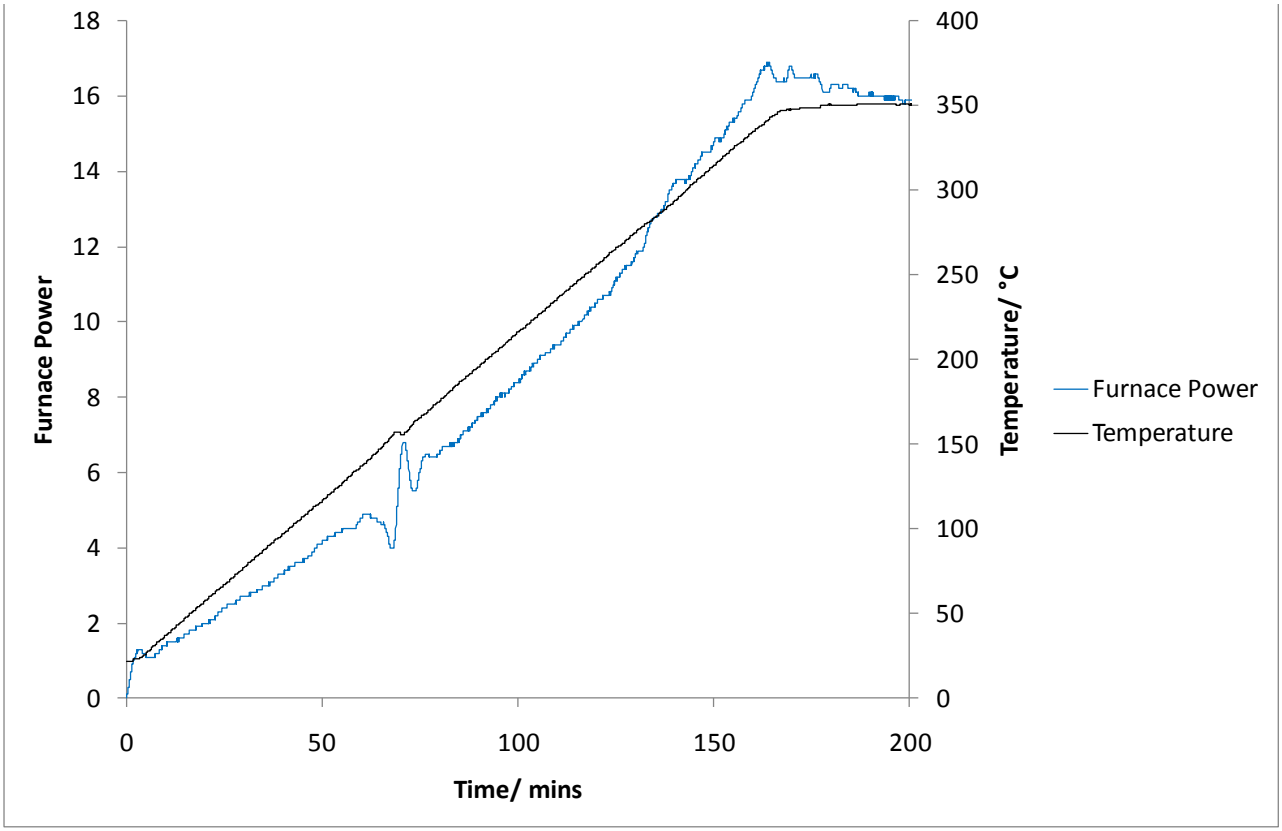

Figure 4-2 Furnace power during the TPD-MS analysis of $2NaNH_2 + 3MgH_2$ reaction to 350 °C. The furnace power and temperature are shown in blue and black respectively.

2. Flowing Line Reactions

As the hydrogen trace showed more than one hydrogen desorption, the reaction was carried out to intermediate temperatures in order to find out more about the reaction mechanism occurring in each temperature regime. The first peak in the TPD trace was observed at 150 °C; therefore the reactants were heated together at 150 °C for 12 hours. This temperature also coincided with the exothermic event identified in the furnace power plot of the TPD-MS apparatus (Figure 4-2). The products identifiable from powder XRD were a mixture of $Mg(NH_2)_2$ and NaH, as well as some of the starting material MgH_2 (Figure 4-7). A very small amount of $NaMgH_3$ was also present in the product mixture.

In order to investigate the origin of the $NaMgH_3$ observed in the reaction products, the formation of $NaMgH_3$ from reaction of the binary hydrides, NaH and MgH_2, was studied. NaH and MgH_2 were reacted in a 1:1 ratio under argon at various temperatures. After reaction at 150 °C, the temperature at which $NaMgH_3$ was observed in the reaction $2NaNH_2 + 3MgH_2$, only the starting binary hydrides were observed in the powder XRD pattern. Heating to the higher temperature of 250 °C was required in order to produce $NaMgH_3$, although the starting materials and some Mg were also present (Figure 4-3). The presence of Mg is not unexpected as the decomposition of MgH_2 to its constituent elements is kinetically slow. The amount of Mg + MgH_2 is comparable to NaH.

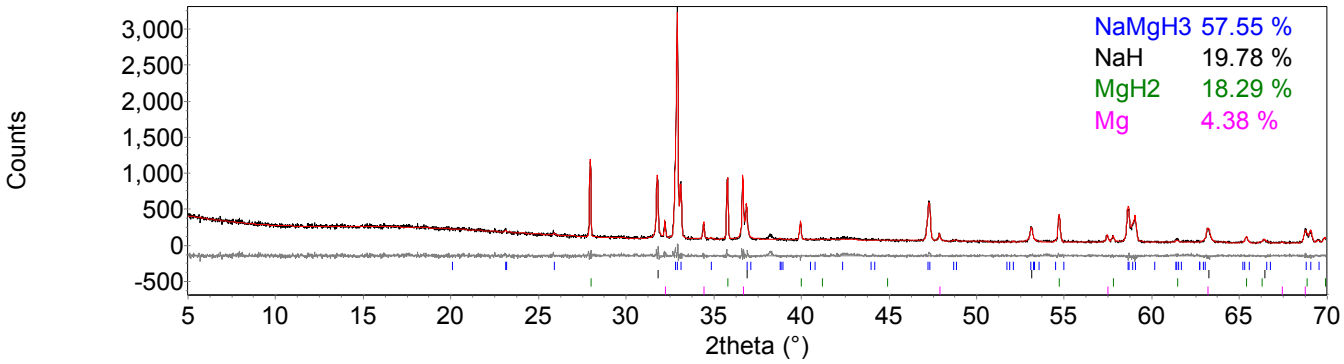

Figure 4-3 Powder XRD pattern of NaH + MgH_2, heated to 250 °C for 24 hours on a flowing line. The observed powder XRD pattern (black line) was fitted using a Rietveld fit (red line) to the observed phases $NaMgH_3$ (blue tick marks), NaH (black tick marks), MgH_2 (green tick marks) and Mg (pink tick marks). R_{wp} = 9.502, R_{exp} = 7.880, X^2 = 1.5.

Table 4-1 Summary table of weight percents and mole fractions of products of NaH + MgH_2 heated to 250 °C for 24 hours.

Phase	*Weight Percent in XRD*	*Mole Fraction/ mol %*
$NaMgH_3$	57.55	40.28
NaH	19.78	28.98
MgH_2	18.29	24.38
Mg	4.38	6.36

On heating the NaH and MgH_2 starting materials to 300 °C all MgH_2 had converted to Mg and the amount of $NaMgH_3$ present had dropped off, possibly because of the sublimation of Mg. Reducing the reaction temperature to 275 °C and heating for 18 hours gave the highest proportion of $NaMgH_3$, along with Mg and minimal starting materials still present.

Longer heating of the $NaMgH_3$ at this temperature appeared to result in the decomposition of $NaMgH_3$ to NaH and Mg; the temperature was too low to decompose NaH. Overall, $NaMgH_3$ was shown to form by the direct reaction of NaH with MgH_2 at temperatures above 250 °C.

The second desorption event of $2NaNH_2 + 3MgH_2$ peaked at 250 °C, with a 1.6 wt% hydrogen loss. The starting materials were heated at 250 °C for 12 hours. The products were then examined by powder XRD and found to be MgH_2 and NaH, along with a greater proportion of $NaMgH_3$ than before. There were also many unidentified peaks (unidentified phase A) in the XRD pattern (Figure 4-7). The positions and relative intensities of these peaks were consistent when the reaction was repeated.

The starting materials were heated for longer (18 and 24 hours) and then ground and annealed in order to attempt to form phase A pure. Quenching was also employed, as well as heating the starting materials to slightly higher and lower temperatures (225 and 275 °C). Attempts to form phase A in high purity were unsuccessful, with a certain amount of starting material always present. In order to investigate the internal bonding of phase A Raman spectroscopy was employed.

3. Raman Spectroscopy

Raman spectroscopy of the products of $2NaNH_2 + 3MgH_2$, heated to 250 °C for 12 hours (unidentified phase A, NaH and MgH_2) were compared to $Mg(NH_2)_2$, $NaNH_2$ and Li_2NH. (Unfortunately no Raman spectra could be found for MgNH in the literature.) The Raman spectrum, Figure 4-4 below, showed peaks present in the imide/amide region.

In the Raman spectrum of the products of this reaction there were two major stretches, each with 2 peaks, at 3177 and 3263 cm^{-1}. When compared to $Mg(NH_2)_2$ and $NaNH_2$ (Figure 4-5), the new phase stretches had been displaced downfield from the amide region. It can be seen from Figure 4-6 that the stretches from unidentified phase A were in the same region as lithium imide N-H stretches.

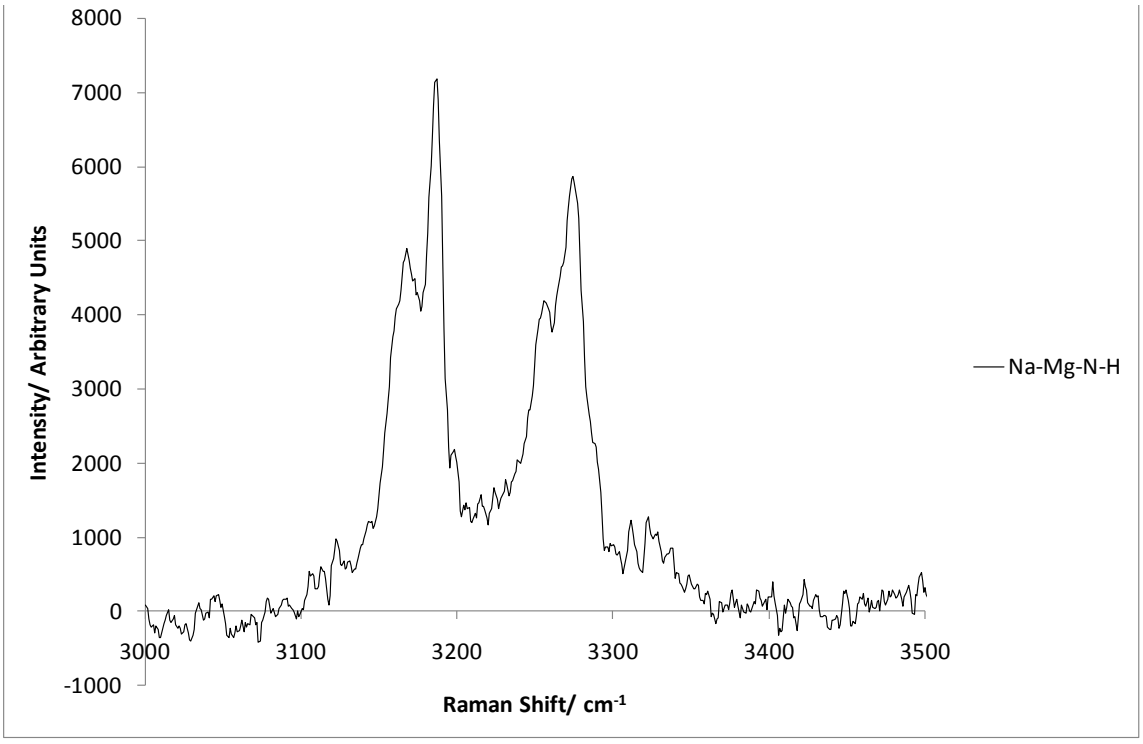

Figure 4-4 Raman spectrum of the N-H region of $2NaNH_2 + 3MgH_2$ heated at 250 °C for 12 hours. The phases present were MgH_2, NaH and phase A.

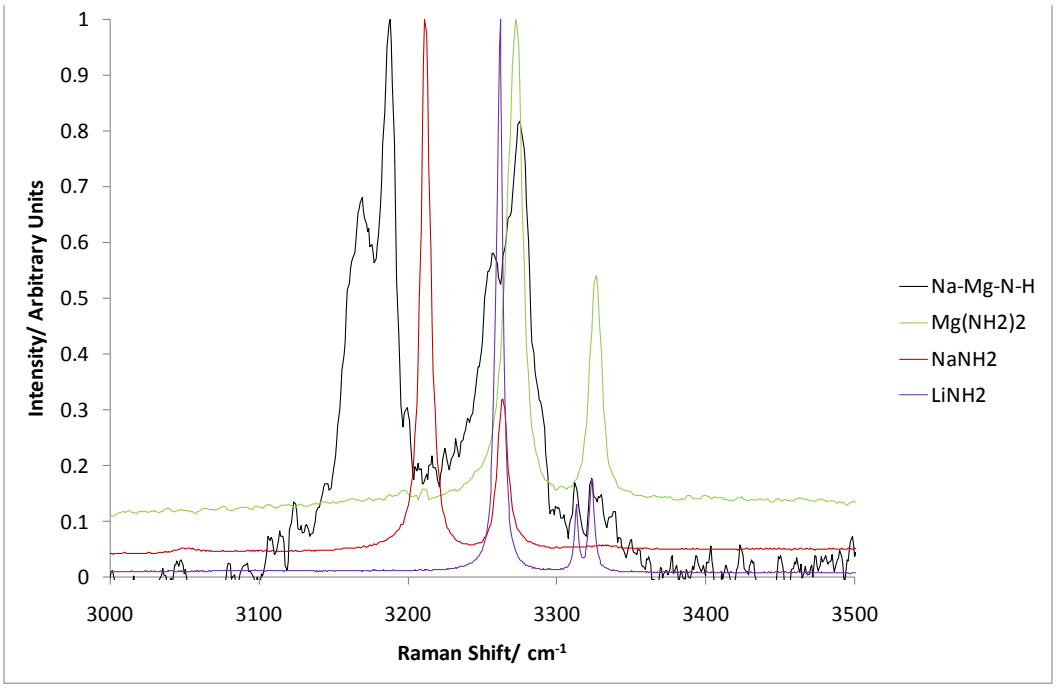

Figure 4-5 Comparison of the Raman spectra of the N-H region of $2NaNH_2 + 3MgH_2$ heated at 250 °C for 12 hours, $NaNH_2$ and $Mg(NH_2)_2$.

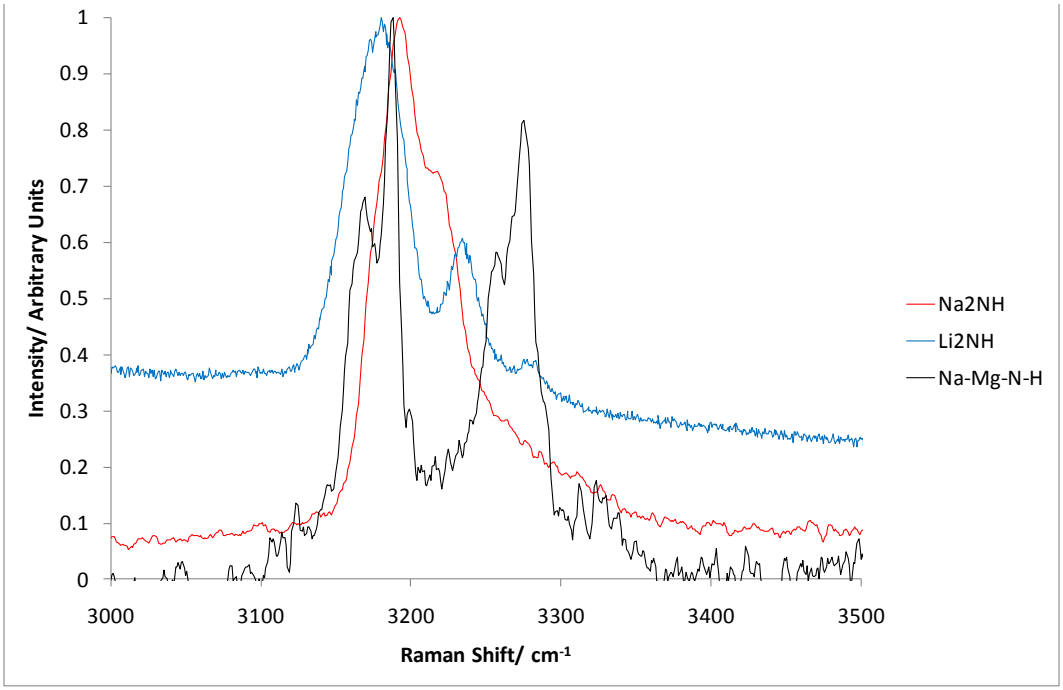

Figure 4-6 Comparison of the Raman spectra of the N-H region of $2NaNH_2 + 3MgH_2$ heated at 250 °C for 12 hours and Li_2NH.

When the $2NaNH_2 + 3MgH_2$ starting materials were heated to 300 °C for 12 hours, there was still evidence of unidentified phase A (Figure 4-7). Phase A was fitted with a Pawley fit. The best fit was for a trigonal unit cell with space group *P*−3*c*1, *P*3*c*1, *P*63*cm*, *P*−6*c*2 or *P*63/*mcm* with lattice parameters $a = 6.1077(7)$ Å and $c = 17.881(3)$. There was also a large amount of Mg_3N_2 and a continued presence of NaH, $NaMgH_3$ and MgH_2 starting material. The lattice parameters of the other phases are known and were fitted using a Rietveld refinement. This means a weight percentage of the total mixture could be estimated. As the structural model for phase A is unknown, no estimate of the percentage in the mixture can be made. This is referred to as Pawley in the table (Table 4-2) where weight percent and mole fractions should appear. The fitting of phase A with a Pawley fitting does not alter the ratios of the other products to each other.

The $2NaNH_2 + 3MgH_2$ reactants were then heated on the flowing gas line at 350 °C for 12 hours. The products were NaH and Mg_3N_2 (Figure 4-7). There was also a large amount of Na present. There was no evidence of phase A at this temperature.

Mg_3N_2 and Na were the fully dehydrided products of this reaction of $2NaNH_2 + 3MgH_2$. The overall reaction could be expressed as:

Equation 4-1 $$2NaNH_2 + 3MgH_2 \rightarrow Mg_3N_2 + 2Na + 5H_2$$

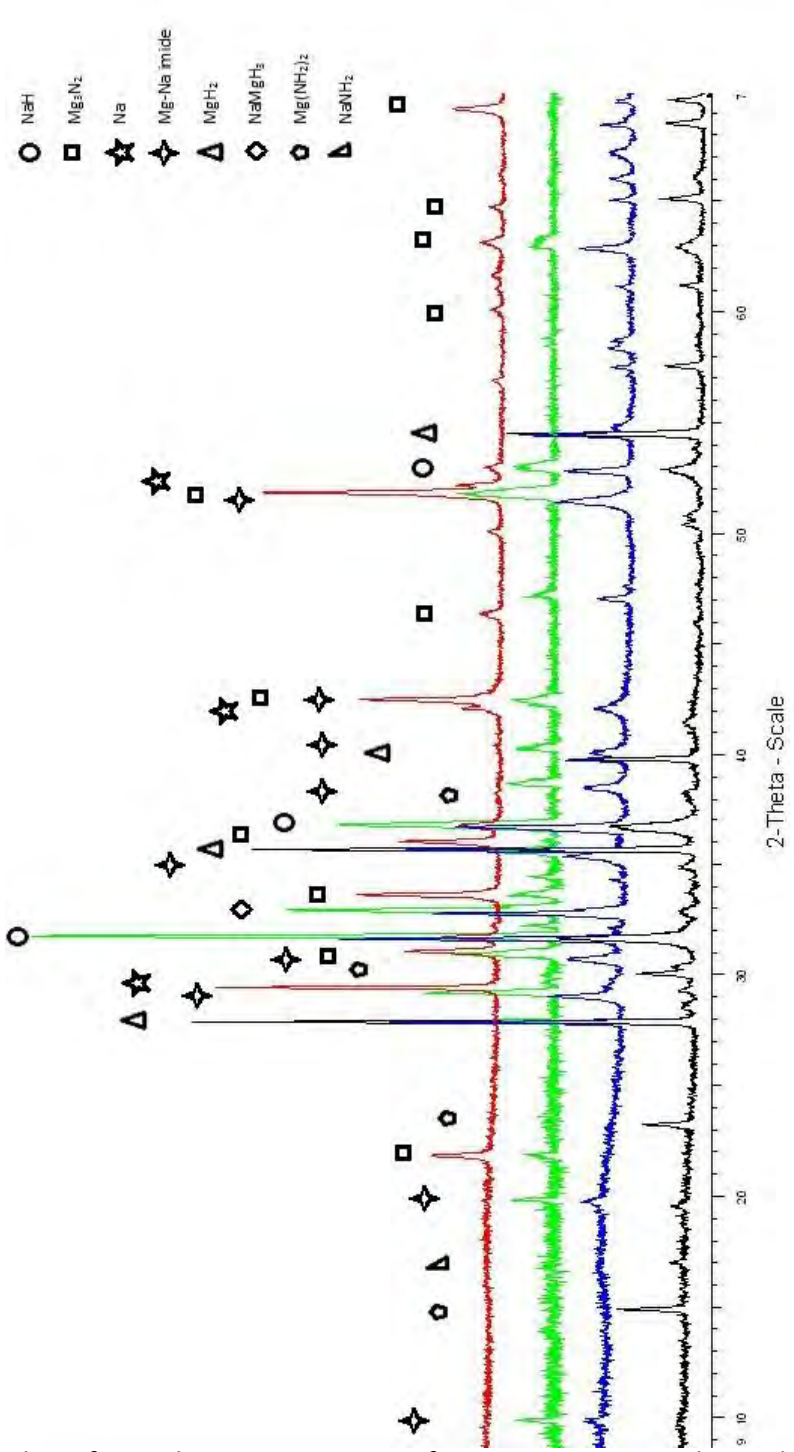

Figure 4-7 Stack plot of powder XRD patterns of $2NaNH_2 + 3MgH_2$ heated to 150 °C (black), 250 °C (blue), 300 °C (green) and 350 °C (red). The individual XRD patterns can be found in the appendix.

Table 4-2 Summary table of weight percents and mole fractions of products of $2NaNH_2 + 3MgH_2$ from powder XRD shown in Figure 4-7.

$2NaNH_2 + 3MgH_2$	Temperature									
	150		250		300		350			
Phase	Weight % in XRD	Mole Fraction	Weight % in XRD	Mole Fraction	Weight % in XRD	Mole Fraction	Weight % in XRD	Mole Fraction		
MgH_2	44.34	49.58	34.95	37.57	4.40	6.01	NA	NA		
NaH	32.27	38.70	42.31	49.72	48.61	72.87	8.73	21.10		
$Mg(NH_2)_2$	18.82	9.54	NA	NA	NA	NA	NA	NA		
$NaNH_2$	3.40	2.60	NA	NA	NA	NA	NA	NA		
$NaMgH_3$	1.17	0.58	22.74	12.71	12.61	8.69	NA	NA		
Mg_3N_2	NA	NA	NA	NA	34.87	12.43	77.76	44.69		
Phase A	NA	NA	NA	NA	Pawley	Pawley	NA	NA		
Na	NA	NA	NA	NA	NA	NA	13.51	34.21		

4. Rehydriding Studies

$2NaNH_2 + 3MgH_2$ were heated together at 250 °C for 12 hours in an attempt to maximise the amount of new phase A present. This sample was then tested on an intelligent gravimetric analyser (IGA) in order to assess its ability to rehydride. The sample was heated to 200 °C under 18 bar hydrogen for 100 hours. Upon heating, the sample immediately started to take up hydrogen. After rehydriding it was found to have absorbed 1.82 wt% H_2 (Figure 4-8). This was in llcomparison to a theoretical uptake of 2.6 wt%. The uptake was not quite complete when the reaction was stopped. Although the hydrogen uptake was not complete, substantial rehydriding had occurred; full rehydriding may only have been possible after a significantly longer time, higher hydrogen pressure or different temperature.

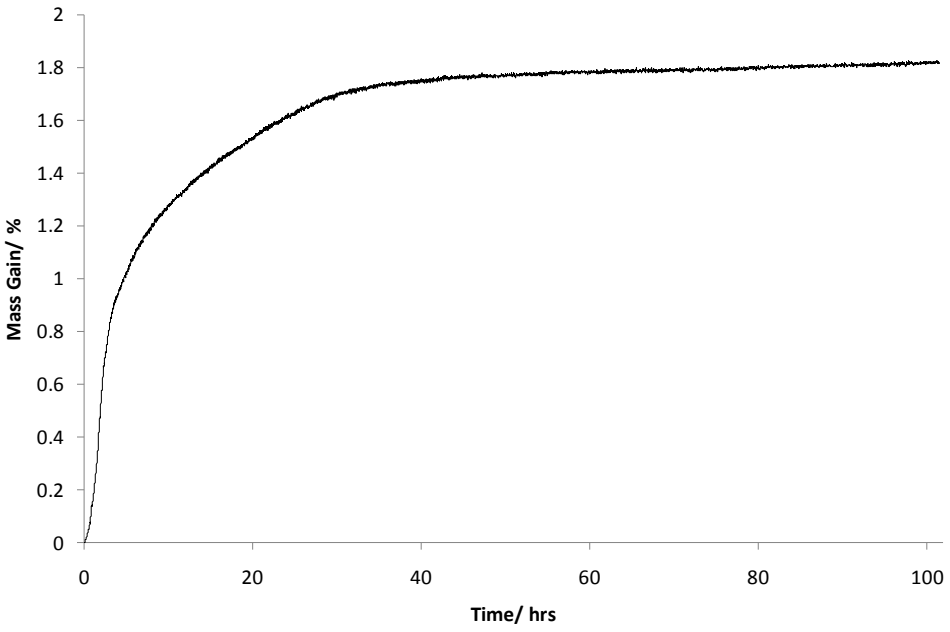

Figure 4-8 Mass gain of the products of $2NaNH_2 + 3MgH_2$ when heated to 250 °C for 2 hours, rehydrided under 18 bar hydrogen at 200 °C for 100 hours.

5. Discussion

The first stage of this multi-step reaction appeared to be an exothermic metathesis reaction, although it was slow and incomplete under the conditions examined here. The products from heating to 150 °C (Figure 4-7) were a mixture of MgH_2 and a small amount of $NaNH_2$ starting materials as well as $Mg(NH_2)_2$ and NaH products. These are products that would be present had a salt metathesis reaction occurred. MgH_2 starting material would also be expected to be present, as it was in excess for the metathesis (Equation 4-2).

Equation 4-2 $$2NaNH_2 + 3MgH_2 \rightarrow Mg(NH_2)_2 + 2NaH + 2MgH_2$$

A salt methathesis reaction between a group one amide $LiNH_2$ and MgH_2 has been shown to occur previously,[22] before going on to react further. A mixture of $2LiNH_2 + MgH_2$ was heated to 220 °C under 100 bar H_2 for 2 hours in order to establish the reaction mechanism. The powder XRD after this experiment showed the presence of $Mg(NH_2)_2$ and LiH, as well as the starting materials $LiNH_2$ and MgH_2. This is analogous to our metathesis observed.

Thermodynamics suggests the enthalpy of formation of $Mg(NH_2)_2$ plus NaH is more exothermic than that of $NaNH_2$ and MgH_2 (Table 4–3). The addition of heat to this reaction was enough to surmount the activation energy and cause the metathesis to take place.

Table 4-3 Enthalpy of formation values for $NaNH_2$, MgH_2, $Mg(NH_2)_2$ and NaH.

Substance	*$\Delta_f H$ ° (kJ mol^{-1})*
$NaNH_2$	–123.8[23]
MgH_2	–75.3
$Mg(NH_2)_2$	–325.0[26]
NaH	–56.3

$$\Delta H^\circ = \left(\Delta_f H^\circ(\mathrm{Mg(NH_2)_2}) + 2\Delta_f H^\circ(\mathrm{NaH})\right) - \left(2\Delta_f H^\circ(\mathrm{NaNH_2}) + \Delta_f H^\circ(\mathrm{MgH_2})\right)$$

$$\Delta H^\circ = \left(-325.0 + (2 \times -56.3)\right) - \left((2 \times -123.8) - 75.3\right)$$

$$\Delta H^\circ = -114.7 \text{ kJ mol}^{-1}$$

Sheppard *et al.*[21] ball-milled $NaNH_2$ + MgH_2 and found a metathesis reaction occurred. They found NaH appeared in their XRD pattern, however $Mg(NH_2)_2$ was not observed due to amorphisation.

The salt metathesis reaction can be identified as the exothermic event that was observed in the furnace power (Figure 4-2). The metathesis involved the exchange of $[NH_2]^-$ and H^- between $NaNH_2$ and MgH_2. Theoretically there should not be any hydrogen desorption associated with the metathesis. The relatively small hydrogen desorption (0.11 wt%) that was observed in the TPD-MS trace was possibly due to the increase in temperature caused by the exothermic nature of the metathesis. This could have raised the temperature enough locally in the sample to promote hydrogen release. The hydrogen desorption was unlikely to have occurred from the starting materials. The decomposition temperature of sodium amide is 210 °C and this would not release only hydrogen; magnesium hydride is well documented to decompose at 280–

300 °C very slowly, with the release of hydrogen. The newly formed magnesium amide decomposes with the release of ammonia at 350 °C and sodium hydride decomposes with the release of hydrogen at above 400 °C.[20] The hydrogen release at 150 °C was likely to have been from the reaction of some of these materials together.

Sheppard *et al.*[21] also observed hydrogen release from their $2NaNH_2 + 3MgH_2$ reaction below 165 °C. This was accounted for by the formation of the imide-like phase.

Both $Mg(NH_2)_2$ and MgH_2 were present after the metathesis. It might be expected they would react together with further heating, *cf*. $LiNH_2$-LiH, to form MgNH.

Nakamori *et al.*,[7] having successfully formed $Mg(NH_2)_2$,[*] investigated the reaction between $Mg(NH_2)_2$ and MgH_2 in 1:1 and 1:2 ratios.

They expected the reactions to proceed as follows:

Equation 4-3 $Mg(NH_2)_2 + MgH_2 \rightarrow 2MgNH + 2H_2$

Equation 4-4 $Mg(NH_2)_2 + 2MgH_2 \rightarrow Mg_3N_2 + 4H_2$

These reactions are analogous to the $LiNH_2$-LiH system. However, from TG data it could be seen that weight loss reactions occurred at 357 °C and 447–477 °C.[7] The weight losses were approximately 24 wt% and 16 wt% for $Mg(NH_2)_2 + MgH_2$ and $Mg(NH_2)_2 + 2MgH_2$, respectively. These mass losses were much greater than expected for the reactions above (Equation 4-3 and

[*] $Mg(NH_2)_2$ was formed by exposing MgH_2 (and Mg present in starting material) to 5 bar of ammonia. This was heated to 330-380 °C for 1 week. $Mg(NH_2)_2$ was optimally formed at 340 °C.

Equation 4-4). (4.9 wt% and 7.4 wt%, respectively.) It was suggested that the release of ammonia along with hydrogen would give rise to these increased mass losses. As the temperature at which the mass losses were observed were the same as for the $Mg(NH_2)_2$ NH_3 releasing decomposition to form MgNH, it can be seen that the addition of MgH_2 to $Mg(NH_2)_2$ did not result in any reaction between the amide and hydride. Nakamori *et al.* reasoned the slow kinetics between MgH_2 and ammonia in order to form $Mg(NH_2)_2$ was the cause of the lack of interaction. This indicated the reaction of MgH_2 and ammonia was in the order of days, unlike LiH and ammonia which is ultra fast (25ms), and therefore unlikely to result in the same kinetic products.

Leng *et al.*[24] ball-milled $Mg(NH_2)_2$[†] with $2MgH_2$ for two hours. The reaction mixture was then heated up to 500 °C. Hydrogen was observed being desorbed from 80 °C, but there was no peak in the desorption until 415 °C. The low desorption temperature was said to be due to the low decomposition temperature of the $Mg(NH_2)_2$ starting material. Leng *et al.* said this was probably due to the ball-milling. The wide temperature range for the hydrogen desorption was said to be due to the slow reaction between MgH_2 and NH_3. This was regarded as disappointing by Leng *et al.* as a major desorption of hydrogen gas was not observed until a higher temperature then the $LiNH_2$ + LiH system to which $Mg(NH_2)_2$ + $2MgH_2$ was compared.

In order to build upon the failed attempts at a reaction between $Mg(NH_2)_2$ and MgH_2 by Nakamori *et al.,*[7] Hu *et al.*[25] ball-milled $Mg(NH_2)_2$[‡] in a 1:1 ratio with MgH_2. Hydrogen was found

[†] $Mg(NH_2)_2$ was formed by heating ball-milled MgH_2 under an ammonia atmosphere of 4 bar.
[‡] Hu *et al*. formed $Mg(NH_2)_2$ by reacting Mg powder with 8.3 bar ammonia at 300 °C.

to be the only gaseous product generated during ball-milling. The reactants were ball-milled for up to 72 h. Up to 5 h of ball-milling no gas was detected. Only with further milling, and therefore a greater decrease in particle size, did any detectable solid state reaction occur.

The reactants, ball-milled for different lengths of time, were then exposed to heating on a TPD-MS apparatus. The sample milled for 5 h released hydrogen above 200 °C whereas after milling for 11 h or longer, the hydrogen started to desorb as low as 65 °C.

Hu *et al.*[26] found their ball-milling of $Mg(NH_2)_2$ + MgH_2 in a 1:1 ratio was successful in releasing only hydrogen. Hu *et al.*[25] continued their work on this system by mixing equimolar amounts of $H^{\delta+}$ in amide and H^- in hydride in a 1:1 ratio i.e. $Mg(NH_2)_2$ + $2MgH_2$. The mixture of starting materials was initially milled for 72 h at room temperature. The pressure inside the ball mill increased with time. The gas responsible for the pressure build-up was found to be pure hydrogen. Hydrogen release started after 2 h and accelerated after 5 h. The rate of release slowed after 20 h. As neither starting material released hydrogen when ball-milled alone, the hydrogen release must have been from the reaction between the $Mg(NH_2)_2$ and MgH_2. The delayed time before release was due to the particle sizes of the reactants being too large. After 72 h ball-milling all the hydrogen was released from the starting materials. From FTIR and XRD the phases present throughout ball-milling where found first to be $Mg(NH_2)_2$, followed by MgNH and finally Mg_3N_2. The enthalpy of formation of $Mg(NH_2)_2$ was found to be $-325\ kJmol^{-1}$. In comparison to work carried out previously by Hu *et al.*,[26] it can be seen the additional MgH_2 caused the reaction mixture to dehydride fully and form Mg_3N_2.

$NaMgH_3$ was also found to be present, although in a very small amount (as shown in Figure 7-1). The formation of $NaMgH_3$ has been reported to occur at 480 °C when NaH was heated with Mg metal in equimolar amounts for 24 hours under 10 bar H_2 (Equation 4-5).[27] Clearly the conditions described here were beneficial for the formation of $NaMgH_3$ at a radically lower temperature than previously reported. $NaMgH_3$ was also observed by Sheppard *et al.*[21] after ball-milling $NaNH_2$ + MgH_2 and heating to 160 °C. The unit cell published by Bouamrane *et al.*[27] is shown in Figure 4-9. It is orthorhombic, space group *Pnma* and lattice parameters of a = 5.4634 Å, b = 7.703 Å and c = 5.4108 Å.

Equation 4-5 $NaH + Mg + H_2 \rightarrow NaMgH_3$

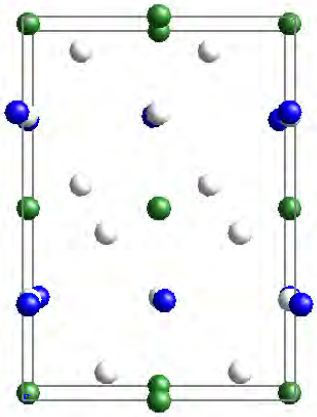

Figure 4-9 Crystal structure of $NaMgH_3$. Sodium is shown in blue, magnesium sites in green and hydrogen in grey. The unit cell is shown in black.[27]

Shortly after this work, Ronnebro *et al.*[28] formed $NaMgH_3$ by heating different ratios of ground NaH and MgH_2 in a pressed tablet up to 380 °C under 70 bar H_2 for 1 week. $NaMgH_3$ only formed when a 1:1 ratio of starting materials was heated to 350 °C under 70 bar H_2 for a few hours.

Several years later Ikeda *et al.*[29] were the first group to synthesise $NaMgH_3$ by ball-milling NaH and MgH_2. This occurred at 300 °C under H_2 for 20 h at room temperature. The crystal structure was found to be thermally stable to 300 °C. They also attempted to form $LiMgH_3$, however under these conditions, it was not possible.

Ikeda *et al.*[30,31] continued their work on $NaMgH_3$ by investigating the reversibility of hydriding and dehydriding the material. The sample was formed as above by ball-milling, and was then heat-treated at 300 and 500 °C, under 10 bar H_2 for 3 hours. The structure here was stable to 500 °C under 10 bar H_2. Upon heating to 400 °C under 10 bar He, the mass loss was found to be 5.8 ± 0.2 wt% within 8 minutes. This mass coincided with the hydrogen content of $NaMgH_3$. Using powder XRD the dehydriding process was found to proceed along the following steps:

Equation 4-6 $NaMgH_3 \rightarrow NaH + Mg + H_2$

Equation 4-7 $NaH + Mg + H_2 \rightarrow Na + Mg + 3/2H_2$

Rehydriding was possible by heating up the elemental Na and Mg to 400 °C for 3 hours under 10 bar of hydrogen.

The same group continued their work[32] and found the charge density distributions[§] indicated that $NaMgH_3$ contained two hydrogen anions on different crystallographic sites.

Wu *et al.*[33] found the hydriding/dehydriding of $NaMgH_3$ could occur at temperatures as low as 350 °C, an improvement of 50 °C compared to Ikeda *et al.*[30]

It is possible that $NaMgH_3$ could be formed under the conditions used in $x$$NaNH_2$ + $y$$MgH_2$ reactions from the decomposition of a mixed Na-Mg amide formed. Alternatively, $NaMgH_3$ may be formed from the diffusing of Na^+ from $NaNH_2$ into MgH_2, therefore forming $NaMgH_3$ as an intermediate, or from a direct reaction between NaH, formed from the metathesis, and MgH_2, starting material.

The peaks from phase A present after heating to 250 °C, in Figure 4-7, were found to be similar to those previously reported by Xiong *et al.*,[4] after heating a ball-milled $2Mg(NH_2)_2$ + 3NaH mixture to 190 °C and recently indexed by Sheppard *et al.*[21] This phase identified by Xiong *et al.*[4] rehydrided to $Mg(NH_2)_2$ and NaH.

Xiong *et al.*[4] did not attempt to index their XRD pattern and therefore identify the material involved. Our attempts to index the peaks have so far suggested a trigonal unit cell with space group *P*−3*c*1, *P*3*c*1, *P*63*cm*, *P*−6*c*2 or *P*63/*mcm* with lattice parameters a = 6.1077(7) Å and c = 17.881(3) Å. Since our indexing of the phase, Sheppard *et al.*[21] published their lattice parameters of the same phase. They also indexed it to a trigonal unit cell with possible space group *P*3*c*1 and lattice constants a = 6.11 Å and c = 17.90 Å. These parameters matched very closely with ours.

[§] Charge density distributions found from maximum entropy method (MEM)/Rietveld method from synchrotron XRD.

It might be expected that an amide minus hydrogen would result in an imide, as is the case with $LiNH_2$ + LiH or $2LiNH_2$ + MgH_2. In this case, with $2NaNH_2$ + $3MgH_2$, a mixed Na-Mg imide could be formed. There was also a lack of nitrogen present in crystalline form in the identified products, along with the lack of ammonia, NH_3, detected. However, in the literature there are no known mixed Na-Mg-cation imides or amides, sodium imide or indeed any sodium containing imides. There was no Na_3N formed at any point during any of these reactions. Na_3N has only been formed with great difficulty by passing electrical discharges through sodium under low nitrogen pressure[34] or more recently by plasma-assisted synthesis.[35,36] Moldenhauer and Mottig[37] disagreed with Wattenberg *et al.*[34] and suggested that evaporating a mixture of sodium azide (NaN_3) and Na could form sodium nitride. Its formation has not been observed under conventional synthesis conditions.

The Raman spectroscopy undertaken (Figure 4-4) showed clear evidence of nitrogen present in the products, due to the presence of peaks in the N-H region of the spectrum. This must have been present in phase A and any amorphous products present, as neither of the known products (NaH and MgH_2) contained nitrogen.

The release of hydrogen from the system, as well as the position of the N-H stretches in the N-H region of the Raman spectrum, point to the formation of an imide rather than a mixed Na-Mg amide. The imide could be either an unknown polymorph of MgNH or a new mixed Na-Mg imide; these suggestions concur with the conclusions of Sheppard *et al*. Sodium imide is unlikely to be formed, as it is unknown in the literature. The two peaks for each of the main stretches were most likely due to two different N-H environments within the phase. If a mixed Na-Mg

imide was formed, and both cations were bonded to N-H groups, the twin peaks in the Raman spectrum could be accounted for.

By charge balancing the possible imide along with the excess hydrides, it was possible to suggest the following idealised reaction (Equation 4-8):

Equation 4-8 $Mg(NH_2)_2 + 2NaH + 2MgH_2 \rightarrow 2\ Mg_{(1-x)}Na_{2x}(NH) + (1+2x)MgH_2 + (2-4x)NaH + 2H_2$

The ratio of moles of MgH_2 to NaH observed was 7:9. This could be used to suggest a value for *x*. For $(1+2x)/(2-4x) = 7/9$, $x = 0.11$. The mixed imide would have the possible formula $Mg_{0.89}Na_{0.22}(NH)$, this approximately equates to $Mg_9Na_2(NH)_{10}$.

Dolotko *et al.*[18] heated their $2NaNH_2 + 3MgH_2$ mixture to 250 °C and found decreased amounts of NaH, MgH_2 and $Mg(NH_2)_2$ (as we did); however, Dolotko *et al.* had an increase in the intensities of the XRD peaks for $NaMgH_3$ and Mg_3N_2. 250 °C is a lower temperature than we found the formation of Mg_3N_2 to occur. They made no mention of finding a new phase at this temperature.

Dolotko *et al.*[18] also investigated the analogous reaction $2LiNH_2 + 3MgH_2$. After heating to 250 °C, LiH (a metathesis product) was present along with $Li_2Mg(NH)_2$, Mg_3N_2 and unreacted starting material MgH_2. These products are equivalent to those found by our $2NaNH_2 + 3MgH_2$ reaction heated to 250 °C.

Mg_3N_2 first appeared as a product of our reaction after heating to 300 °C (Figure 4-7). There was no longer MgH_2 starting material present. As mentioned above, nitrides can result from the

reaction of an appropriate imide and a hydride. The Mg_3N_2 was thought to be present due to decomposition of the mixed imide upon reaction with excess MgH_2. This was backed up by the observation of continued hydrogen desorption (Equation 4-9).

Equation 4-9 $$2Mg_{(1-x)}Na_{2x}(NH) + (1+2x)MgH_2 + (2-4x)NaH \rightarrow Mg_3N_2 + 2NaH + 2H_2$$

On further heating their sample, Dolotko *et al.* found a decreased amount of MgH_2 and an increased proportion of LiH and Mg_3N_2.

Sheppard *et al.*[21] found the products after heating $2NaNH_2 + 3MgH_2$ to 335 °C to be Mg_3N_2, NaH and the possible mixed imide. No MgH_2 or $NaMgH_3$ was present.

In Figure 4-7, the products from our reaction at 350 °C were Mg_3N_2 and Na. The Na present was thought to be due to the decomposition of NaH (Equation 4-10). The long tail off of hydrogen at 350 °C in Figure 4-1 is consistent with this. The decomposition of NaH to its elemental form has been reported to occur at temperatures around 425 °C.[20] It is possible the conditions that were present during this reaction may be conducive to lowering this temperature, to just below 350 °C. Further investigations by us showed NaH alone to decompose to Na and hydrogen under flowing argon gas (zero hydrogen partial pressure) at 350 °C (Equation 4-10).

Equation 4-10 $$2NaH \rightarrow 2Na + H_2$$

Sheppard *et al.*[21] also found Na present after heating their sample to 370 °C and also put it down to the decomposition of NaH to Na.

Dolotko *et al.*[18] heated a sample of $2NaNH_2 + 3MgH_2$ to 395 °C. They found the final products were Mg_3N_2 and NaH along with desorbed H_2. After ball-milling, they heated their starting materials to 147 °C, and found products similar to ours: no $NaNH_2$, decreased MgH_2 and newly formed $Mg(NH_2)_2$, NaH and $NaMgH_3$. They also observed the metathesis reaction. Their mixture was then heated to 320 °C and the products were found to be an increased amount of Mg_3N_2 and decreased amounts of MgH_2 and $NaMgH_3$.

The overall reaction scheme for our $2NaNH_2 + 3MgH_2$ heated on a flowing line is shown below, in Table 4-4.

Table 4-4 Overall reaction scheme of $2NaNH_2 + 3MgH_2$ heated to various temperatures. The products from each temperature are shown, the temperature at which new phases form and the lattice parameters of the new phases.

Temp/ °C	*Reaction Scheme*	*Products*	*New Phase(s)*	*Lattice Parameters/ Å*
150	$2NaNH_2 + 3MgH_2 \rightarrow$	$Mg(NH_2)_2$, NaH, $NaMgH_3$, MgH_2	–	–
250	$Mg(NH_2)_2 + 2NaH + 2MgH_2 \rightarrow$	MgH_2, NaH, H_2	$Mg_{(1-x)}Na_{2x}(NH)$ (Phase A)	a = 6.1382(4), c = 17.945(19)
275	$NaH + MgH_2$	$NaMgH_3$	–	–
300	$2Mg_{(1-x)}Na_{2x}(NH) + (1+2x)MgH_2 + (2-2x)NaH \rightarrow$	Mg_3N_2, NaH, H_2	$Mg_{(1-x)}Na_{2x}(NH)$ (Phase A)	a = 6.1077(7), c = 17.881(3)
350	$NaH \rightarrow$	Na, H_2	–	–

Dolotko *et al.*[18] also investigated the reversibility of this reaction and found an uptake of 2.1 wt% on heating Mg_3N_2 and NaH to 395 °C for 48 hours. This was carried out under 190 bar

hydrogen, in contrast to our reaction at 18 bar. The products of Dolotko *et al*. were MgNH, Mg_3N_2 and NaH. 2.1 wt% hydrogen uptake was consistent with the products found, as the theoretical mass gain for Equation 4-11 is 2.7 wt%.

Equation 4-11 $Mg_3N_2 + 2NaH + 2H_2 \rightarrow 2MgNH + 2NaH + MgH_2$

The continued presence of Mg_3N_2 showed the reaction had not managed to complete the first stage of rehydrogenation. The ideal equation for the first step of rehydrogenation is shown in Equation 4-12.

Equation 4-12 $Mg_3N_2 + 2H_2 \leftrightarrow 2MgNH + MgH_2$

Our hydrogen uptake value was similar to Dolotko *et al.* although Dolotko *et al.* were rehydriding from Mg_3N_2, whereas we attempted the rehydriding of the $Mg_{(1-x)}Na_{2x}(NH)$ intermediate. It was thought longer heating and greater pressure would be required in order to complete our rehydrogenation forming $Mg(NH_2)_2$ from MgNH. Dolotko *et al.* may have further problems as Kojima *et al.*[38] investigated the hydriding of Mg_3N_2 by ball-milling under 10 bar H_2 at room temperature. Mg_3N_2 only had a 0.5 wt% uptake under these conditions. This was put down to small heats of formation.[39] These were −2 and −43 kJ mol^{-1} H_2, respectively from first principle calculations (Equation 4-12 and Equation 4-13). It can be suggested that if Kojima *et al.*

increased the pressure of the hydrogen gas, a more successful hydrogen uptake may have been achieved.

Equation 4-13 $2MgNH + 2H_2 \leftrightarrow Mg(NH_2)_2 + MgH_2$

It was seen in the case of Dolotko *et al.* that additional pressure did not force the rehydrogenation any further than ours. Their problem appeared to be reforming an intermediate that could promote further hydrogenation. If the reaction was fully reversible back to $Mg(NH_2)_2$, the theoretical hydrogen uptake value would be 5.1 wt% (Equation 4-14).

Equation 4-14 $Mg_3N_2 + 4H_2 + 2NaH \rightarrow Mg(NH_2)_2 + 2MgH_2 + 2NaH$

It is interesting to note that attempts by Dolotko *et al.* to rehydride the Mg_3N_2 and LiH products from the analogous $2LiNH_2$-$3MgH_2$ system were not successful. They suggested the presence of NaH is important to the rehydriding of Mg_3N_2 as no NaH was present when rehydriding failed with LiH.

Xiong *et al.*[19] rehydrided their unidentified phase under H_2. The products were $Mg(NH_2)_2$ and NaH, which were their original starting materials. Evidence (Table 4–3) suggests $Mg(NH_2)_2$ and NaH represent a lower energy state than $NaNH_2$ and MgH_2. It is well documented that $Li_2Mg(NH)_2$ rehydrides to $Mg(NH_2)_2$ and LiH, whether formed from $2LiNH_2 + MgH_2$ or $Mg(NH_2)_2 + 2LiH$.[4,5,6]

It was published by Juza *et al.*[40] that $Mg(NH_2)_2$ could be formed directly from the reaction of Mg_3N_2 under 10 bar NH_3 at 350 °C for 4–6 weeks.[41] If this reaction could be speeded up, it would ensure the full reaction could be reversed and make an excellent fully reversible hydrogen storage solution.

Cycling of the sample would be beneficial in order to clarify whether the sample maintains its level of dehydriding/rehydriding.

2. $2NaNH_2 + MgH_2$

1. *Temperature Programmed Desorption-Mass Spectrometry*

Having investigated the magnesium rich reaction $2NaNH_2 + 3MgH_2$, our interest turned to a direct comparison of $2NaNH_2 + MgH_2$ with $2LiNH_2 + MgH_2$, therefore, $2NaNH_2 + MgH_2$ was heated in order to establish whether a mixed sodium-magnesium imide could again be formed. $NaNH_2$ and MgH_2 were heated together in a 2:1 ratio. The reaction was initially carried out on a TPD-MS apparatus, at a heating rate of 2 °C min^{-1} to 350 °C.

It can be seen from Figure 4-10 that hydrogen was the majority gas desorbed from the reaction of $2NaNH_2$ and MgH_2. There appeared to be a very small amount of ammonia desorbed at the peak of the hydrogen desorption. The hydrogen desorption peaked at three different temperatures; 155, 234 and 316 °C. The desorption started at about 115 °C when a small amount of hydrogen release occurred. This peaked at 155 °C and was accompanied by a fluctuation in the temperature trace. The rate of hydrogen desorption then decreased until 180 °C when the rate of release increased again up to a peak at 234 °C. This peak was the major

desorption event. Again, the rate of desorption decreased, until 316 °C when a small increase occurred, followed by a long slow tail off as the isothermal heating region commenced. A comparison between this hydrogen desorption and that of the other xNaNH$_2$ + yMgH$_2$ reactions can be seen in Figure 4-30.

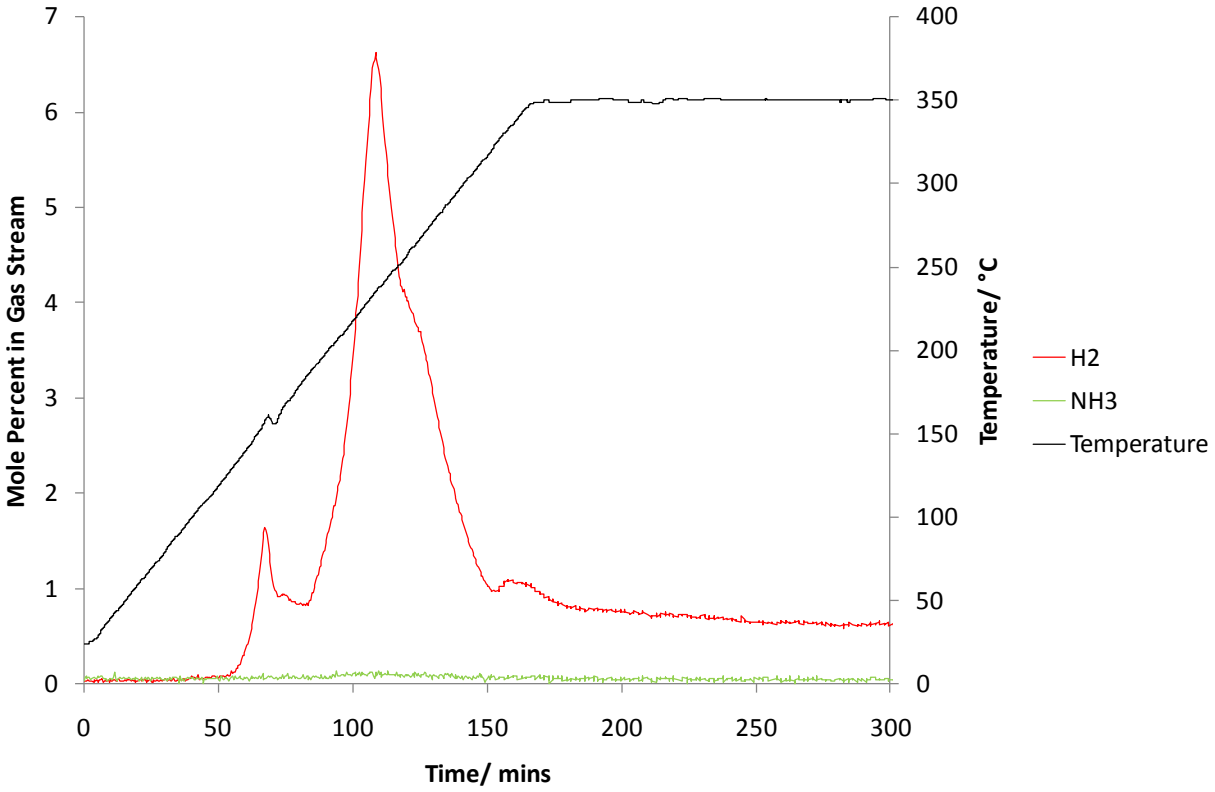

Figure 4-10 TPD-MS analysis of the 2NaNH$_2$ + MgH$_2$ reaction. The temperature trace is shown in black and the MS traces for H$_2$ and NH$_3$ are shown in red and green, respectively.

The temperature trace was then compared to that of the furnace power. It could be seen that the fluctuation in the temperature trace at 155 °C was echoed in the furnace power at the same temperature (Figure 4-10). The temperature trace showed an increase followed by a small drop.

The power of the furnace dropped first and was followed by a rise. This was indicative of an exothermic event occurring within the sample. This occurred at the same temperature as for $2NaNH_2 + 3MgH_2$.

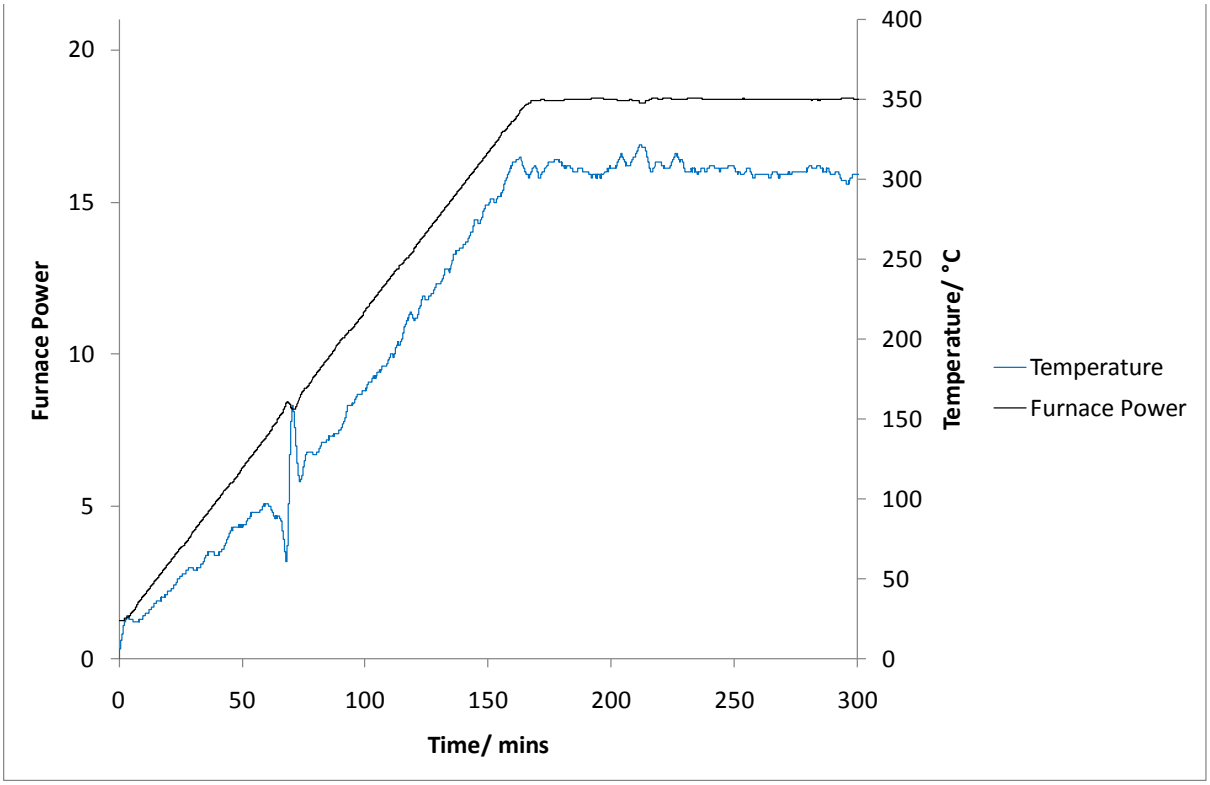

Figure 4-11 Furnace power during the TPD-MS analysis of $2NaNH_2 + MgH_2$ reaction. The furnace power and temperature are shown in blue and black respectively.

After heating in the TPD-MS apparatus the products were analysed by powder XRD and found to be Na, NaH, a little MgNH and $NaNH_2$ remaining starting material. The majority of the peaks were due the phase designated the Na-Mg imide.

In order to quantify the amount of hydrogen released at each desorption event, thermogravimetric analysis (TGA) was performed.

2. *Thermogravimetric Analysis*

The $2NaNH_2 + MgH_2$ starting materials were heated on a TGA-MS apparatus, at a rate of 2 °C min^{-1} to 350 °C where heating ceased. It was found that only hydrogen gas was desorbed (Figure 4-12). No ammonia was seen above the detection limit of the mass spectrometer. The hydrogen desorption occurred in 3 peaks as in the TPD-MS experiment (Figure 4-10). The peaks of hydrogen desorption occurred at 182, 246 and 328 °C. The initial hydrogen desorption occurred roughly 30 °C later on the TGA-MS apparatus than on the TPD-MS apparatus. The reaction was again exothermic and the accompanying hydrogen release was large and sharp. What had been the main desorption on TPD-MS was comparatively small on TGA-MS, although it did occur at the same temperature.

The overall mass loss from this experiment was 3.7 wt %, very close to the theoretical mass loss value of 3.9 wt % for the imide product (Equation 4-15).

Equation 4-15 $$2NaNH_2 + MgH_2 \rightarrow MgNa_{2y}(NH)_{1+y} + (2-y)NaH + 0.5yMgH_2 + 1.5H_2$$ [**]

[**] In this case the mixed cation imide formula has been recast as $Mg_{(1-x)}Na_{2x}(NH)_{1+y}$ as it is the only magnesium containing product.

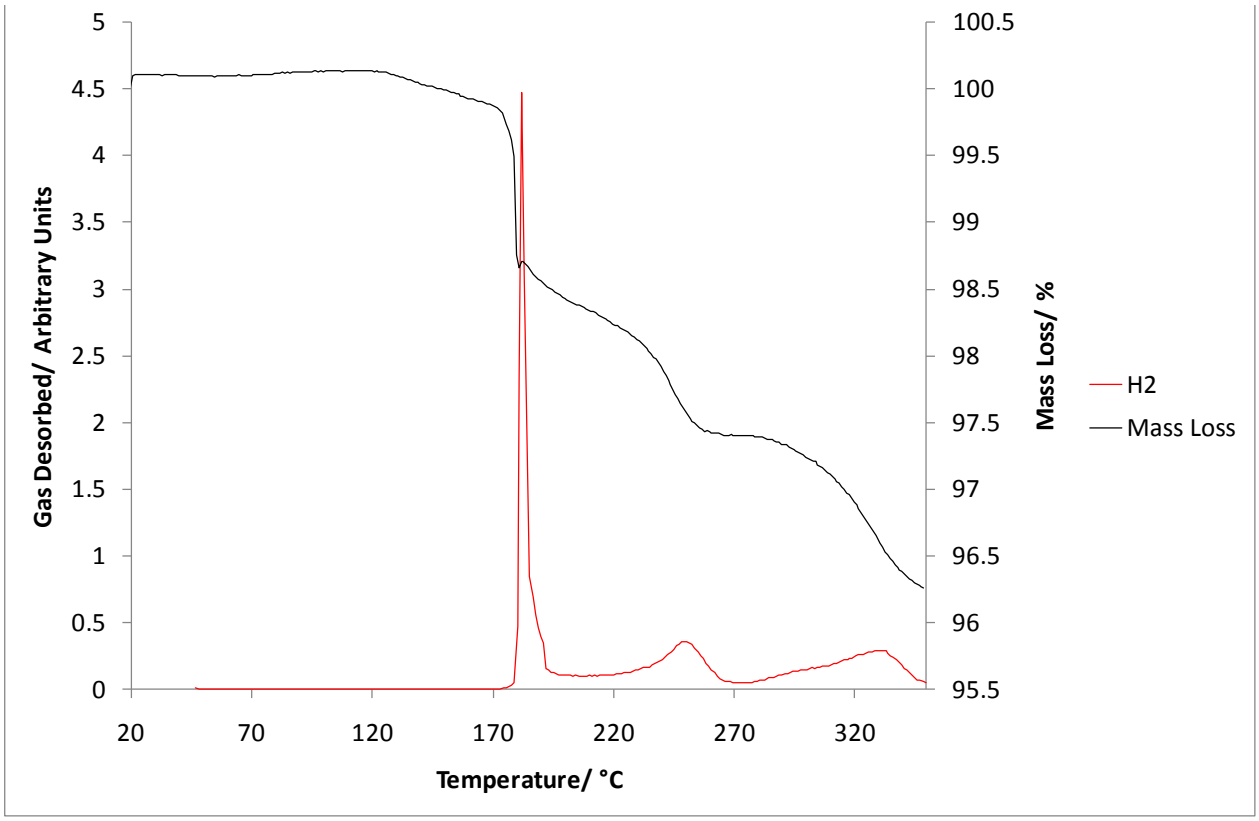

Figure 4-12 TGA-MS of the $2NaNH_2 + MgH_2$ reaction. The H_2 release is shown in red and the percentage mass loss is shown in black.

The desorption of $2NaNH_2 + MgH_2$ makes an interesting comparison with that of $Mg(NH_2)_2 + 2NaH$ as they have equivalent amounts of each ion in the reaction. (Background and formation of $Mg(NH_2)_2$ is in section 4.2.1.5.) The reaction $Mg(NH_2)_2 + 2NaH$ was carried out on a TGA-MS apparatus (Figure 4-13). The reaction was heated up to 350 °C. There was hydrogen desorbed along with a small rise in ammonia from 315 °C. It was seen that hydrogen was desorbed in two steps. The initial desorption started slowly at 145 °C. The rate of hydrogen desorption increased at 170 °C up to a peak at 234 °C. The rate of desorption decreased to 261 °C before increasing up to about 306 °C. The rate of desorption then dropped off rapidly.

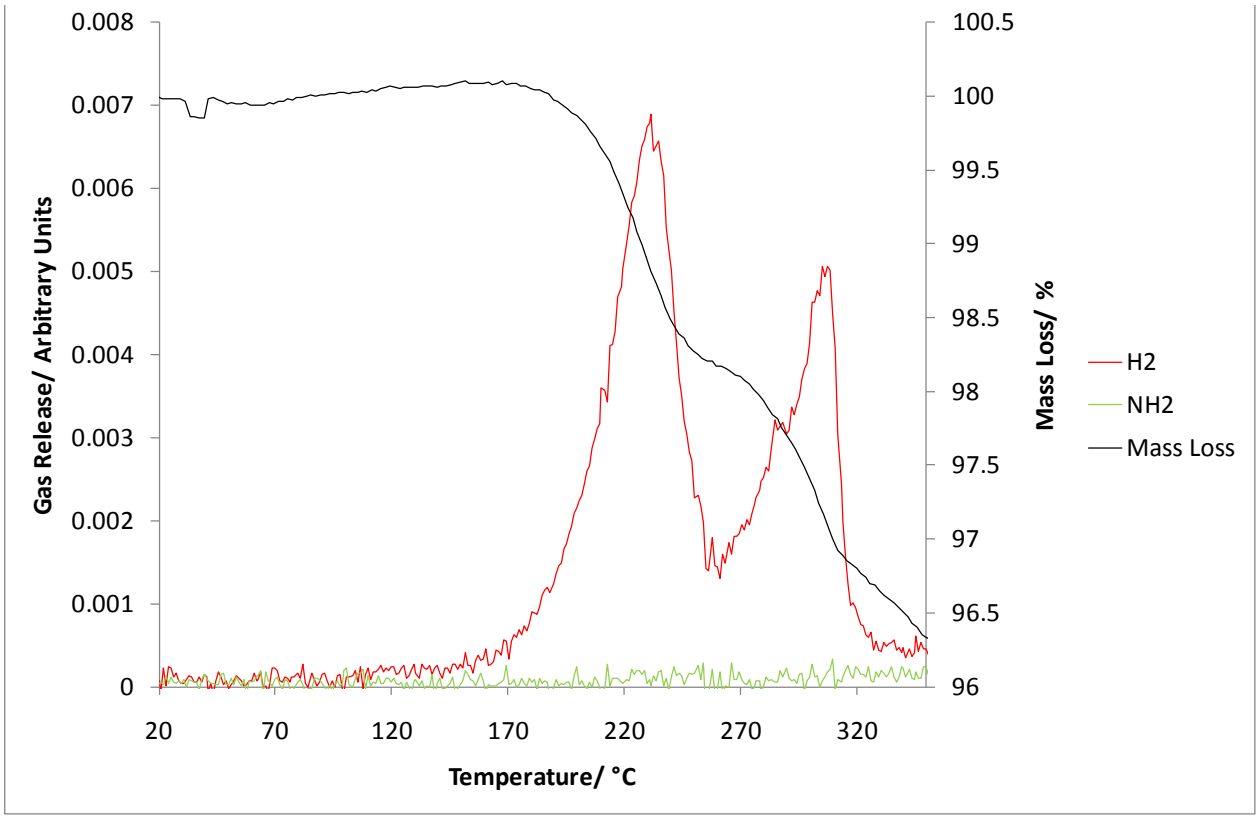

Figure 4-13 TGA-MS of the $Mg(NH_2)_2$ + 2NaH reaction. The MS traces for H_2 and NH_2 are shown in red and green, respectively, and the percentage mass loss is shown in black.

3. *Flowing Line Reactions*

In order to investigate the first step in the observed reaction, a flowing line reaction was carried out by heating $2NaNH_2$ + MgH_2 to 150 °C for 12 hours. This was at the same temperature as the first, small hydrogen desorption in the TPD-MS data and the major desorption even in the TGA data. The products from this reaction were found to be starting materials, $NaNH_2$ and MgH_2, as well as NaH and $Mg(NH_2)_2$ (Figure 4-14). There were also a few new unidentified peaks (phase B) which did not match $NaMgH_3$, NaOH, MgO, Na_2O, MgNH, Na, Mg or the trigonal phase assigned as a sodium-magnesium imide (phase A).

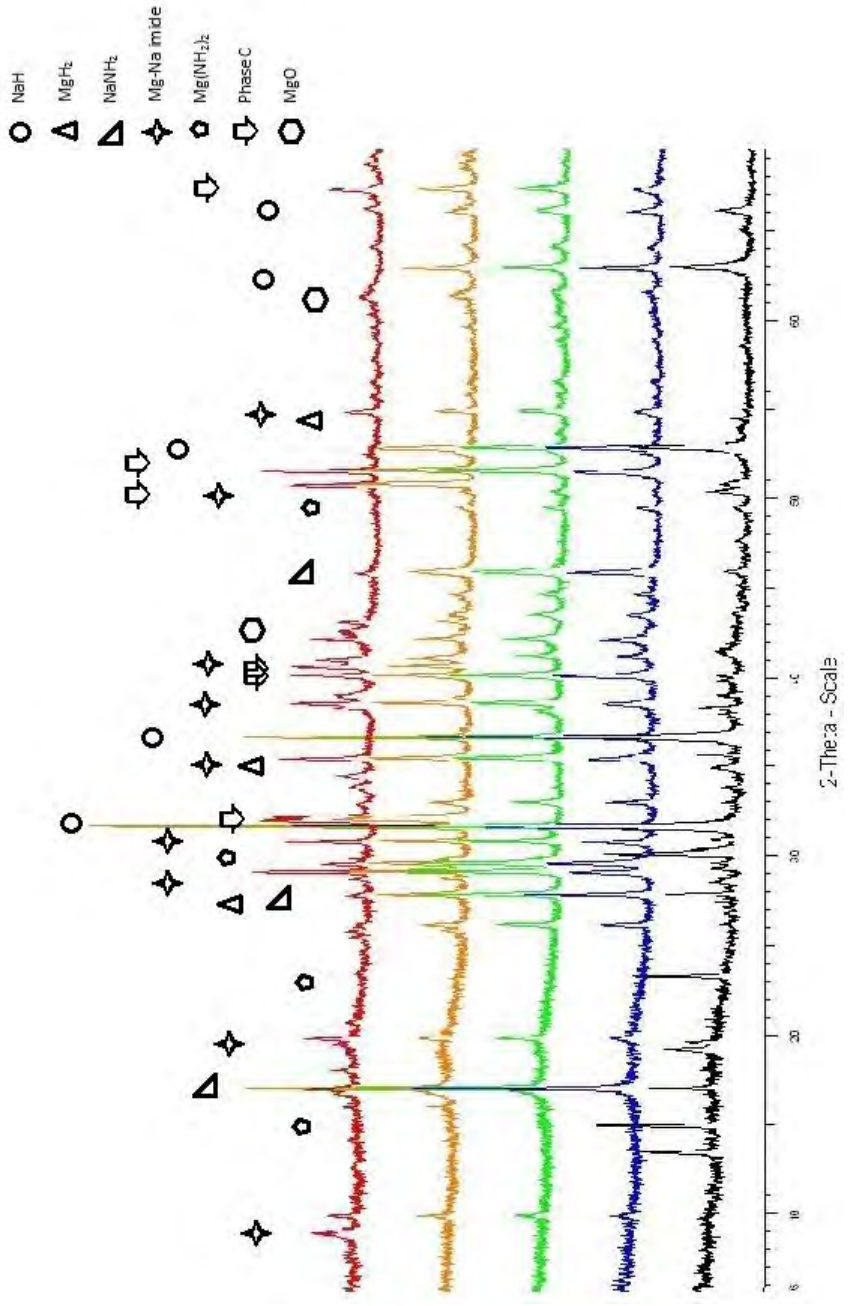

Figure 4-14 Stack plot of powder XRD patterns of $2NaNH_2 + MgH_2$ heated to 150 °C (black), 200 °C (blue), 250 °C (green), 300 °C (orange) and 350 °C (red). The individual XRD patterns can be found in the appendix.

Table 4-5 Summary table of weight percents and mole fractions of products of $2NaNH_2 + MgH_2$ from powder XRD shown in Figure 4-14.

$2NaNH_2 + MgH_2$	Temperature													
	150		200			250			300			350		
Phase	Weight % in XRD	Mole Fraction	Weight % in XRD	Mole Fraction		Weight % in XRD	Mole Fraction		Weight % in XRD	Mole Fraction		Weight % in XRD	Mole Fraction	
MgH_2	4.55	5.26	NA	NA		NA	NA		NA	NA		NA	NA	
NaH	56.77	71.95	35.34	47.05		32.85	44.30		36.74	48.56		NA	NA	
$Mg(NH_2)_2$	30.70	16.57	NA	NA		NA	NA		NA	NA		NA	NA	
$NaNH_2$	7.98	6.22	64.66	52.95		67.15	55.70		63.26	51.44		66.08	66.84	
$MgNa_{2y}(NH)_{1+y}$	NA	NA	Pawley	Pawley		Pawley	Pawley		Pawley	Pawley		Pawley	Pawley	
Phase C	NA	NA	NA	NA		NA	NA		Pawley	Pawley		Pawley	Pawley	
MgO	NA	NA	NA	NA		NA	NA		NA	NA		33.92	33.16	

It was plausible that the new phase observed could be due to the formation of a mixed Na-Mg amide, as is observed for $LiNa_2(NH_2)_3$,[13] $Li_3Na(NH_2)_4$,[13] $K_2Li(NH_2)_3$[15] and $K_2Li(NH_2)_3$.[15] In order to investigate whether the formation of a mixed sodium-magnesium amide was favourable $NaNH_2$ was heated with $Mg(NH_2)_2$ in a 1:1 ratio to 220 °C for 12 hours (Figure 4-15).

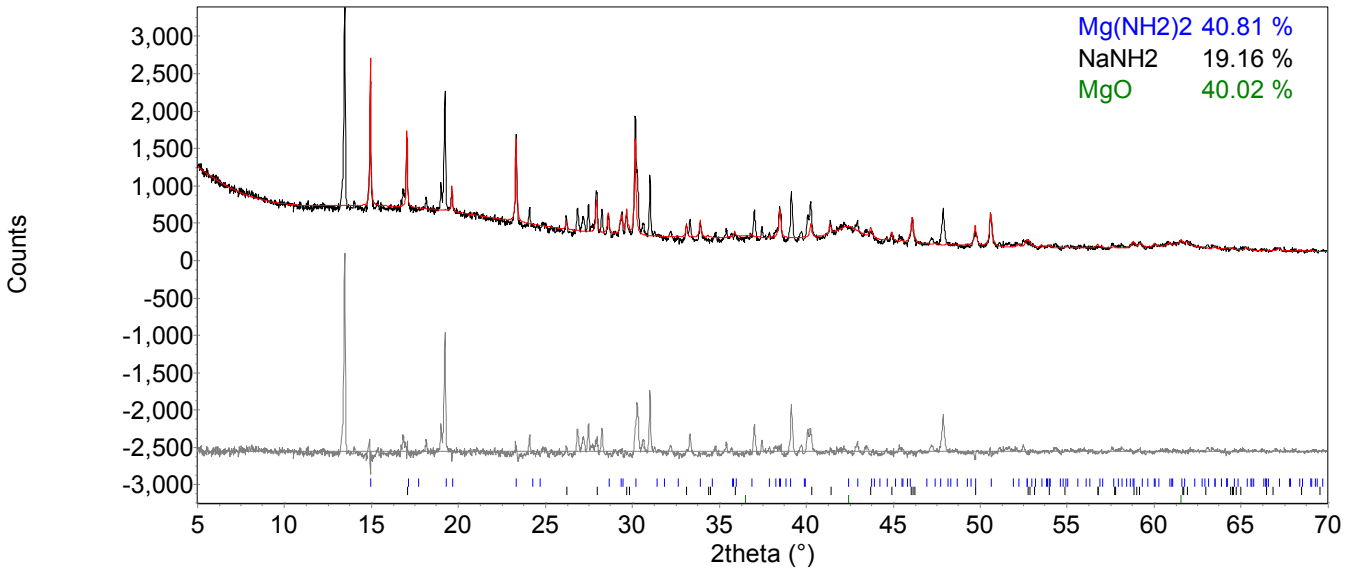

Figure 4-15 Powder XRD pattern of $NaNH_2$ + $Mg(NH_2)_2$, heated at 220 °C for 12 hours under flowing argon. The observed powder XRD pattern (black line) was fitted using a Rietveld fit (red line) to the observed phases $Mg(NH_2)_2$ (blue tick marks), $NaNH_2$ (black tick marks) and MgO (green tick marks). R_{wp} = 16.124, R_{exp} = 4.755, X^2 = 11.5.

Table 4-6 Summary table of weight percents and mole fractions of products of $NaNH_2$ + $Mg(NH_2)_2$ heated to 220 °C for 12 hours.

Phase	*Weight Percent in XRD*	*Mole Fraction/ mol %*
$Mg(NH_2)_2$	40.81	32.79
$NaNH_2$	19.16	22.24
MgO	40.02	44.97

The result of this reaction was a powder XRD pattern that showed the presence of both starting materials, but also a range of unidentified peaks (Figure 4-15). The positions and relative intensities of the 4 largest unidentified Bragg peaks closely match those of the unidentified peaks present in the sample of $2NaNH_2 + MgH_2$ heated to 150 °C for 12 hours (Figure 4–14). This is consistent with the partial formation of a sodium-magnesium amide which did not go to completion under the reaction conditions investigated.

The known products $Mg(NH_2)_2$ and NaH from the reaction $2NaNH_2 + MgH_2$ heated to 150 °C for 12 hours indicated the same metathesis as for $2NaNH_2 + 3MgH_2$ occurred (Equation 4-16).

Equation 4-16 $2NaNH_2 + MgH_2 \rightarrow Mg(NH_2)_2 + 2NaH$

The salt metathesis again was the cause of the exothermic event at 155 °C.

The $2NaNH_2 + MgH_2$ starting materials were then heated to 200 °C for 12 hours. This was just above the temperature at which the main hydrogen desorption started when heated on TPD-

MS apparatus (Figure 4-10). The products from this reaction were found to be NaH and $MgNa_{2y}(NH)_{1+y}$ (Figure 4-14) along with remaining $NaNH_2$ starting material.

The $2NaNH_2 + MgH_2$ mixture was then heated to 250 °C for 12 hours. This temperature was after the main peak of hydrogen. Again, the crystalline products were identified as $NaNH_2$, NaH and $MgNa_{2y}(NH)_{1+y}$ (Figure 4-14, Figure 7-7)

The $2NaNH_2 + MgH_2$ mixture was also heated to 300 °C for 12 hours. 300 °C was between the second and third hydrogen desorptions. As before, the products found by powder XRD were NaH, $MgNa_{2y}(NH)_{1+y}$ and remaining $NaNH_2$ starting material (Figure 4–16). There was also the appearance of another set of 8 major peaks which had not been observed previously (phase C). The *hkl* values, peak positions, *d*-spacings and intensities of the Bragg peaks are shown in Table 4-7. The table includes the peaks less easy to distinguish from the XRD pattern, but of great enough intensity to be in the phase C pattern (below).

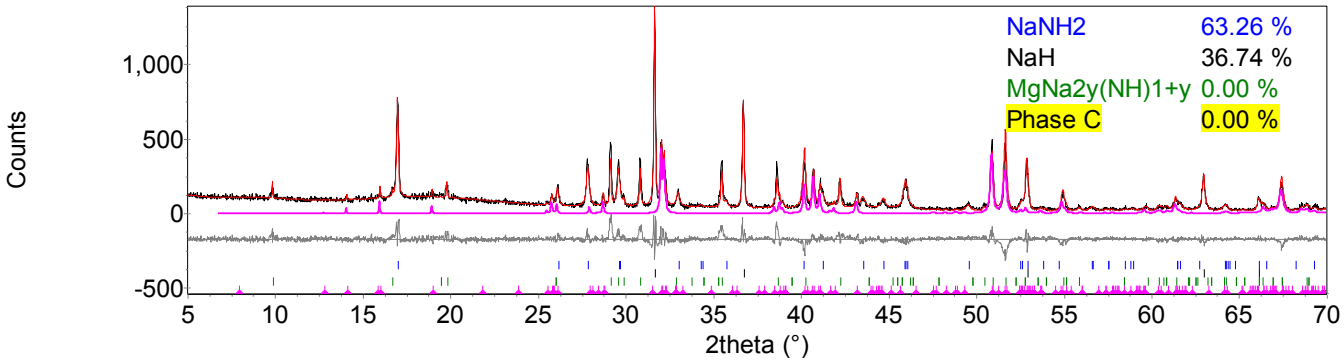

Figure 4-16 Powder XRD pattern of $2NaNH_2 + MgH_2$, heated at 300 °C for 12 hours under flowing argon. The observed powder XRD pattern (black line) was fitted using a Rietveld fit (red line) to the observed phases $NaNH_2$ (blue tick marks) and NaH (black tick marks). Phase A (green tick marks) and phase C (pink tick marks) were fitted using a Pawley fit (red line). $R_{wp} = 17.251$, $R_{exp} = 10.587$, $X^2 = 2.7$.

Table 4-7 Peak positions, hkl, *d*-spacings and intensities of phase C, as identified by $2NaNH_2$ + MgH_2 heated to 300 °C for 12 hours (Figure 4-16).

hkl	d-*spacing*	*Peak Position/ 2θ*	*Intensity*
2 0 0	6.27892	14.1	0.021
-2 0 2	5.52923	16.0	0.082
2 0 1	4.67371	19.0	0.095
1 1 0	3.44887	25.8	0.164
-4 0 2	3.44969	25.8	0.201
1 -1 -1	3.41181	26.1	0.293
1 1 1	3.18961	28.0	0.276
4 0 0	3.13946	28.4	0.126
1 -1 -2	3.10383	28.7	0.411
1 1 2	2.78884	32.1	2.641
3 -1 -2	2.77608	32.2	2.420
-4 0 4	2.76462	32.4	0.775
3 1 0	2.72367	32.9	0.081
3 -1 -3	2.57065	34.9	0.106
1 1 3	2.39105	37.6	0.031
-4 0 5	2.36805	38.0	0.095
1 -1 -4	2.30777	39.0	0.445
-6 0 1	2.24082	40.2	1.113
2 0 4	2.21743	40.7	0.471
3 1 2	2.21363	40.7	3.560
-6 0 4	2.19203	41.1	2.028
5 -1 -1	2.16511	41.7	0.294
5 -1 -3	2.15352	41.9	0.410
6 0 0	2.09297	43.2	1.700
5 1 0	2.05734	44.0	0.195
-4 0 6	2.03331	44.5	0.235

4. Rehydriding

The products from the starting materials that had been heated to 300 °C for 12 hours were subjected to high pressure hydrogen at a range of temperatures in order to assess whether the products would readily reform the reactants. The products of the reaction $2NaNH_2 + MgH_2$ (NaH and $MgNa_{2y}(NH)_{1+y}$, with $NaNH_2$ starting material) were heated under a hydrogen atmosphere

for 24 hours at a pressure of 75 bar H_2. After the rehydrogenation attempt, the observed products were $Mg(NH_2)_2$ and MgNH along with NaH present at the start (Figure 4-17). $Mg(NH_2)_2$ and NaH are the expected products from the initial metathesis of the starting materials $NaNH_2$ and MgH_2, indicating that similarly to the Li-Mg system, the alkaline earth metal amide is the rehydrogenation product of the mixed imide in preference to the alkali metal amide.

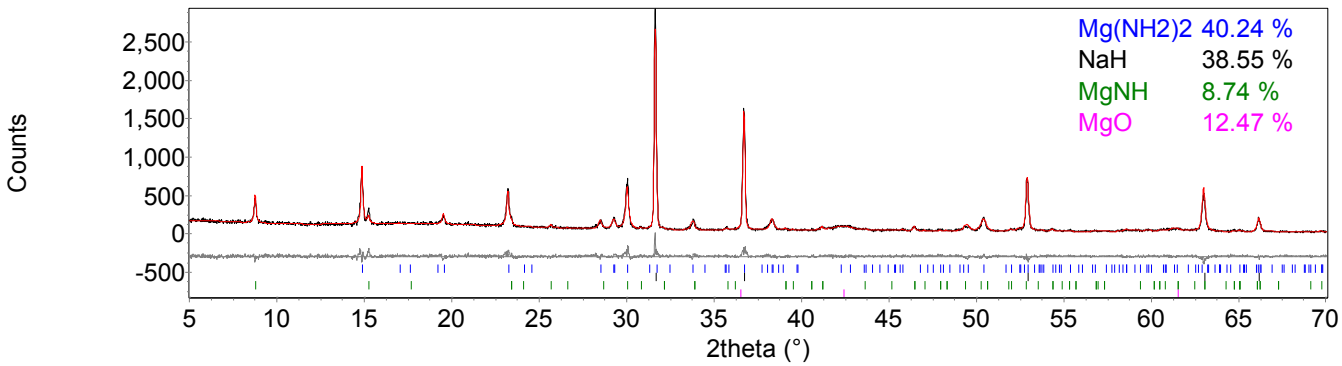

Figure 4-17 Powder XRD pattern of $2NaNH_2 + MgH_2$ heated at 300 °C and rehydrided at 300 °C for 24 hours under 75 bar H_2. The observed powder XRD pattern (black line) was fitted using a Rietveld fit (red line) to the observed phases $Mg(NH_2)_2$ (blue tick marks), NaH (black tick marks), MgNH (green tick marks) and MgO (pink tick marks). R_{wp} = 12.041, R_{exp} = 9.625, X^2 = 1.6.

Table 4-8 Summary table of weight percents and mole fractions of products of $2NaNH_2 + MgH_2$ heated to 300 °C and rehydrided at 300 °C for 24 hours under 75 bar H_2.

Phase	*Weight Percent in XRD*	*Mole Fraction/ mol %*
$Mg(NH_2)_2$	40.24	25.04
NaH	38.55	56.32
MgNH	8.74	7.79
MgO	12.47	10.85

5. Discussion

A small amount of ammonia was desorbed at the peak of the hydrogen desorption shown in Figure 4-10. After heating the sample to 350 °C on the TPD-MS apparatus, MgNH was present. The MgNH could have resulted from the decomposition of $Mg(NH_2)_2$ (Equation 4-17). The formation of MgNH from $Mg(NH_2)_2$ would cause the small ammonia desorption. The $Mg(NH_2)_2$ could be present from not being used in forming $MgNa_{2y}(NH)_{1+y}$, and would not yet have formed Mg_3N_2 as the sample was not heated long enough.

Equation 4-17 $Mg(NH_2)_2 \rightarrow MgNH + NH_3$

The peaks present after heating the starting materials to 150 °C were $NaNH_2$, $Mg(NH_2)_2$, NaH and MgH_2 as well as unidentified phase B (comparatively in Figure 4–14 and Figure 7-5). These Bragg peaks did not match any known Na-N-H or Mg-N-H phase, or mixed cation imide as found in the $2NaNH_2 + 3MgH_2$ reaction. A brief investigation into the identity of phase B peaks was

carried out (Figure 4-15). As there are known compounds of both sodium and magnesium amides ($NaNH_2$, $Mg(NH_2)_2$) and hydrides (NaH, MgH_2) as well as a mixed sodium-magnesium hydride ($NaMgH_3$) it was possible a mixed sodium-magnesium amide may have been formed. Reactions of $Mg(NH_2)_2$ with $NaNH_2$ indicated that phase B was most likely a mixed Na-Mg amide.

Mixed group 1 and 2 amides have been formed before. Jacobs *et al.*[42] formed $NaCa(NH_2)_3$ in 1979 using ammonothermal synthesis between 297–397 °C. It was found to have an orthorhombic unit cell with lattice parameters given as a = 21.78 Å, b = 10.44 Å and c = 7.37 Å with an *Fddd* space group. On decomposition the mixed Na-Ca amide formed $NaNH_2$ and MgNH with the release of NH_3 (Equation 4-18).

Equation 4-18 $NaCa(NH_2)_3 \rightarrow NaNH_2 + CaNH + NH_3$

Jacobs *et al.*[43] further investigated the formation of $NaCa(NH_2)_3$ and compared it to the amides of heavier group 1 and 2 cations. Jacobs *et al.* formed their mixed amides by reacting the metals (in this case sodium and calcium) with supercritical ammonia at about 5 kbar in autoclaves at temperatures in the range 200 to 500 °C. They found well-crystallised amides were produced under these conditions.

In investigating the caesium-magnesium system Birkenbeul *et al.*[44] found one ternary amide $Cs_2[Mg(NH_2)_4]$. It was formed in an autoclave at 142 °C and with an ammonia pressure of 2 kbar

for 2 days. It was monoclinic with the space group $P12_1/c1$ and with lattice parameters of a = 9.447 Å, b = 7.027 Å, c = 12.372 Å and β = 94.80 °.

It appeared that our new phase (Figure 4–14) could only form in very small amounts at low temperatures during the $2NaNH_2 + MgH_2$ reaction, because at temperatures a little higher, the hydrogen desorption became more prevalent and overwhelmed the formation of this new compound. It is unknown what stoichiometry this new phase took and further investigations would be necessary to form it pure and characterise it. Reactions under supercritical ammonia similar to those mentioned previously may be necessary for the formation of the mixed amide in order to suppress the decomposition reaction.

The decomposition of the mixed Na-Ca amide formed by Jacobs *et al.*[43] produced a group 2 imide as well as ammonia. It is possible following the small investigation above into a possible Na-Mg amide that a similar decomposition of Na-Mg amide had occurred. This is another possibility for the MgNH and ammonia present after heating to 350 °C (Equation 4-19). This could also account for some of the large amount of $NaNH_2$ present on heating the $2NaNH_2 + MgH_2$ starting materials to various temperatures. The apparent deficiency of MgNH present could be due to it existing as a poorly crystalline phase.[45]

Equation 4-19 $NaMg(NH_2)_3 \rightarrow NaNH_2 + MgNH + NH_3$

In the temperature range investigated the $2NaNH_2 + MgH_2$ reaction appeared to have gone to completion by forming $MgNa_{2y}(NH)_{1+y}$. This phase had lattice parameters of a = 6.1249(3) Å and

c = 17.916(11) Å after being formed at 250 °C. This was in comparison to those from our investigations into $2NaNH_2 + 3MgH_2$ which found lattice parameters of a = 6.1077(7) Å and c = 17.881(3) Å. Sheppard *et al.*[21] found lattice parameters of a = 6.11 Å and c = 17.90 Å. This product was an imide, and therefore was not fully dehydrided. This is in comparison to $2NaNH_2 + 3MgH_2$ which saw fully dehydrided products, Na and Mg_3N_2. It could be suggested that the additional MgH_2 present in $2NaNH_2 + 3MgH_2$ could react with the mixed imide to form Mg_3N_2, as the mixture is stoichiometric with regard to magnesium and nitrogen (Equation 4-9). The lack of magnesium in $2NaNH_2 + MgH_2$ could inhibit Mg_3N_2 formation.

This is analogous to work carried out on $2LiNH_2 + (3)MgH_2$. It has been shown by Dolotko *et al.*[12] that $3MgH_2$ reacted with $2LiNH_2$ forms LiH and Mg_3N_2 as products, whereas other work by Rijssenbeek *et al.*[49] showed the reaction between $2LiNH_2$ and MgH_2 can only go as far as $Li_2Mg(NH)_2$. Up to 530 °C only $Li_2Mg(NH)_2$ and no Mg_3N_2 was found.

Because of relatively small amounts of phase B observed in the powder XRD patterns of the reaction products, so far it has not been possible to confirm the identity of phase B. The few peaks present in Figure 4–16 that were unidentified (phase C) matched another previously unidentified phase published by Sheppard *et al.*[21] Figure 4–18 below shows the unidentified peaks fitted with the lattice parameters suggested by Sheppard *et al.* Their lattice parameters were a = 13.92 Å, b = 3.58 Å, c = 12.39 Å and β = 115.8 °. Using the lattice parameters of Sheppard *et al.,* we indexed phase C and refined it to be a = 13.945(1) Å, b = 3.5847(18) Å, c = 12.405(1) Å and β = 115.78(6) °. As our parameters were fitted to a minority phase, they

compare well to those of Sheppard *et al.*, who made a case for this new phase to be a mixed Na-Mg nitride as they found no FTIR peaks for an amide or imide.

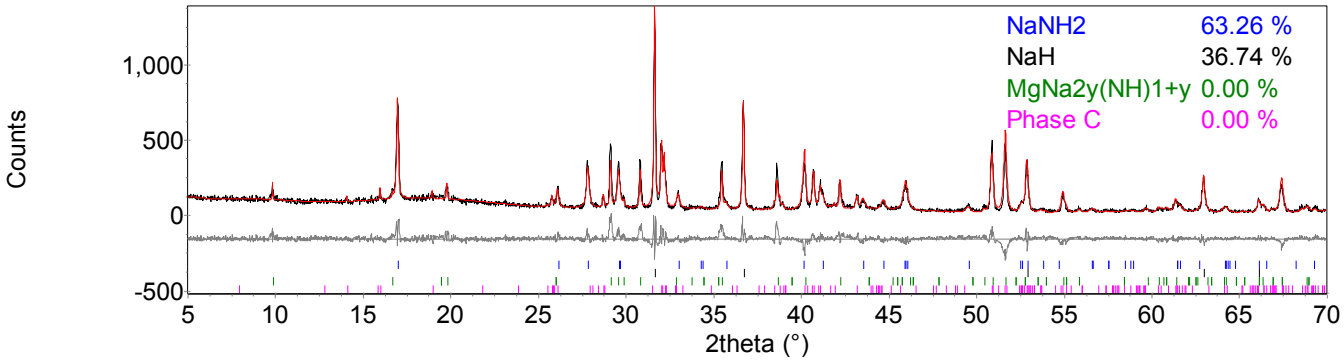

Figure 4-18 Powder XRD pattern of $2NaNH_2 + MgH_2$, heated at 300 °C for 12 hours under flowing argon, with peaks due to Phase C as determined for a Pawley refinement highlighted. The observed powder XRD pattern (black line) was fitted using a Rietveld fit (red line) to the observed phases $NaNH_2$ (blue tick marks), NaH (black tick marks) and $MgNa_{2y}(NH)_{1+y}$ (green tick marks) and phase C (pink tick marks) fitted using a Pawley fit (red line). $R_{wp} = 17.252$, $R_{exp} = 10.587$, $X^2 = 2.7$.

The overall reaction scheme for $2NaNH_2 + MgH_2$ heated to various temperatures is shown in Table 4–9.

Table 4-9 Overall reaction scheme $2NaNH_2 + MgH_2$ of heated to various temperatures. The products from each temperature are shown, the temperature at which new phases form and the lattice parameters of the new phases.

Temp/ °C	*Reaction Scheme*	*Products*	*New Phase(s)*	*Lattice Parameters/ Å*
150	$2NaNH_2 + MgH_2 \rightarrow$	$Mg(NH_2)_2$, 2NaH	Na-Mg amide (Phase B)	–
200	$Mg(NH_2)_2 + 2NaH \rightarrow$	$NaNH_2$, NaH, H_2	$MgNa_{2y}(NH)_{1+y}$ (Phase A)	a = 6.1372(4), c = 17.935(2)
220	$Mg(NH_2)_2 + NaNH_2 \rightarrow$		Na-Mg amide (Phase B)	–
250	$Mg(NH_2)_2 + 2NaH \rightarrow$	$NaNH_2$, NaH, H_2	$MgNa_{2y}(NH)_{1+y}$ (Phase A)	a = 6.1249(3), c = 17.916(10)
300		$NaNH_2$, NaH, H_2	$MgNa_{2y}(NH)_{1+y}$ (Phase A) Na-Mg nitride Phase C	a = 6.1230(3), c = 17.913(16) a = 13.945(10) b = 3.5847(18) c = 12.405(10) β = 115.777(6)

The comparison between the TGA-MS graphs of $2NaNH_2 + MgH_2$ (Figure 4-12) and $Mg(NH_2)_2$ + 2NaH (Figure 4-13) shows only slight differences. The TGA-MS graph of $2NaNH_2 + MgH_2$ has three peaks, whereas $Mg(NH_2)_2$ + 2NaH only had the latter two. This was due to there being no metathesis reaction present in $Mg(NH_2)_2$ + 2NaH. The latter temperature two peaks from the TGA-MS graph of $2NaNH_2 + MgH_2$ match reasonably well to the peaks present in $Mg(NH_2)_2$ + 2NaH. The amount of hydrogen desorbed in the latter two peaks in Figure 4-12 was much less than that shown in Figure 4-13 from $Mg(NH_2)_2$ + 2NaH. This was due to the initial reaction in Figure 4-12 being very exothermic. This raised the heat locally enough to desorb the majority of hydrogen at the lower peak temperature. The later peaks were therefore smaller. Overall this would cause the same amount of hydrogen to be desorbed, but the relative amount of

hydrogen released at different peak temperatures to differ. The total mass loss after heating the reactions to 350 °C was the same for both $2NaNH_2 + MgH_2$ and $Mg(NH_2)_2 + 2NaH$, 3.7 wt% H_2.

The TPD-MS hydrogen desorption peaks from Figure 4-10 match the temperatures well in comparison to TGA-MS $2NaNH_2 + MgH_2$ (Figure 4-12), but slightly better to $Mg(NH_2)_2 + 2NaH$ (Figure 4-13) as there was no large exothermic event to disrupt to rest of the hydrogen desorption.

$Mg(NH_2)_2 + 2NaH$ (Figure 4-13) was heated for an hour at 350 °C, whereas $2NaNH_2 + MgH_2$ (Figure 4-12) had heating stopped as soon as the thermocouple reached 350 °C. A comparison of the products showed the $Mg(NH_2)_2 + 2NaH$ products to be $NaNH_2$, Na and phase C, whereas $2NaNH_2 + MgH_2$ had Na, $MgNa_{2y}(NH)_{1+y}$, phase C and $NaNH_2$ starting material. This fitted in well with the suggestion that phase C was a nitride because it would indicate the more prolonged heating of $Mg(NH_2)_2 + 2NaH$ caused the products to be more hydrogen deficient compared to the products of $2NaNH_2 + MgH_2$. The final mass losses of the two TGA reactions back this up. Although after heating to 350 °C both had lost 3.7 wt% H_2, after the additional isothermal heating of $Mg(NH_2)_2 + 2NaH$, 4.9 wt% H_2 had been lost in total. This was in agreement with the observed products being a mixture of hydrogen deficient (phase C-possible nitride) and those not [Na, $MgNa_{2y}(NH)_{1+y}$]. If a pure Na-Mg nitride were formed *cf.* LiMgN,[46] then there would be a theoretical mass loss of 5.8 wt% H_2 from these reactions (Equation 4-20). It can be seen from Equation 4-20 that $NaNH_2$ appeared as a starting material and as a product.

Equation 4-20 $2NaNH_2 + MgH_2 \rightarrow Mg(NH_2)_2 + 2NaH \rightarrow NaMgN + NaNH_2 + 2H_2$

Xiong *et al.*[19] heated $Mg(NH_2)_2 + 2NaH$ to 390 °C after ball-milling. The desorption characteristics of the reaction included the release of hydrogen at 180 °C, as well as the release of ammonia and nitrogen above 300 °C. They suggested the nitrogen released was probably due to the decomposition of NH_3 desorbed. In contrast, we observed no evidence of N_2 desorption. The reaction by Xiong *et al.* releasing hydrogen at a slightly lower temperature was probably due to the initial ball-milling carried out on the reactants. The smaller particle size means shorter diffusion lengths for desorbed gases from the bulk phase, as well as the possible addition of catalytic metal during milling as steel pots and balls were used.

$2NaNH_2 + MgH_2$ after dehydrogenation at 300 °C for 12 hours was subjected to 75 bar hydrogen for 12 hours at 300 °C. It could be seen from the XRD pattern (Figure 4-17), that the products were more hydrogen rich than before rehydrogenation. $Mg(NH_2)_2$ as well as a small amount of MgNH was present, along with NaH. This is consistent with the argument that phase A, from $2NaNH_2 + 3MgH_2$, was an imide, as it was possible to rehydride it back to the lowest energy starting materials, namely the $Mg(NH_2)_2$ and NaH (post metathesis products).

$2NaNH_2 + MgH_2$ was originally investigated to provide a comparison to $2LiNH_2 + MgH_2$. When $2LiNH_2 + MgH_2$ is heated up it forms $Li_2Mg(NH)_2$. On rehydriding, this reaction also was also found to revert to $Mg(NH_2)_2$ + group 1 hydride (Equation 4-22).[4,5,6,7] It would therefore not be surprising with sodium amide and magnesium hydride that after heating and then rehydriding, magnesium amide was formed along with NaH. The MgNH present would presumably

rehydrogenate to $Mg(NH_2)_2$ and MgH_2 if exposed to the rehydriding conditions for a longer time or at a higher temperature pressure than 75 bar.

Equation 4-21 $2NaNH_2 + MgH_2 \rightarrow Mg(NH_2)_2 + 2NaH \leftrightarrow MgNa_{2y}(NH)_{1+y} + (1-x)NaNH_2 + (1-x)NaH + (1+x)H_2$

Equation 4-22 $2LiNH_2 + MgH_2 \rightarrow Mg(NH_2)_2 + 2LiH \leftrightarrow Li_2Mg(NH)_2 + 2H_2$

It can be seen in Equation 4-21 that NaH along with $NaNH_2$ starting material were both present from the reaction in a 1:1 ratio. Converting the wt% calculated by quantitative phase analysis using Topas into mole% produces $NaNH_2$:NaH as approximately a 1:1 ratio as predicted.

From Figure 4-18, 63.27 wt% / 39.01235 = 1.62 mol% for $NaNH_2$; 36.73 wt% / 23.99771 = 1.53 mol%. As the mol% for $NaNH_2$ and NaH were consistent throughout heating, the ratio of $NaNH_2$:NaH as products also remained at approximately 1:1.

3. $3NaNH_2 + 2MgH_2$

When the sodium rich reaction $2NaNH_2 + MgH_2$ was carried out the products were $NaNH_2$, NaH and $MgNa_{2y}(NH)_{1+y}$. As $NaNH_2$ was consistently the major product of $2NaNH_2 + MgH_2$, we therefore reduced the amount of Na in the ratio of Na:Mg by investigating the reaction of $NaNH_2$ and MgH_2 in a 3:2 ratio.

1. *Temperature Programmed Desorption-Mass Spectrometry*

$NaNH_2$ and MgH_2 were heated together in a 3:2 ratio. The reaction was carried out on a TPD-MS apparatus in order to establish whether this system desorbed hydrogen like the other $NaNH_2$–MgH_2 systems. It was heated at 2 °C min^{-1} to 350 °C and held there for approximately 1 hour.

It can be seen from Figure 4-19 that, like other $x$$NaNH_2$ + $y$$MgH_2$ reactions (Figure 4-30), hydrogen was desorbed from this reaction also. There was only a very small amount of ammonia desorbed at the peak of the second major hydrogen desorption. The hydrogen desorption started at 126 °C and increased to a peak at 154 °C. The rate of desorption quickly slowed. A second increase in the rate of hydrogen desorption started at 182 °C and peaked twice at 243 and 265 °C before the hydrogen desorption dropped away. At 325 °C there was a small additional hydrogen desorption which tailed off slowly.

There was a very small fluctuation in the temperature trace that occurred at the same temperature as the first hydrogen desorption. This was same as temperature fluctuations for the other $x$$NaNH_2$ + $y$$MgH_2$ reactions (Figure 4-2 and Figure 4-11). The fluctuation was mirrored in the furnace power indicating an exothermic event as described previously. This indicated an exothermic event.

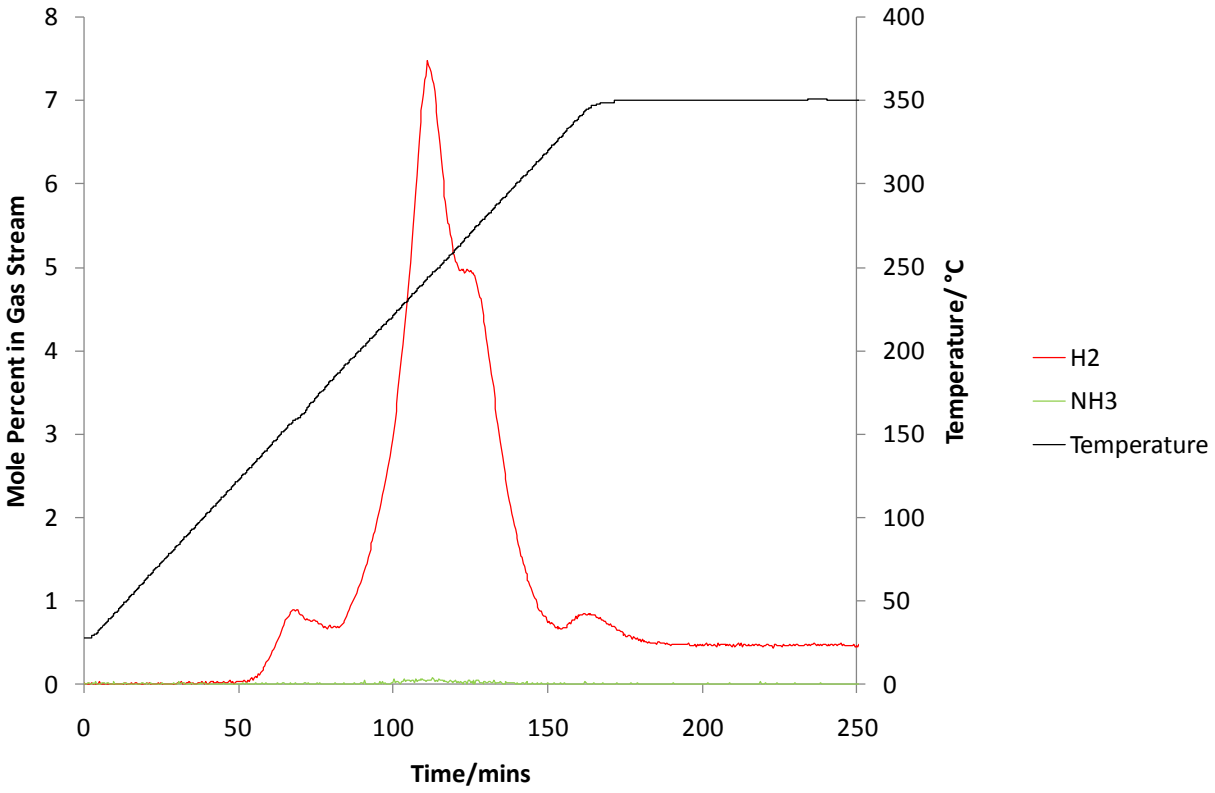

Figure 4-19 TPD–MS analysis of the $3NaNH_2 + 2MgH_2$ reaction. The temperature trace is shown in black and the MS traces for H_2 and NH_3 released are shown in red and green, respectively.

The products after TPD–MS analysis of the $3NaNH_2 + 2MgH_2$ reaction were NaH and $MgNa_{2y}(NH)_{1+y}$ along with $NaNH_2$ starting material (Figure 4-20). These are the same products as from the reaction $2NaNH_2 + MgH_2$.

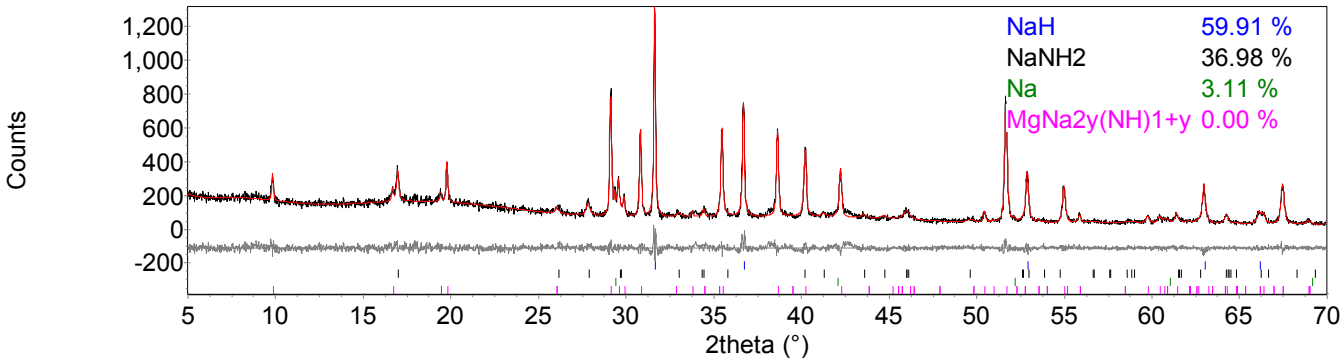

Figure 4-20 Powder XRD pattern of $3NaNH_2$ + $2MgH_2$, after TPD-MS analysis to 350 °C. The observed powder XRD pattern (black line) was fitted using a Rietveld fit (red line) to the observed phases NaH (blue tick marks), $NaNH_2$ (black tick marks), Na (green tick marks) and $MgNa_{2y}(NH)_{1+y}$ (pink tick marks) fitted using a Pawley fit (red line). R_{wp} = 10.767, R_{exp} = 9.032, X^2 = 1.4.

Table 4-10 Summary table of weight percents and mole fractions of products of $3NaNH_2$ + $2MgH_2$ after TPD-MS analysis to 350 °C.

Phase	*Weight Percent in XRD*	*Mole Fraction/ mol %*
NaH	59.91	69.72
$NaNH_2$	36.98	26.49
Na	3.11	3.79
$MgNa_{2y}(NH)_{1+y}$	Pawley	NA

2. *Thermogravimetric Analysis*

It can be seen from the TGA–MS trace that a similar hydrogen desorption to that in the TPD-MS was observed. The 3 main hydrogen desorptions were visible (Figure 4-21). The first, sharp peak occurred at 181 °C, 30 °C after the initial peak on TPD-MS. No ammonia was detected in TGA, although the sample size was smaller than in the TPD-MS therefore releasing a smaller amount

of ammonia which may not be detectable above the detection limit of the mass spectrometer. Heating was stopped at 350 °C. The products after TGA were Na and phase C along with remaining $NaNH_2$ (Figure 4-22). There was no $MgNa_{2y}(NH)_{1+y}$ present here. This was the first time the presence of phase C was observed in the absence of $MgNa_{2y}(NH)_{1+y}$.

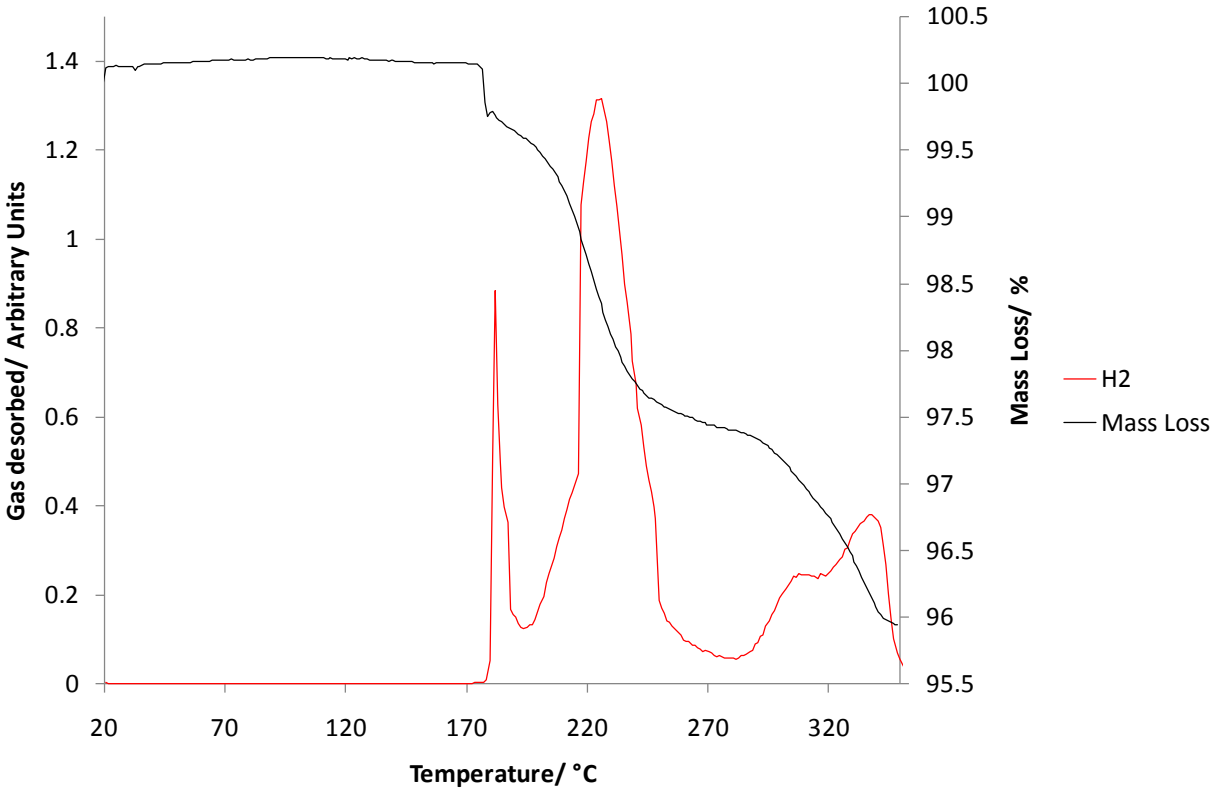

Figure 4-21 TGA–MS of the $3NaNH_2 + 2MgH_2$ reaction. The H_2 release is shown in red and the percentage mass loss is shown in black.

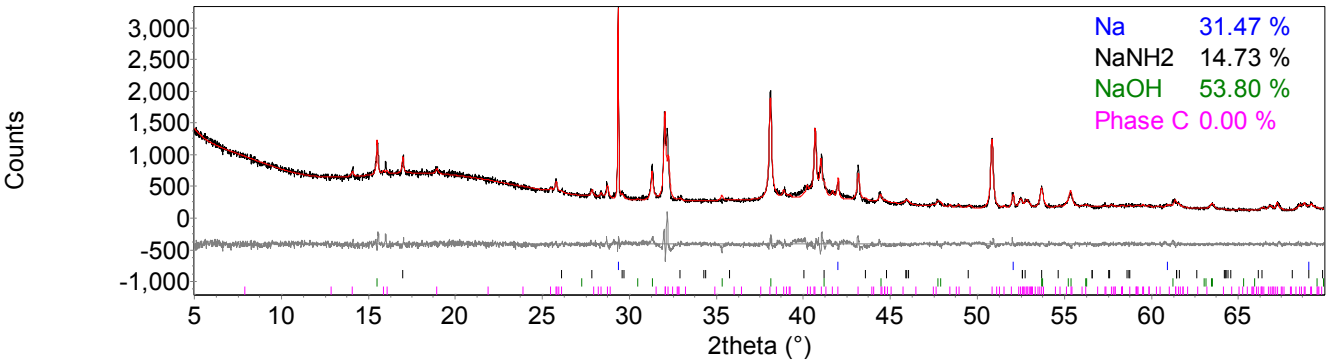

Figure 4-22 Powder XRD of $3NaNH_2$ + $2MgH_2$ heated to 350 °C on a TGA-MS apparatus. The observed powder XRD pattern (black line) was fitted using a Rietveld fit (red line) to the observed phases Na (blue tick marks), $NaNH_2$ (black tick marks), NaOH (green tick marks) and phase C (pink tick marks) fitted using a Pawley fit (red line). R_{wp} = 6.903, R_{exp} = 4.745, X^2 = 2.1.

Table 4-11 Summary table of weight percents and mole fractions of products of $3NaNH_2$ + $2MgH_2$ heated to 350 °C on TGA-MS apparatus.

Phase	*Weight Percent in XRD*	*Mole Fraction/ mol %*
Na	31.47	44.28
$NaNH_2$	14.73	12.21
NaOH	53.80	43.51
Phase C	Pawley	NA

3. Flowing Line Reactions

As in previous sections, (section 4.2.1 and 4.2.2) the reaction was carried out at intermediate temperatures in order to establish the desorption mechanism. The starting materials were first heated to 150 °C for 12 hours. This was shortly before the exothermic event and the start of the hydrogen desorption. The products after heating under these conditions were starting

materials, $NaNH_2$ and MgH_2, as well as NaH and $Mg(NH_2)_2$, which have previously been shown to be metathesis products (Figure 4–24, Equation 4-2). The few unidentified peaks present are the same as those labelled 'phase B' in section 4.2.2 from the reaction of $NaNH_2$ with $Mg(NH_2)_2$ – the possible Na-Mg amide.

The starting materials were then heated to 200 °C for 12 hours. This was the approximate temperature at which the second desorption started. The known product was NaH along with $NaNH_2$ starting material. The peaks from $MgNa_{2y}(NH)_{1+y}$ were also present (Figure 4-24).

The $3NaNH_2 + 2MgH_2$ reaction mixture was also heated to 250 °C for 12 hours. This temperature was between the two peaks of the second desorption. The products were the same as those after heating to 200 °C, NaH and $MgNa_{2y}(NH)_{1+y}$ as well as $NaNH_2$ (Figure 4–24).

After the temperature in the TPD-MS experiment reached 300 °C the major hydrogen desorption was over. The products from heating the starting materials to 300 °C on a flowing line experiment were as identified after heating to 250 °C, NaH and $MgNa_{2y}(NH)_{1+y}$ and remaining $NaNH_2$ (Figure 4-24) as well as the higher temperature phase C found earlier in section 4.2.2 (Figure 4–18).

The same reaction was carried out at 350 °C and held there for 4 hours. The observed products were more crystalline than observed after reaction at 300 °C, as evidenced by sharper Bragg peaks in the powder XRD pattern. There was no evidence of phase C that had been present at 300 °C. The products were NaH and $MgNa_{2y}(NH)_{1+y}$ in addition to $NaNH_2$ (Figure 4-23).

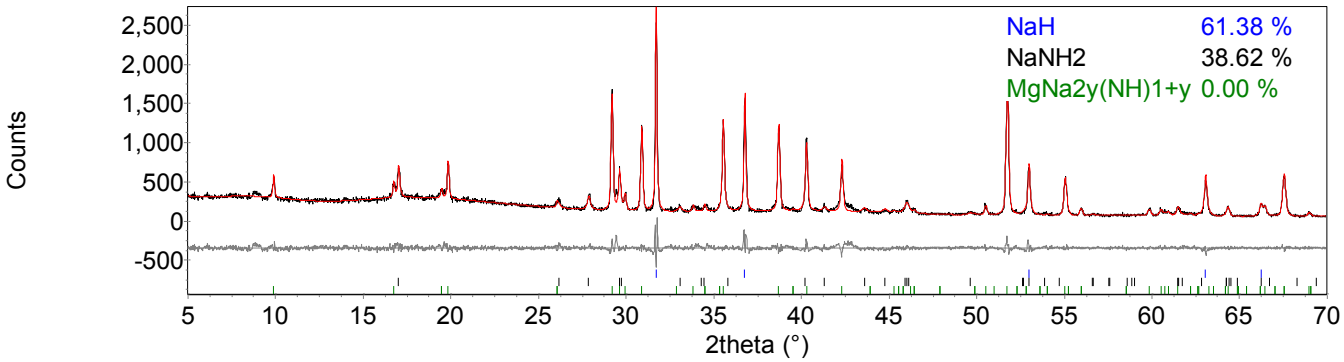

Figure 4-23 Powder XRD pattern of $3NaNH_2$ + $2MgH_2$, heated to 350 °C for 4 hours under flowing argon. The observed powder XRD pattern (black line) was fitted using a Rietveld fit (red line) to the observed phases NaH (blue tick marks), $NaNH_2$ (black tick marks) and $MgNa_{2y}(NH)_{1+y}$ (green tick marks) fitted using a Pawley fit (red line). R_{wp} = 9.865, R_{exp} = 6.803, X^2 = 2.1.

Table 4-12 Summary table of weight percents and mole fractions of products of $3NaNH_2$ + $2MgH_2$ heated to 350 °C for 4 hours.

Phase	*Weight Percent in XRD*	*Mole Fraction/ mol %*
NaH	61.38	72.10
$NaNH_2$	38.62	27.90
$MgNa_{2y}(NH)_{1+y}$	Pawley	NA

The starting materials were heated together to 350 °C and held there for 12 hours. Again, $NaNH_2$ was present along with the products, but this time Na was present with no NaH. The $MgNa_{2y}(NH)_{1+y}$ phase was again present (Figure 4-24). 350 °C was above the final hydrogen desorption temperature and this final desorption can be put down to the decomposition of NaH to Na and hydrogen (Equation 4-10).

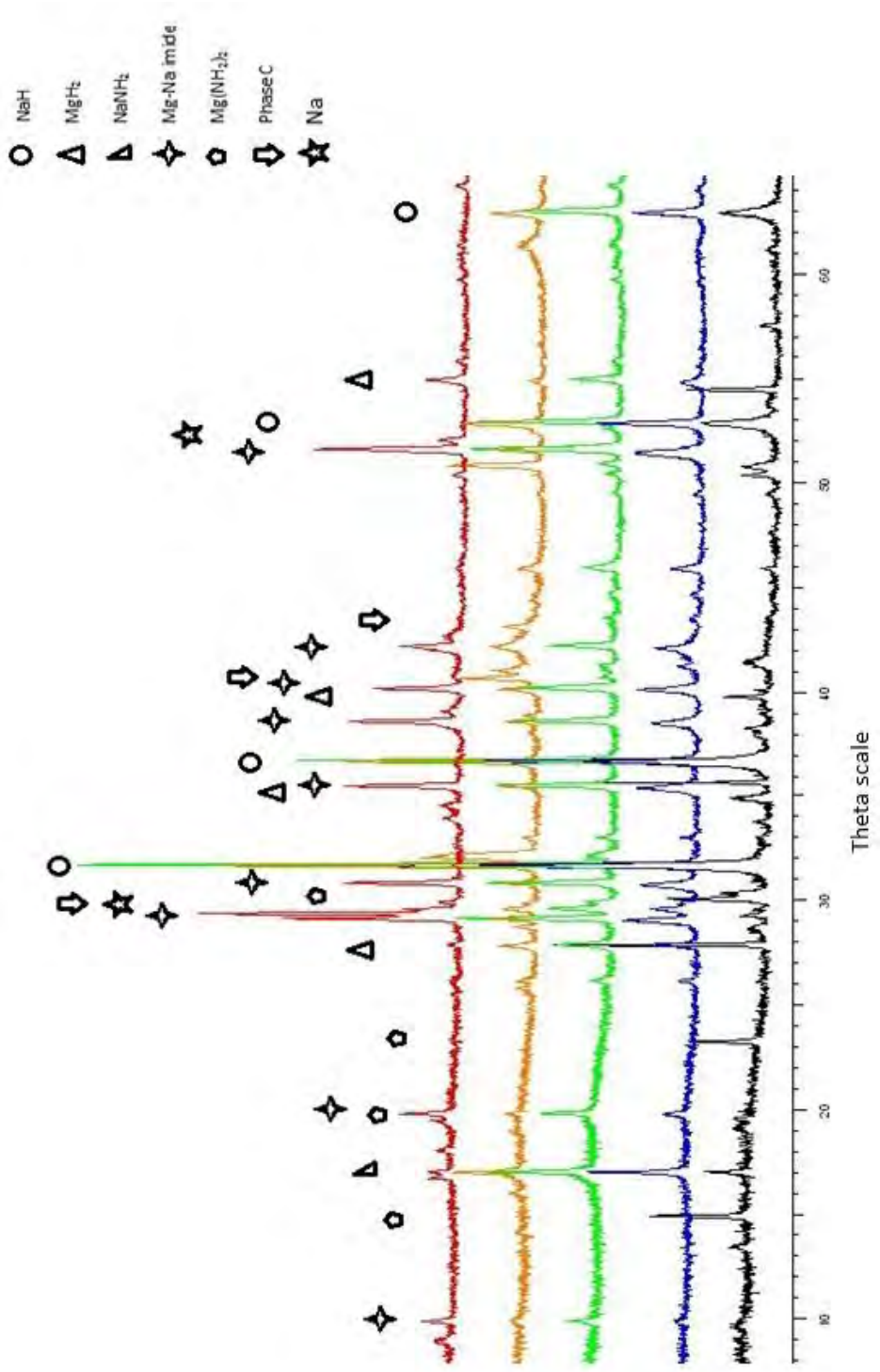

Figure 4-24 Stack plot of powder XRD patterns of $3NaNH_2 + 2MgH_2$ heated to 150, 200, 250, 300 and 350 °C. The individual XRD patterns can be found in the appendix.

Table 4-13 Summary table of weight percents and mole fractions of products of $3NaNH_2$ + $2MgH_2$ from powder XRD shown in Figure 4–24.

$3NaNH_2$ + $2MgH_2$	Temperature													
	150		200			250			300			350		
Phase	Weight % in XRD	Mole Fraction	Weight % in XRD	Mole Fraction		Weight % in XRD	Mole Fraction		Weight % in XRD	Mole Fraction		Weight % in XRD	Mole Fraction	
MgH_2	17.39	19.47	NA	NA		NA	NA		NA	NA		NA	NA	
NaH	51.47	63.22	62.22	72.81		57.31	68.58		60.33	71.20		3.66	3.99	
$Mg(NH_2)_2$	26.76	14.00	NA	NA		NA	NA		NA	NA		NA	NA	
$NaNH_2$	4.38	3.31	37.78	27.19		42.69	31.42		39.67	28.80		32.20	21.95	
$MgNa_{2y}(NH)_{1+y}$	NA	NA	Pawley	Pawley		Pawley	Pawley		Pawley	Pawley		Pawley	Pawley	
Phase C	NA	NA	NA	NA		NA	NA		Pawley	Pawley		NA	NA	
Na	NA	NA	NA	NA		NA	NA		NA	NA		64.14	74.14	

4. Rehydriding

The products after heating $3NaNH_2 + 2MgH_2$ to 300 °C for 12 hours were then exposed to a hydrogen atmosphere in order to rehydride the sample. The phases present before hydrogenation were $NaNH_2$, NaH, $MgNa_{2y}(NH)_{1+y}$ and phase C, and they were heated under hydrogen to 300 °C for 24 hours at 75 bar H_2. The products after this attempted rehydriding were MgO, NaH, $Mg(NH_2)_2$ and a very small amount of MgNH (Figure 4-25). The oxidation was most probably due to poor cycling of the high pressure system to remove the air.

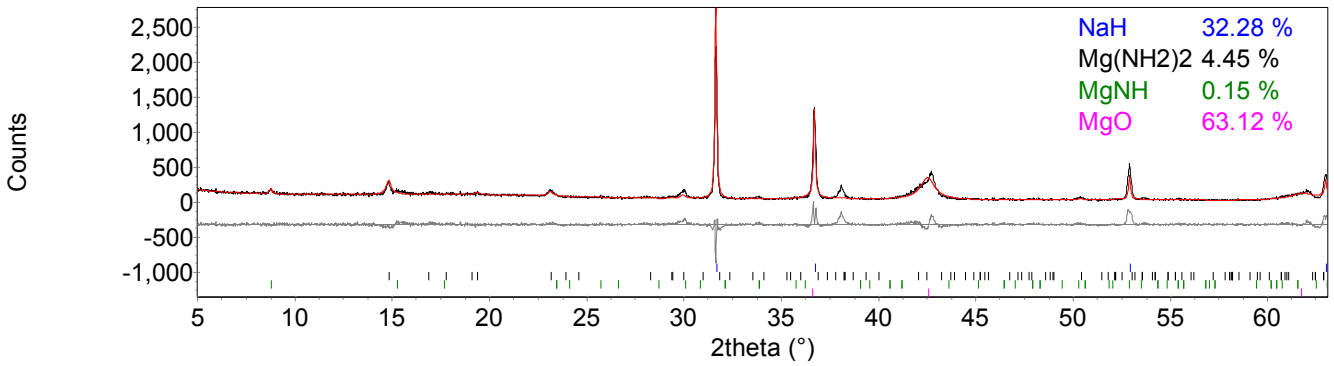

Figure 4-25 Powder XRD pattern of $3NaNH_2 + 2MgH_2$ heated to 300 °C and then rehydrided at 350 °C for 24 hours under 75 bar H_2. The observed powder XRD pattern (black line) was fitted using a Rietveld fit (red line) to the observed phases NaH (blue tick marks), $Mg(NH_2)_2$ (black tick marks), MgNH (green tick marks) and MgO (pink tick marks) fitted using a Pawley fit (red line). R_{wp} = 18.706, R_{exp} = 9.866, X^2 = 3.6.

Table 4-14 Summary table of weight percents and mole fractions of products of $3NaNH_2$ + $2MgH_2$ heated to 300 °C and then rehydrided at 350 °C for 24 hours under 75 bar H_2.

Phase	*Weight Percent in XRD*	*Mole Fraction/ mol %*
NaH	32.28	94.15
$Mg(NH_2)_2$	4.45	5.58
MgNH	0.15	0.27
MgO	63.12	

5. Discussion

The fluctuation in the furnace power and its appearance in the temperature trace of the TPD-MS trace (Figure 4-19) showed less of an exothermic reaction than had been evidenced before (Figure 4-2, Figure 4-11). This was as expected as the reaction was not stoichiometric with respect to the metathesis.

After heating the starting materials, the products from the salt metathesis were seen to occur. The metathesis had nearly gone to completion; only a little $NaNH_2$ was still present (Figure 4-13). The idealised metathesis reaction for $3NaNH_2 + 2MgH_2$ is shown in Equation 4-23.

Equation 4-23 $$6NaNH_2 + 4MgH_2 \rightarrow 3Mg(NH_2)_2 + 6NaH + MgH_2$$

By 200 °C all the $Mg(NH_2)_2$ and MgH_2 had either become amorphous ($Mg(NH_2)_2$) or been used up (MgH_2). Only $NaNH_2$, NaH and $MgNa_{2y}(NH)_{1+y}$ could be seen from the powder XRD pattern

(Figure 4–24). The lattice parameters of $MgNa_{2y}(NH)_{1+y}$ were a little larger than published – a = 6.1431(4) Å and c = 17.941(19) Å in comparison to a = 6.11 Å and c = 17.90 Å.[21]

Equation 4-24 $3Mg(NH_2)_2 + 6NaH + MgH_2 \rightarrow MgNa_{2y}(NH)_{1+y} + (2\text{-}4x)NaNH_2 + (4\text{-}4x)NaH + (4+4x)H_2$

Using the starting materials heated to 350 °C (Figure 4-24) which shows Na product, if we assume that all the Na comes from NaH, $(2\text{-}4y)/(4\text{-}4y)$= 2/7 (ratio of $NaNH_2$:NaH), this gives y = 0.3 and the imide has the possible formula $MgNa_{0.6}(NH)_{1.3}$.

Some very small peaks belonging to phase C were visible in the XRD pattern for the starting materials heated to 250 °C. These occurred along with the same products seen at 200 °C. This was the lowest temperature at which phase C had been observed. The lattice parameters for $MgNa_{2y}(NH)_{1+y}$ formed at this temperature were as published.[21]

By 300 °C, the lattice parameters had shrunk to a = 6.1242(3) Å and c = 17.9253(8) Å, and by 350 °C the lattice parameters were a = 6.1158(19) Å and c = 17.8967(7) Å for 4 hours and a = 6.1199(4) Å and c = 17.909(12) Å for 12 hours of heating.

Throughout all of the temperatures investigated, the lattice parameters of $NaNH_2$ were larger than those published by Nagib.[47] This may mean that some Mg was present within the $NaNH_2$ although there has previously been no suggestion of $NaNH_2$ of having a mixed stoichiometry. However, the formula unit size of $Mg(NH_2)_2$ compared to $NaNH_2$ is smaller, 33.86 $Å^3$ versus 47.14 $Å^3$, not larger, meaning it would be unlikely the inclusion of Mg within the $NaNH_2$ unit cell

would increase its lattice parameters. The lattice parameters of NaH were consistent with those published, throughout.

It appeared the proportion of $MgNa_{2y}(NH)_{1+y}$ had increased with increasing temperature, but there were no additional Mg containing phases seen. It was possible that amorphous Mg phases were still present.

The products of the $3NaNH_2 + 2MgH_2$ reactions were the same as $2NaNH_2 + MgH_2$. However, the percentages of NaH and $NaNH_2$ refined by powder XRD using quantitative phase analysis were different (although no account is taken of $MgNa_{2y}(NH)_{1+y}$ – the ratios of $NaNH_2$ to NaH were comparable). It is possible the $MgNa_{2y}(NH)_{1+y}$ phase had a variable stoichiometry. Here there was more NaH present, however in $2NaNH_2 + MgH_2$ there was more $NaNH_2$. This suggests that there was too much amide present in $2NaNH_2 + MgH_2$. For both sodium rich reactions, $2NaNH_2 + MgH_2$ and $3NaNH_2 + 2MgH_2$, sodium phases were dominant in the XRD patterns. Therefore, suggesting that there must have been too much sodium present in the starting materials. It is therefore proposed that using $x Mg(NH_2)_2 + y NaH$ as the starting reaction would give better control over the number of starting material units (Mg^{2+}, Na^+, NH_2^- and H^-). For example:

$2NaNH_2 + MgH_2$ gave 2Na, $2[(NH_2)^-]$, 1Mg and 2H, the reaction products gave excess $NaNH_2$. We then reduced the amount of sodium amide present to react $3NaNH_2 + 2MgH_2$ which gave 3Na, $3[(NH_2)^-]$, 2Mg and 4H. This reaction gave excess NaH. Therefore, by having $x Mg(NH_2)_2 + y NaH$ starting materials, the reactants can have less sodium hydride added to them, whilst

maintaining the $[(NH_2)^-]$:H^- ratio. This ratio is important as it defines how far the reaction can proceed.

The peaks of phase C seen after heating to 300 °C were fitted using the parameters found by Sheppard *et al.*[21] for a phase suggested to be a nitride. The fitted peaks can be seen in Figure 4–26. Our lattice parameters were a = 13.950(14) Å, b = 3.5849(5) Å, c = 12.403(15) Å and β = 115.753(8) °. These compare well to those published by Sheppard *et al.* of a = 13.92 Å, b = 3.58 Å, c = 12.39 Å and β = 115.8 °.

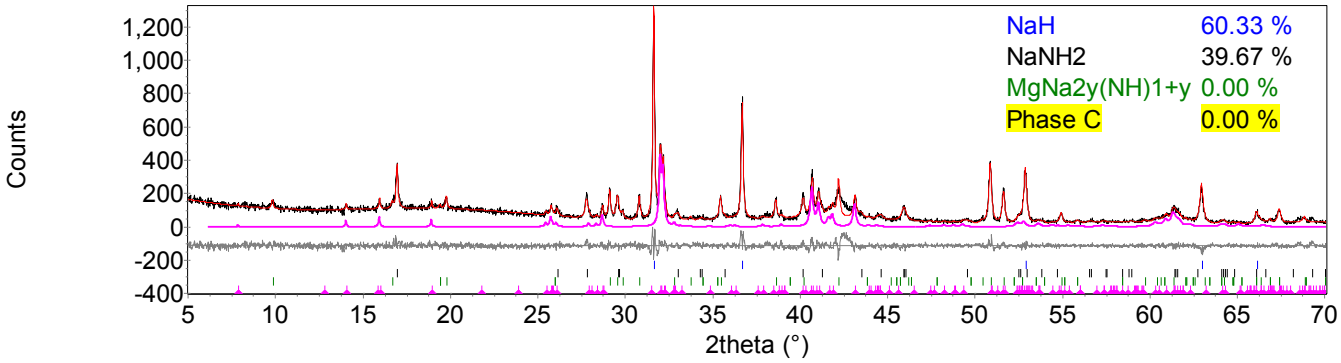

Figure 4-26 Powder XRD pattern of $3NaNH_2 + 2MgH_2$, heated to 300 °C for 12 hours under flowing argon with phase C fitted. The observed powder XRD pattern (black line) was fitted using a Rietveld fit (red line) to the observed phases NaH (blue tick marks), $NaNH_2$ (black tick marks) and $MgNa_{2y}(NH)_{1+y}$ (green tick marks) and phase C (pink tick marks) fitted using a Pawley fit (red line). R_{wp} = 13.469, R_{exp} = 10.482, X^2 = 1.7.

The full set of reactions for $3NaNH_2 + 2MgH_2$ heated on a flowing line is shown in Table 4-15.

Table 4-15 Overall reaction scheme $3NaNH_2 + 2MgH_2$ of heated to various temperatures. The products from each temperature are shown, the temperature at which new phases form and the lattice parameters of the new phases.

Temp/ °C	*Reaction Scheme*	*Products*	*New Phase(s)*	*Lattice Parameters/ Å*
150	$3NaNH_2 + 2MgH_2 \rightarrow$	$Mg(NH_2)_2$, NaH, MgH_2	–	–
200	$3Mg(NH_2)_2 + 6NaH + MgH_2 \rightarrow$	NaH, $NaNH_2$, H_2	$MgNa_{2y}(NH)_{1+y}$ (Phase A)	a = 6.1431(4), c = 17.941(19)
250		NaH, $NaNH_2$, H_2	$MgNa_{2y}(NH)_{1+y}$ (Phase A)	a = 6.1195(2), c = 17.8966(9)
300		NaH, $NaNH_2$, H_2	$MgNa_{2y}(NH)_{1+y}$ (Phase A) Na-Mg nitride Phase C	a = 6.1243(3), c = 17.9254(8) a = 13.950(14), b = 3.5849(5), c = 12.403(15), β = 115.753(8)
350		Na, $NaNH_2$, NaH, H_2	$MgNa_{2y}(NH)_{1+y}$ (Phase A)	a = 6.1199(4), c = 17.909(12)
350	NaH →	Na, H_2	–	–

The reaction heated on the TGA apparatus gave the first appearance of phase C without any $MgNa_{2y}(NH)_{1+y}$ (Figure 4-22). We fitted the Sheppard *et al.*[21] phase to our XRD pattern (Figure 4-27). This gave lattice parameters of a = 13.918(10) Å, b = 3.5891(19) Å, c = 12.356(15) Å and β = 115.460(5) °, slightly smaller than those of Sheppard *et al.* The oxidation as evidenced by the presence of NaOH may have been due to poor sample preparation for XRD.

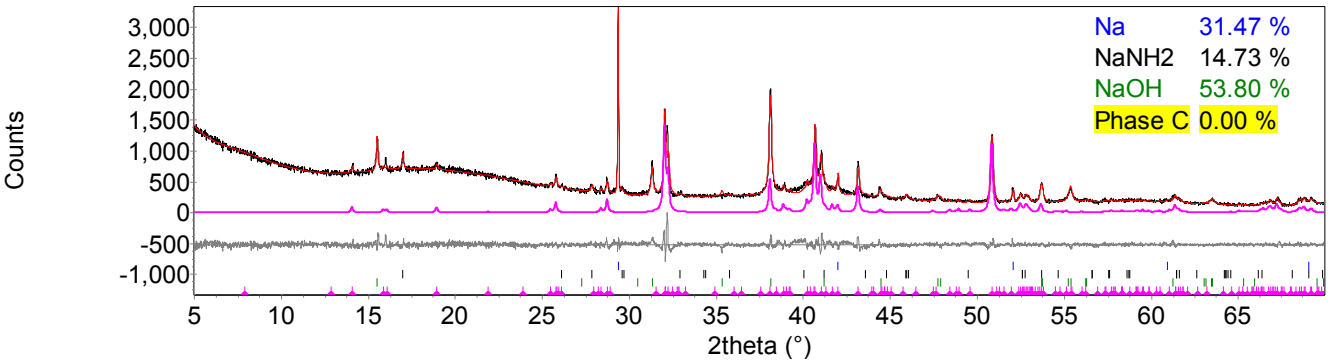

Figure 4-27 Powder XRD of $3NaNH_2$ + $2MgH_2$ heated to 350 °C on a TGA-MS apparatus with Phase C fitted. The observed powder XRD pattern (black line) was fitted using a Rietveld fit (red line) to the observed phases Na (blue tick marks), $NaNH_2$ (black tick marks), NaOH (green tick marks) and phase C (pink line) fitted using a Pawley fit (red line) R_{wp} = 6.903, R_{exp} = 4.745, X^2 = 2.1.

NaH was present in a large amount in the phases that were to be rehydrided. NaH was a rehydrided product and therefore would not be expected to change upon being exposed to a hydrogen atmosphere.

The products from the rehydrogenation included a large amount of MgO, unfortunately. There was, however, a small amount of $Mg(NH_2)_2$ present which showed that at least part of the sample was able to be rehydrided, as $2NaNH_2$ + MgH_2 was (Figure 4-18).

Having concluded that there was too much sodium amide present in the starting materials of the sodium rich reactions, $2NaNH_2$ + MgH_2 and $3NaNH_2$ + $2MgH_2$, in the next section we investigate starting materials with less sodium amide present i.e., the reaction of $NaNH_2$ and MgH_2 in a 1:1 ratio.

4. $NaNH_2 + MgH_2$

1. *Temperature Programmed Desorption-Mass Spectrometry*

$NaNH_2$ and MgH_2 were heated together in a 1:1 ratio. The reactants were first heated together on a TPD–MS apparatus at a heating rate of 2 °C min^{-1} to 350 °C and held at 350 °C for approximately 2 hours. From Figure 4-28, it can be seen that hydrogen was the major gas desorbed, with a very small amount of ammonia desorbed at the peak of hydrogen release. The hydrogen desorption started very slowly around 72 °C, significantly lower temperature then observed for other compositions, with the rate increasing around 120 °C. This desorption peaked at 155 °C before dropping off. The rate increased again at around 183 °C. The second desorption was the major hydrogen release that peaked at 245 °C. As the rate decreased there were 2 shoulders: one at 260 °C, the other at 320 °C. The hydrogen desorption then tailed off. The TPD-MS trace for hydrogen desorbed from $NaNH_2 + MgH_2$ can be compared to gas release from other $x NaNH_2 + y MgH_2$ reactions (Figure 4-30)

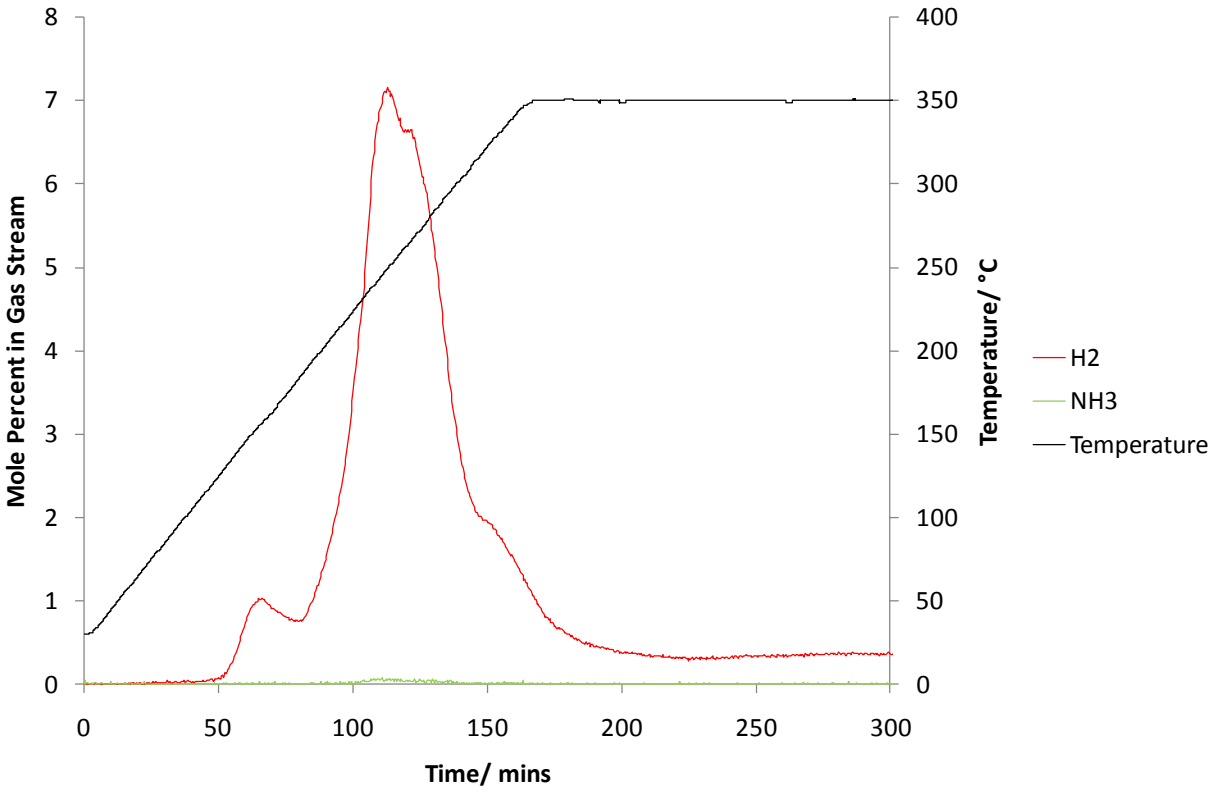

Figure 4-28 TPD–MS analysis of the $NaNH_2$ + MgH_2 reaction. The temperature trace is shown in black and MS traces of H_2 and NH_3 released are shown in red and green respectively.

The temperature trace was then compared to the furnace power in order to see whether there was any thermal event in the furnace power that had not been translated onto the temperature trace. As seen in Figure 4-29 there was no obvious alteration the furnace power in comparison to other furnace power traces. There may be a small fluctuation at 150 °C, which would match with fluctuations seen in other compositions, but this event was significantly smaller.

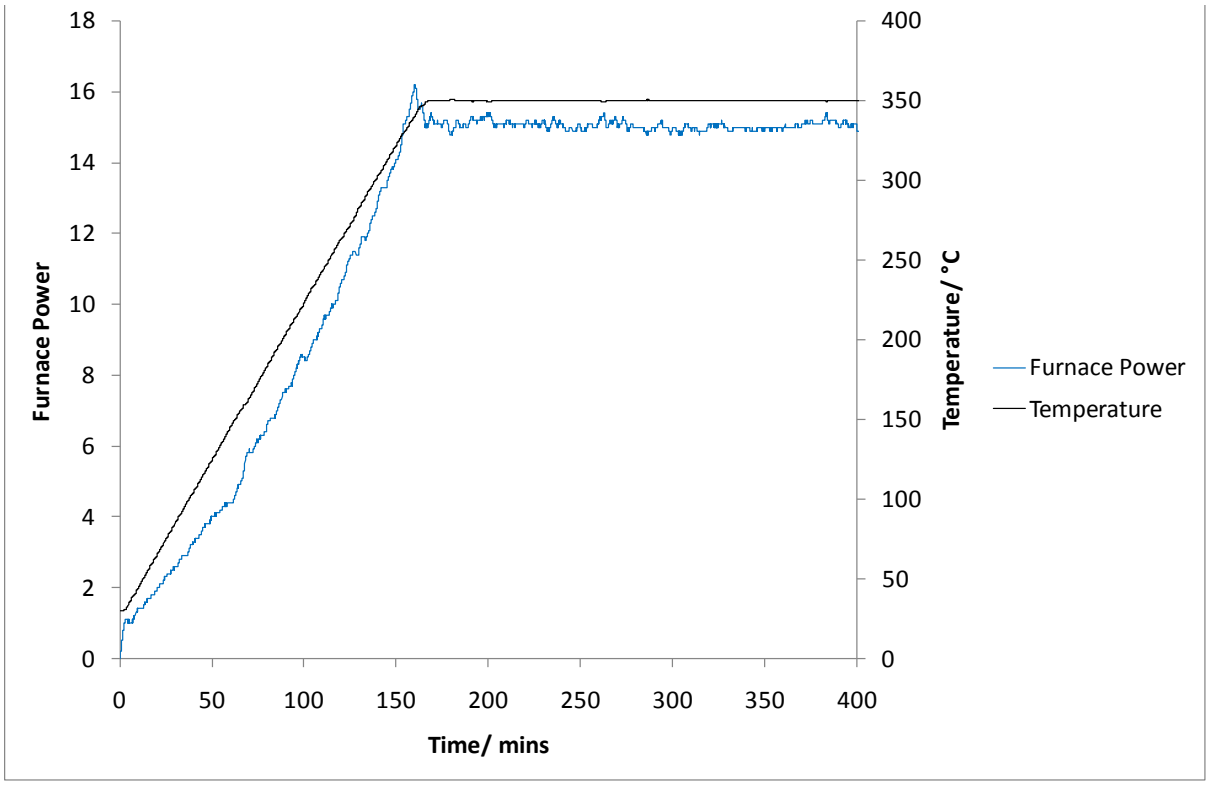

Figure 4-29 Furnace power during the TPD-MS analysis of $NaNH_2$ + MgH_2 reaction. The furnace power and temperature are shown in blue and black respectively.

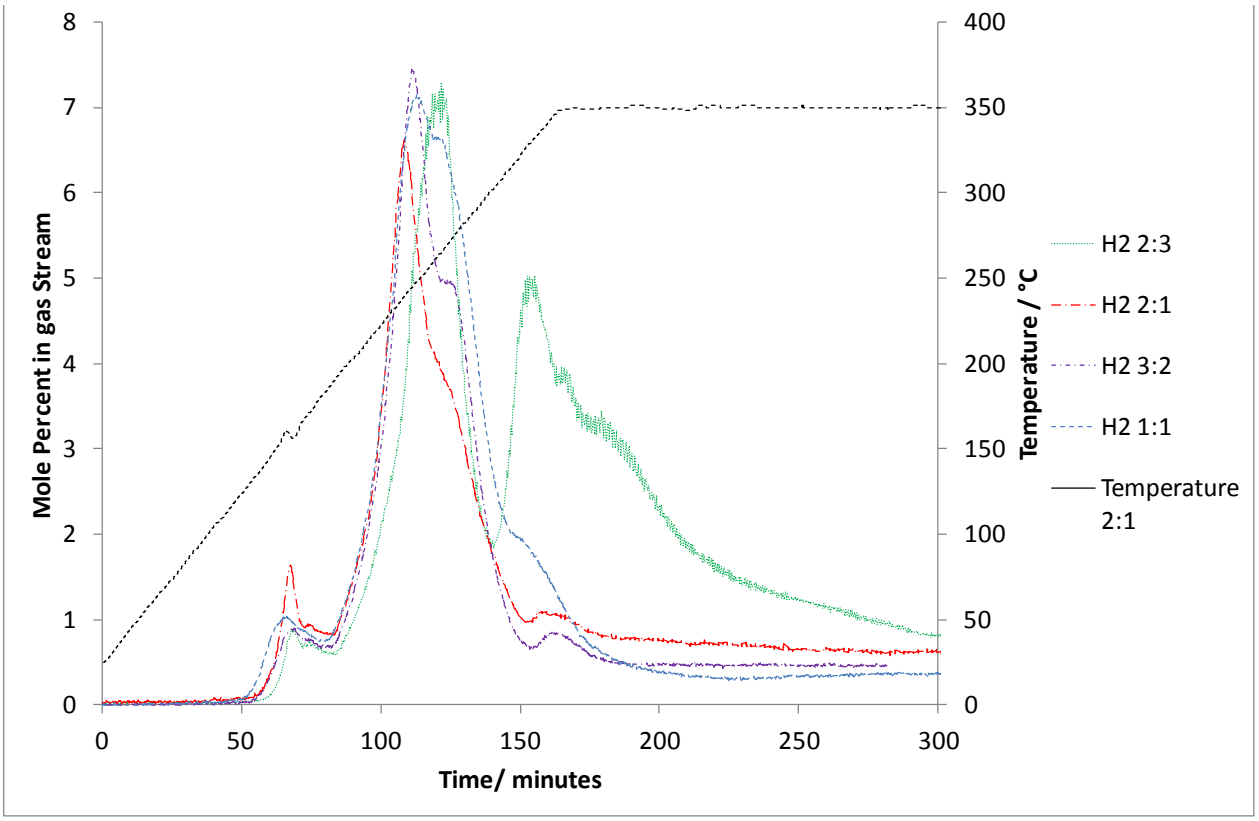

Figure 4-30 Comparison of TPD–MS analysis of the xNaNH$_2$ + yMgH$_2$ reactions. The temperature trace is shown in black and MS traces of H_2 released are shown in green, (2:3), red, (2:1), purple (3:2) and blue (1:1).

The products after TPD-MS were analysed using powder XRD. They were found to be NaH, Na, Mg_3N_2 and $MgNa_{2y}(NH)_{1+y}$ (Figure 4-31).

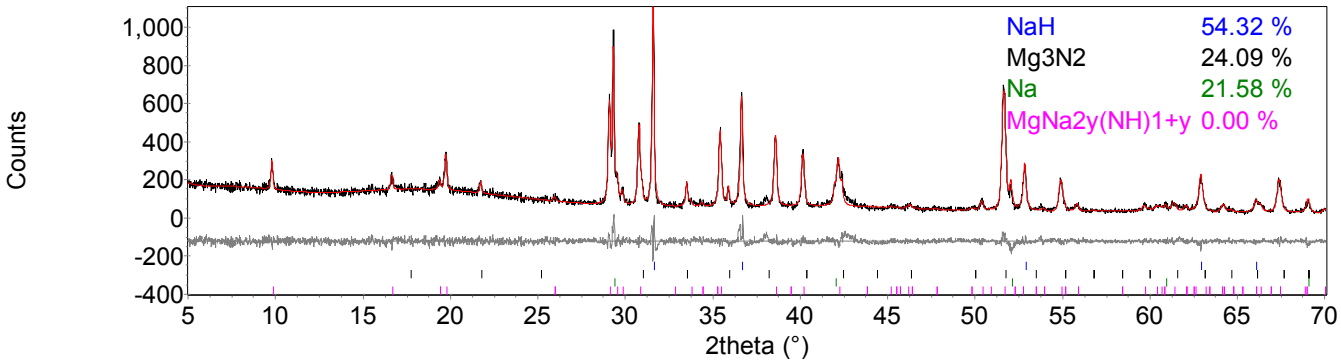

Figure 4-31 Powder XRD pattern of $NaNH_2$ + MgH_2, after TPD–MS analysis to 350 °C. The observed powder XRD pattern (black line) was fitted using a Rietveld fit (red line) to the observed phases NaH (blue tick marks), Mg_3N_2 (black tick marks), Na (green tick marks) and $MgNa_{2y}(NH)_{1+y}$ (pink tick marks) fitted using a Pawley fit (red line). R_{wp} = 11.625, R_{exp} = 9.413, X^2 = 1.5.

Table 4-16 Summary table of weight percents and mole fractions of products of $NaNH_2$ + MgH_2 heated to 350 °C on TPD-MS apparatus.

Phase	*Weight Percent in XRD*	*Mole Fraction/ mol %*
NaH	54.32	65.71
Mg_3N_2	24.09	6.98
Na	21.58	27.33
$MgNa_{2y}(NH)_{1+y}$	Pawley	NA

2. *Thermogravimetric Analysis*

The $NaNH_2$ + MgH_2 reaction mixture was heated at 2 °C min^{-1} to 350 °C where heating ceased. The sample desorbed only H_2 (Figure 4-32). Again there was a large, sharp initial desorption. This occurred at 170 °C, before rapidly dropping off. There were two other desorptions which peaked at 222 and 350 °C. The mass loss after heating to 350 °C was 5.3 wt%. This agreed well

with the theoretical mass loss of 5.4 wt% for this reaction if all NaH is converted to Na (Equation 4-10).

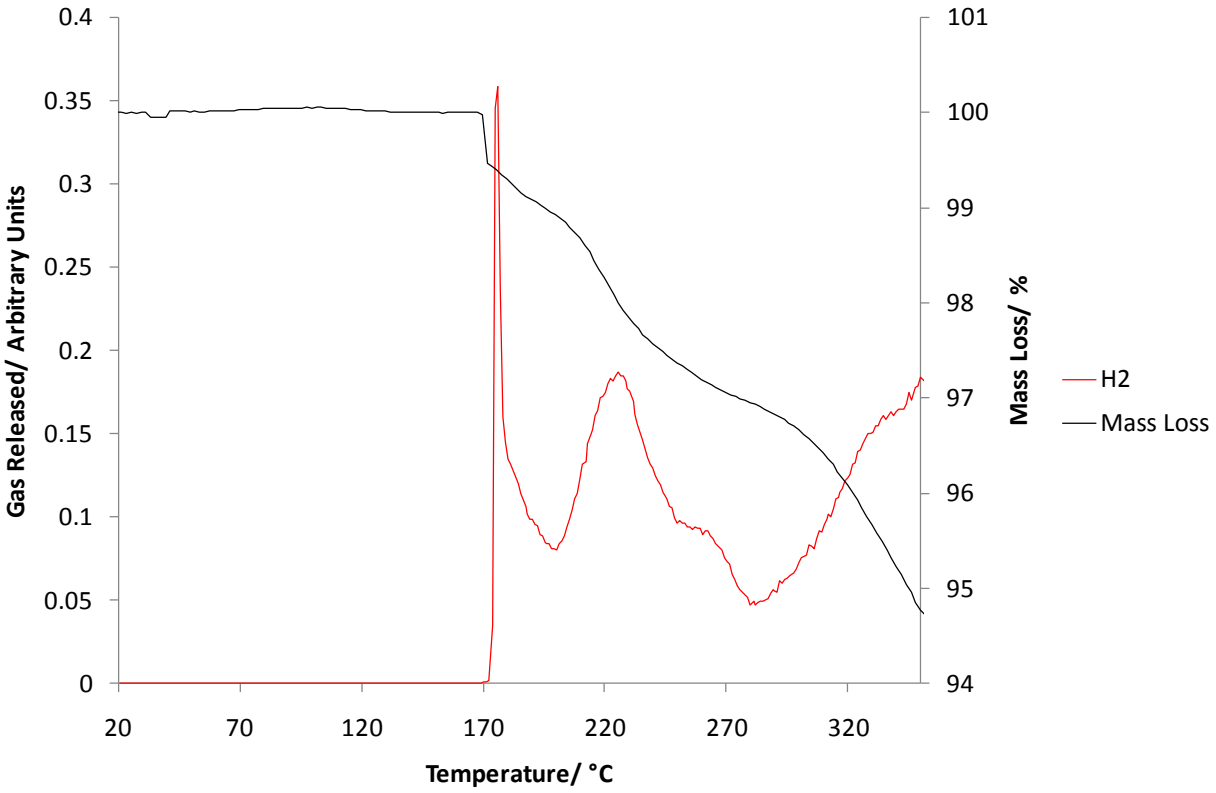

Figure 4-32 TGA–MS of the $NaNH_2$ + MgH_2 reaction. The H_2 release is shown in red and the percentage mass loss is shown in black.

3. *Flowing Line Reactions*

The starting materials were again heated at intermediate temperatures in order to investigate the chemical processes involved during dehydrogenation. $NaNH_2$ + MgH_2 were heated to 150 °C for 12 hours. This was after the first, small hydrogen desorption observed in the TPD-MS experiment. The products after heating under these conditions were NaH, $Mg(NH_2)_2$, $NaMgH_3$

and remaining MgH_2 (Figure 4-33), as well as some small phase B peaks, previously suggested to be a mixed Mg-Na amide.

The starting materials, $NaNH_2$ and MgH_2, were then heated together for 12 hours to 200 °C. At this temperature, the rate of hydrogen desorption was increasing towards its peak. The products from heating were NaH, $Mg(NH_2)_2$, $NaMgH_3$ and $MgNa_{2y}(NH)_{1+y}$ and remaining MgH_2 (Figure 4-33).

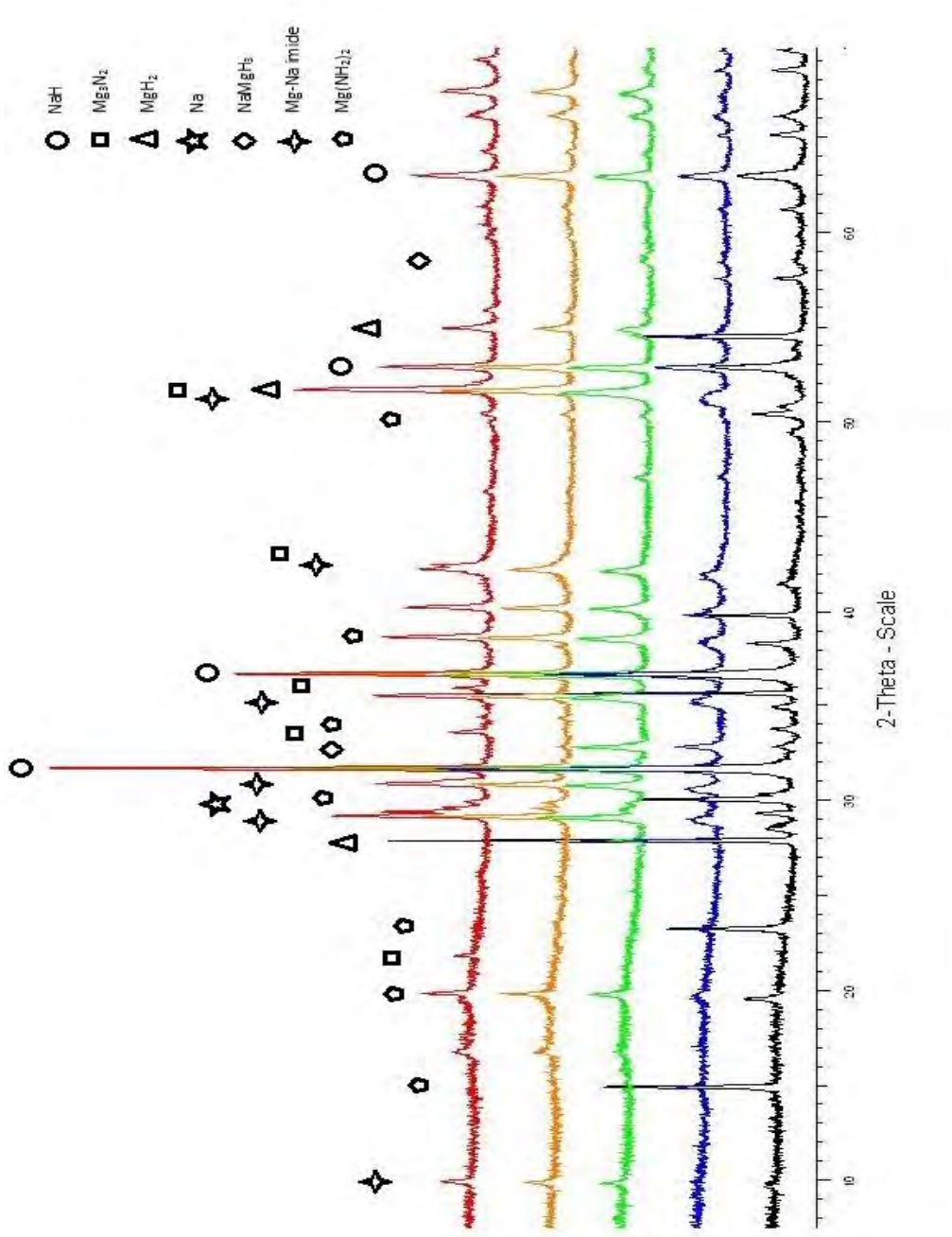

Figure 4-33 Stack plot of powder XRD patterns of $NaNH_2$ + MgH_2 heated to 150 °C (black), 200 °C (blue), 250 °C (green), 300 °C (orange) and 350 °C (red).

Table 4-17 Summary table of weight percents and mole fractions of products of $NaNH_2$ + MgH_2 from powder XRD shown in Figure 4–33.

$NaNH_2$ + MgH_2	Temperature													
	150		200			250			300			350		
Phase	Weight % in XRD	Mole Fraction	Weight % in XRD	Mole Fraction		Weight % in XRD	Mole Fraction		Weight % in XRD	Mole Fraction		Weight % in XRD	Mole Fraction	
MgH_2	25.26	29.63	20.88	21.77		7.19	7.03		NA	NA		NA	NA	
NaH	39.79	51.23	59.80	68.39		78.93	85.69		100	100		63.58	80.30	
$Mg(NH_2)_2$	34.05	18.52	12.10	5.89		NA	NA		NA	NA		NA	NA	
$NaMgH_3$	0.90	0.62	7.22	3.94		13.87	7.29		NA	NA		NA	NA	
$MgNa_{2y}(NH)_{1+y}$	NA	NA	Pawley	Pawley		Pawley	Pawley		Pawley	Pawley		Pawley	Pawley	
Mg_3N_2	NA	NA	NA	NA		NA	NA		NA	NA		27.71	8.18	
Na	NA	NA	NA	NA		NA	NA		NA	NA		8.71	11.52	

The starting materials were also heated to 250 °C. At this temperature the hydrogen desorption had peaked. The products after analysis with powder XRD were NaH, $NaMgH_3$, and $MgNa_{2y}(NH)_{1+y}$ as well as remaining MgH_2 starting material (Figure 4-33).

The reaction was carried out to 300 °C for 12 hours. The only products were NaH and $MgNa_{2y}(NH)_{1+y}$ (Figure 4-33).

When the reaction was carried out at 350 °C for 4 hours, the final products were the same as those after heating on the TPD–MS apparatus: NaH, Mg_3N_2 and $MgNa_{2y}(NH)_{1+y}$ along with some Na (Figure 4-33). Phase C, the suggested mixed Mg-Na nitride, was not seen in the XRD products for this series of reactions.

The full reaction scheme can be written as:

Equation 4-25 $$4NaNH_2 + 4MgH_2 \rightarrow 2MgNa_{2y}(NH)_{1+y} + (1-y)Mg_3N_2 + (4-4y)NaH + (3y-1)MgH_2 + (6-2y)H_2$$

No excess MgH_2 was observed in the reaction products. For $y = ⅓$, MgH_2 would be 0. This would give a formula for the imide as $Mg_3Na_2(NH)_4$. This was close to the possible value for y calculated for $3NaNH_2 + 2MgH_2$, $y = 0.3$.

We found a hydrogen desorption of 3.6 wt% from the TPD-MS apparatus data. This is less than the theoretical mass loss of 4.6 wt% for this reaction.

4. Rehydriding

The products after heating $NaNH_2$ + MgH_2 to 300 °C for 12 hours were then subjected to rehydriding conditions. The phases observed by powder XRD prior to rehydrogenation were NaH and $MgNa_{2y}(NH)_{1+y}$. These materials were then heated to 350 °C for 24 hours under 75 bar H_2 in order to assess whether it was possible to rehydride this system. The products after rehydriding were NaH, MgNH and $Mg(NH_2)_2$ (Figure 4-34). Unfortunately, there was also a large amount of MgO present.

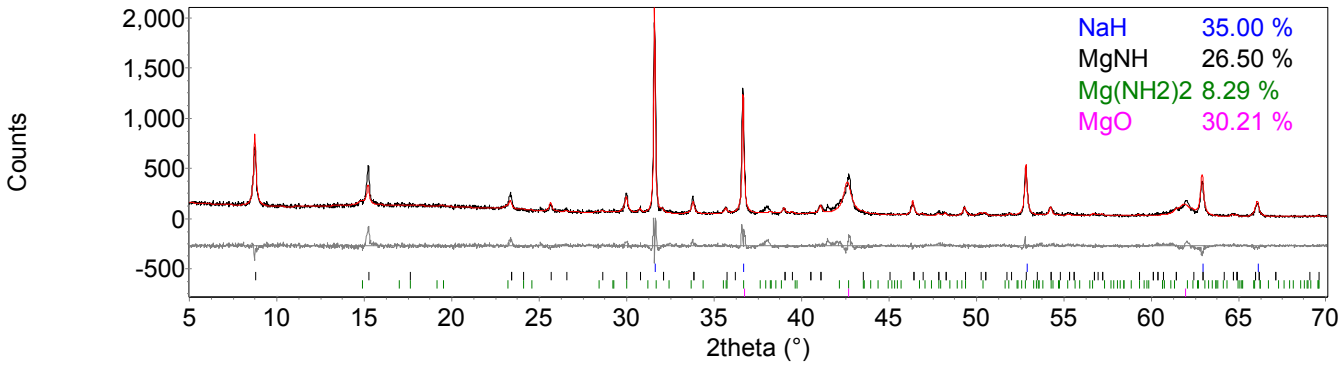

Figure 4-34 Powder XRD pattern of $NaNH_2$ + MgH_2 heated to 300 °C and then rehydrided at 350 °C for 24 hours under 75 bar H_2. The observed powder XRD pattern (black line) was fitted using a Rietveld fit (red line) to the observed phases NaH (blue tick marks), MgNH (black tick marks), $Mg(NH_2)_2$ (green tick marks) and MgO (pink tick marks). R_{wp} = 15.101, R_{exp} = 9.964, X^2 = 2.3.

Table 4-18 Summary table of weight percents and mole fractions of products of $NaNH_2$ + MgH_2 heated to 300 °C and then rehydrided at 350 °C for 24 hours under 75 bar H_2.

Phase	*Weight Percent in XRD*	*Mole Fraction/ mol %*
NaH	35.00	48.15
MgNH	26.50	22.25
$Mg(NH_2)_2$	8.29	4.85
MgO	30.21	24.75

5. Discussion

The initial hydrogen desorption peaked at the same temperature as for $3NaNH_2$ + $2MgH_2$. This was also at the same temperature as the salt metathesis in the other $NaNH_2$ and MgH_2 reactions, about 150 °C. The furnace power had only a little fluctuation at the metathesis temperature. This indicated minimal metathesis had occurred. This was as expected as less of a metathesis in comparison to $2NaNH_2$ + MgH_2 could occur, due to less $NaNH_2$ being present.

The products after heating $NaNH_2$ + MgH_2 to 350 °C on TPD-MS (Figure 4–31) were $MgNa_{2y}(NH)_{1+y}$ which was a major product from the sodium rich reactions, $2NaNH_2$ + MgH_2 and $3NaNH_2$ + 2NaH (sections 4.2.2, 4.2.3) and Mg_3N_2 which was the majority product from $2NaNH_2$ + $3MgH_2$ without any $MgNa_{2y}(NH)_{1+y}$ present (section 4.2.1).

After heating for 12 hours at 150 °C the full salt metathesis had occurred (Equation 4-26).

Equation 4-26 $2NaNH_2 + 2MgH_2 \rightarrow Mg(NH_2)_2 + NaH + MgH_2$

The reaction of $NaNH_2$ with MgH_2 in a 1:1 molar ratio can be compared to that of $LiNH_2 + MgH_2$ (1:1). The starting materials ($LiNH_2 + MgH_2$) in the work of Liu *et al*.[48] were ball-milled together, and after 12 hours of milling at room temperature, the products were: $Mg(NH_2)_2$, LiH and MgH_2 (Equation 4-27). These are the equivalent metathesis products to our reaction.

Equation 4-27 $LiNH_2 + MgH_2 \rightarrow Mg(NH_2)_2 + LiH + MgH_2$

From the reaction to 350 °C there was no amide phase present (Figure 4-33). This indicated a complete desorption reaction had occurred at this temperature.

The products from this reaction concur with the analogous $2LiNH_2 + (3)MgH_2$ reactions. As mentioned above, the $2LiNH_2 + MgH_2$ reaction[49] only goes as far as $Li_2Mg(NH)_2$, whereas $2LiNH_2 + 3MgH_2$[12] went to completion, giving Mg_3N_2 and LiH as products. A ratio of starting materials between $2LiNH_2 + MgH_2$ and $2LiNH_2 + 3MgH_2$ would be expected to have mixed products. The Na observed was due to the thermal decomposition of NaH (Equation 4-10).

The final products from $NaNH_2 + MgH_2$ also agree with $LiNH_2 + MgH_2$ from Liu *et al.*[48] Their final products were Mg_3N_2, LiH and $Li_2Mg(NH)_2$ (Equation 4-28). We have the equivalents for our system, Mg_3N_2, NaH and $MgNa_{2y}(NH)_{1+y}$ (Equation 4-25).

Equation 4-28 $4LiNH_2 + 4MgH_2 \rightarrow Mg_3N_2 + 2LiH + Li_2Mg(NH)_2 + 6H_2$

The lack of $MgNa_{2y}(NH)_{1+y}$ and the presence of $Mg(NH_2)_2$ in the XRD pattern after rehydriding showed that the rehydriding attempt was partially successful (Figure 4-34). Usually, it would be suggested that longer heating or increased hydrogen pressure would force the MgNH to convert fully to $Mg(NH_2)_2$ and MgH_2. However, as there was not enough nitrogen present, MgNH could not go directly to $Mg(NH_2)_2$. There was much more MgNH present after this rehydriding in comparison to other rehydrogenation reactions of $x NaNH_2 + y MgH_2$ reactions shown above. This may be related to the large amount of MgO present.

Liu *et al.*[52] attempted to rehydride the products of heating $LiNH_2 + MgH_2$ to 390 °C (Mg_3N_2, $Li_2Mg(NH)_2$ and LiH). After rehydriding, the products were Mg_3N_2, LiH and $Mg(NH_2)_2$. This result was similar to Dolotko *et al.* who rehydrided the products from $2LiNH_2 + 3MgH_2$ [Mg_3N_2 and LiH]. It can be seen the mixed imide could be rehydrided, whereas the Mg_3N_2 could not. The Mg_3N_2 remaining from both these rehydrogenation attempts showed that by stopping the forward reaction before Mg_3N_2 was formed a complete rehydrogenation was much more likely to go fully under moderate temperatures and pressures.

Xiong *et al.*[19] investigated the reaction between $Mg(NH_2)_2$ and NaH in a 1:1 ratio. However, rehydrogenation was only attempted for $Mg(NH_2)_2$ + NaH in a 2:3 ratio. This reaction, when heated, formed the same $MgNa_{2y}(NH)_{1+y}$ phase as formed by Sheppard *et al*.[21] When rehydrided the products were $Mg(NH_2)_2$ and NaH.

The full reaction scheme for $NaNH_2 + MgH_2$ heated in a flowing line is shown in Table 4-19.

Table 4-19 Overall reaction scheme of $NaNH_2$ + MgH_2 heated to various temperatures. The products from each temperature are shown, the temperature at which new phases form and the lattice parameters of the new phases.

Temp/ °C	*Reaction Scheme*	*Products*	*New Phase(s)*	*Lattice Parameters/ Å*
150	$NaNH_2 + MgH_2 \rightarrow$	NaH, $Mg(NH_2)_2$, MgH_2	–	–
200	$Mg(NH_2)_2 + 2NaH + MgH_2 \rightarrow$	NaH, MgH_2, $Mg(NH_2)_2$, $NaMgH_3$, H_2	$MgNa_{2y}(NH)_{1+y}$ (Phase A)	a = 6.1677(8), c = 17.997(5)
250		NaH, $NaMgH_3$, MgH_2	$MgNa_{2y}(NH)_{1+y}$ (Phase A)	a = 6.1299(4), c = 17.928(14)
275	$NaH + MgH_2 \rightarrow$	$NaMgH_3$	–	–
350	$Mg(NH_2)_2 + 2NaH + MgH_2 \rightarrow$	NaH, Mg_3N_2, Na, H_2	$MgNa_{2y}(NH)_{1+y}$ (Phase A)	a = 6.1182(3), c = 17.9117(9)
350	$NaH \rightarrow$	Na, H_2	–	–

In this study, it was found over the course of the investigation that excess MgH_2 after metathesis was always present when Mg_3N_2 was formed. Therefore, we conclude that excess MgH_2 is the reason that Mg_3N_2 is formed in some $x$$NaNH_2$ + $y$$MgH_2$ reactions and not others.

One possibility is that the MgH_2 still present after heating the reaction to 250 °C reacted with $MgNa_{2y}(NH)_{1+y}$ in order to form Mg_3N_2. Where there was a limited amount of MgH_2, only some of the $MgNa_{2y}(NH)_{1+y}$ could be converted into Mg_3N_2 ($NaNH_2$ + MgH_2). It was found that heating magnesium metal with $NaNH_2$ formed Mg_3N_2 along with sodium metal with the release of hydrogen (Equation 4-29).[50] It might therefore be possible for the remaining MgH_2 after forming $MgNa_{2y}(NH)_{1+y}$, to decompose to Mg metal which could have gone on to displace Na from $MgNa_{2y}(NH)_{1+y}$ to form Mg_3N_2. The continued hydrogen release suggests this was a possible mechanism for the formation of Mg_3N_2. It may be unlikely however, due to electrode potentials.

The formation of the Mg_3N_2 was the driving factor for the decomposition of $Mg_{(1-0.5x)}Na_x(NH)$ as sodium does not form a stable nitride.

Equation 4-29 $2NaNH_2 + 3Mg \rightarrow Mg_3N_2 + 2Na + 2H_2$

Mg_3N_2 was present with $NaNH_2 + MgH_2$ as with $2NaNH_2 + 3MgH_2$, therefore enough MgH_2 was present. In order to make $MgNa_{2y}(NH)_{1+y}$ pure, less MgH_2 is needed. $4NaNH_2 + 3MgH_2$ may help in the formation of a pure $MgNa_{2y}(NH)_{1+y}$, although it would be difficult to make it pure without knowing the exact stoichiometry. The results from $3NaNH_2 + 2MgH_2$ and $NaNH_2 + MgH_2$ suggest $x = 0.3–0.333$, this would help in defining the optimum starting materials to form the mixed imide pure.

The overall reaction schemes of each of the $xNaNH_2 + yMgH_2$ reactions have been detailed by Table 4-4, Table 4-9, Table 4-15 and Table 4-19. It can be seen at what temperatures the new phases (A, B and C) form at and how their lattice parameters vary with temperatures at which they were formed. It can also be seen at what temperatures the side reactions form at when independent of the other starting materials.

Throughout this work it could be seen that $Mg_{(1-0.5x)}Na_x(NH)/MgNa_{2y}(NH)_{1+y}$ could be rehydrided back to $Mg(NH_2)_2$ and NaH. Sometimes a longer heating time, greater pressure or ball-milling may have been needed to complete the rehydrogenation. As the rehydriding was carried out on hand ground mixtures was shown to be partially successful, the increased surface area that comes with ball-milling could significantly improve rehydrogenation kinetics. The only reaction

to attempt to rehydride Mg_3N_2 and Na was from $2NaNH_2 + 3MgH_2$ reacted at 250 °C. This rehydrogenation could only form NaH and a little MgNH. A higher pressure of 190 bar H_2 was found not to assist in the rehydrogenation of this reaction.[12] In order to allow for a completely reversible reaction pathway, the products from heating must go no further than $Mg_{(1-0.5x)}Na_x(NH)/MgNa_{2y}(NH)_{1+y}$. Rehydrogenation of Mg_3N_2 was not possible under the conditions investigated in this study or in the literature (Kojima[38]) although Leng *et al.* and Nakamori *et al.* found it possible.[6,51]

Liu *et al.*[52] investigated the effect of Na compounds upon the Li-Mg-N-H system with partial substitution of $Mg(NH_2)_2$ for $NaNH_2$ and LiH for NaH. It was found that the hydrogen desorption kinetics of the Na containing reactions were markedly improved. NH_3 desorption was also lessened. As the activation energies were less, the Na containing reactions desorbed their hydrogen quicker and at lower temperatures. Due to the higher mass of Na compared to Li, the gravimetric hydrogen capacity of the system is less than in the Li-Mg system. The dehydrogenation products were different depending on the molar ratios between Li, Mg and Na.

A comparison of the lattice parameters of $Mg_{(1-0.5x)}Na_x(NH)/MgNa_{2y}(NH)_{1+y}$ (phase A) throughout the reactions at different temperatures was carried out. The $Mg_{(1-0.5x)}Na_x(NH)/MgNa_{2y}(NH)_{1+y}$ phase occurring at 200 °C for all reactions had significantly larger lattice parameters than the phase appearing at higher temperatures. The phases at 200 °C had much broader peaks in their respective XRD patterns than at higher temperatures. This may be due to higher temperatures being necessary to form a more crystalline form of

$Mg_{(1-0.5x)}Na_x(NH)/MgNa_{2y}(NH)_{1+y}$. The most crystalline peaks were those formed at 300 °C. The variation in the lattice parameters may also be due to the variability in stoichiometry of the imide or a solid solution being formed. There are already known stoichiometric and non-stoichiometric phases associated with group 1/2 phases. For example a non-stoichiometric amide like $Li_xMg_{2-x}(NH_2)_{2+x}$ for $0 < x < 1$,[40] a stoichiometric imide $Li_2Mg(NH)_2$[46] or non-stoichiometric nitrides—$(Li_xMg_{1-x})_3N_{2-x}$, $0 < x < 0.2$ and $(Li_xMg_{1-x})_2N(_{2-x})_{2/3}$, $0.5 < x < 0.6$.[53] Mixed amide/imides were also formed by Aoki et *al.*[54] when reacting $3Mg(NH_2)_2$ with 12LiH. They found new tetragonal and orthorhombic phases. These corresponded to $Li_4Mg_3(NH_2)_2(NH)_4$ and $Li_{4+x}Mg_3(NH_2)_{2-x}(NH)_{4+x}$ (x = 0.4, 1, 2) respectively. Of course, $LiNH_2$ and Li_2NH can also be non-stoichiometric as described in Equation 4-30.

Equation 4-30 $$Li_{2-x}NH_{1+x} + \varepsilon H_2 \rightarrow Li_{2-(x+\varepsilon)}NH_{1+(x+\varepsilon)} + \varepsilon LiH$$

where non-stoichiometric lithium imide has a lithium deficient/proton excess composition. x denotes the number of lithium vacancies which must equal the number of excess protons.[55] Lithium is also known to form both stoichiometric and non-stoichiometric amides with sodium ($LiNa_2(NH_2)_3$) and $Li_{4-x}Na_x(NH_2)_4$ for $0 \leq x \leq 1$.[55] Sheppard *et al.* suggested the $MgNa_{2y}(NH)_{1+y}$ phase was a solid solution due to the peak shift occurring at different temperatures. This was thought to occur due to compositional changes in the imide structure due to Na or Mg migration to or from the phase as a function of reaction and/or temperature.

Luo and Sickafoose *et al.*[22] also found another Li-Mg-N-H phase on rehydriding $Li_2Mg(NH)_2$, $Li_2MgN_2H_{3.2}$ (Equation 4-31).

Equation 4-31 $Li_2MgN_2H_2 + 0.6H_2 \rightarrow Li_2MgN_2H_{3.2}$

The reactions of xNaNH$_2$ + yMgH$_2$ and xLiNH$_2$ + yMgH$_2$ appear to be very similar in mechanism. The stoichiometric and non-stoichiometric phases above show the possible phases that may be formed by a mixed Na-Mg-N-H system. Further work would need to be carried out in order to establish how many Li-Mg-N-H phases have analogous Na-Mg-N-H counterparts.

[1] P. Chen, Z. Xiong, J. Luo, J. Lin, K. Lee Tan, *Nature,* 420 (2002) 302–304
[2] P. Chen, Z. Xiong, J. Luo, J. Lin, K. Lee Tan, *J. Phys. Chem. B,* 107 (2003) 10967–10970
[3] T. Ichikawa, N. Hanada, S. Isobe, H. Leng, H. Fujii, *J. Phys. Chem. B,* 108 (2004) 7887–7892
[4] Z. Xiong, G. Wu, J. Hu, P. Chen, *Adv. Mater.,* 16 (2004) 1522–1525
[5] W. Luo, *J. Alloys Compds.,* 381 (2004) 284–287
[6] H.Y. Leng, T. Ichikawa, S. Hino, N. Hanada, S. Isobe, H. Fujii, *J. Phys. Chem. B,* 108 (2004) 8763–8765
[7] Y. Nakamori, G. Kitahara, S. Orimo, *J. Pow. Sources,* 138 (2004) 309–312
[8] K. Tokoyoda, S. Hino, T. Ichikawa, K. Okamoto, H. Fujii, *J. Alloys Compds.,* 439 (2007) 337–341
[9] G. Wu, Z. Xiong, T. Liu, Y. Liu, J. Hu, P. Chen, Y. Feng, A. T. S. Wee, *Inorg. Chem.,* 46 (2007) 517–521
[10] H. Wu, *J. Am. Chem. Soc., 130* (2008) 6515–6522
[11] S. Bhattacharya, G. Wu, P. Chen, Y. P. Feng, G. P. Das, *J. Phys. Chem. B*, 112 (2008) 11381–11384
[12] O. Dolotko, H. Zhang, O. Ugurlu, J. W. Wiench, M. Pruski, L. Scott Chumbley, V. Pecharsky, *Acta Mater.,* 55 (2007) 3121–3130
[13] H. Jacobs, B. Harbrecht, *J. Less-Common Met.,* 85 (1982) 87–95
[14] R. L. Lowton, M. O. Jones, W. I. F. David, S. R. Johnson, M. Sommariva, P. P. Edwards, *J. Mater. Chem*., 18 (2008) 2355–2360

[15] F. Kraus, N. Korber, *J. Solid State Chem.,* 178 (2005) 1241–1246
[16] Y. Nakamori, *Mater. Sci. Eng. B,* 108 (2004) 48–50
[17] D. F. Shriver, P. W. Atkins, C.H. Langford (Eds.), *Inorg. Chem*., Oxford University Press, Oxford, Tokyo, 1990
[18] O. Dolotko, N. Paulson, V. K. Pecharsky, *Int. J. Hydrogen Energy,* 35 (2010) 4562–4568
[19] Z. Xiong, J. Hu, G. Wu, P. Chen*, J. Alloys Compds.,* 395 (2005) 209–212
[20] W. Grochala, P.P. Edwards, *Chem. Rev.,* 104 (2004) 1283–1315
[21] D. A. Sheppard, M. Paskevicius, C. E. Buckley, *J. Phys. Chem. C,* 115 (2011) 8407–8413
[22] W. Luo and S. Sickafoose, *J. Alloys Compds.,* 407 (2006) 274−281
[23] Handbook of Chemistry and Physics, 91st edition, 2010–2011
[24] H. Y. Leng, T. Ichikawa, S. Isobe, S. Hino, N. Hanada and H. Fujii, *J. Alloys Compds.,* 404–406 (2005) 443-447
[25] J. Hu, Z. Xiong, G. Wu, P. Chen, K. Murata, K. Sakata, *J. Pow. Sources,* 159 (2006) 120–125
[26] J. Hu, G. Wu, Y. Liu, Z. Xiong, P. Chen, *J. Phys. Chem. B,* 110 (2006) 14688–14692
[27] A. Bouamrane, J-P. Laval, J-P. Soulie, J. P.Bastide, *Mater. Res. Bull.,* 35 (2000) 545–554
[28] E. Ronnebro, D. Noreus, K. Kadir, A. Reiser, B. Bogdanovic, *J. Alloys Compds.,* 299 (2000) 101–106
[29] K. Ikeda, Y. Nakamori, S. Orimo *Acta Mater.,* 53 (2005) 3453–3457
[30] K. Ikeda, Y. Kogure, Y. Nakamori, S. Orimo *Scripta Mater.,* 53 (2005) 319–322
[31] K. Ikeda, Y. Kogure, Y. Nakamori, S. Orimo *Progress in Solid State Chemistry,* 35 (2007) 329–337
[32] K. Ikeda, S. Kato, Y. Shinzato, N. Okudaa, Y. Nakamori, A. Kitano, H. Yukawa, M. Morinaga, S. Orimo, *J. Alloys Compds.,* 446–447 (2007) 162–165
[33] H. Wu, W. Zhou, T. J. Udovic, J. J. Rush, T. Yildirim, *Chem. Mater., 20* (2008) 2335–2342
[34] H. Wattenberg *Ber.,* 63 (1930) 1667–1672
[35] G. V. Vajenine, *Inorg. Chem.*, 46 (2007) 5146–5148
[36] G. V. Vajenine, *Solid State Synthesis*, 10 (2008) 450–454
[37] W. Moldenhauer and H. Mottig, *Ber.,* 62 (1929) 1954
[38] Y. Kojima, Y. Kawai, N. Ohba, *J. Pow. Sources*, 159 (2006) 81–87
[39] Report of the New Energy and Industrial Technology Development Organization (NEDO), Basic Technology Development Project for Hydrogen Safety and Utilization, Developments of lithium-based hydrogen storage materials for fuel cell vehicles, 04000549–0, 2003–2004
[40] R. Juza *Angew. Chem. Internat. Edit.,* 3 (1964) 471–481
[41] H. Jacobs, Universitat Kiel, unpublished work
[42] H. Jacobs, U. Fink, *J. Less-Common Met.,* 63 (1979) 273–286
[43] H. Jacobs, J. Kockelkorn, J. Birkenbeul, *J. Less-Common Met.,* 87 (1982) 215–224
[44] H. Jacobs, J. Birkenbeul, D. Schmitz, *J. Less-Common Met.,* 85 (1982) 79–86
[45] F. Dolci, E. Napolitano, E. Weidner, S. Enzo, P. Moretto, M. Brunelli, T. Hansen, M. Fichtner, W. Lohstroh, *Inorg. Chem*., 50 (2011) 1116–1122
[46] J. Lu, Y. J. Choi, Z. Z. Fang, H. Y. Sohn, *J. Pow. Sources,* 195 (2010) 1992–1997
[47] M. Nagib, H. Kistrup, H. Jacobs, *Atomkernenergie,* 26 (1975) 87–90

[48] Y. Liu, K. Zhong, M. Gao, J. Wang, H. Pan, Q. Wang *Chem. Mater.,* 20 (2008) 3521–3527
[49] J. Rijssenbeek, *J. Alloys Compds.,* 454 (2008) 233–244
[50] F. Ephraim, *Zeitschrift für Anorganische Chemie,* 44 (1905) 185–199
[51] Y. Nakamori, G. Kitahara, K. Miwa, S. Towata, S. Orimo, *Appl. Phys. A,* 80 (2005) 1–3
[52] Y. Liu, J. Hu, Z. Xiong, G. Wu, *J. Mater. Res.,* 22 (2007) 1339–1345
[53] H. Yamane, T. H. Okabe, O. Ishiyama, Y. Waseda, M. Shimada, *J. Alloys Compds.,* 319 (2001) 124–130
[54] M. Aoki, T. Noritake, G. Kitahara, Y. Nakamori, S. Towata, S. Orimo *J. Alloys Compds.,* 428 (2007) 307–311
[55] W. I. F. David, M. O. Jones, D. H. Gregory, C. M. Jewell, S. R. Johnson, A. Walton, P. P. Edwards, *J. Am. Chem. Soc.,* 129 (2007) 1594–1601

5. $NaNH_2$ + NaH

1. Introduction

1. $NaNH_2$

Although interesting products and reaction schemes have been discovered in the process of reacting light metal amides and hydrides together, it is important to understand as fully as possible what reaction pathways the starting materials take when they are heated alone. Most of the starting materials used in this research have been fully investigated outside of this work; however, $NaNH_2$ has been relatively neglected and therefore further experiments were required in order to confirm the decomposition products of $NaNH_2$. Also of interest was whether there are any similarities between the reactions of $NaNH_2$ + NaH and $LiNH_2$ + LiH. In the Li-based system, it is well known that $LiNH_2$ decomposes, both alone and when heated with LiH, to Li_2NH.[1,2] There is, however, no known analogous sodium imide phase.

Titherley *et al.*[3] originally investigated the decomposition of $NaNH_2$ heated under vacuum. They found there was no change until 200 °C when the sodium amide started to distil as an almost colourless liquid with a green tinge. 210 °C is the known melting point of $NaNH_2$. At 300–400 °C the liquid appeared dark green and apparently unchanged, but at 500–600 °C gas was evolved owing to the decomposition of the amide. The sample was kept at that temperature for 1 hour. Sodium metal was the only observed product, but there was no evidence of sodium nitride.

When Titherley *et al.*[3] investigated the decomposition of sodium amide, they found it decomposed down to its elements and not sodium nitride as suggested by Gay Lussac *et al.*[4]

Titherley *et al.* did find, however, that the ratio of N_2 to H_2 release was not 1:2 as expected. The deficiency of hydrogen was put down to its reducing action on the glass of the reacting vessel and some absorption by the metallic sodium. There was only slight decomposition on approaching 600 °C and none at all at 300–400 °C.

Further experiments done on heating sodium amide at 300–350 °C for 1 h under hydrogen found a scarcely appreciable amount of gas desorbed and the sodium amide remained unchanged. When repeated at 450 °C the decomposition was again scarcely appreciable with gas evolved very slowly. The gas comprised chiefly of ammonia, with a little hydrogen and nitrogen. At higher temperatures the same result as under vacuum occurred. However, on heating sodium amide under flowing ammonia at "dull-redness" temperature (500–600 °C) the ammonia is continuously decomposed to its elements. Titherley *et al.* concluded that the sodium amide split into its constituent elements, nitrogen, hydrogen and sodium, with sodium going to reform sodium amide under the ammonia atmosphere and decomposing again, therefore forming endless amounts of nitrogen and hydrogen at a lower temperature than normal, in other words sodium amide was a catalyst for the decomposition of ammonia. They concluded that neither Na_2NH nor Na_3N could be formed by heating $NaNH_2$.

The authors[3] then investigated whether the action of sodium on sodium amide could form either of the above products. Excess sodium was heated with sodium amide under hydrogen. If Na_2NH were formed hydrogen would be released (Equation 5-1). If the sodium merely remained in solution with the sodium amide, no gas release would be observed.

Equation 5-1 $$2NaNH_2 + 2Na \rightarrow 2Na_2NH + H_2$$

The reaction was carried out under vacuum, hydrogen and nitrogen but no gas release was observed. It was suggested that compounds of formula $(NaNH_3)_2$ (sodammonium) or $(Na.NaNH_2)_2$ (disodammonium, alternatively written as $Na_2H_2N.NH_2Na_2$) was formed[5] but no experiments were carried out to ascertain exactly what had been formed.

McGee *et al.*[6] found the rate of decomposition of $NaNH_2$ at 210 °C (the melting temperature) was slow, but increased with increasing temperature. The evolved gas at 300 °C was collected and tested. It was found to be ammonia, with no evidence of nitrogen or hydrogen. Further testing was carried out on the residue left in the cell. When decomposed with absolute alcohol and distilled water, only ammonia was desorbed, with no hydrogen, as would have been expected had sodium metal been present. The conclusion of McGee *et al.* was that the residue was either sodium imide (Equation 5-2) or nitride (Equation 5-3), and not sodium metal, along with undecomposed amide.

Equation 5-2 $2NaNH_2 \rightarrow Na_2NH + NH_3$

Equation 5-3 $3NaNH_2 \rightarrow Na_3N + 2NH_3$

Although a little unclear, the conclusions of Titherley *et al.*[3] result from $NaNH_2$ being heated to between 500 and 600 °C, and therefore not comparable with the work of McGee *et al.*[6] carried out at 300 °C. Bergstrom *et al.*[7] commented directly on the work of McGee *et al.* to suggest the decomposition of the amide into imide had its origin in the reaction of the amide with the glass container and, possibly, also in the reaction with platinum present.

In 1933, Bergstrom *et al.*[7] carried out further work. They commented on $NaNH_2$ heated at 300–400 °C only to say it was unchanged, except for a little darkening of the liquid. At 400 °C they commented that the substance started to volatilize and then rapidly evolved gas between 500 and 600 °C. Bergstrom *et al.* found this gas to be hydrogen and nitrogen evolved in a 2:1 ratio with metallic sodium remaining. This suggests the reaction:

Equation 5-4 $2NaNH_2 \rightarrow 2Na + 2H_2 + N_2$

However, it depends on how well the volumes of each could be measured, as it is possible NH_3 was decomposing to give the H_2 and N_2 evolved. It may be possible that although the ultimate decomposition is to the elements, that a nitrogen containing intermediate product could be formed (Equation 5-2 or Equation 5-3) along with the release of ammonia. The intermediate may then decompose to sodium metal with the release of nitrogen, along with the decomposition of ammonia gas.

Further investigations into the decomposition of $NaNH_2$ were carried out by Sakurazawa *et al.*[8] referenced by Juza *et al.*[9] This work suggested that between 335 and 400 °C two possible modes of thermal decomposition of sodium amide can occur depending on the overall pressure of the system. If the pressure of the system is greater than the dissociation pressure of NaH, then NaH is the solid product accompanied by N_2 and H_2 (Equation 5-5).

Equation 5-5 $2NaNH_2 \rightarrow 2NaH + N_2 + H_2$

However, if the total pressure is below the dissociation pressure of NaH, then the NaH decomposes to Na giving a greater desorption of H_2, along with N_2, (Equation 5–4). Ammonia was also produced along with the nitrogen and hydrogen, but they gave no indication of how much.

The crystal structure of $NaNH_2$ was first solved in 1956 concurrently by Juza *et al.*[10] and Zalkin *et al.*[11] The conclusion of both groups found it to be an orthorhombic structure of space group *Fddd*. Zalkin *et al.* found the lattice parameters were a = 8.964(3) Å, b = 10.456(3) Å (Figure 5-1) and c = 8.073(3) Å, in comparison to a = 8.06 Å, b = 8.929 Å and c = 10.427 Å published by Juza *et al*.

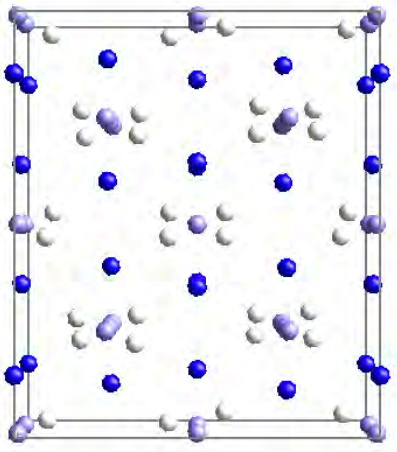

Figure 5-1 Crystal structure of $NaNH_2$. Sodium sites are shown in dark blue, nitrogen sites in light blue and hydrogen sites in white. The unit cell is shown in black.[11]

2. Na_3N

Research has also been carried out into the viability of the formation of Na_3N. Gay-Lussac *et al.*[4] first suggested the formation of Na_3N on the decomposition of $NaNH_2$. They identified a dark, infusible mass, when $NaNH_2$ was heated in a glass tube, as Na_3N (Equation 5-3). This

was dismissed by Titherley *et al.*[3] because sodium amide behaves differently when not heated in contact with glass. The dark colour quoted by Gay-Lussac *et al.*[4] was not present when $NaNH_2$ was heated in a different vessel. The liquid $NaNH_2$ was observed to have a pale green colour that became colourless on cooling. As it is now known that sodium and other alkali metals react with glass turning it dark brown, the differences in reactions observed can be explained by the reaction of sodium amide with the vessel the experiment was carried out in. Titherley *et al.*[3] tried to form Na_3N by heating $NaNH_2$ with Na_2O unsuccessfully. The reactants only fused and mixed together and were possible to separate again by heating strongly and distilling off the amide from the oxide.

Moldenhauer and Mottig suggested that evaporating a mixture of sodium azide (NaN_3) and Na could go to form sodium nitride (Equation 5-6).[12] However, no further work has been investigated in order to confirm the results of Moldenhauer and Mottig.

Equation 5-6 $$NaN_3 + 8Na \rightarrow 3Na_3N$$

Na_3N was formed by passing electrical discharges through sodium under low nitrogen pressure.[13,14] Na_3N was also prepared by reacting metallic Na or liquid Na-K alloy with plasma activated nitrogen at low pressure. Its formation seems not to be possible under more conventional chemical conditions.

The crystal structure of Na_3N, as formed by Vajenine *et al.* is shown below (Figure 5-2). It was found to be cubic, space group *Pm*−3*m*, with a lattice parameter of a = 4.7250(16) Å.

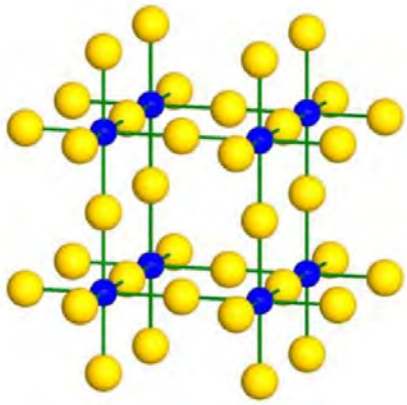

Figure 5-2 Crystal structure of Na_3N. Sodium sites are shown in yellow and nitrogen sites in blue. The unit cell is shown in black. Taken from Vajenine *et al*.[14]

In stark contrast to Na_3N, Li_3N forms spontaneously from the elements at room temperature. Na_3N does not form spontaneously and evidence so far seems to be that Na_3N is only formed under unusual conditions. Fischer and Jansen formed Na_3N from generating Na and N_2 in a vacuum chamber and co-depositing them on a cooled substrate.[15] This resulted in a statistical mixture of the atoms. This was then heated to room temperature. Their XRD pattern showed a pattern that could be refined to Na_3N.

The difficulty in making Na_3N highlights a difference from the Li-system. It is unlikely that if Na_2NH did form, that Na_3N would result from the decomposition of it. This effectively excludes Equation 5-3 as a possibility. Na_2NH has been discounted as forming (Equation 5-2) therefore other than that, it seems the solid product expected from the decomposition of $NaNH_2$ can only be Na or NaH.

2. Results

1. $NaNH_2$

1. *Temperature Programmed Desorption-Mass Spectrometry*

$NaNH_2$ starting material was heated at 2 °C min^{-1} to 350 °C for 4 hours on a flowing gas line. The powder XRD pattern taken after heating gave a set of peaks that did not match any known phase in the JCPDS database (Figure 5-3). There was no evidence of NaH or Na. A small amount of $NaNH_2$ was present. $NaNH_2$ is labelled in Figure 5-3 as 100% as it was the only Rietveld refined phase present.

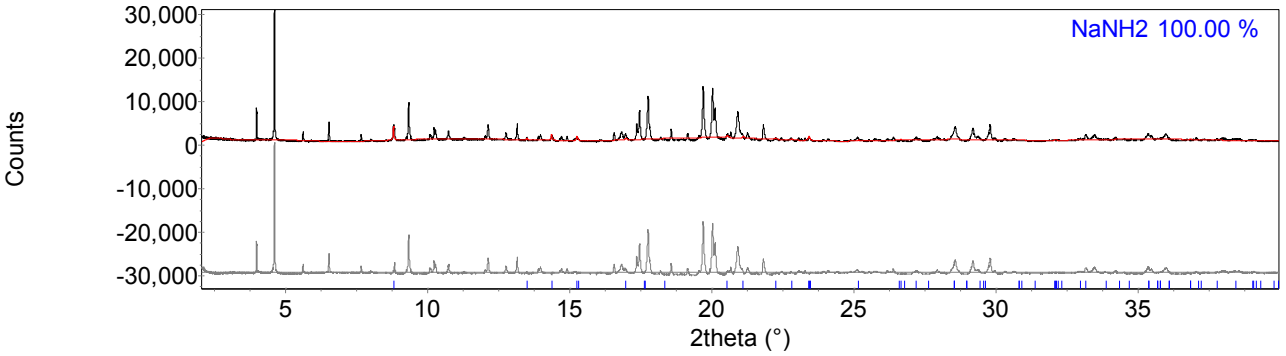

Figure 5-3 Powder XRD pattern (from ID31, ESRF) of $NaNH_2$ heated to 350 °C for 4 hours. The observed powder XRD pattern (black line) was fitted using a Rietveld fit (red line) to the observed phase $NaNH_2$ (blue tick marks). R_{wp} = 34.699, R_{exp} = 3.403, X^2 = 104.0.

The same reaction was carried out on a TPD-MS apparatus in order to establish whether any gas had been desorbed. From the desorption profile of $NaNH_2$ (Figure 5-4), it was seen that ammonia, NH_3, was the major gas desorbed. It can be seen that N_2 was also desorbed at the peak of NH_3 desorption. It was possible that an equilibrium between NH_3 and N_2/H_2 was present here. The H_2 desorption level also increased slightly at the same point (0.3 wt%

total). Unfortunately we were unable to quantify accurately the amount of N_2 released as the TPD-MS apparatus used was not calibrated for N_2.

There was a fluctuation in the temperature trace at around 200 °C. This is close to the melting point of $NaNH_2$ (210 °C). The onset of ammonia release was shortly after the sample had melted, at 220 °C. A comparison of the temperature fluctuation in Figure 5-4 with the furnace power (Figure 5-5) at the same temperature can see the power input into the sample increases before decreasing. This was a sign of an endothermic event occurring which was consistent with a melting event. The peak of desorption was at 330 °C, just before the isotherm at 350 °C. The total ammonia desorbed was 17.5 wt%.

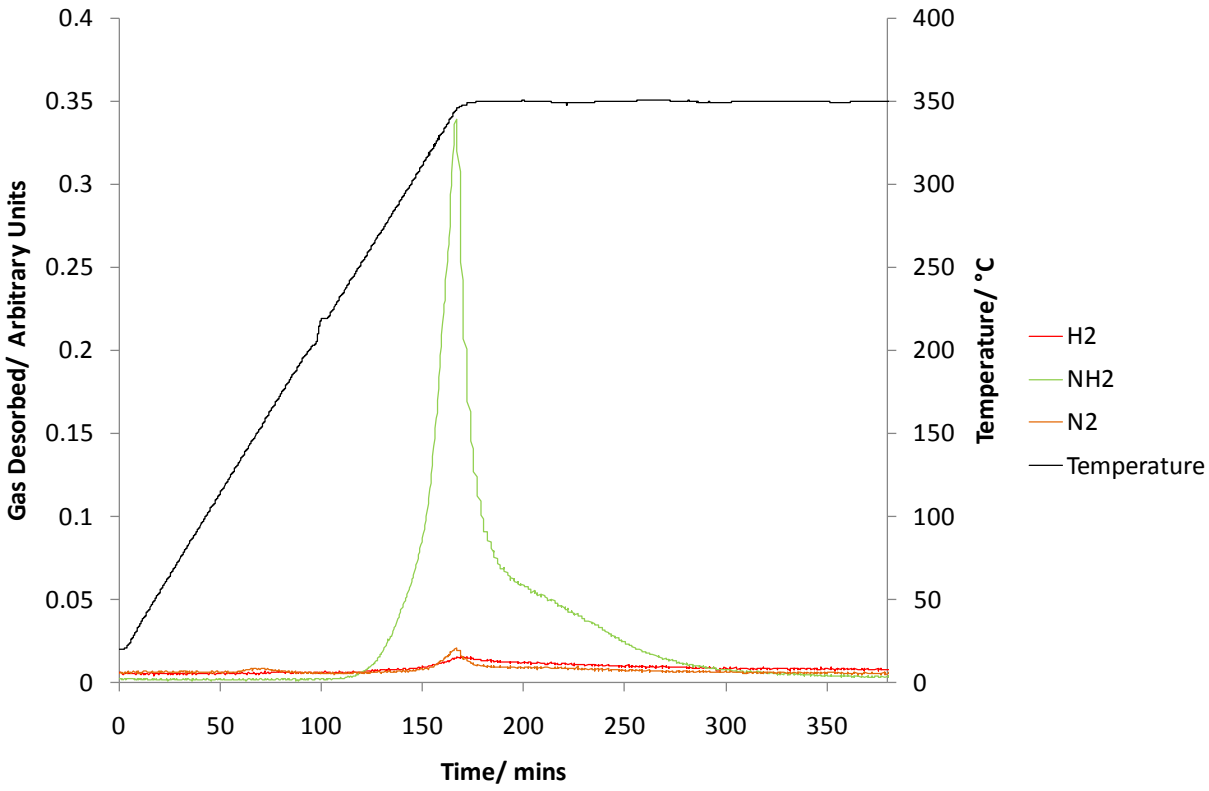

Figure 5-4 TPD-MS analysis of the heating of $NaNH_2$. The temperature trace is shown in black and the MS traces for H_2, NH_3 and N_2 are shown in red, green and orange, respectively.

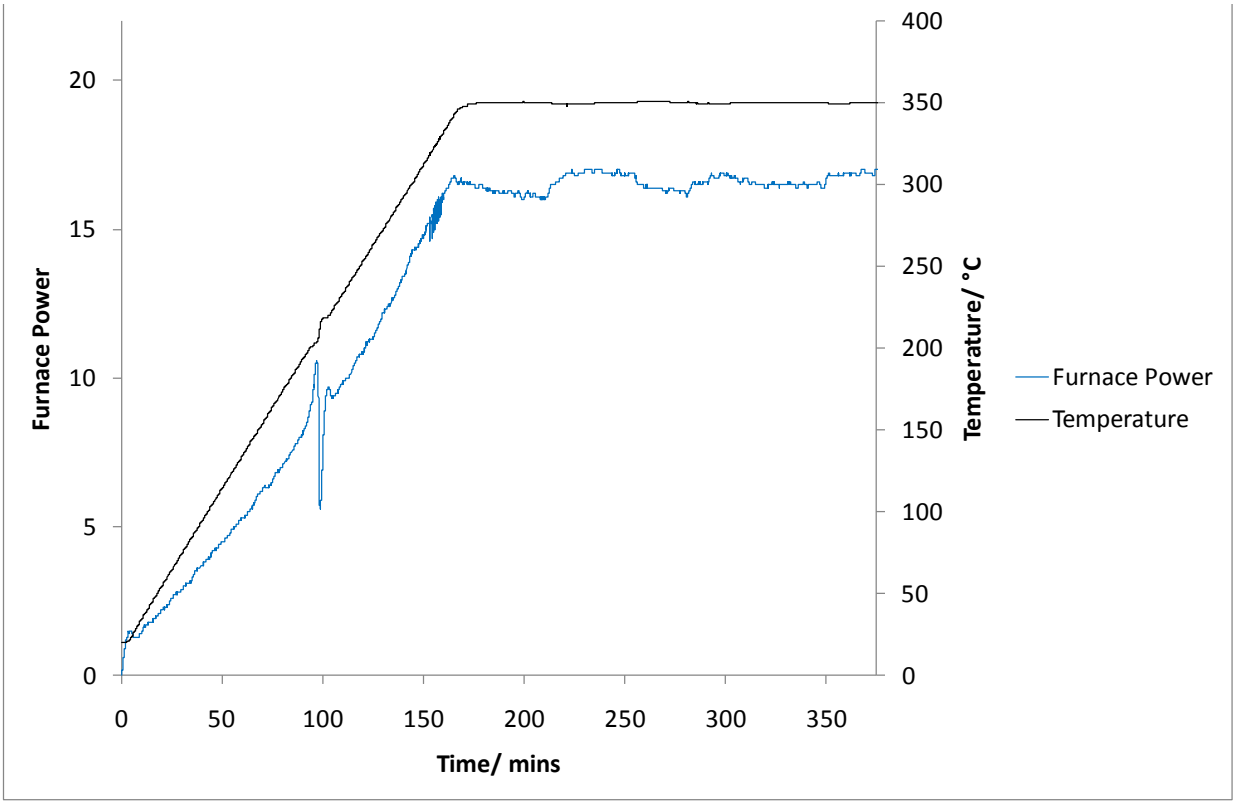

Figure 5-5 Furnace power during the TPD-MS analysis of $NaNH_2$ reaction. The furnace power and temperature are shown in blue and black respectively.

2. *Flowing Line Reactions*

The same reaction was carried out at 20 °C intervals between 230 and 350 °C for 4 hours. From the powder XRD patterns shown in Figure 5-6, it can be seen in comparison to $NaNH_2$ heated to 230 °C (no change to starting material) that the unidentified peaks were first visible after heating $NaNH_2$ to 270 °C. By 350 °C, the majority of $NaNH_2$ had disappeared although a small amount still remained. The starting material peaks were very distinctive until 330 °C. At no point was NaH or Na visible. Indexing was unsuccessful when attempted on the product from heating to 350 °C for 4 hours.

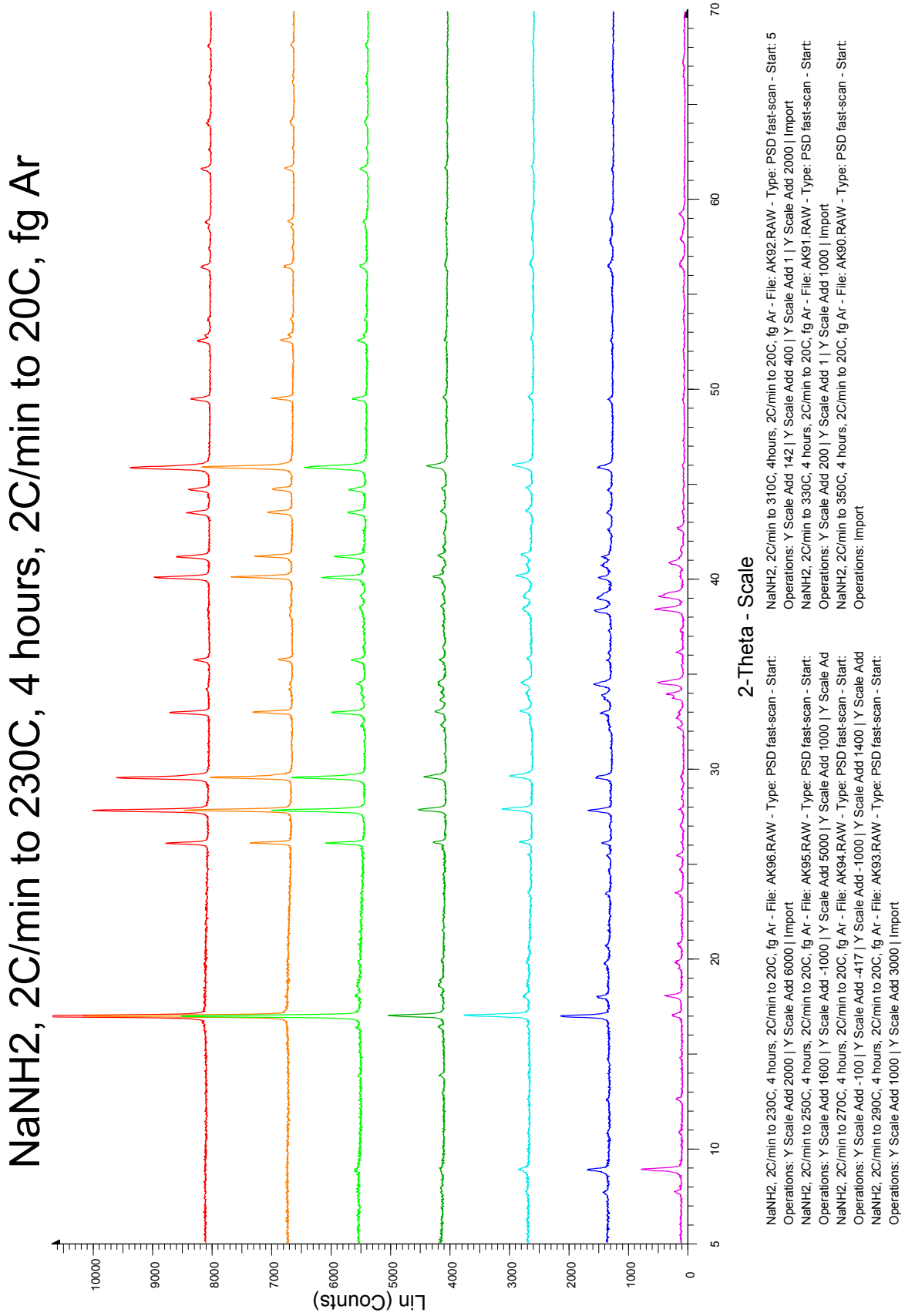

Figure 5-6 Powder XRD patterns of $NaNH_2$ heated to 230 °C (red), 250 °C (orange), 270 °C (light green), 290 °C (dark green), 310 °C (light blue), 330 °C (dark blue) and 350 °C (purple). The spectra are offset on the vertical scale for clarity.

There was little change to the lattice parameters of $NaNH_2$ throughout the heating of these reactions (Table 5-1). The possible variation of $NaNH_2$ lattice parameters were compared in order to establish whether a $Na_{2-x}NH_{1+x}$ type solid solution would be formed. This would be similar to the solid solution observed for $LiNH_2$-Li_2NH. The unit cell volume reduced upon heating in comparison to the lattice parameters found for the $NaNH_2$ starting material. The greatest difference in volume of $NaNH_2$ unit cell was noticed for samples heated to 230 °C and 250 °C.

Table 5-1 Lattice parameters of $NaNH_2$ heated to between 230 and 350 °C.

Temp/ °C	*a/ Å*	*b/ Å*	*c/ Å*	*Volume/ Å^3*	*% difference*
R. T.[16]	8.968	10.458	8.076	757.427	–
230	8.96097(4)	10.45227(5)	8.07276(4)	756.115(6)	-0.172
250	8.96046(4)	10.45341(5)	8.07316(4)	756.192(7)	-0.174
270	8.96300(9)	10.4477(12)	8.07462(9)	756.13(14)	-0.164
290	8.9638(2)	10.4464(3)	8.0757(2)	756.20(4)	-0.159
310	8.9642(3)	10.4472(3)	8.0767(2)	756.39(4)	-0.137
330	8.9666(5)	10.4424(6)	8.0772(5)	756.29(7)	-0.152
350	8.966(3)	10.435(3)	8.085(2)	756.4(4)	-0.131

Although there was a small amount of $NaNH_2$ still present at 350 °C, this was greatly reduced in comparison to the sample heated to 330 °C. $NaNH_2$ was heated to 350 °C for 12 hours in order to see if the transformation to the new phase would complete over a longer time. No $NaNH_2$ was present after the longer heating time (Figure 5-7).

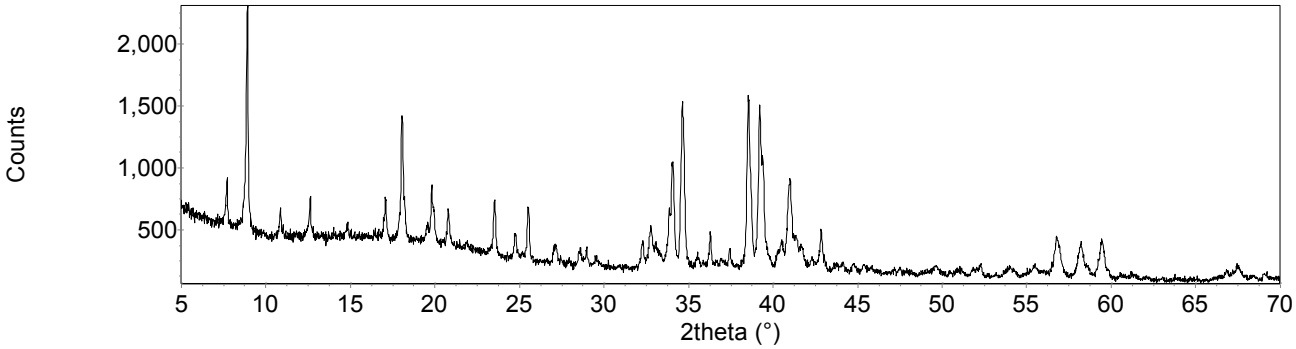

Figure 5-7 Powder XRD pattern of $NaNH_2$ heated to 350 °C for 12 hours.

3. Rehydriding

A sample of $NaNH_2$ heated to 350 °C was put under 100 bar H_2 pressure at 300 °C for 48 hours in order to see if it would take up hydrogen. These experiments were unsuccessful and the only peaks present in the XRD pattern afterwards were the previously unidentified peaks (Figure 5-8).

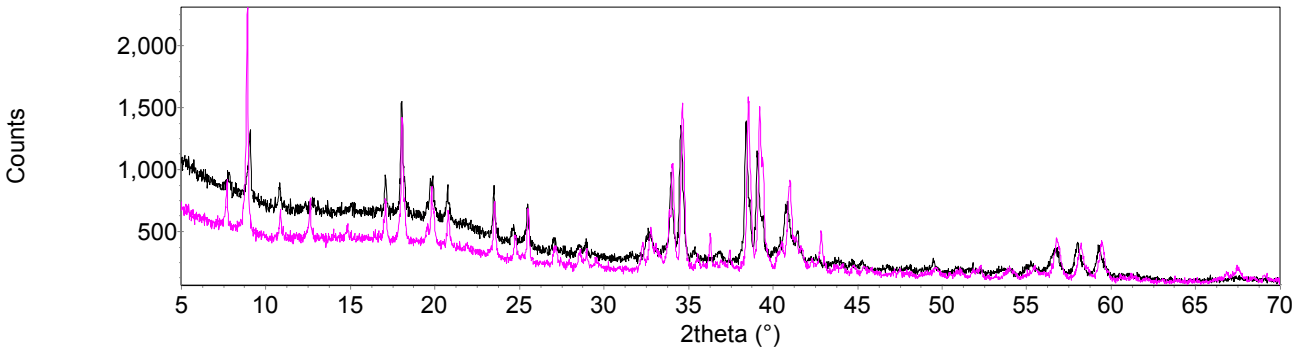

Figure 5-8 Powder XRD pattern comparison of $NaNH_2$ heated to 350 °C (purple pattern) put under 100 bar H_2 at 300 °C for 48 hours (black pattern).

2. $NaNH_2$ + NaH

1. *Temperature Programmed Desorption-Mass Spectrometry*

No previous work has been reported on the reaction of $NaNH_2$ with NaH. This reaction was of interest to investigate as it could then be compared to the reaction of lithium amide with lithium hydride (Equation 5-7). In the latter reaction, lithium imide was formed with the release of hydrogen (Equation 5-7). Of interest was whether the reaction of $NaNH_2$ with NaH would release ammonia, like $NaNH_2$ alone (Figure 5-4), or hydrogen, like $LiNH_2$ + LiH.

Equation 5-7 $LiNH_2 + LiH \rightarrow Li_2NH + H_2$

$NaNH_2$ and NaH were heated together in a 1:1 ratio at 2 °C min^{-1} to 350 °C and held for 4 hours. The XRD pattern from this reaction (Figure 5-9) gave the same set of unidentified peaks as $NaNH_2$ heated alone to 350 °C (Figure 5-3) alongside some $NaNH_2$ remaining.

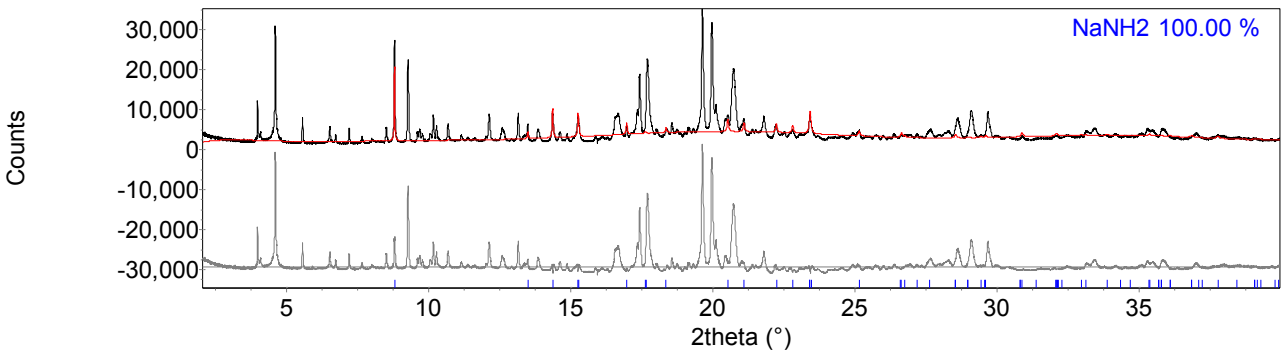

Figure 5-9 Powder XRD pattern (from ID31, ESRF) of $NaNH_2$ + NaH heated to 350 °C for 4 hours. The observed powder XRD pattern (black line) was fitted using a Rietveld fit (red line) to the observed phases $NaNH_2$ (blue tick marks). R_{wp} = 33.107, R_{exp} = 2.546, X^2 = 169.1.

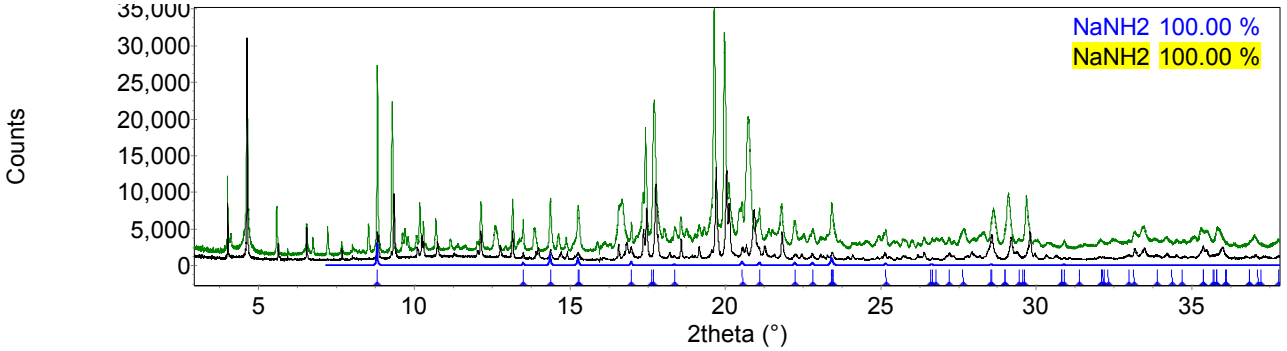

Figure 5-10 Powder XRD patterns (from ID31, ESRF) comparing $NaNH_2$ (black) heated to 350 °C for 4 hours and $NaNH_2$ + NaH (green) heated to 350 °C for 4 hours. The powder XRD patterns with the observed phase of $NaNH_2$ (blue tick marks) beneath are shown.

As before, the reaction was then carried out on a TPD-MS apparatus in order to establish what gas(es), if any, were desorbed. As can be seen in Figure 5-11, only hydrogen gas was released. The desorption started slowly as soon as heating was commenced. The rate of desorption increased at about 200 °C and peaked at about 318 °C. As the rate of desorption decreased, a second amount of hydrogen was desorbed as the isothermal heating started and slowly tailed off.

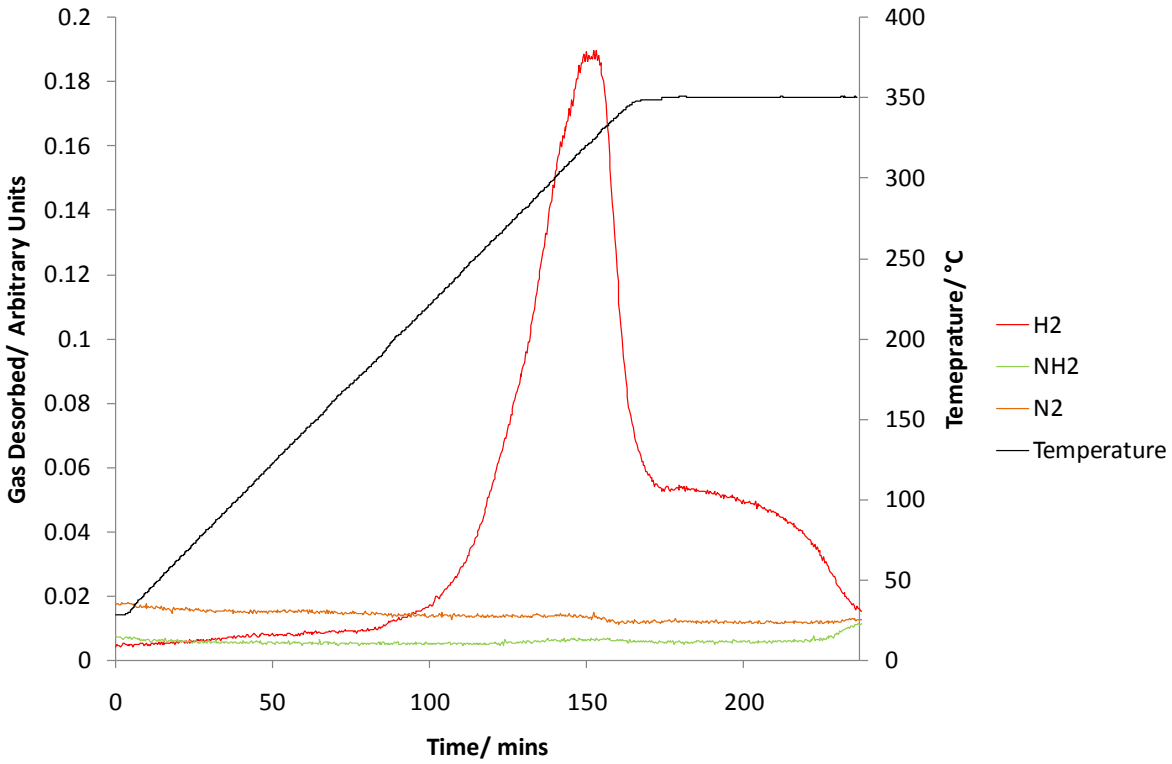

Figure 5-11 TPD-MS analysis of the reaction of $NaNH_2$ + NaH. The temperature trace is shown in black and the MS traces for H_2, NH_3 and N_2 are shown in red, green and orange, respectively.

2. *Flowing Line Reactions*

As with heating $NaNH_2$ alone, we heated the $NaNH_2$ + NaH mixture to intermediate temperatures between 230 and 350 °C for 4 hours. Heating to below 350 °C for the same length of time gave starting materials as well as the unidentified new peaks present in the XRD pattern. The new peaks first appeared at 290 °C. At 350 °C there was still $NaNH_2$ present. No NaH or Na was found at any temperature (Figure 5-12).

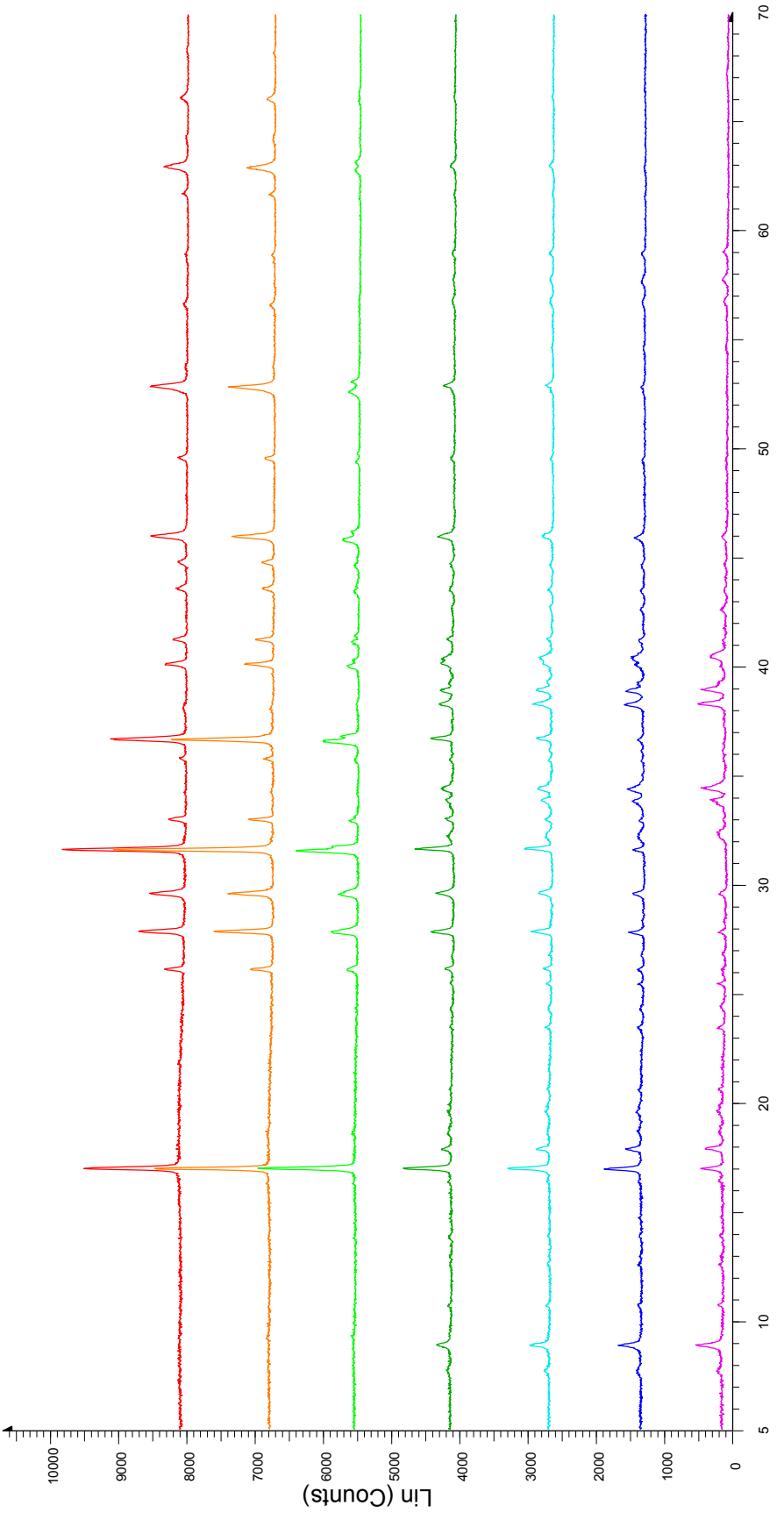

Figure 5-12 Powder XRD patterns of $NaNH_2$ + NaH heated to 230 °C (red), 250 °C (orange), 270 °C (light green), 290 °C (dark green), 310 °C (light blue), 330 °C (dark blue) and 350 °C (purple). The spectra are offset on the vertical scale for clarity.

The lattice parameters for the $NaNH_2$ and NaH starting materials after heating were compared to the lattice parameters established from the starting materials at room temperature (Table 5-2). For $NaNH_2$, the greatest difference was for the samples heated to 230, 250 and 270 °C. The unit cell volume had decreased by approximately 0.3 %. This was a greater decrease than observed on heating $NaNH_2$ alone, where the unit cell volume decreased only slightly. After heating at 290 °C the decrease in the unit cell volume had decreased to approximately 0.1 %. This temperature was the first for which the unidentified phase was first seen.

The lattice parameters of NaH were consistent after heating at different temperatures (Table 5-3), although they were all smaller than the unheated sample. There is no literature referring to hydrogen deficient NaH. The percentage difference was greater than that for $NaNH_2$.

Table 5-2 Lattice parameters of $NaNH_2$ after heating to between 230 and 350 °C with NaH. The errors for each parameter are included. The percentage difference between the volume of the starting material and those heated was included for comparison.

Temp/ °C	*a/ Å*	*b/ Å*	*c/ Å*	*Volume/ Å^3*	*% difference*
R. T.[16]	8.968	10.458	8.076	757.427	0.000
230	8.96357(7)	10.4380(10)	8.06982(7)	755.03(12)	-0.310
250	8.96349(9)	10.4341(12)	8.07003(9)	754.75(14)	-0.359
270	8.96283(8)	10.4344(11)	8.07134(8)	754.84(13)	-0.347
290	8.9643(5)	10.4320(6)	8.0897(4)	756.51(7)	-0.120
310	8.9654(7)	10.4300(8)	8.0897(7)	756.5(10)	-0.138
330	8.9683(8)	10.429(10)	8.0902(8)	756.7(13)	-0.104
350	8.972(18)	10.434(2)	8.085(18)	756.9(3)	-0.074

Table 5-3 Lattice parameters of NaH after heating to between 230 and 350 °C with $NaNH_2$. The errors for the parameter are included. The percentage difference between the volume of the starting material and those heated was included for comparison.

Temp/ °C	*a/ Å*	*Volume/ Å^3*	*% difference*
R. T.	4.89858(6)	117.547(5)	0.000
230	4.88483(2)	116.560(13)	-0.855
250	4.88527(3)	116.591(3)	-0.855
270	4.88475(3)	116.554(2)	-0.855
290	4.8841(15)	116.51(10)	-0.916
310	4.8840(2)	116.50(16)	-0.916
330	4.8845(5)	116.54(3)	-0.855
350	N/A	N/A	N/A

The starting materials were then heated to 350 °C for 24 hours. It was found that there was no change in the unidentified phase after this longer period of time. The starting materials were also heated to 400 °C for 24 hours. Again, the product was the same as before.

$NaNH_2$ and NaH were then heated together to 350 °C for 7 days (168 hours). The products, although similar, were not identical to the others observed after heating for a shorter time. The peak positions in the powder XRD were similar but some peaks had diminished in relative size and other new peaks had appeared (Figure 5-13). This was an indication that either the relative amount of difference phases change over time, or that there is a change in the crystal structure of the phase responsible for the Bragg reflections.

The phase could be compared after heating for 4 hours and 168 hours (Figure 5-14). It could be seen the peaks were similar in position, but some peak intensities had varied. The longer heating had resulted in a more crystalline XRD pattern, as evidenced by the sharpness of the Bragg reflections. The comparison of $NaNH_2$ heated to 350 °C for 168 hours and $NaNH_2$ + NaH for 168 hours showed the same level of crystallinity, but the peak ratios varied and peaks had shifted to both higher and lower *d*-spacings (Figure 5-15).

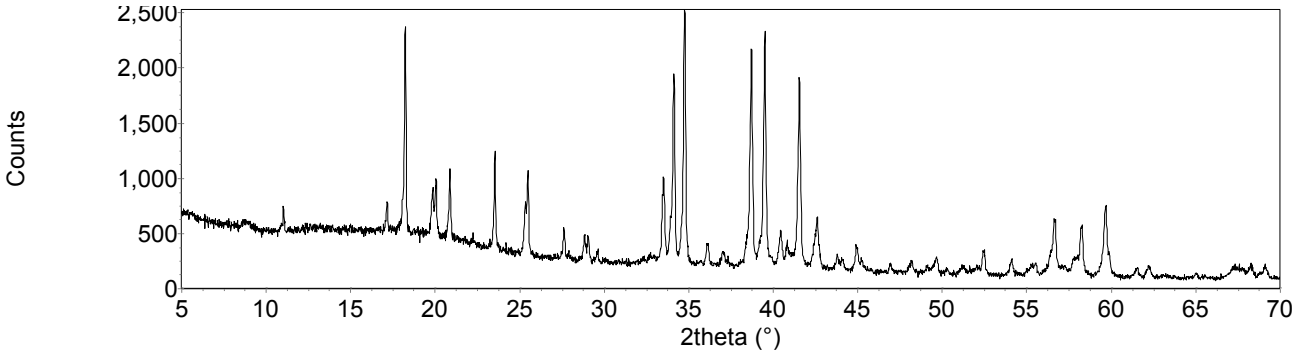

Figure 5-13 Powder XRD pattern of $NaNH_2$ + NaH heated to 350 °C for 168 hours.

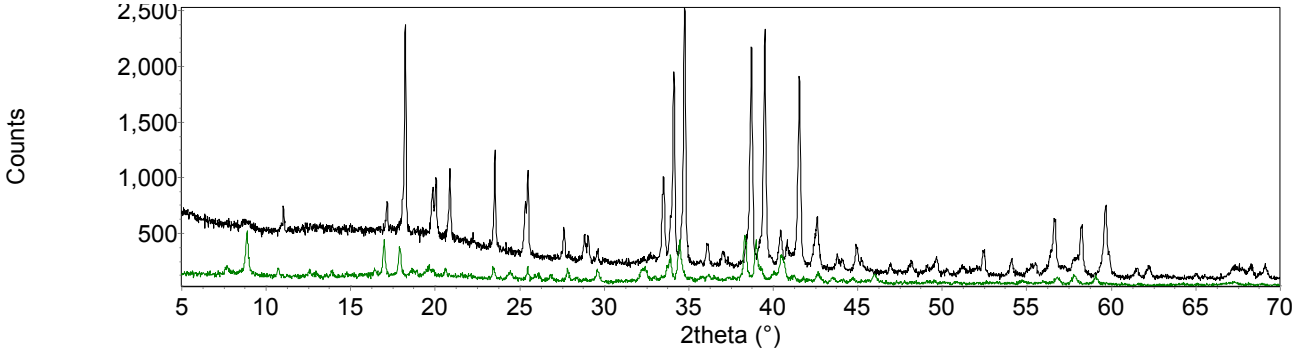

Figure 5-14 Powder XRD patterns of comparison of $NaNH_2$ + NaH (black) (from ID31, ESRF) heated to 350 °C for 168 hours and $NaNH_2$ + NaH (green) heated to 350 °C for 4 hours.

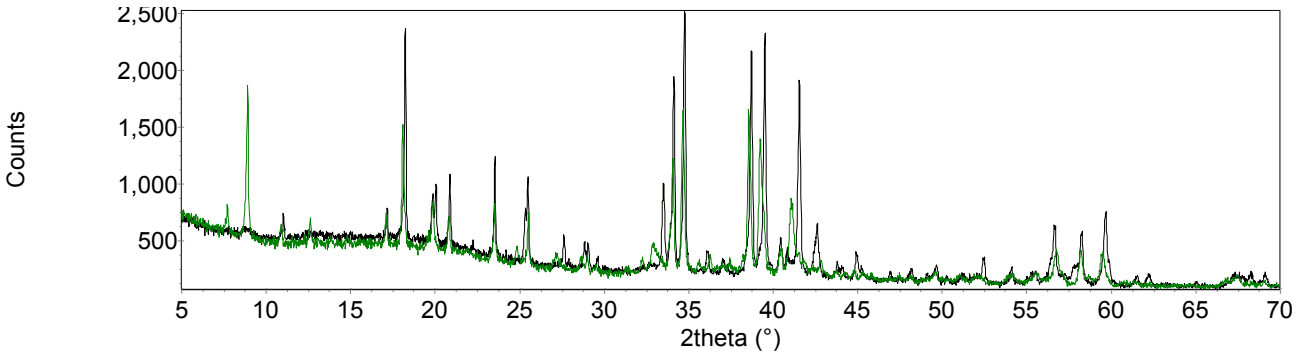

Figure 5-15 Powder XRD patterns of comparison of $NaNH_2$ (black) heated to 350 °C for 168 hours and $NaNH_2$ + NaH (green) heated to 350 °C for 168 hours.

3. *Raman*

The Raman spectrum of $NaNH_2$ + NaH heated to 350 °C for 12 hours is shown in Figure 5-16. It can be seen that peaks were present in the N-H stretching region. $NaNH_2$ + NaH heated to 350 °C can be compared to the spectrum of $NaNH_2$ starting material (Figure 5-16). The sodium phases can also be compared with Li^+-$[NH_2]^-$ with Li^+_2-$[NH]^{2-}$, as shown in Figure 5-17. The N-H stretches of $NaNH_2$ were observed at 3211.48 and 3252.14 cm^{-1}; whereas the main peak from the reaction product of $NaNH_2$ + NaH occurred at 3192.10 cm^{-1}.

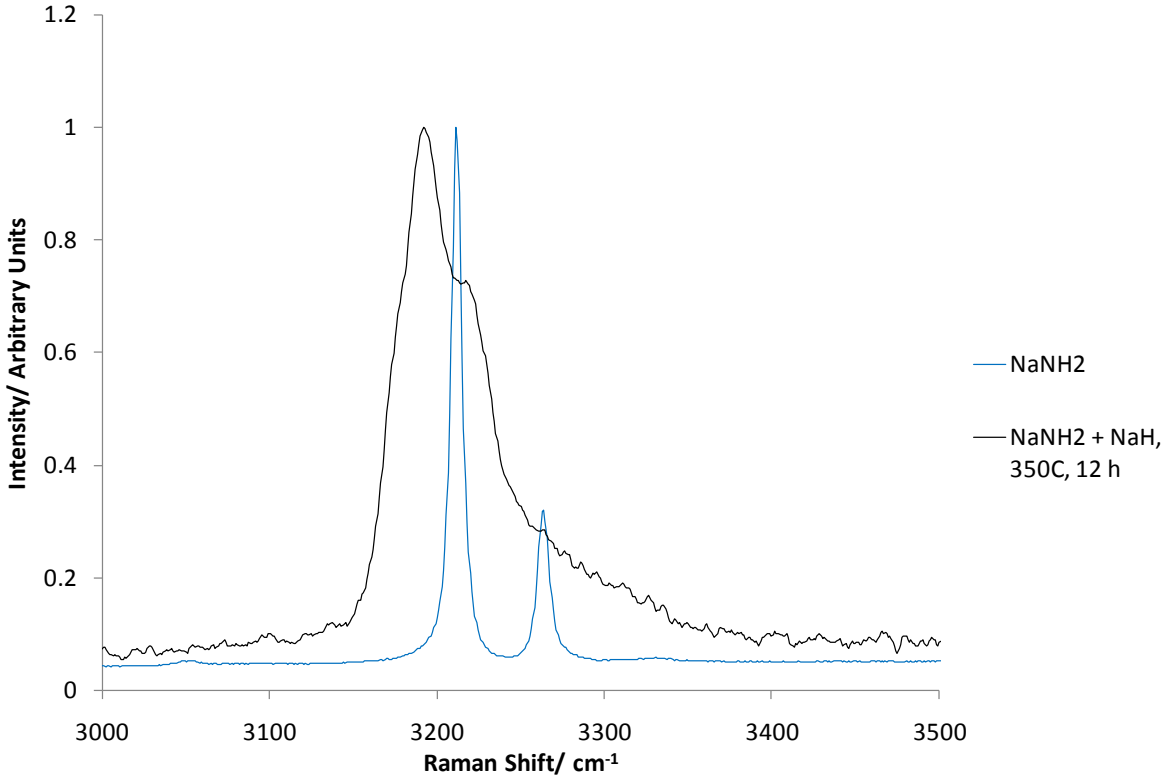

Figure 5-16 Raman spectra of $NaNH_2$ at room temperature and $NaNH_2$ + NaH, heated to 350 °C: amide stretching region.

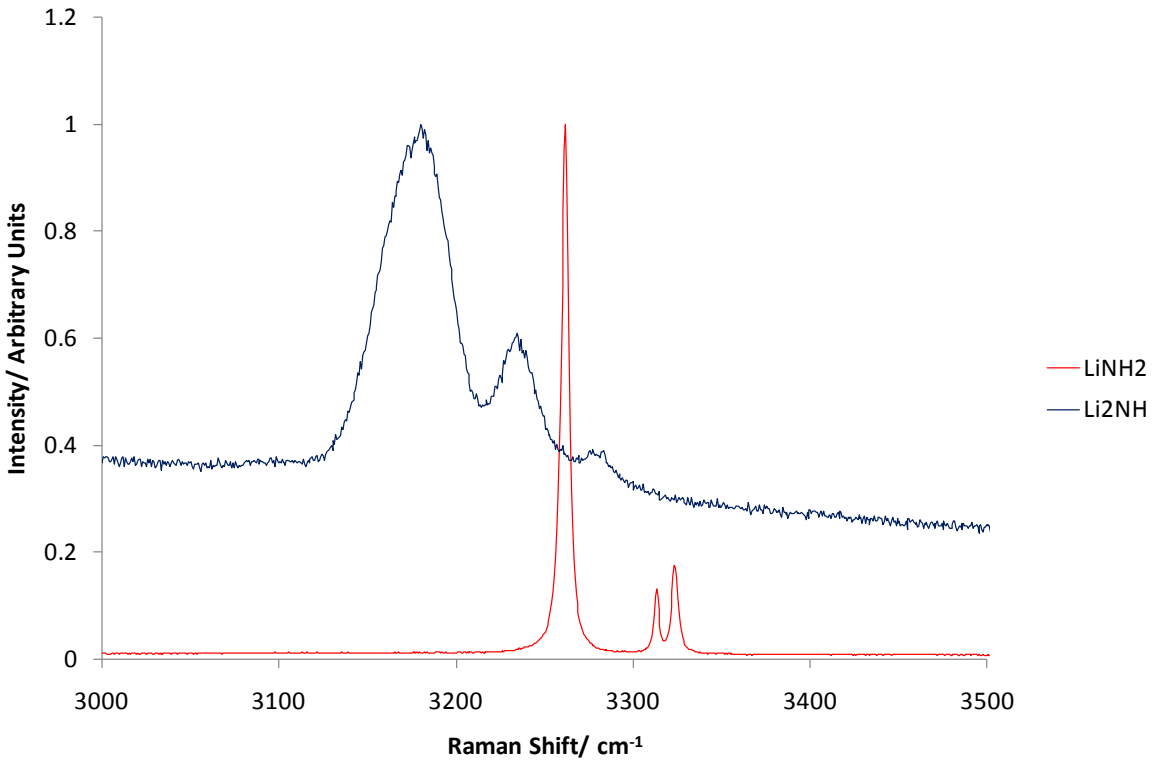

Figure 5-17 Raman spectra of $LiNH_2$ and Li_2NH: amide stretching region.

4. Rehydriding

The unidentified products after heating $NaNH_2$ + NaH to 350 °C were exposed to 100 bar hydrogen at 200 °C for 48 hours. Attempts to rehydride the unidentified phase failed as they did for $NaNH_2$ heated alone. There was no evidence of any additional phase, other than the unidentified peaks present before hydriding, although the peak positions and intensities had altered from $NaNH_2$ + NaH heated to 350 °C before rehydriding was attempted.

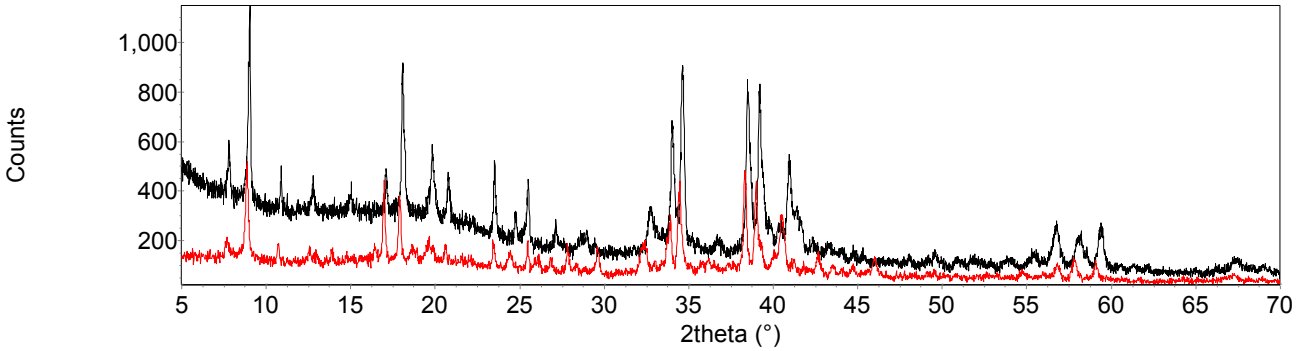

Figure 5-18 Powder XRD patterns of $NaNH_2$ + NaH heated to 350 °C for 4 hours (red pattern) put under 100 bar H_2 at 200 °C for 48 hours (black pattern).

3. Discussion

It could be seen that when $NaNH_2$ alone was heated it formed a previously unidentified diffraction pattern with the release of ammonia. This could be analogous to $LiNH_2$. When $LiNH_2$ is heated alone it releases ammonia and forms Li_2NH[1] (Equation 5-8), raising the possibility that a previously dismissed sodium imide phase may have been formed through these reactions.

Equation 5-8 $2LiNH_2 \rightarrow Li_2NH + NH_3$

If Na_2NH was formed from the heating of $NaNH_2$ (Equation 5-2), there would be a theoretical mass loss of 21.8 wt% NH_3 (1 mole NH_3), which can be compared to the 17.5 wt% loss inferred from the MS data, although the 17.5 wt% loss does not include the nitrogen and hydrogen released. This is the equivalent of 0.8 NH_3 moles released.

In the temperature trace (Figure 5-5) it could be seen that there was a fluctuation at 210 °C. This was accompanied by a large variation in the furnace power. This started with an

increase in power, swiftly followed by a drop in power and was indicative of an endothermic event. As 210 °C is the melting point of $NaNH_2$, it can be assumed that the fluctuation was due to the melting of $NaNH_2$.

$NaNH_2$ has a significant vapour pressure below its 210 °C melting point. This could lead to sodium loss from the system. It is possible that the unknown phase is a hydrogen rich non-stoichiometric version of Na_2NH ($Na_{2-x}NH_{1+x}$) (analogous to that observed in the lithium system–$Li_{2-(x+\varepsilon)}NH_{1+(x+\varepsilon)}$).

When $NaNH_2$ was heated with NaH the only gas released was hydrogen. The XRD gave the same pattern as for $NaNH_2$ heated alone (Figure 5-10). Again, this is similar to the $LiNH_2$-LiH system. When $LiNH_2$ and LiH are heated together, they form Li_2NH along with the release of hydrogen (Equation 5-7).

The amount of hydrogen desorbed after heating $NaNH_2$ + NaH together was 2.1 wt%. This was in comparison to a theoretical release of 3.2 wt% if the reaction proceeded as the analogous $LiNH_2$-LiH reaction, forming Na_2NH.

An often proposed mechanism for the release of hydrogen desorption from the reaction of $LiNH_2$ + LiH is an ammonia mediated one. The $LiNH_2$ decomposes to Li_2NH with the release of NH_3. The NH_3 then reacts "ultrafast"[17] with the LiH present to form further $LiNH_2$ with the release of hydrogen and the cycle begins again.

Equation 5-9 $\quad LiH + NH_3 \rightarrow LiNH_2 + H_2$

As seen above, $NaNH_2$ decomposed to an unknown phase with the release of ammonia. It has been reported that NaH, when ball-milled with ammonia gas, can form $NaNH_2$ after

1 hour whereas the formation of $LiNH_2$ (Equation 5-9) took 2 hours.[18] This suggests that there could also be a fast reaction between NaH and ammonia equivalent to lithium hydride. The NaH and NH_3 react to form further $NaNH_2$ and release the hydrogen observed in the reaction $NaNH_2$ + NaH (Figure 5-11).

In the TPD-MS trace (Figure 5-11), the above mechanism could account for the first hydrogen desorption peak and the second, slower higher temperature peak may result from any NaH, left over, decomposing to Na and H_2 (Equation 5-10). Although no Na was detected in the products of the reaction heated to 350 °C, it is possible the Na came off the reaction as a vapour and was therefore not detectable. A small amount of $NaNH_2$ was still present in the products after heating by TPD-MS. There was a small rise in ammonia at the end of the heating on TPD-MS. This may have come from the remaining $NaNH_2$ continuing to release ammonia, but with no NaH to react with due to NaH decomposing to Na.

Equation 5-10 $2NaH \rightarrow 2Na + H_2$

The longer heating time for $NaNH_2$ + NaH appeared to give a more crystalline XRD pattern and a pattern that indicated different content (Figure 5-14). There was no change in the XRD pattern between heating $NaNH_2$ at 350 °C for 4 hours and 168 hours.

Evidence from the Raman spectra showed nitrogen was still present in the product (Figure 5-16), due to the peaks present in the N-H stretching region of the Raman spectra. This suggested either $[NH_2]^-$ or $[NH]^{2-}$ units were present in the unidentified phase after heating $NaNH_2$ with NaH.

The $[NH_2]^-$ units from $NaNH_2$ were shown in Figure 5-16 to exhibit peaks at higher wavenumbers than the N-H stretches in the unknown phase. Interestingly, the N-H stretching peaks of $LiNH_2$ are known to occur at a higher wavenumber than those of Li_2NH (Figure 5-17). This was also found by Kojima *et al.*[19], and Bohger *et al.*[20] confirmed the position of the $LiNH_2$ peaks. $Mg(NH_2)_2$ peaks occur at 3274 and 3333 cm^{-1},[21,22] whereas the peaks of MgNH occur at lower wavenumbers: 3251 and 3199 cm^{-1}.[21,23] It would therefore be expected that the peaks of Na_2NH would be shifted from the higher wavenumber of $NaNH_2$ to a lower wavenumber, like MgNH and Li_2NH.

The published positions for the IR N-H stretching bands of $LiNH_2$ are 3260 and 3315 cm^{-1}. $LiNH_2$ has two stretches- the symmetric and the asymmetric bands. The symmetric band appears alone at approximately 3260 cm^{-1}, whereas there can be evidence of 2 asymmetric bands occurring at slightly higher wavenumbers, 3310 and 3315 cm^{-1}.[20] However the numbers of stretches within Li_2NH has not been confirmed. It has been noted by Ichikawa *et al.*[24,25] that Li_2NH has one IR band, by Kojima *et al.* and Bogher *et al.*[19,20,26] that it has 2 bands (3180 and 3250 cm^{-1}) and by Varin *et al.*[27] that it has 3 bands in the N-H region. The variation in number of bands observed within Li_2NH IR/Raman, may be due to the non-stoichiometry possible within Li_2NH.[28]

The Li_2NH $[N\text{-}H]^{2-}$ peaks were found to be broader than those for $LiNH_2$ and $NaNH_2$. Kojima *et al.* also showed the same broadening in their Li_2NH Raman peaks produced from the thermal decomposition of $LiNH_2$. They put the broadening down to small crystallite size and/or disorder in the crystallites. Chen *et al.*[25] suggested the broadening of the IR band of Li_2NH was due to some unknown chemical/structural environments within the Li-N-H crystal.

The bands of the unknown phase were also found to be broader than $LiNH_2$ and $NaNH_2$, in the same way as Li_2NH.

The Raman evidence is consistent with the suggestion that the N-H bands in the unknown phase could be from $[NH]^{2-}$ as these peaks are known to appear at a lower wavenumber to amide units as well as having a broader peak width.

Another possibility was that a mixed sodium amide-imide was formed ($Na_{2-x}(NH_2)_x(NH)_{1-x}$, $0 \leq x \leq 1$). $LiNH_2$-Li_2NH is known to be non-stoichiometric with respect to the Li^+/H^+ ions.[28] The mixed stoichiometry possible from a mixed amide-imide could account for the similarities in the XRD patterns from heating $NaNH_2$ and $NaNH_2$ + NaH, and forming similar, but obviously not the same, products.

Further investigation is needed in order to confirm the structure of the possible $Na_{2-x}NH_{1+x}$. The $NaNH_2$-NaH system did not appear to be successful for hydrogen storage as although hydrogen *was* released, it was not at a lower temperature than hydrogen desorption in the $LiNH_2$-LiH and $LiNH_2$- MgH_2 systems. However, the information garnered from this research and from further investigations into $NaNH_2$ may well assist in the understanding of the mechanism of hydrogen desorption for other amide-imide systems.

---

[1] P. Chen, Z. Xiong, J. Luo, J. Lin, K. Lee Tan, *Nature,* 420 (2002) 302–304
[2] T. Ichikawa, N. Hanada, S. Isobe, H. Leng, H. Fujii, *J. Phys. Chem. B,* 108 (2004) 7887–7892
[3] A. W. Titherley, *J. Chem. Soc. Trans.,* 65 (1894) 504–522
[4] J. L. Gay-Lussac, L. J. Thenard, *Recherches Physico-chimiques,* 1 (1811) 337–356
[5] A. Joannis, *Compt. Rend*., 115 820–823
[6] J. M. McGee, *J. Am. Chem. Soc.*, 43 (1921) 586–591
[7] F. W. Bergstrom, W. C. Fernelius, *Chem. Rev.,* 12 (1933) 43–179
[8] K. Sakurazawa, R. Hara, *J. Soc. Chem. Ind., Japan,* 40 (1937) Suppl. Binding 10

[9] R. Juza, *Angew*. *Chem*., *76* (1964) 290–300
[10] R. Juza, H. H. Weber, K. Opp, *Naturwissenschaften*, 42 (1955) 125, 73–82
[11] A. Zalkin, D. H. Templeton, *J. Phys. Chem.*, 60 (1956) 821–823
[12] W. Moldenhauer, H. Mottig, *Ber*., 62 (1929) 1954–1959
[13] H. Wattenberg, *Ber*., 63 (1930) 1667–1672
[14] G. V. Vajenine, *Inorg. Chem.,* 46 (2007) 5146–5148
[15] D. Fischer, M. Jansen, *Angew. Chem. Internat. Edit.*, 41 (2002) 1701–1702
[16] M. Nagib, H. Kistrup, H. Jacobs, *Atomkernenergie,* 26 (1975) 87–90
[17] Y. H. Hu, E. Ruckenstein, *J. Phys. Chem. A,* 107 (2003) 9737–9739
[18] H. Y. Leng, T. Ichikawa, S. Hino, N. Hanada, S. Isobe, H. Fujii, *J. Pow. Sources*, 156 (2006) 166–170
[19] Y. Kojima, Y. Kawai, *J. Alloys Compds.,* 395 (2005) 236–239
[20] J-P. 0. Bohger, R. R. Essmann, H. Jacobs, *J. Mol. Struct.,* 348 (1995) 325–328
[21] J. Hu, Z. Xiong, G. Wu, P. Chen, K. Murata, K. Sakata, *J. Pow. Sources,* 159 (2006) 120–125
[22] C. Tian, H-B. Yang, *Science in China Series B: Chemistry,* 52 (2009) 1412–1416
[23] W. Lohstroh, M. Fichtner, *J. Alloys Compds.,* 446-447 (2007) 332–335
[24] T. Ichikawa, H. Y. Leng, S. Isobe, N. Hanada, H. Fujii, *J. Pow. Sources,* 159 (2006) 126–131
[25] P. Chen, Z. Xiong, J. Luo, J. Lin, K. L. Tan, *J. Phys. Chem. B,* 107 (2003) 10967–10970
[26] Y. Kojima, Y. Kawai, *Chem. Commun.,* (2004) 2210–2211
[27] R. A. Varin, M. Jang, M. Polanski, *J. Alloys Compds*., 491 (2010) 658–667
[28] W. I. F. David, M. O. Jones, D. H. Gregory, C. M. Jewell, S. R. Johnson, A. Walton, P. P. Edwards, *J. Am. Chem. Soc.,* 129 (2007) 1594–1601

6. Conclusions

From this work it could be seen that the mixed cation amides, $Li_3Na(NH_2)_4$ and $LiNa_2(NH_2)_3$, desorbed substantial amounts of hydrogen when heated with lithium hydride and magnesium hydride. When heated with sodium hydride only the decomposition of NaH was observed. This indicates that, in contrast to simple amides like $LiNH_2$ and consistent with TPD results on the mixed amides, the production of hydrogen did not occur *via* reaction of the hydrides with NH_3,[1] but through direct reaction between amide and hydride. Sodium hydride was found to be unreactive in this respect, but was observed as a product of the reactions of the amides with both LiH and MgH_2. As NaH decomposes at relatively low temperatures, this is more likely to reflect the lack of stable alternative sodium-containing products (imide or nitride) than any special thermodynamic stability of the hydride itself. It was also found that minimal ammonia was desorbed which is consistent with the conclusions above and potentially of considerable benefit for a hydrogen storage material. When the mixed cation amides were heated with MgH_2 the hydrogen was desorbed at a temperature almost 100 °C lower than when heated with LiH. Unlike when lithium amide is heated with LiH and desorbs hydrogen with the formation of lithium imide, when the mixed cation amides were heated with LiH, no mixed imide was formed; instead lithium imide and NaH were formed. The products after heating the mixed cation amides with MgH_2 contained one or more unidentified phases, along with the known products.

Future work is needed to differentiate between the unidentified phases formed from the mixed cation amide reactions with MgH_2 and characterise them. Improvements to the

kinetics of the mixed cation amide + MgH_2 reactions could be made by ball-milling the starting materials and/or seeding with decomposition products [Li_2NH or $Li_2Mg(NH)$].

All the reactions of $x NaNH_2$ + $y MgH_2$ were found to react together to desorb hydrogen, without any ammonia detected. The stoichiometry of the magnesium with respect to Mg_3N_2 was important as it was an indication as to how far the reaction would go to full dehydrogenation.

The ratio of the starting materials was also important in the reversibility of the system. The heating of the $2NaNH_2$ + $3MgH_2$ system gave fully dehydrogenated products of Na and Mg_3N_2. These products were very difficult to rehydride under the conditions investigated here. By the addition of less MgH_2 ($2NaNH_2$ + MgH_2) the final product on heating to 350 °C was a mixed Na-Mg imide. This was possible to rehydride to $Mg(NH_2)_2$ and NaH at 300 °C, under 75 bar H_2 for 24 hours. On heating $2NaNH_2$ + $3MgH_2$, Na-Mg imide was formed at a lower temperature than Mg_3N_2, however the temperature at which to stop heating in order to only form the mixed imide was difficult to determine.

The unknown products of these reactions were thought to be a mixed Na-Mg amide, Na-Mg imide and Na-Mg nitride. Further work is required to characterise these phases.

From the work on $NaNH_2$ It was found that when heated to 350 °C $NaNH_2$ decomposed to an unknown phase and ammonia. When $NaNH_2$ was heated with NaH to 350 °C, an unknown phase, similar to that produced on heating $NaNH_2$ alone, was formed along with the release of hydrogen. This is analogous to the products of $LiNH_2$ when heated alone (Equation 5-8) and with LiH (Equation 5-7), indicating it is possible a sodium imide was formed. This had previously been dismissed in the literature.

The powder XRD patterns of the two phases (after heating $NaNH_2$ alone and with NaH) were similar, but not the same. This indicated possible non-stoichiometry, which is also present in the $LiNH_2$-Li_2NH system.

Attempts to rehydrogenate both unknown phase(s) did not reform the original reactant(s), although both XRD patterns were different to those before rehydrogenation.

Further work on this system would involve characterisation of the new phase(s). Continued work on the rehydrogenation of the possible imide should also be carried out.

[1] T. Ichikawa, N. Hanada, S. Isobe, H. Leng, H. Fujii, *J. Phys. Chem. B,* 108 (2004) 7887–7892

7. Appendix

1. $2NaNH_2 + 3MgH_2$

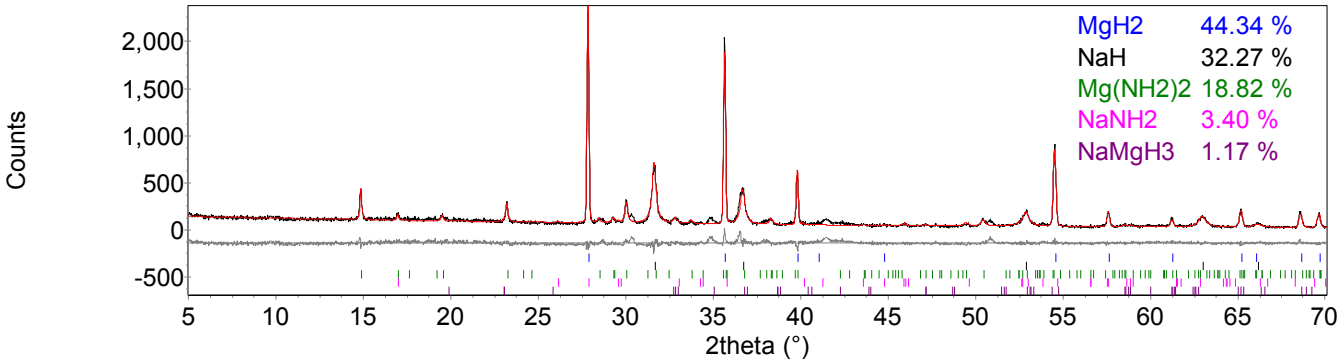

Figure 7-1 Powder XRD pattern of $2NaNH_2 + 3MgH_2$ after heating to 150 °C for 12 hours on a flowing line. The observed powder XRD pattern (black line) was fitted using a Rietveld fit (red line) to the observed phases MgH_2 (blue tick marks), NaH (black tick marks), $Mg(NH_2)_2$ (green tick marks), $NaNH_2$ (pink tick marks) and $NaMgH_3$ (purple tick marks). R_{wp} = 14.980, R_{exp} = 9.842, X^2 = 2.3.

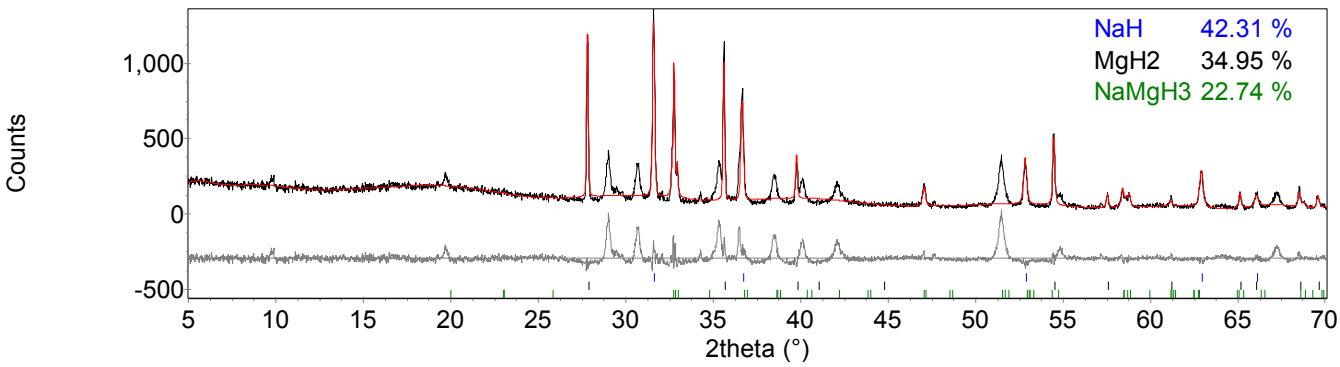

Figure 7-2 Powder XRD pattern of $2NaNH_2 + 3MgH_2$, heated to 250 °C for 12 hours on a flowing line. The observed powder XRD pattern (black line) was fitted using a Rietveld fit (red line) to the observed phases NaH (blue tick marks), MgH_2 (black tick marks) and $NaMgH_3$ (green tick marks). R_{wp} = 22.184, R_{exp} = 8.665, X^2 = 6.6.

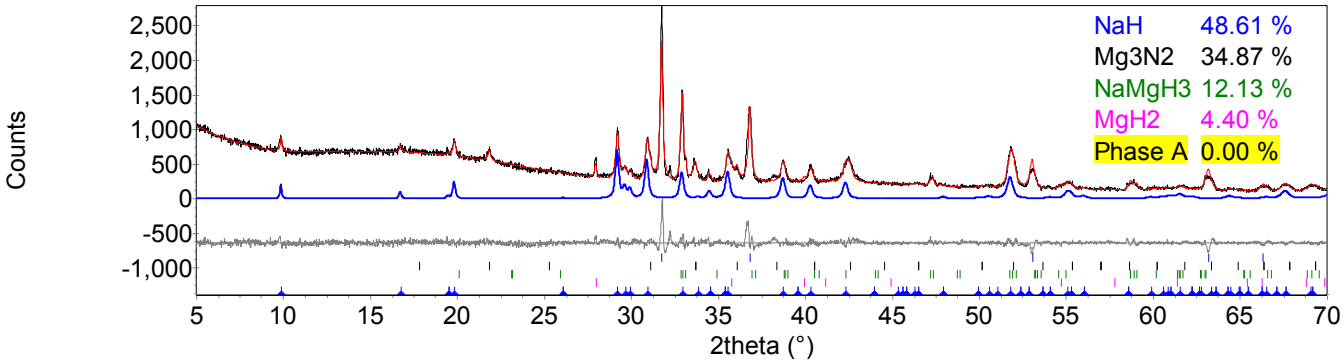

Figure 7-3 Powder XRD pattern of $2NaNH_2 + 3MgH_2$, heated at 300 °C for 12 hours on flowing line. The observed powder XRD pattern (black line) was fitted using a Rietveld fit (red line) to the observed phases NaH (blue tick marks), Mg_3N_2 (black tick marks), $NaMgH_3$ (green tick marks), MgH_2 (pink tick marks) and phase A (blue arrows) fitted using a Pawley fit (red line).* R_{wp} = 7.681, R_{exp} = 4.905, X^2 = 2.5.

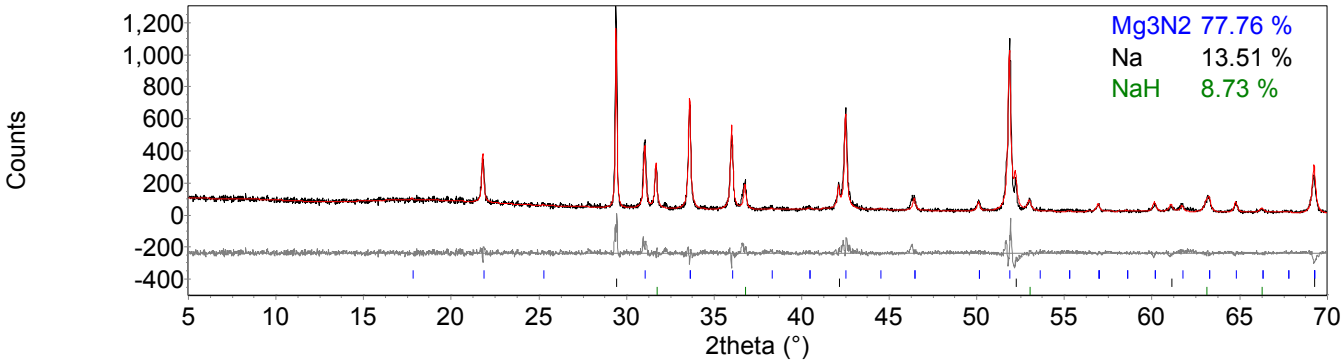

Figure 7-4 Powder XRD pattern of $2NaNH_2 + 3MgH_2$, heated at 350 °C for 12 hours on a flowing line. The observed powder XRD pattern (black line) was fitted using a Rietveld fit (red line) to the observed phases Mg_3N_2 (blue tick marks), Na (black tick marks) and NaH (green tick marks). R_{wp} = 15.975, R_{exp} = 11.615, X^2 = 1.9.

* Phase A is marked as 0% on the XRD pattern, because it was fitted to the pattern using a Pawley fit.

2. $2NaNH_2 + MgH_2$

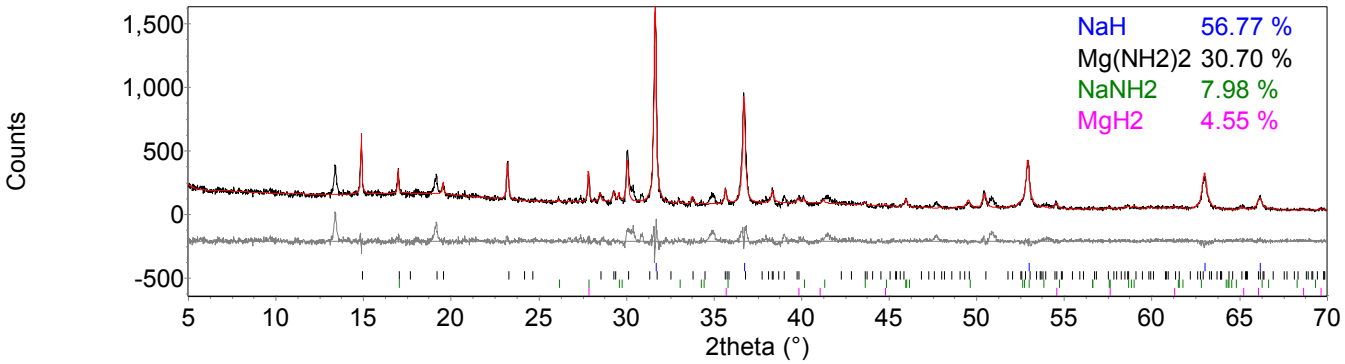

Figure 7-5 Powder XRD pattern of $2NaNH_2$ + MgH_2, heated at 150 °C for 12 hours under flowing argon. The observed powder XRD pattern (black line) was fitted using a Rietveld fit (red line) to the observed phases NaH (blue tick marks), $Mg(NH_2)_2$ (black tick marks), $NaNH_2$ (green tick marks) and MgH_2 (pink tick marks). R_{wp} = 14.906, R_{exp} = 9.139, X^2 = 2.7.

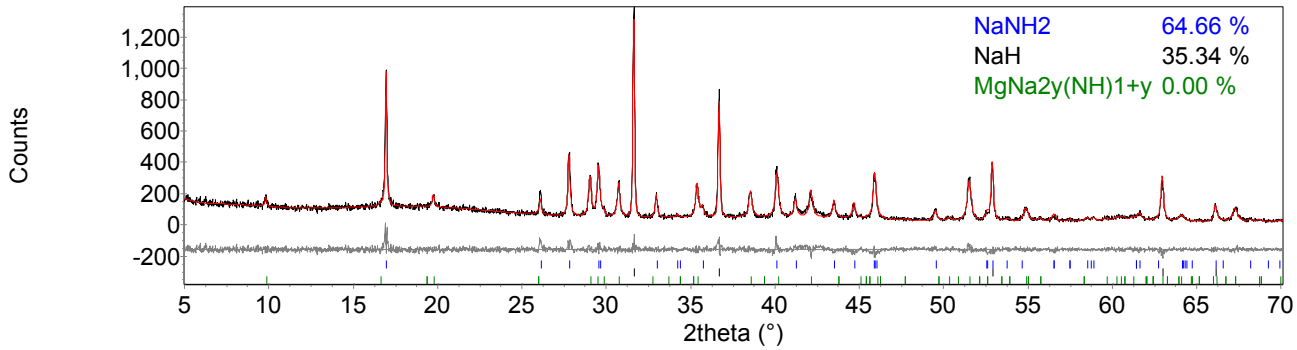

Figure 7-6 Powder XRD pattern of $2NaNH_2$ + MgH_2, heated at 200 °C for 12 hours under flowing argon. The observed powder XRD pattern (black line) was fitted using a Rietveld fit (red line) to the observed phases $NaNH_2$ (blue tick marks), NaH (black tick marks) and $MgNa_{2y}(NH)_{1+y}$ (green tick marks) fitted using a Pawley fit (red line). R_{wp} = 12.454, R_{exp} = 10.39, X^2 = 1.4.

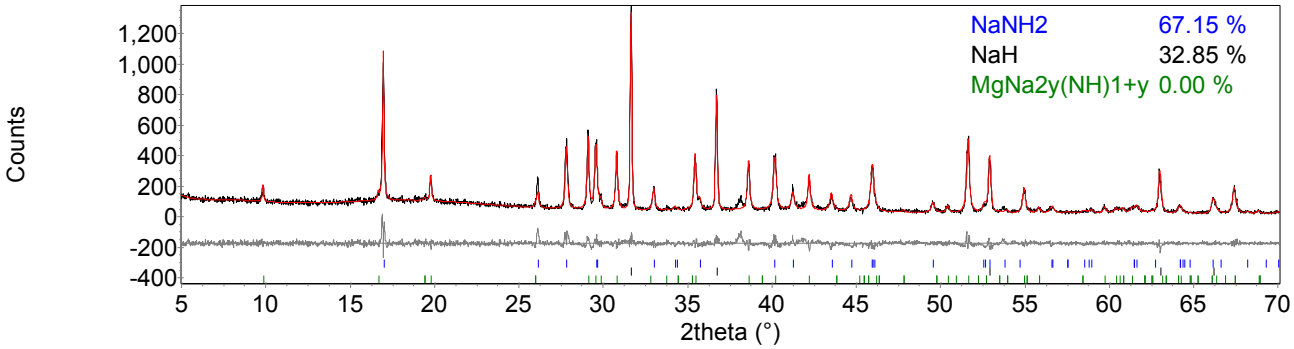

Figure 7-7 Powder XRD pattern of $2NaNH_2$ + MgH_2, heated at 250 °C for 12 hours under flowing argon. The observed powder XRD pattern (black line) was fitted using a Pawley fit (red line) to the observed phases $NaNH_2$ (blue tick marks), NaH (black tick marks) and $MgNa_{2y}(NH)_{1+y}$ (green tick marks) fitted using a Pawley fit (red line). R_{wp} = 13.643, R_{exp} = 10.475, X^2 = 1.7.

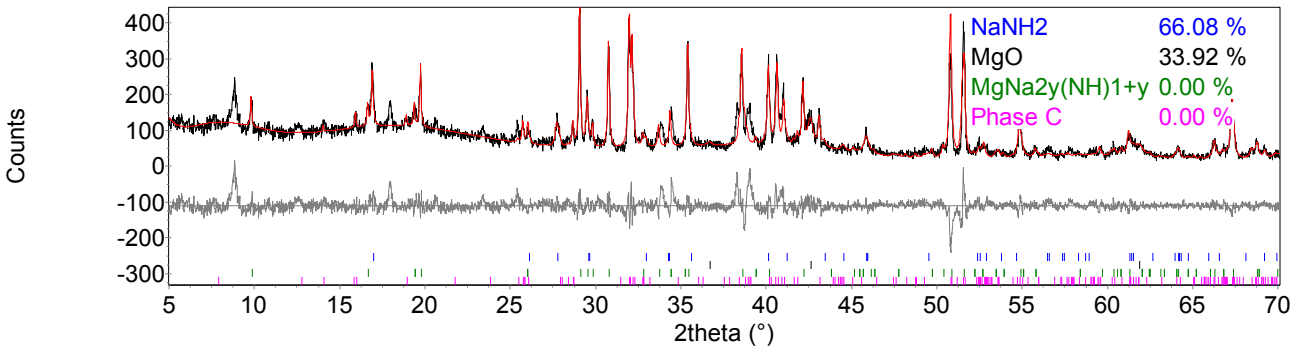

Figure 7-8 Powder XRD pattern of $2NaNH_2$ + MgH_2, heated at 350 °C for 12 hours under flowing argon. The observed powder XRD pattern (black line) was fitted using a Rietveld fit (red line) to the observed phases $NaNH_2$ (blue tick marks) and MgO (black tick marks). $MgNa_{2y}(NH)_{1+y}$ (green tick marks) and phase C (pink tick marks) were fitted using a Pawley fit (red line). R_{wp} = 17.511, R_{exp} = 10.828, X^2 = 2.6.

3. $3NaNH_2 + 2MgH_2$

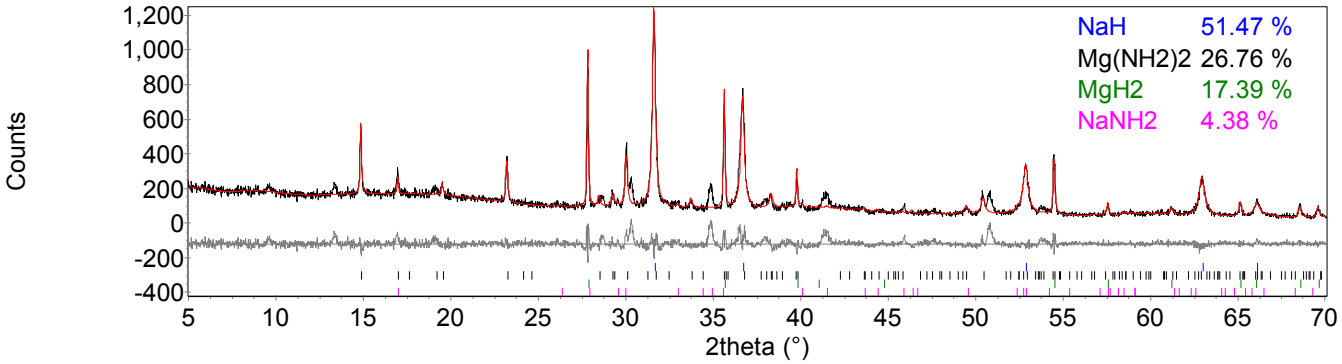

Figure 7-9 Powder XRD pattern of $3NaNH_2 + 2MgH_2$, heated to 150 °C for 12 hours under flowing argon. The observed powder XRD pattern (black line) was fitted using a Rietveld fit (red line) to the observed phases NaH (blue tick marks), $Mg(NH_2)_2$ (black tick marks), MgH_2 (green tick marks) and $NaNH_2$ (pink tick marks). R_{wp} = 14.232, R_{exp} = 8.904, X^2 = 2.6.

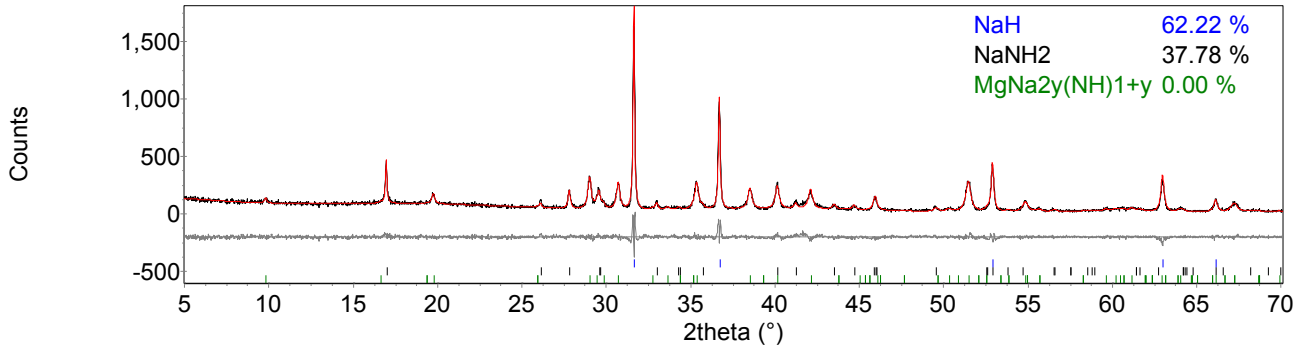

Figure 7-10 Powder XRD pattern of $3NaNH_2 + 2MgH_2$, heated to 200 °C for 12 hours under flowing argon. The observed powder XRD pattern (black line) was fitted using a Rietveld fit (red line) to the observed phases NaH (blue tick marks), $NaNH_2$ (black tick marks) and $MgNa_{2y}(NH)_{1+y}$ (green tick marks) fitted using a Pawley fit (red line). R_{wp} = 13.406, R_{exp} = 10.986, X^2 = 1.5.

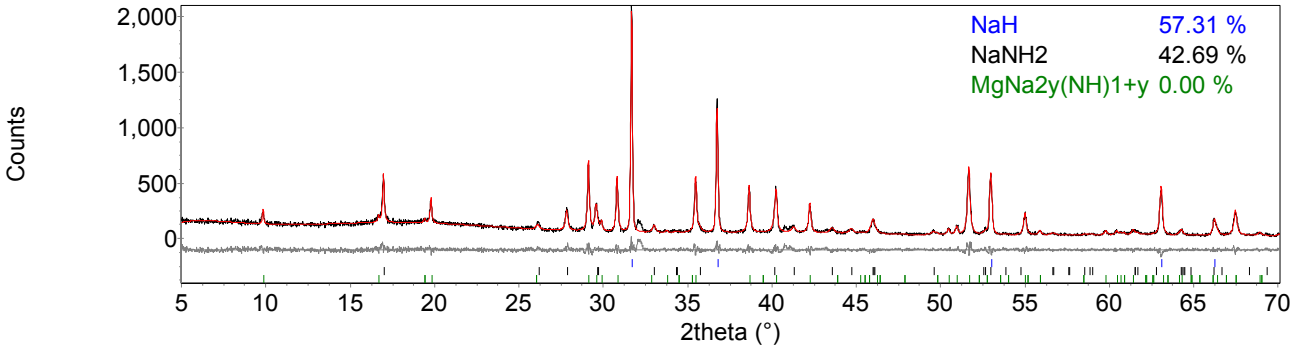

Figure 7-11 Powder XRD pattern of $3NaNH_2 + 2MgH_2$, heated to 250 °C for 12 hours under flowing argon. The observed powder XRD pattern (black line) was fitted using a Rietveld fit (red line) to the observed phases NaH (blue tick marks), $NaNH_2$ (black tick marks) and $MgNa_{2y}(NH)_{1+y}$ (green tick marks) fitted using a Pawley fit (red line). A small selection of the peaks of phase C were also visible. R_{wp} = 12.253, R_{exp} = 9.550, X^2 = 1.6.

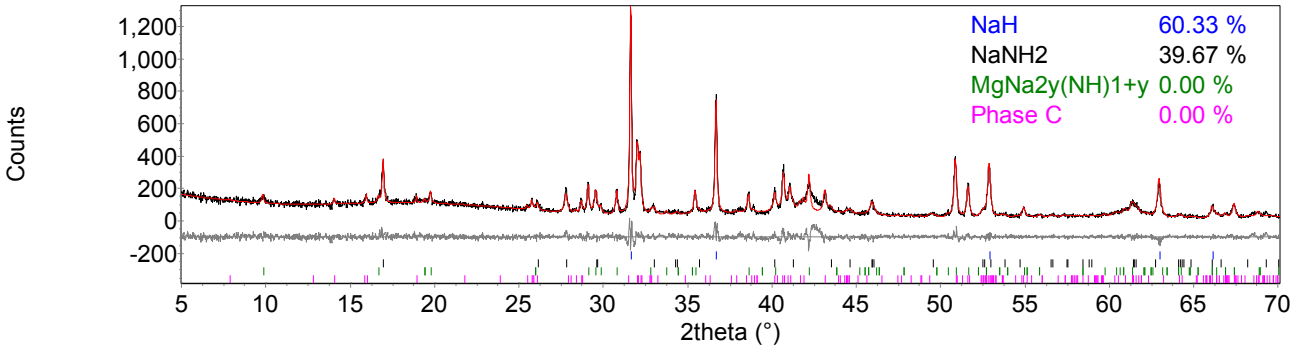

Figure 7-12 Powder XRD pattern of $3NaNH_2 + 2MgH_2$, heated to 300 °C for 12 hours under flowing argon. The observed powder XRD pattern (black line) was fitted using a Rietveld fit (red line) to the observed phases NaH (blue tick marks), $NaNH_2$ (black tick marks) and $MgNa_{2y}(NH)_{1+y}$ (green tick marks) and phase C (pink tick marks) fitted using a Pawley fit (red line). R_{wp} = 13.469, R_{exp} = 10.482, X^2 = 1.7.

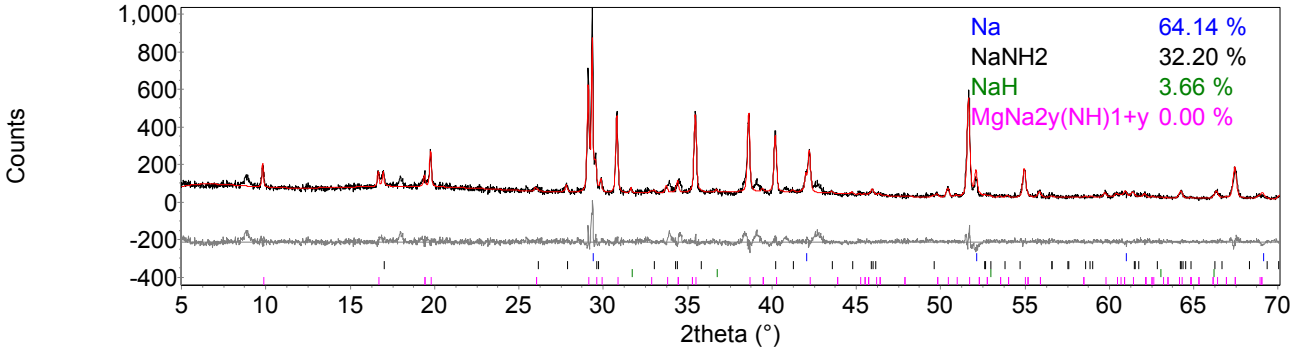

Figure 7-13 Powder XRD pattern of $3NaNH_2 + 2MgH_2$, heated to 350 °C for 12 hours under flowing argon. The observed powder XRD pattern (black line) was fitted using a Rietveld fit (red line) to the observed phases Na (blue tick marks), $NaNH_2$ (black tick marks), NaH (green tick marks) and $MgNa_{2y}(NH)_{1+y}$ (pink tick marks) fitted using a Pawley fit (red line). R_{wp} = 16.345, R_{exp} = 11.887, X_2 = 1.9.

4. $NaNH_2 + MgH_2$

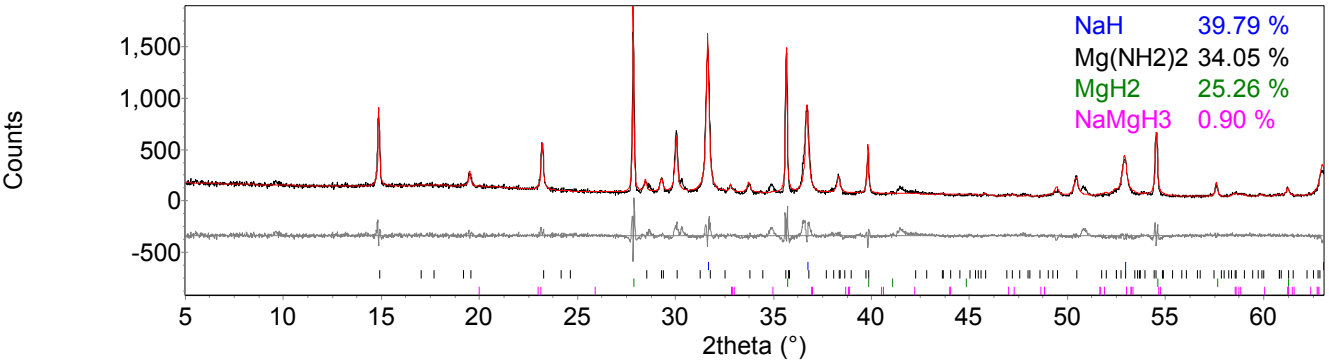

Figure 7-14 Powder XRD pattern of $NaNH_2 + MgH_2$, heated to 150 °C for 12 hours under flowing argon. The observed powder XRD pattern (black line) was fitted using a Rietveld fit (red line) to the observed phases NaH (blue tick marks), $Mg(NH_2)_2$ (black tick marks), MgH_2 (green tick marks) and $MgNa_{2y}(NH)_{1+y}$ (pink tick marks). R_{wp} = 15.020, R_{exp} = 8.970, X^2 = 2.8.

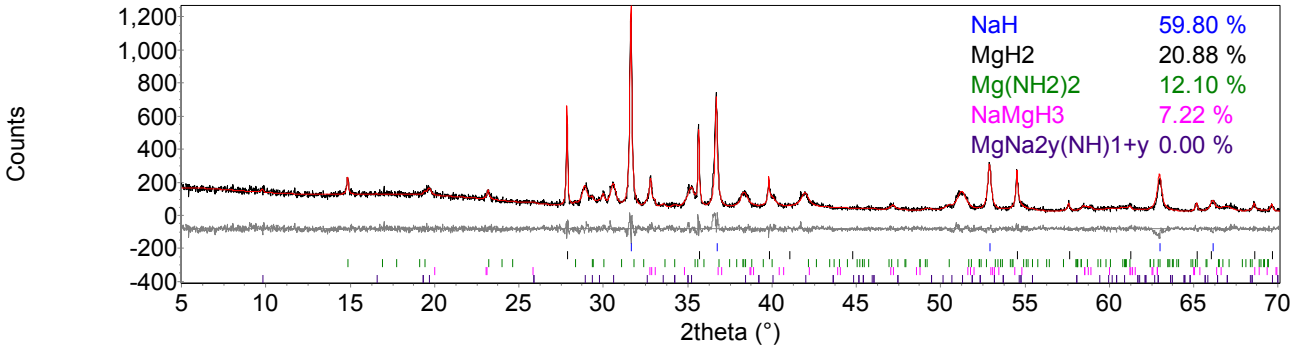

Figure 7-15 Powder XRD pattern of $NaNH_2$ + MgH_2, heated to 200 °C for 12 hours under flowing argon. The observed powder XRD pattern (black line) was fitted using a Rietveld fit (red line) to the observed phases NaH (blue tick marks), MgH_2 (black tick marks), $Mg(NH_2)_2$ (green tick marks), $NaMgH_3$ (pink tick marks) and $MgNa_{2y}(NH)_{1+y}$ (purple tick marks) fitted using a Pawley fit (red line). R_{wp} = 12.188, R_{exp} = 10.238, X^2 = 1.4.

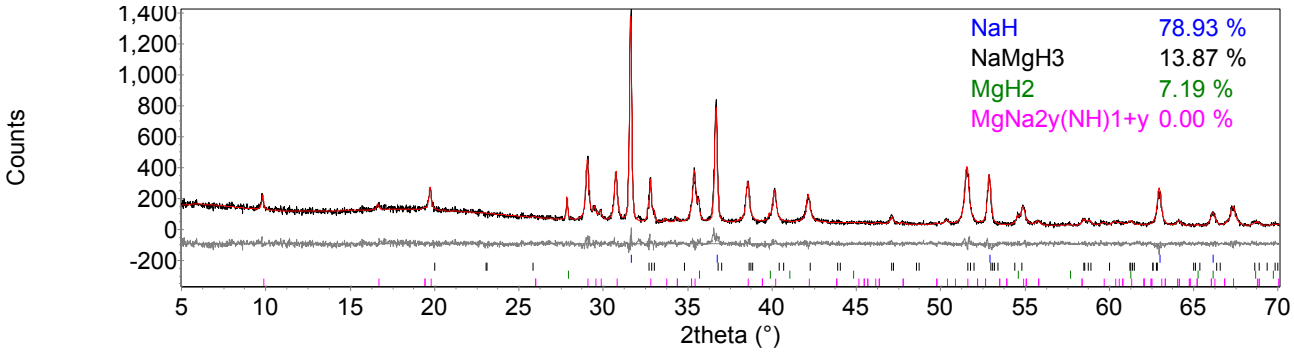

Figure 7-16 Powder XRD pattern of $NaNH_2$ + MgH_2, heated to 250 °C for 12 hours under flowing argon. The observed powder XRD pattern (black line) was fitted using a Rietveld fit (red line) to the observed phases NaH (blue tick marks), $NaMgH_3$ (black tick marks), MgH_2 (green tick marks) and $MgNa_{2y}(NH)_{1+y}$ (pink tick marks) fitted using a Pawley fit (red line). R_{wp} = 11.588, R_{exp} = 10.109, X^2 = 1.3.

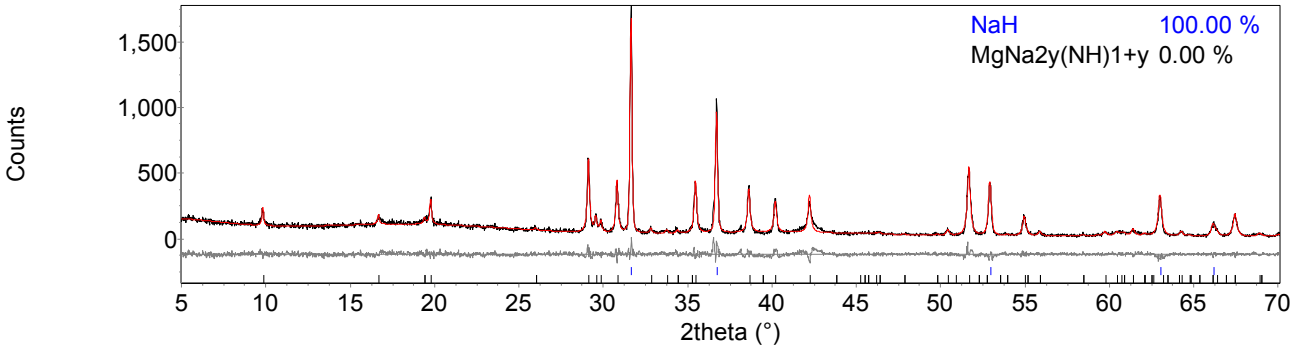

Figure 7-17 Powder XRD pattern of $NaNH_2$ + MgH_2, heated to 300 °C for 12 hours under flowing argon. The observed powder XRD pattern (black line) was fitted using a Rietveld fit (red line) to the observed phases NaH (blue tick marks). $MgNa_{2y}(NH)_{1+y}$) (black tick marks) was fitted using a Pawley fit (red line). R_{wp} = 13.861, R_{exp} = 10.430, X^2 = 1.8.

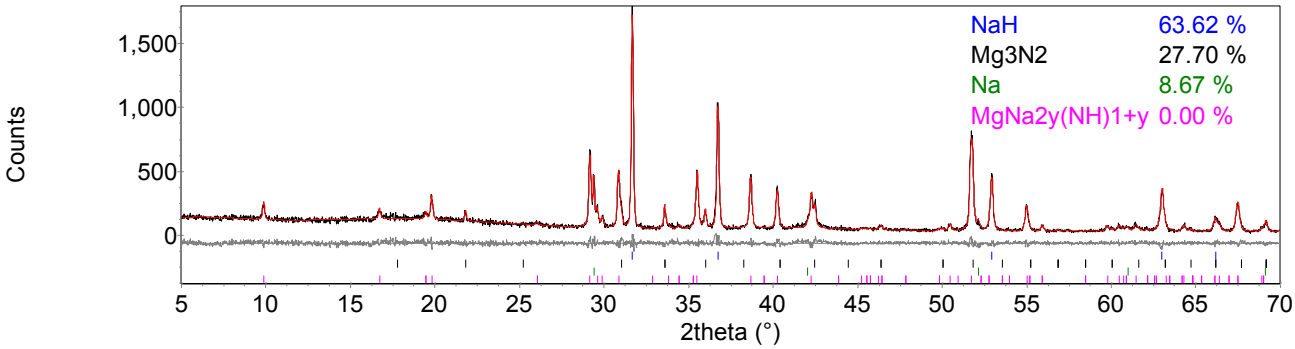

Figure 7-18 Powder XRD pattern of $NaNH_2$ + MgH_2, heated to 350 °C for 4 hours under flowing argon. The observed powder XRD pattern (black line) was fitted using a Rietveld fit (red line) to the observed phases NaH (blue tick marks), Mg_3N_2 (black tick marks), Na (green tick marks) and $MgNa_{2y}(NH)_{1+y}$ (pink tick marks) fitted using a Pawley fit (red line). R_{wp} = 11.258, R_{exp} = 9.669, X^2 = 1.4.

List of Illustrations